

2

AGARD-CP-391

AGARD-CP-391

AGARD

ADVISORY GROUP FOR AEROSPACE RESEARCH & DEVELOPMENT

7 RUE ANCELLE 92200 NEUILLY SUR SEINE FRANCE

AD-A166 652

DTIC
SELECTE
APR 15 1986
S D

AGARD CONFERENCE PROCEEDINGS No.391

Smokeless Propellants

This document has been approved for public release and sale; its distribution is unlimited.

DTIC FILE COPY

NORTH ATLANTIC TREATY ORGANIZATION



DISTRIBUTION AND AVAILABILITY
ON BACK COVER

86 4

AGARD-CP-391

NORTH ATLANTIC TREATY ORGANIZATION
ADVISORY GROUP FOR AEROSPACE RESEARCH AND DEVELOPMENT
(ORGANISATION DU TRAITE DE L'ATLANTIQUE NORD)

AGARD Conference Proceedings No.391
SMOKELESS PROPELLANTS

Papers presented at the Propulsion and Energetics Panel 66th (A) Specialists' Meeting, held in
Florence, Italy, 12-13 September 1985.

THE MISSION OF AGARD

The mission of AGARD is to bring together the leading personalities of the NATO nations in the fields of science and technology relating to aerospace for the following purposes:

- Exchanging of scientific and technical information;
- Continuously stimulating advances in the aerospace sciences relevant to strengthening the common defence posture;
- Improving the co-operation among member nations in aerospace research and development;
- Providing scientific and technical advice and assistance to the Military Committee in the field of aerospace research and development (with particular regard to its military application);
- Rendering scientific and technical assistance, as requested, to other NATO bodies and to member nations in connection with research and development problems in the aerospace field;
- Providing assistance to member nations for the purpose of increasing their scientific and technical potential;
- Recommending effective ways for the member nations to use their research and development capabilities for the common benefit of the NATO community.

The highest authority within AGARD is the National Delegates Board consisting of officially appointed senior representatives from each member nation. The mission of AGARD is carried out through the Panels which are composed of experts appointed by the National Delegates, the Consultant and Exchange Programme and the Aerospace Applications Studies Programme. The results of AGARD work are reported to the member nations and the NATO Authorities through the AGARD series of publications of which this is one.

Participation in AGARD activities is by invitation only and is normally limited to citizens of the NATO nations.

The content of this publication has been reproduced directly from material supplied by AGARD or the authors.

Published January 1986

Copyright © AGARD 1986
All Rights Reserved

ISBN 92-835-0387-2



Printed by *Specialised Printing Services Limited*
40 Chigwell Lane, Loughton, Essex IG10 3TZ

RECENT PUBLICATIONS OF THE PROPULSION AND ENERGETICS PANEL

Conference Proceedings

Testing and Measurement Techniques in Heat Transfer and Combustion
AGARD Conference Proceedings No.281, 55th A Meeting, May 1980

Centrifugal Compressors, Flow Phenomena and Performance
AGARD Conference Proceedings No.282, 56th B Meeting, May 1980

Turbine Engine Testing
AGARD Conference Proceedings No.293, 56th Meeting, Sep/October 1980

Helicopter Propulsion Systems
AGARD Conference Proceedings No.302, 57th Meeting, May 1981

Ramjets and Ramrockets for Military Applications
AGARD Conference Proceedings No.307, 58th Meeting, October 1981

Problems in Bearings and Lubrication
AGARD Conference Proceedings No.323, 59th Meeting, May/June 1982

Engine Handling
AGARD Conference Proceedings No.324, 60th Meeting, October 1982

Viscous Effects in Turbomachines
AGARD Conference Proceedings No.351, 61st A Meeting, June 1983

Auxiliary Power Systems
AGARD Conference Proceedings 352, 61st B Meeting, May 1983

Combustion Problems in Turbine Engines
AGARD Conference Proceedings 353, 62nd Meeting, October 1983

Hazard Studies for Solid Propellant Rocket Motors
AGARD Conference Proceedings 367, 63rd A Meeting, May/June 1984

Engine Cyclic Durability by Analysis and Testing
AGARD Conference Proceedings No.368, 63rd B Meeting, May/June 1984

Gears and Power Transmission Systems for Helicopters and Turboprops
AGARD Conference Proceedings No.369, 64th Meeting October 1984

Heat Transfer and Cooling in Gas Turbines
AGARD Conference Proceedings No.390, 65th Meeting, May 1985

Smokeless Propellants
AGARD Conference Proceedings No.391, 66th A Meeting, September 1985

Working Group Reports

Aircraft Fire Safety
AGARD Advisory Report 132, Vol.1 and Vol.2. Results of WG11 (September and November 1979)

Turbulent Transport Phenomena (in English and French)
AGARD Advisory Report 150. Results of WG 09 (February 1980)

Through Flow Calculations in Axial Turbomachines
AGARD Advisory Report 175. Results of WG 12 (October 1981)

Alternative Jet Engine Fuels
AGARD Advisory Report 181, Vol.1 and Vol.2. Results of WG 13 (July 1982)

Suitable Averaging Techniques in Non-Uniform Internal Flows
AGARD Advisory Report 182 (in English and French). Results of WG 14 (June/August 1983)

Lecture Series

Non-Destructive Inspection Methods for Propulsion Systems and Components
AGARD LS 103 (April 1979)

The Application of Design to Cost and Life Cycle Cost to Aircraft Engines
AGARD LS 107 (May 1980)

Microcomputer Applications in Power and Propulsion Systems
AGARD LS 113 (April 1981)

Aircraft Fire Safety
AGARD LS 123 (June 1982)

Operation and Performance Measurement of Engines in Sea Level Test Facilities
AGARD LS 132 (April 1984)

Ramjet and Ramrocket Propulsion Systems for Missiles
AGARD LS 136 (September 1984)

3-D Computation Techniques Applied to Internal Flows in Propulsion Systems
AGARD LS 140 (June 1985)

Other Publications

Airbreathing Engine Test Facility Register
AGARD AG 269 (July 1981)

THEME

In the PEP 53rd Symposium on "Solid Rocket Motor Technology" held in Spring 1979, diverging views on smoke and visibility were stated, and a follow-on activity was suggested. In this two-day Specialists' Meeting on "Smokeless Propellants", it was intended to bring together specialized experts in this field to discuss their problems and the definition of smokeless propellants. The scope included: smokeless propellant chemistry; experimental results and their comparisons on smokelessness, minimum smoke and reduced smoke of propellants; smokeless inhibitors; smoke measurements, particle collection, different wave lengths; light diffusion and contrast; plume analysis.

* * * *

Lors du 53^e Symposium du PEP sur "La Technologie des Moteurs Fusées à Propergol Solide", qui eut lieu au printemps 1979, des vues divergentes sur la fumée et la visibilité furent déjà exprimées et il fut suggéré de poursuivre l'étude de ce domaine. Au cours de la réunion de spécialistes, d'une durée de deux jours, qui vous a été proposée, sur le thème de "Propergols non Générateurs de Fumée", nous avons réunis des experts du domaine en cause pour examiner leurs problèmes et discuter de la définition des propergols non générateurs de fumée. Les sujets étudiés furent les suivants: chimie des propergols non générateurs de fumée; résultats expérimentaux et comparaison de ces résultats en ce qui concerne l'absence de fumée, l'émission minimale de fumée et l'émission réduite de fumée des propergols; les inhibiteurs non générateurs de fumée; les mesures de la fumée, le recueil des particules, les différentes longueurs d'ondes; la diffusion de la lumière et le contraste; l'analyse du panache de fumée.

Accession For	
NTIS CRA&I	<input checked="" type="checkbox"/>
DTIC TAB	<input type="checkbox"/>
Unannounced	<input type="checkbox"/>
Justification	
By	
Distribution /	
Availability Codes	
Dist	Avail and/or Special
A-1	

QUALITY
CHECKED
3

PROPULSION AND ENERGETICS PANEL

Chairman: Prof. H.Wittenberg
Delft University
Dept. of Aerospace Engineering
Kluyverweg 1
2629 HS Delft, Netherlands

Deputy Chairman: Dr W.L.Macmillan
National Defence Headquarters
CRAD/DRDA
101 Colonel By Drive
Ottawa, Ontario K1A 0K2, Canada

PROGRAMME COMMITTEE

Prof. Dr A.Ücer (Chairman)
Middle East Technical University O D T Ü
Makina Müh. Bölümü
Ankara, Turkey

Ten. Col. Gari L.Gagliardi
Ministero della Difesa
Direzione Generale Costruzioni AAAS
Viale dell'Università 4, 00185 Roma, Italy

Dip.-Ing. B.Crispin
Messerschmitt-Bölkow-Blohm GmbH, Abt AE 15
Postfach 801149, 8000 München Germany

Dr W.L.Macmillan
National Defence Headquarters
CRAD/DRDA 6
101 Colonel By Drive
Ottawa, Ontario K1A 0K2, Canada

Mr A.Cruttenden
Royal Ordnance Factories
Explosives Division HQ
Westcott, Aylesbury, Bucks HP18 0NZ, UK

Mr L.Vailhe
Société Européenne de Propulsion
Le Haillan, Boîte Postale 37
33165 Saint Médard en Jalles, France

Prof. F.E.Culick
201 Karman Laboratory
Mail Stop 301-46
California Institute of Technology
Pasadena, California 91125, US

Prof. Ir. H.Wittenberg
Delft University of Technology
Department of Aerospace Engineering
Kluyverweg 1, 2629 HS Delft, Netherlands

M.B.Zeller
Société Nationale des Poudres et Explosifs
91710 Vert-le-Petit, France

HOST NATION COORDINATOR

Lt Col. A.Castrucci

PANEL EXECUTIVE

Dr E.Riester
AGARD-NATO
7 rue Ancelle
92200 Neuilly sur Seine
France

ACKNOWLEDGEMENT

The Propulsion and Energetics Panel wishes to express its thanks to the Italian National Delegates for the invitation to hold this meeting in Florence, Italy, and for the facilities and personnel which made the meeting possible.

CONTENTS

	Page
RECENT PUBLICATIONS OF PEP	iii
THEME	v
PROPULSION AND ENERGETICS PANEL	vi
TECHNICAL EVALUATION REPORT by G.I.Evans	ix
	Reference

SESSION I – A REVIEW OF SMOKELESS PROPELLANT TECHNOLOGY

HAZARDS/PERFORMANCE TRADEOFFS FOR SMOKELESS SOLID PROPELLANT ROCKET MOTORS* by R.L.Derr and T.L.Boggs	1
---	---

SESSION II – PREDICTION AND MEASUREMENTS OF SIGNATURE

ROCKET CONDENSATION TRAILS: PROPELLANT AND ALTITUDE EFFECTS FOR TACTICAL MISSILES* by D.E.Jensen and A.C.H.Mace	2
METHODOLOGIE ET MOYEN D'ETUDE DE LA DISCRETION DES MOTEURS A PROPERGOL SOLIDE* par E.Ajdari	3
EXHAUST SIGNATURE PREDICTIONS FOR ROCKET MOTORS* by A.C.H.Mace	4

SESSION III – CHEMISTRY OF SMOKELESS PROPELLANTS (I)

PROPERGOLS SANS FUMEE CONTENANT DES NITRAMINES* par R.Couturier	5
SMOKELESS PROPELLANTS OF IMPROVED PERFORMANCE by E.A.Baker	6
NITRAMIN SOLID ROCKET PROPELLANTS WITH REDUCED SIGNATURE* by W.Klöhn and S.Eisele	7
COMBUSTION DES PROPERGOLS A BASE D'OCTOGENE par G.Lengelle et J.Duterque	8
STABILITY OF NITROCELLULOSE PROPELLANTS ASSESSED VIA THERMAL DECOMPOSITION AND ALTERATION OF THE STABILIZER COMPOSITION by P.van de Mey and A.H.Heemskerk	9
BURNING STABILITY OF DOUBLE BASE PROPELLANTS by L. De Luca, C.Zanotti, G.Riva, R.Dondé, A.Volpi, C.Grimaldi and G.Colombo	10
ENERGETIC BINDERS AS INGREDIENTS FOR MINIMUM SMOKE PROPELLANTS* by R.Reed, Jr, T.L.Boggs and M.L.Chan	11
LOW VISCOSITY SATURATED HYDROXYL TERMINATED POLYMERS FOR COMPOSITE PROPELLANTS* by R.A.H.Strecker and I.Harrer	12
ELASTOMER MODIFIED CAST DOUBLE BASE PROPELLANTS by G.I.Evans and D.Facer	13

*Issued in classified publication CP 391 (Supplement)

Reference

Paper 14 withdrawn 0

INHIBITEURS POUR MOTEURS D'ENGINS TACTIQUES SANS FUMÉES²
par B.Gonthier et J.N.Tauzia

15 7

SESSION IV – CHEMISTRY OF SMOKELESS PROPELLANTS (II)

THE REDUCTION OF EXHAUST SIGNATURE IN SOLID PROPELLANT ROCKET
MOTORS

by G.I.Evans and P.K.Smith

16

THE CHEMICAL INTERACTION OF BALLISTIC MODIFIERS IN CDB PROPELLANT –
ITS EFFECT UPON BALLISTICS AND STABILITY

by J.D.M.Pearson, A.C.J.Shedden and I.A.Duncan

17

SESSION V – SMOKE MEASUREMENTS (I)

DIRECT EROSIVE BURNING MEASUREMENTS OF A REDUCED-SMOKE SOLID
PROPELLANT ROCKET BY FLASH X-RAYS

by T.Constantinou and D.Greatrix

18

SESSION VI – SMOKE MEASUREMENTS (II)

EXPERIMENTAL TECHNIQUES FOR OBTAINING PARTICLE BEHAVIOR IN SOLID
PROPELLANT COMBUSTION

by D.W.Netzer and J.P.Powers

19

ANALYSE DES GAZ DANS L'ETUDE DE LA COMBUSTION DES PROPERGOLS
DOUBLE BASE ET DE L'OCTOGENE

par J-F.Trubert

20

MEASUREMENTS OF DISTRIBUTED COMBUSTION

by M.W.Beckstead, P.C.Braithwaite and D.L.Gordon

21

*Issued in classified publication CP 391 (Supplement)

TECHNICAL EVALUATION REPORT*

by

G.I.Evans
IMI Summerfield
Kidderminster, Worcs DY11 7RZ
UK

This conference's papers show significant advances in some areas of smokeless propellants since the 53rd PEP Meeting in Oslo. In other areas the advances are not so obvious and further work remains within the AGARD Community.

Smoke consists of condensed phase particles suspended in a gas. Accordingly, metals such as aluminium fuel materials which inevitably give rise to condensed phase as propellant ingredients are eliminated from the definition of smokeless propellants. Paper No 3 by Mr Ajdari of SNPE showed even small proportions of aluminium give unacceptable smoke penalty. For example 2% aluminium in a double base matrix resulted in only 58% transmission through the plume of a visible wavelength beam. Of interest this paper showed that at the 2% aluminium level the transparency of the plume in the infra-red region was much higher than in the visible. This phenomenon is explainable, however, from the optical properties of particulate clouds. The light or beam scattering coefficient of a single particle reaches a peak at a specific particle size. This peak in the scattering coefficient shifts to the high particle size regions at the longer infra-red wavelengths. Thus the relatively dilute cloud of aluminium oxide smoke in Mr Ajdari's example becomes more transparent in the infra-red regions. Nevertheless, at slightly higher aluminium contents the particulate cloud would become more dense and when entering the state of multiple particle scattering of the incident beam, the attenuation in the infra-red wavelengths would also climb steeply.

It follows from the above that, since aluminium or other metal fuels are not compatible with smokeless propellants, an energy penalty is inevitable as a trade-off for desirable plume properties. The conference papers reflect the attempts to minimise this energy penalty and achieve other utilisable propellant properties by propellant formulation advances.

This latter task has to be constrained by the definition of smokeless propellant. It is noteworthy that this conference programme preamble referred to the findings of the 53rd PEP Meeting**. The latter referred to differences of view on the definitions of smoke and visibility and the "further need for specialists to consider further, etc".

The evaluator considers the conference in general did not address itself to this specific question and there is a need for an agreed quantitative measure and methodology for defining smoke properties of propellants.

Paper No 1 by Dr R.L.Derr was the only paper in the conference specifically devoted to attempting this definition and this paper also introduced the important subject of hazard classification associated with minimum smoke which is referred to later. This paper No 1 classified propellants into smoky, reduced smoke, minimum smoke, smokeless related to classification of propellant types, i.e. binder and fillers, under these headings. Whilst valuable in qualitatively stating generally observed principles this classification is too imprecise and broad-brush to serve as a meaningful definition, which is fundamental to this subject area. There is the danger of a proliferation of terminology which furthers confusion rather than clarity, for example, the imprecise sub-division of "minimum smoke" and "smokeless" where the latter is an esoteric ideal of no hydrogen in propellant (because of the special case of potential water contrails at high altitudes).

The evaluator would wish to see a return to basics centring around the real requirements of missile systems and guidance/signature requirements of the propulsion plume. From this a quantitative definition of a *smokeless* propellant would be one that gives 90% or more transmission of an incident beam wavelength when such a beam is directed through the axis of the plume or at a narrow angle (e.g. 7°) to the plume. Instrumented measurements of rocket motor firings along these lines have been in practice for many years in the UK and, to the writer's knowledge, in France. Such a plume transparency property implies dilute particulate clouds manifesting single particle scattering of an incident beam. In flight, therefore, the plume is virtually invisible and the definition of visibility may be, at worst, conveniently circumvented. Similarly quantitative, instrumented measurements of other plume signature and transparency features at other wavelengths are established practice and may serve for definition purposes.

If we move from "smokeless" to the so called "reduced smoke" terminology, confusion arises. The practitioners in propellants and systems in this area have not defined what is meant by reduced smoke or by how much the "smoke" has to be

* The report reflects the personal opinion of the author. Some Members of the Programme Committee do not always concur with the author's considerations

**AGARD Conference Proceedings No.259

reduced to qualify. If we are to be persuaded that the latter has relevance to the conference subject area then a visibility contrast definition is clearly required. The latter has to be in the context of external ambient light with either a clear, bright sky with direct solar radiation or a dark, cloudy overcast sky in conjunction alternatively with a bright or a dark background (land or sea). Similarly, transparency definitions of a "reduced smoke" cloud are required.

In this elastic area of reduced smoke definitions and the work tasks involved, the evaluator would advise careful consideration to the foreseeable and more difficult task of defining the broad band of the unacceptable. This is pertinent since the term "reduced smoke" has arisen because of the attempts to accommodate halogens — particularly ammonium perchlorate — into the subject area of smokeless propellants.

Papers Nos 2, 3 and 4 by Dr Mace and Mr Ajdari reinforce previous disclosures. These papers give the boundary conditions for formation of HCL condensates or secondary smoke arising from AP. Study of these humidity conditions inevitably leads to the conclusion that service deployment, more particularly in temperate and tropical regions (as defined in NATO documents), will realise these boundary conditions on the vast majority of occasions.

Thus although special climatic conditions can be contrived in trials to avoid or minimise condensates, this cannot disguise the fact that a service weapon with an AP propellant will give highly visible and opaque secondary smoke plumes. This is the case with modest mass fraction of AP in the propellant. Mr Ajdari presented data on 15% AP in a smokeless double base binder. Dr Mace gave data on the number of molecules of HCL per cubic metre of gas to form visible condensates.

Moreover there is a further conclusive feature which renders "reduced smoke" AP propellants *non-progredi est regredi* in this conference subject area.

Advances in smokeless propellant requirements have, as a concomitant, secondary flame suppression in the plume. Missile requirements are calling for and will increasingly stress "stealth" features, implying low signature not only with respect to visible smoke but visible flame, emission radiance through the infra-red spectrum and radar signature. Missile guidance requirements, not only in microwave radar frequencies but increasingly with lasers, are important. All these features demand cool plumes which are associated with secondary flame suppression. Paper No 16 presented by G.I. Evans addressed this area in some detail. The necessary precursor of efficient flame suppression is a smokeless or minimum smoke propellant (or rocket motor). Particulate smoke reduces the efficiency of potassium salt suppression, resulting in the vicious circle of increased potassium salt and increasing potassium smoke penalty. More importantly, the HCL from AP, even in modest proportions, prevents the mechanism of potassium salt flame suppression by formation of the stable KCL.

The aforementioned has dealt at some length on the subject of a quantitative definition of smokeless propellant and on AP "reduced smoke" propellants. It is important to relate the relevance of the latter to smokeless and plume properties which are the subject of the conference. A number of the papers including some with propellant formulation developments, involved continuing use of AP, in the light of the Oslo 53rd PEP reported findings the evaluator felt it may be useful to lay the emphasis given in the foregoing.

Moving to the area of smokeless propellants, defined on the quantitative lines suggested previously (or, if preferred, the more imprecise "minimum smoke"), a substantial number of papers were of importance. It is noteworthy that all such propellants showed a convergence on and heavy dependence on the nitramine crystalline fillers RDX and HMX. These performance lead to departure from the classical composite propellant binders towards energetic binders. The latter fell into two groups:

- (i) An inert elastomer with energetic plasticisers of nitric esters, most typically nitroglycerine, and
- (ii) The classical double base nitrocellulose-nitroglycerine binders.

The EMCDB class of propellants given in paper No 13 by G.I. Evans is a hybrid of these two groups.

The above two groups of propellant lead to three critical features in the field of tactical service use:—

1. *Ballistics*. The first group of propellants, essentially the slurry cast mix or nitramite G are dominated by the energetic binder/nitramine filler propensity for high temperature coefficient of burning rate, high pressure exponent and the limitation on burning rate range, notably restrictions in the boost region. The limitations on burning rate and temperature coefficient of rate are serious constraints on their applicability in tactical missile requirements. Paper No 5 by Mr Couturier and Paper No 8 by Mr Lengéie were erudite in presenting this aspect. These papers showed, with this group of propellants, the current inability to achieve burning rate catalysis and platonisation (to obtain temperature coefficient effects). The papers 5 and 8 showed HMX filler is not conducive to burning rate modulation as is possible by AP size variation.

The reasons are not hard to envisage. The evidence for catalysis and platonisation of energetic binder propellants is accompanied by formation of carbon fibrils at the burning surface during rate catalysis, followed by progressive depletion and disappearance of the carbon fibrils and catalysis at higher pressure regions, the latter resulting in a plateau effect. This phenomenon has only been seen in the group (ii) binders based on NC/NG. The presence of nitrocellulose is the key. Following rupture of the CO—NO₂ bond the catalysts appear to promote dehydrogenation of the cellulose to carbon fibrils. The molecular structure of the cellulose is obviously important but the morphology of the naturally occurring cotton fibre may also be important.

With regard to group (ii) nitrocellulose double base propellants and its derivatives, the conference papers showed significant advances made in such burning rate catalysts. This is evident in paper No 5 by Mr Couturier, paper No 6 by Mr E. Baker, papers 13 and 16 Mr G.I. Evans and paper No 17 by Dr I. Duncan. These papers showed advances in catalysis, platonisation and temperature coefficients for tactical systems. These effects are now achieved with RDX/HMX levels up to 40% in energetic binders with specific impulse up to 2450 Ns/kg over a wide range of boost/sustain burning rates. It has to be said that such advances are made by empirical and experimental means relying on experience and innovative flair. No definitive understanding of the basic chemical reaction mechanism exists to give a predictive means to design and guide propellants advances.

Accordingly, to enhance the utility of the group (i) propellants for tactical missiles, either the introduction of sufficient amounts of such nitrocellulose or an equivalent alternative ingredient to promote such active carbon fibril formation appears desirable. There is evidently a great need for fundamental studies of the mechanisms of burning rate catalysis and platonisation. Only one paper in the conference was devoted to this basic study, that is paper No 20 by Mr Trubert of ONERA. This work examined the combustion regions of interest by a technique of linear pyrolysis of double base propellants under vacuum using radiant heat source. The reaction products were measured. The paper does not elucidate the basic reaction mechanism of catalysis/platonisation but its conclusion does identify that catalysis occurs in the primary flame (presumably the fizz zone) and not in the secondary flame. This conclusion correlates with the aforementioned observation of the importance of the carbon fibrils at the combustion surface (i.e. the condensed phase/fizz zone region). The evaluator would add, however, that the secondary flame is important to the overall effect. At high pressures the secondary combustion flame moves progressively closer to the propellant surface from experimental observations. The resulting increased heat transfer rate to the surface would result in increased reaction rate of the carbon fibrils. The rapidity of removal of the latter would result in cessation of catalysis. In that event the propellant combustion rate would return progressively to that of the basic propellant at the high pressure i.e. the plateau or mesa effect.

Whilst the group (i) propellants are currently deficient in the means of catalysis inherent in the double base group (ii) they have the advantage of superior mechanical properties, particularly low temperature strain capability. Conversely, the double base propellants have poor low temperature strain capability and high brittle points (-20 to -30°C) which constrain their use in case bond motors. The EMCDB class in paper No 13 is a hybrid to achieve the mechanical properties of group (i) whilst retaining the minimum of nitrocellulose (12%) required to achieve catalysis/platonisation.

Paper No 1 by Dr R.L. Derr was the only conference paper devoted to Hazard Classification. This subject area will dominate the field of smokeless propellants and its advances in the future. The importance is accentuated by the increasing demands of the NATO service users for insensitive munitions. The munitions are required to give a low order response of controlled burning rather than violent explosive pressure bursts or detonation under specified types of thermo-mechanical attack. The latter are defined attacks of cook-off (eg fuel fire), bullet and fragment attack and sympathetic detonation. Thus the work to minimise the energy penalty inherent in smokeless propellants, versus the traditional aluminised propellants has to take account of the defined constraints of acceptable insensitive munitions.

The NATA STANAG 4170 attempted to correlate universal criteria and methodology of hazard classifications. Each national authority, within this, develops its own interpretation and application, (for example in the UK in OB Proc 41779). Also the STANAG, ambitiously, has embraced all explosives (HE, pyrotechnics, gun propellants and rocket propellants) under one umbrella. Confusion and imprecision of significant impact to the direction of the field of smokeless propellants has arisen and is evident in this conference.

In paper No 1 Mr Derr expressed the US Navy view that "reduced smoke" propellants are not mass detonatable (1.3 class) but that "minimum smoke" propellants are mass detonatable (1.1 class). It is not clear to the writer the extent to which the US view is as sharp and immutable as that quoted, but it is likely to be regarded elsewhere as too broad-brush. Significant work on rocket motors in the UK using bullet/fragment/sympathetic detonation trials have shown instances of designs with composite HTPB propellants giving violent responses not complying with the definition of an insensitive munition given in US Navy specifications. Whereas by contrast, certain RDX filled "minimum smoke" propellants under such attack do comply. Moreover to further illustrate the terminological confusion that can arise in this field the UK authorities recently under STANAG 4170 methodology have classified as 1.3 an RDX filled EMCDB smokeless propellant for service use. Other examples in both France and UK have classified smokeless propellants of the type classical CDB, epitetete, RDX filled CDB, nitramite E and RDX filled EMCDB as 1.3 (i.e. not mass detonation risk).

The common ground may be in thresholds of RDX/HMX filler loading level, perhaps 40% in some systems and that the threshold may be dependent on the particular binder rheological properties. To further illustrate these considerations, the importance of the differences between the Group (i) propellants (slurry cast, nitramite G etc) which feature large μ in the US smokeless propellant field and Group (ii) and EMCDB which are noteworthy:—

(a) Colloidal Aspects of Binder

The group (i) propellants have little (< 2%) or no nitrocellulose. Where used it variously takes the form of ball powder, flakes or NC lacquer solutions. Group (ii) have high nitrocellulose content e.g. even the filled EMCDB has 12 to 16%. Moreover the NC is in the form of a gelatinised fibre based on the morphology of the naturally occurring cotton fibre.

(b) RDX/HMX Encapsulation

In the case of the group (ii) propellants the RDX is encapsulated in yet higher nitrocellulose, highly viscous doughs during the intermediate powder granule manufacture. In the group (i) case the RDX is suspended in a highly plasticised elastomeric gel.

The use of resin coated RDX/HMX to enhance filler/binder adhesion and nitramine particle size may also be important.

The above (a), (b) rheological features can be important to the response under the instantaneous shock load of thermo-mechanical attack.

The evaluator has dealt at some length on the hazard classification because as Dr Derr's message makes clear, it will dominate this field and should determine the direction of further work. No other paper specifically addressed this relevant subject. The timely initiative of paper No 1 would suggest a specialist conference be planned on this specific subject. It would cover exchange of test results, test methods and the influence of formulatory (chemical and physical) aspects on results. In addition the application of STANAG 4170 laboratory methodology to specifically rocket solid propellants should be covered. The correlation or relevance of these to real thermo-mechanical tests specified in missile requirements and US Military Standards is important. For example the relevance of the sharp and arbitrary sentencing threshold of the card-gap test, which is central to some establishments classification theology. Importantly the now well known influence of motor design aspects to the acceptability, hence classification of propellants under thermo-mechanical attack, should be on the agenda.

There is a danger that advanced, exploratory work of the kind presented by Mr T. Boggs (NWC) in paper No 11 can be prejudiced and influenced by erroneous or imperfect prognostications or tests for the threshold of propellant acceptability. The latter can be influenced by motor design and also by formulatory rheology and methodology of testing.

Paper No 11 by Mr T. Boggs was of particular interest in its approach to finding an alternative filler to RDX or HMX but hopefully of less hazard sensitivity. Using elemental chemistry and molecular orbital calculations for heat of formation, a theoretical compound DNDFP (dinitro difluorazano piperazine) promises increased energy/density compared to the nitramines. This compound does not exist but attempts are currently under way to synthesise it. Following this, sensitivity tests will be undertaken. However, the compound contains a significant amount of the halogen fluorine and hence HF in the plume with consequent secondary smoke. At the conference Dr Roberto (AFRPI) and Dr Mace (Westcott UK) confirmed that their modelling of the boundary conditions reveals HF is essentially the same as HCL from AP in its secondary smoke behaviour. HF will also prevent secondary flame suppression by potassium salts. Accordingly, DNDFP is unlikely to be central to future smokeless propellants. The approach given by Mr T. Boggs may allow exploration of other possible non-halogen alternatives for the nitramines.

Paper No 18 by Mr I. Constantinou describes an interesting technique of flash x-rays of full scale motors to monitor burning rate in erosive burning studies. The publication of the paper will be of interest to rocket designers to assess whether flash x-rays can be used as a diagnostic tool to study motor design performance.

Paper No 10 by Professor De Luca gave an erudite presentation of the development of a combustion model for catalysed double base propellant. However, catalysed double base combustion is a much more complex challenge than modelling composite propellants. For a given double base propellant the addition of various metal salt catalysts markedly changes combustion rate over a wide range e.g. from 3 to 5 mm/s to 30-40 mm/s with accompanying plateau/mesa effects. Basic chemistry studies and understanding of the catalysis mechanism and reactions are needed first. The absence of this will severely constrain the success of a predictive model for the combustion of catalysed double base propellant.

Papers 19 and 21 are pertinent to smokeless propellants in their study of particulate properties. Paper No 19 by Dr Netzer studied particle properties in the grain port and nozzle region. The means used or proposed consisted of high speed cine, light scattering optical properties of the particles, holography and sampling. The paper dealt with aluminium/aluminium oxide particles which are not directly relevant to "minimum smoke" propellants. However, the extension of these techniques and the potential data for acoustic combustion instability additives and condensed phase potassium species in smokeless propellants would be very valuable.

Paper No 21 by Mr Beckstead dealt with "distributed combustion" of particles commonly used in some areas for acoustic instability suppression. The particles studied were aluminium and zirconium carbide. The paper showed that the apparent divergence of experimental data from the particulate damping theory based on Professor Culick's work, is explained by the gas phase burning of these particles. A paper presented at the 53rd PEP Meeting in Oslo described the use of particles chosen to be both refractory and chemically inert in the gas stream. The objective was to obtain the most efficient dampening by tuning the particle size/density function to the acoustic frequency in accordance with Culick's theory. Thus the mass fraction of particles is at the most efficient minimum desirable for low smoke purposes. In addition the size element in the size/density function was adjusted to avoid the peak in the light scattering coefficient of the particulate cloud. Aluminium and zirconium carbide were shown to be not the best material for this purpose.

Mr Beckstead's paper showed aluminium is not a refractory or inert and ZrC is not inert. Therefore, control of particle properties is not possible to correlate with theory or the most efficient dampening. Moreover, as Mr Beckstead showed, the heat of reaction of the burning particles can add to the acoustic gain of the oscillations. This further reduces the efficiency of such particles. For smokeless propellants using the minimum mass fraction of particles, of given size, this paper

reinforces the need to choose particles for refractory and chemical inertness in the combustion chamber.

Proposals for Future Work

The evaluator suggests 5 points for attention:--

- (1) An agreed quantitative and instrumented measure should be agreed, universally applicable in the AGARD community as a definition of smokeless propellants.
- (2) In the field of smokeless propellants, the emphasis should be broadened beyond visible smoke to other wavelengths in signature and transparency, with quantitative, instrumented measures for definition.
- (3) Fundamental studies of burning rate catalysis and platonisation reaction chemistry are required in double base propellants to enable or guide similar effects in other energetic binder smokeless propellants.
- (4) Hazard classification studies need to be increased in priority and collaboration within AGARD. A specialist conference is suggested to cover test results, methods, formulation effects on threshold sensitivity, STANAG 4170 review of test methods and their correlation with real missile thermo-mechanical attack, and the influence of motor design on propellant response.
- (5) Considerable scope for improvement of elastomeric binders in smokeless propellants exists. Such improvements will not only improve the mechanical properties of current smokeless propellants, but more importantly can have a bearing on advances in points 3 and 4 above.

Finally the writer would like to thank all participants and authors for their forbearance and the privilege of commenting on the theme of the many excellent papers. Because of the classified nature of the papers and the AGARD proceedings administrative deadline, the author has not seen copies of the classified papers. The above comments are based on the verbal presentation at the conference. Therefore the evaluator apologises if any important aspects or emphasis has been omitted from any of the papers.

SMOKELESS PROPELLANTS OF
IMPROVED PERFORMANCE

E A Baker
ROYAL ORDNANCE PLC
Research and Development Centre
Sewardstone Road
Waltham Abbey
Essex EN9 1AY
England

For double-base propellants the high density of nitramines compared with nitrocellulose/nitroglycerine matrices of equivalent energy levels is particularly attractive where propellant energy levels or charge volumes are restrictive.

The inclusion of nitramines generally reduced plateau burning rates and impairs plateau quality, but RDX-filled extruded propellants with good plateau ballistics and low temperature dependence, suitable for boost applications have been developed. No departure from conventional EDB processing is involved.

1. INTRODUCTION

1.1 Nitramines, RDX and HMX, are dense, energetic, and chemically stable. They are compatible with nitrocellulose and nitroglycerine and will not increase smoke to any significant extent. These properties make them attractive as additions to existing double-base propellants.

Both in density and calorimetric value RDX offers advantages over the whole range of nitrocellulose/nitroglycerine paste ratios used in typical unfilled UK extruded propellants:

Propellant	NC/NG Ratio	Density (ρ) kg/litre	Calorimetric Value kJ/kg	Product $\rho \times CV$ (units)
(i)	52/48	1641	5500	9025
(ii)	56/44	1643	5360	8805
(iii)	58/42	1644	5290	8700
(iv)	61/39	1645	5180	8521
(v)	65/35	1647	5040	8300
RDX	-	1800	5690	10240

Whilst potential gains appear to be small where nitrocellulose/nitroglycerine ratios are low, useful improvements have been achieved even at these levels by other adjustments to formulations.

1.2 Double base propellants containing up to 20 per cent of an inert solid ingredient, with physical properties suitable for large extruded grains were made in the UK in the 1950's. The propellants could be processed successfully by the standard UK methods, including even speed rolling. Inert loadings up to 30 per cent were processed in small experimental lots. This experience was the basis for the decision to investigate RDX levels of up to 25 per cent. At this loading, improvements of from 10 to 25 per cent in density impulse were predicted.

1.3 The adverse effects of RDX on plateau ballistics using a wider range of ballistic modifiers was accepted at the start of the programme. Thus no efforts were made to achieve the fastest burning rates. Ballistic modifier combinations capable of retaining good plateaux or mesas over a wide range of energies with up to 25 per cent RDX have been identified. Formulations with plateau rates from 3 mm/s to 28 mm/s have been developed and their suitability for conventional production demonstrated. The energy levels and ballistics are suitable for boost, sustain and power cartridge operations.

1.4 Retention of good plateau ballistics in RDX filled propellants to which flash suppression salts have been added has also been achieved. Standard solventless processing is used.

2. CHOICE OF NITRAMINE

Both HMX and RDX are readily available through their use as explosives. Although HMX has the higher density this advantage is partially offset by its slightly lower calorimetric value. Limited work in double-base systems indicated generally similar ballistic behaviour. Since HMX is appreciably more costly, full propellant development has been restricted to RDX.

3. SAFETY

Considerable data from small scale tests exists to indicate that RDX is less friction and impact sensitive than the other major ingredients, nitrocellulose (if dry) and nitroglycerine. Early experiments confirmed that the nitramine can be introduced into the process in water wet form with no adverse impact on propellant properties.

UK processing includes rolling dry paste on even speed rolls and the possibility of a violent incident, rather than a fire, at this stage was considered to be the major risk. Experiments demonstrated that the depth of RDX filled (25%) paste necessary for 'detonation' comfortably exceeded that likely to occur in propellant processing and also that required for an unfilled formulation of similar energy which has been in regular production for many years. Rolling machines are already equipped with fast acting drenching units and no additional precautions are considered necessary for current nitramine levels. There is no evidence of an increased incident of fires at the rolling stage or in machining.

4. FORMULATION STUDIES

4.1 Boost Propellants

4.1.1 Initial studies were designed to produce propellants burning between 20 and 30 mm/s suitable for boost motor applications. Two ballistic modifier combinations known to give plateau burning rates in excess of 25 mm/s were selected for study. The first, a mixture of lead and copper compounds yielded a range of useful propellants with plateau rates of about 30 mm/s. Control of burning rate levels is achieved by adjustment of carbon black loadings. Properties of a typical composition are shown in Figure 1 (EB1).

4.1.2 The second combination of modifiers has given plateau burning rates at 22 mm/s or less over a wide range of energy levels. Burning rates can be controlled by simple adjustment to the ratio of the two modifiers. Properties of two formulations, are summarised in Figure 1 (EB2) and Figure 2 (EB3).

With EB2 increases of 9-10 per cent in impulse have been confirmed in large diameter boost motors with retention of low temperature coefficients. Burning rates can be tailored to deliver the additional energy over longer burning times, permitting mid-term improvements with minimum impact on other design aspects.

Burning rate curves for EB3 illustrate the very extended plateau pressure ranges associated with nitramine filled propellants using this combination of ballistic modifiers. The formulation can contain up to 2 per cent of a flash suppression salt with no impairment of plateau ballistic yielding low temperature coefficients (mp/r) over a wide pressure range. Low temperature dependence has been confirmed in motor firings with up to 10 second burn times.

4.2 Slow Burning Propellants

Plateau burning rates of less than 5 mm/s at energy levels required for sustain applications are difficult to achieve in unfilled compositions. A careful study of matrix (unmodified) propellant burning rates indicated that some advantages could be gained by inclusion of RDX. In these studies nitramine is used to achieve slower burning rates rather than to enhance energy output. A ballistic modifier combination tolerant of RDX addition has been identified. Properties of a typical formulation in this series are summarised in Figure 2 (EB4). Plateau burning rates down to 3 mm/s have been demonstrated in small experimental lots.

5. GENERAL PROPELLANT PROPERTIES

Ballistic modifier systems chosen for use in nitramine propellants are well established by use in unfilled propellant motors in service. Trials at elevated temperatures up to 80 °C confirm that the ballistic and chemical stability of the nitramine filled propellants are as good as equivalent unfilled formulations.

No unusual problems have been encountered in bonding inhibitors, including ethyl cellulose, to nitramine propellants. Inhibited charges have been successfully fired after temperature cycling.

The introduction of nitramine is in most cases accompanied by changes in nitrocellulose/plasticiser ratio. Thus the physical properties, including tensile strength and elongation are very similar to those of the range of existing UK unfilled propellants.

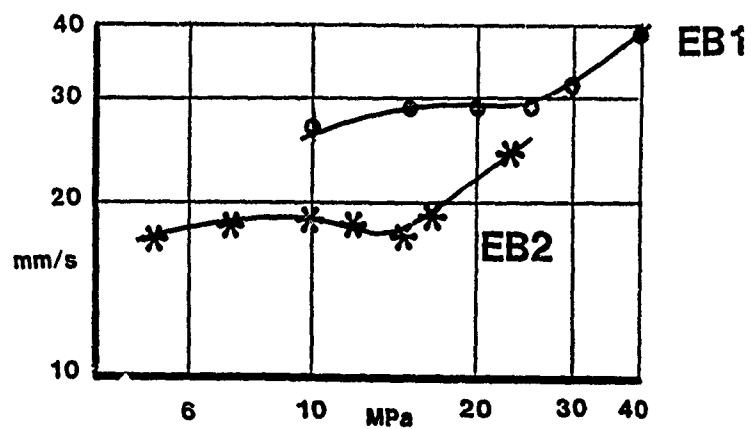
Motors have been fired successfully after cycled temperature storage and vibration tests.

6. CONCLUSIONS

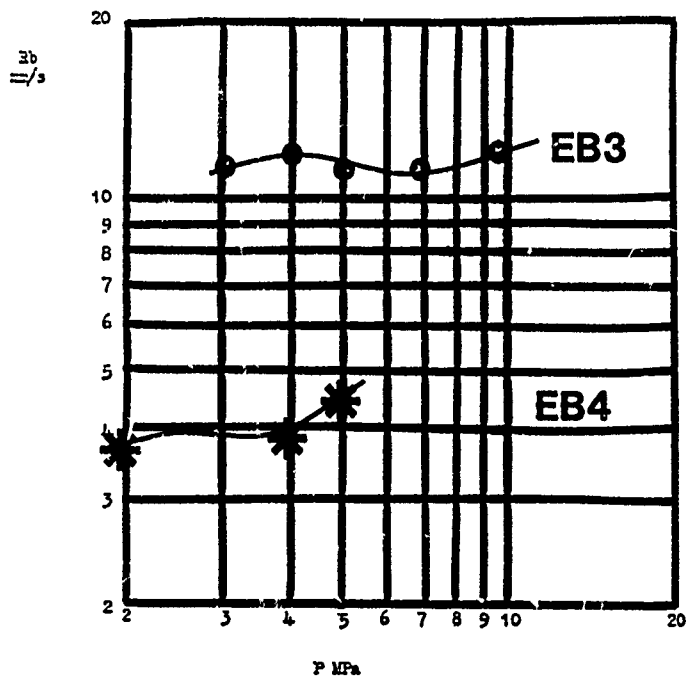
Improvements in performance (density x impulse) can be achieved in extruded double-base propellants by addition of nitramines. Ballistic modifier combinations which permit retention of good plateau ballistics over the burning rate range (3-30 mm/s) have been identified.

The propellants can be safely processed using standard UK manufacturing techniques.

	EB2	EB1
Calorimetric Value (kJ/kg)	5219	5200
C*	1514	1500
S.I. (Ns/Kg)	2437	2400
Density (Kg/litre)	1712	1685
Chamber Flame Temperature (°K)	3130	3100
Temperature Coefficient /°K (% per °C)	<0.1	<0.15



	EB3	EB4
Calorimetric Value (kJ/kg)	4300	4120
C*	1460	1440
S.I. (Ns/Kg)	2308	2280
Density (Kg/litre)	1661	1620
Chamber Flame Temperature (°K)	2738	-
Temperature Coefficient /°K (% per °C)	<0.15	<0.25



DISCUSSION**C.Brongniart, FR**

You described the critical height of the RDX propellant as higher than that of the non-RDX propellant. Critical height is a concept normally applied to granular, powder propellant. Can you describe what you mean in your context?

Author's Reply

In this context, by critical height is meant the minimum depth of propellant paste at which an ignition will lead to burning to detonation. The tests showed that the paste in question, with 25% RDX, had a critical height or depth greater than would occur in practice in this rolling process.

COMBUSTION DES PROPERGOLS A BASE D'OCTOGENE*

par Guy LENGELLÉ et Jean DUTERQUE

Office National d'Etudes et de Recherches Aérospatiales
29, avenue de la Division Leclerc
92320 CHATILLON (France)Résumé

L'étude de la combustion des propergols solides à base d'octogène et de liant "énergétique" a porté sur l'investigation de l'octogène et du liant en combustion autonome et de leur combinaison en propergols.

- Le comportement en phase condensée des composants a été étudié au moyen d'essais d'allumage, de thermogravimétrie, d'analyse thermique différentielle et par des relevés de profils de température (microthermocouples), complétés par une analyse des gaz issus de la phase condensée. On en déduit, en particulier pour l'octogène, la loi de pyrolyse V_c (T_{surface}) et l'énergie dégagée à la surface.
- A très basse pression, l'octogène donne lieu à une flamme étagée similaire à celle des propergols homogènes. Au-delà d'environ 10 bars, les réactions se confondent en une flamme unique prémélangée. En conséquence, la loi V_c (p) est quasi-linéaire.
- Le comportement du liant est proche de celui des propergols homogènes (flamme étagée et forte sensibilité de la vitesse de combustion à la pression). Les combinaisons d'additifs, efficaces pour les propergols homogènes, ont cependant des effets moins importants. La trame carbonée de la surface est aussi moins importante.
- La vitesse de combustion du propergol est une pondération des vitesses de chaque constituant, sans interaction entre la flamme de l'octogène et celle du liant (ainsi, la granulométrie de l'octogène est sans influence). Les effets de survitesse sont faibles et sans grande possibilité de modulation. L'introduction de faibles quantités de perchlorate d'ammonium permet cette modulation par la présence de flammes d'interaction P.A.-liant. L'action est en conséquence liée à la granulométrie du P.A.

Summary

The investigation of the combustion of solid propellants based on H.M.X. and an "energetic" binder has been carried out through the study of H.M.X. and the energetic binder in self-burning, as well as that of their combination in propellants.

- The condensed phase behavior of the components has been looked into by means of thermogravimetric analysis, differential scanning calorimetry, ignition and temperature (microthermocouples) profile measurements, as well as sampling and analysis of the gases produced from the condensed phase. In particular for H.M.X., the r_b (T_s) law and the energy evolved at the surface can be deduced.
- At very low pressure, H.M.X. sustains a staged flame, much like that of homogeneous propellants. Above about 10 atm., the reactions merge into a single premixed flame. The r_b (p) law thus becomes nearly linear.
- The behavior of the binder is close to that of homogeneous propellants (staged flame and high sensitivity of the burning rate to pressure). Additives, known to be efficient in homogeneous propellants, are however less active. The carbon residue on the surface is also less abundant.
- The burning rate of the propellant is a compromise between the rates of the components, without interaction between the H.M.X. flame and that of the binder (thus the H.M.X. particle size has no influence). The super-rate effects are moderate and without much possibility of modulation. The introduction of small quantities of ammonium perchlorate allows such a modulation due to the A.P.-binder interaction flames. The activity of the A.P. is then related to its particle size.

* Travaux menés sous contrat de la Direction des Recherches, Etudes et Techniques (DRET), de la Délégation Générale à l'Armement (DGA), et en étroite collaboration avec la Société Nationale des Poudres et Explosifs (SNPE) et l'Ecole Nationale Supérieure des Techniques Avancées (ENSTA).

1 - INTRODUCTION

Les propergols solides font l'objet d'une évolution rapide liée à la nécessité de satisfaire des caractéristiques recherchées. Dans le domaine des engins tactiques, l'absence de fumées en est une. La figure 1 résume les qualités des différents types de propergols existants ou en cours de développement.

Les propergols homogènes à base de nitrocellulose et de nitroglycérine sont sans fumées, mais possèdent des qualités énergétiques limitées.

Les propergols composites perchlorate d'ammonium (P.A.)-liant combustible (le polybutadiène par exemple), plus énergétiques, produisent des fumées secondaires (par condensation de gouttelettes de H₂O et HCl). En présence d'aluminium, producteur de fumées primaires, ils sont réservés aux applications (lanceurs, missiles stratégiques, certains étages de missiles tactiques) pour lesquelles l'absence de discrétion importe peu.

Les propergols composites à base d'octogène et de liant énergétique, objets de cet exposé, conservent la qualité sans fumées tout en permettant d'atteindre des performances élevées. Leur utilisation en présence d'aluminium est réservée aux engins stratégiques avancés.

La présentation qui suit fait le bilan des activités menées à l'ONERA sur le comportement des composants en combustion autonome et de leur combinaison en propergols. Le texte principal présente les résultats et conclusions obtenus, les annexes donnent certains détails complémentaires.

1 - Propergols homogènes (double - base)
$i_0 \leq 220s$, sans fumées
2 - Propergols perchlorate d'ammonium-liant combustible
$i_0 \leq 242s$, fumées secondaires avec aluminium
$i_0 \leq 265s$, fumées primaires
3 - Propergols octogène - liant énergétique
$i_0 \leq 256s$, sans fumées avec aluminium
$i_0 \leq 273s$, fumées primaires

Fig. 1 - Différents propergols solides.

* i_0 théorique pour une détente 70/1 à l'équilibre

Sources: AIR et COSMOS n° 1000 - 1984
GIFAS n° 1288 - 1981

2 - COMBUSTION AUTONOME DE L'OCTOGENE

Le comportement en combustion autonome de l'octogène, dont la composition en éléments oxydants et réducteurs est équilibrée et permet d'atteindre une température d'environ 3280 K, est caractérisé par les données relatives d'une part à la dégradation en phase condensée et d'autre part à la structure de flamme.

2.1 - Dégradation en phase condensée

La cinétique de la dégradation de l'octogène peut être déterminée par des essais d'analyse enthalpique différentielle (A.E.D.) ou de thermogravimétrie. De nombreuses études ont été réalisées et se trouvent dans la bibliographie, voir le tableau 1 pour quelques exemples. BOGGS [5], dans un exposé de synthèse, donne une liste plus complète. La figure 2 rassemble les résultats obtenus en A.E.D. au voisinage de la fusion-décomposition de l'octogène. En supposant un ordre de réaction de 1 vis-à-vis de l'octogène restant on obtient les caractéristiques cinétiques indiquées.

Une autre méthode qui permet de déterminer la cinétique de décomposition est celle de l'allumage par exposition à un flux de chaleur, le délai détecté étant celui de la première manifestation de réactions exothermiques. La figure 3 indique les résultats obtenus. La corrélation de ces résultats, en attribuant la première réaction exothermique à la décomposition en phase condensée, conduit aux valeurs indiquées, c'est-à-dire à une confirmation de la cinétique obtenue à partir des analyses en A.E.D.

L'étude du comportement en phase condensée est complétée par le relevé en cours de combustion des profils de température à l'aide de microthermocouples. On sait que l'épaisseur de propagation du profil de température dans un matériau en régression est donnée (conventionnellement) par :

$$e = 4 \lambda_{10} \sqrt{p / V_{\text{régression}}}$$

soit pour une vitesse de 1 à 10 mm/s e de 250 à 25 μm . Il est donc nécessaire d'utiliser des thermocouples aussi fins que possible. Ceux-ci sont réalisés à partir de fils de 2,5 μm ou 5 μm , soudés bout à bout par décharge électrique, de telle façon que la jonction est pratiquement de la taille des fils. Le thermocouple est ensuite pris entre deux plaquettes d'échantillon, toutes les manipulations étant faites sous microscope avec déplacements microniques, figure 4. Un exemple de relevé est indiqué sur cette figure.

A partir de ces relevés il est possible d'obtenir une estimation de la température de surface (indiquée en général par une rupture de pente perceptible) et de l'énergie dégagée, correspondant à la transformation matériau solide \rightarrow gaz de dégradation, par le bilan :

$$\lambda \left. \frac{dT}{dx} \right|_{x=0} = \dot{m} [\bar{c}_p (T_s - T_0) - Q_s]$$

Le gradient à la surface est relevé sur les profils de température et la conductivité des gaz est estimée en fonction de la composition mesurée des espèces issues de la surface, évoquée par la suite. Les résultats obtenus pour Q_s sont donnés sur la figure 5. Le bilan de la transformation de l'octogène en gaz est exothermique, l'énergie absorbée par la dégradation des liaisons moléculaires étant vraisemblablement plus que compensée par l'énergie dégagée par le début des réactions de recombinaison entre gaz oxydants, NO_2 , N_2O , et réducteurs, HCHO , HCN , dans la zone superficielle du matériau.

L'évolution vitesse de régression-température de surface de l'octogène est reportée sur la figure 6. On y trouve d'une part les températures de surface mesurées par microthermocouples et d'autre part la loi de pyrolyse $v_c(T_s)$ évaluée en tenant compte de la cinétique de décomposition déterminée précédemment. On voit que, si l'on tient compte de l'incertitude (traduite par une dispersion sur T_s d'environ 50 K) liée à la mesure des températures de surface, il y a continuité entre le mécanisme de dégradation (phénomène thermique irréversible de rupture des liaisons moléculaires, sans participation importante, selon toute vraisemblance, d'évaporation de l'octogène et donc sans influence de la pression) observé en A.E.D., à partir de $\approx 240^\circ\text{C}$, en allumage, aux environs de 350°C , et en combustion autonome pour des températures superficielles de 500 à 650°C . Cette conclusion sur la continuité du mécanisme de dégradation avait également été obtenue dans le cas des propergols homogènes nitrocellulose-nitroglycérine [6].

Le prélèvement et l'analyse des gaz par spectrométrie de masse en l'absence de réactions en phase gazeuse (la régression du matériau sous vide étant entretenue par apport de chaleur extérieur, par contact sur une plaquette chauffée par courant électrique) permet une détermination quantitative des gaz résultant de la dégradation en phase condensée. Cette étude fait l'objet d'une présentation parallèle [7]. Les résultats obtenus sont résumés sur la figure 7. On y voit que la dégradation produit en quantités voisines (en masse) les gaz oxydants NO_2 , NO et N_2O , résultant de la décomposition initiale de la molécule d'octogène avec, dans le cas de NO , un début de recombinaison dans la phase condensée, et les gaz réducteurs HCHO et HCN . Les autres gaz, mineurs, N_2 , CO_2 , CO , H_2O , sont le résultat du début de la réaction de combustion dès la phase condensée. Leur présence est en accord avec l'exothermicité globale de la transformation solide \rightarrow gaz de l'octogène.

TABLEAU 1

Etudes de la décomposition de l'octogène

("T fusion" $\approx 275^\circ\text{C}$)

Auteurs	Gamme de température ($^\circ\text{C}$)	E_c (kcal/mole)	A_c (s^{-1})
SINCLAIR et HONDEE [1]	> 241	52,7	--
SURYANARAYANA [2]	> 268	52	--
ROGERS [3]	270-285	51,3	$6,4 \cdot 10^{18}$
ROBERTSON [4]	271-314	52,7	$5 \cdot 10^{19}$
ONERA (A.E.D.)	240-280	50 (209 kJ/mole)	$0,7 \text{ à } 1,6 \cdot 10^{17}$
ONERA (Allumage)	≈ 350	50	$1,1 \cdot 10^{17}$

TABLEAU 2

Valeurs considérées comme représentatives de l'octogène

$$\bar{c}_p = \bar{c}_g = 0,35 \text{ cal/g K.}$$

$$\rho_p = 1,9 \text{ g/cm}^3.$$

$$d_p = \lambda_p / \rho_p \bar{c}_p = 1 \text{ à } 1,2 \cdot 10^{-3} \text{ cm}^2/\text{s, diffusivité thermique.}$$

$$\lambda_p = 7,3 \cdot 10^{-4} \text{ cal/cm s K.}$$

$E_c = 50 \text{ kcal/mole}$, $A_c = 0,7 \text{ à } 1,6 \cdot 10^{17} \text{ s}^{-1}$, cinétique de la décomposition en phase condensée.

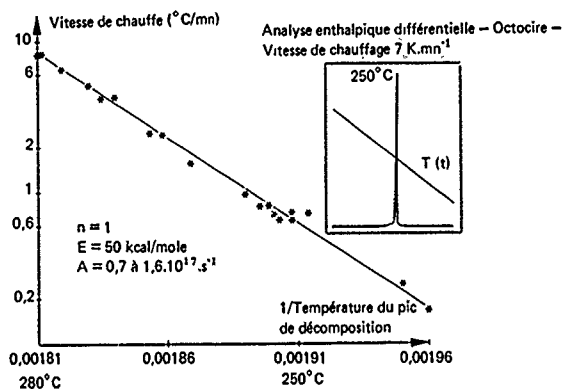
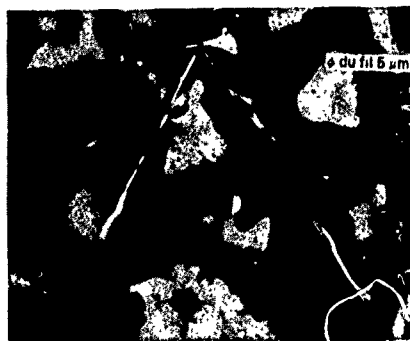
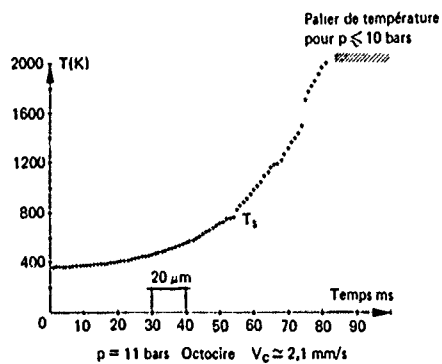
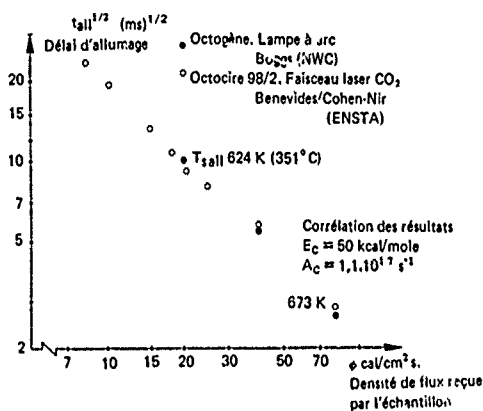


Fig. 2 - Décomposition thermique en A.E.D.

Fig. 3 - Loi d'allumage de l'octogène.



Thermocouple Pt - Pt/Rh collé sur l'échantillon

Fig. 4 - Relevé des profils de température par microthermocouples.

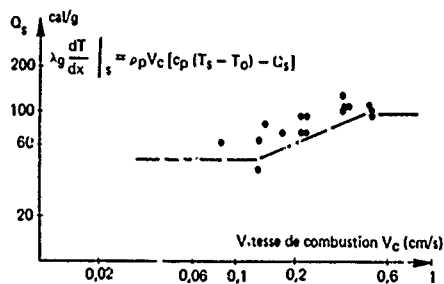


Fig. 5 - Chaleur dégagée par la décomposition de l'octogène.

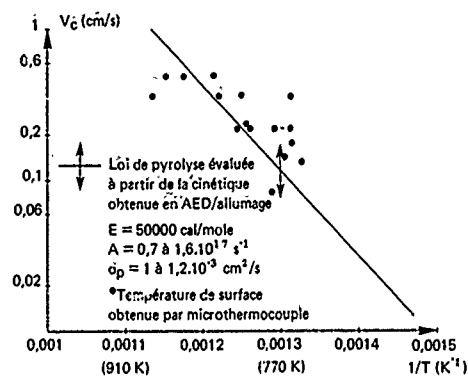
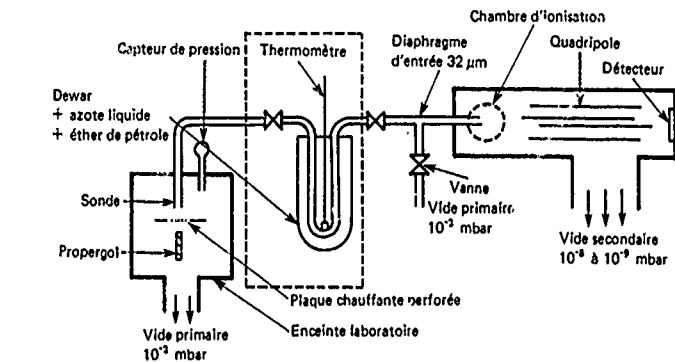


Fig. 6 - Pyrolyse en phase condensée de l'octogène



Composés	NO ₂	NO	N ₂ O	N ₂	CO ₂	CO	H ₂ O	H ₂	HCOOH	HCHO	HCN	NH ₃
% Masse	22,2	17,5	19,1	3	1,4	1,6	3,7	0,07	0,2	14,1	16,8	0,3
	59%						31%					

BILAN MASSIQUE	C	H	O	N
Octogène de départ	16,2	2,7	43,2	37,8
Gaz de dégradation	14,2	2,1	44,8	39

Fig. 7 - Analyse des gaz de pyrolyse de l'octogène.

2.2 - Réactions en phase gazeuse

La production dans la phase condensée de plusieurs gaz oxydants, NO₂, N₂O et NO, peut conduire à la création d'une flamme étagée. C'est ce qui est observé dans le cas bien connu des propergols homogènes [6, 7] pour lesquels NO₂ et NO sont produits et donnent lieu respectivement à une flamme primaire NO₂-aldéhydes et à une flamme secondaire NO-CO, qui sont nettement séparées en dessous de ≈ 50 bars et qui se confondent au-delà de ≈ 200 bars. L'observation de la combustion de l'octogène à basse pression ≤ 10 bars montre la présence d'une zone sombre d'induction et d'une flamme lumineuse détachée de la surface, très semblables à celle des propergols homogènes. Cette observation a également été faite par KUBOTA [8], dans le cas de compositions octogène-liant combustible (la présence de ce dernier refroidissant la combustion de l'octogène et éloignant la flamme secondaire). Par ailleurs, le relevé des profils de température par microthermocouples révèle l'existence pour les pressions ≤ 10 bars d'un palier de température aux environs de 2000 K, avant l'amorce de la flamme qui permet d'atteindre la température de fin de combustion de 3280 K.

La vitesse de combustion de l'octogène, sous forme de cristaux uniques ou d'échantillons concrétés, a été déterminée par BOGGS [9] (quelques points de recoupement ont été obtenus à l'ONERA sur échantillons concrétés), figure 8. Une composition proche d'octocire, à 98 % d'octogène et 2 % de cire servant de liant, donne lieu à une évolution parallèle (le décalage en niveau étant lié au refroidissement apporté par le liant). L'évolution de la vitesse de combustion avec la pression montre l'atteinte dès environ 10 bars d'un régime unique, caractérisé par un exposant de pression élevé ($n \approx 0,85$ à 0,9 dans une loi $V_c \sim P^n$). Cette évolution est révélatrice du fait que, lorsque la pression augmente, rapidement la flamme finale vient se rapprocher de la surface et que la vitesse de combustion de l'octogène

est alors sous l'influence d'une réaction globale, impliquant les différents oxydes d'azote, d'un ordre proche de 2. La schématisation de ces phénomènes, réalisée par le couplage de la description d'une zone de flamme prémélangée avec celle de la phase condensée, par une réaction globale d'ordre 1 (caractéristique de la réaction de NO_2 [6]) à $p \lesssim 30$ bars et d'ordre 2 à $p > 30$ bars permet de rendre compte de l'évolution de la vitesse de combustion avec la pression.

L'introduction d'un sel de plomb dans des échantillons d'octogène concrété, figure 9, fait apparaître une première zone de survitesse qui se termine à ≈ 20 bars. Cette action est à rapprocher de celle observée sur les propergols homogènes [6], pour lesquels il a été établi que la présence du sel de plomb renforce les résidus de carbone à la surface et favorise le rapprochement des réactions impliquant NO . Dans le cas des propergols homogènes cette première survitesse peut être prolongée jusqu'à $\approx 200-300$ bars et son amplitude peut être modulée par le choix des additifs. Dans le cas de l'octogène, la flamme secondaire venant se plaquer à la surface vers 20-30 bars, une extension de la survitesse au-delà est exclue, selon toute vraisemblance. Une deuxième survitesse apparaît au-delà de 200 bars, de même que pour les propergols homogènes [6], pour lesquels cette action avait été attribuée à un effet d'accroche-flamme des résidus de PbO que l'on observe à la surface du propergol.

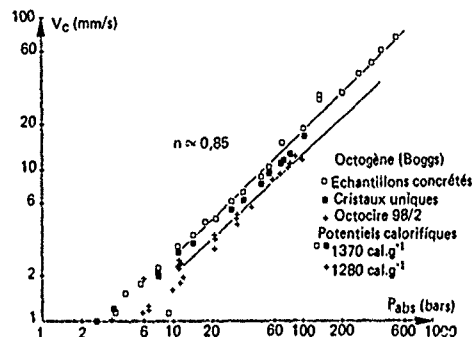
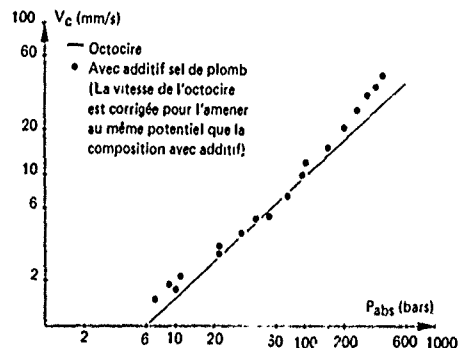


Fig. 9 - Octocire avec additif au plomb

Fig. 8 - Vitesse de combustion de l'octogène et de l'octocire.



3 - COMBUSTION AUTONOME DU LIANT

Les liants "énergétiques" sont constitués par un polymère (polyester ou polyéther) contenant 70 % de nitroglycérine. La nature des liaisons polymère-nitroglycérine n'est pas clairement établie ; il semble qu'elles soient de type Van Der Waals (assez faibles). Il a été supposé, a priori, que le comportement en combustion des deux liants étudiés devait être assez voisin. En réalité, on a constaté des différences assez marquées tant sur le plan de la vitesse de combustion (figure 17) que sur celui de la structure des résidus de combustion.

On a tout d'abord utilisé les mêmes techniques d'étude (A.S.D., thermogravimétrie) que dans le chapitre précédent. Toutefois l'expérience a montré que l'appareillage utilisé n'était pas adapté à ce type de matériaux. L'étude thermogravimétrique du liant 2 (figure 10) montre que, même au maximum de la vitesse de chauffage de notre appareillage ($9 \text{ K} \cdot \text{mn}^{-1}$), toute la nitroglycérine présente initialement (70 %) disparaît par évaporation à une température inférieure à 210°C . Il n'est donc pas possible d'obtenir une cinétique de dégradation par cette méthode. Les mesures de température de surface (par incorporation de microthermocouples dans l'échantillon) sont actuellement en cours de réalisation.

Un autre point étudié, relatif à la phase condensée, concerne les résidus de combustion. En effet, pour les propergols homogènes à basse pression (< 200 bars), on considère que le niveau de vitesse est lié au potentiel et à la présence d'une trame carbonée à la surface. Il a donc semblé intéressant de vérifier si la teneur et la texture des résidus différaient d'un liant à l'autre. On a mesuré la quantité de résidus obtenue par des essais de combustion sous pression modérée (en l'absence de flamme secondaire pour éviter une consommation du carbone). A 10 bars on recueille environ 0,6 % pour les SD (le terme SD qualifie un propergol homogène préparé sans solvant) et les liants 2 et ≈ 1 % pour le liant 1. Pour les SD, l'allure des résidus reste la même, quelle que soit la pression. Pour les liants nitrés, à basse pression, on recueille un magma pâteux qui se structure progressivement lorsque la pression augmente : dès 4 bars pour le liant 2, vers 10 bars pour le liant 1. Sur la figure 11, on compare les résidus obtenus à 10 bars. Pour le propergol SD on observe une trame très fine et très dense. Une allure semblable est observée avec le liant 2, la trame est toutefois moins dense. Dans le cas du liant 1 la trame est presque inexistante.

On conçoit donc bien que, si le niveau de vitesse dépend de la présence de cette trame, il sera plus élevé pour les SD et pour le liant 2 que pour le liant 1 (fig. 12). Sur cette figure on a reporté les vitesses de combustion d'un propergol SD, du liant 1 et du liant 2, les trois compositions ayant un potentiel voisin (≈ 830 cal/g). On note que si la SD et le liant 2 ont une loi de vitesse pratiquement identique, le liant 1 présente une vitesse plus faible à partir de 30 bars.

Des additifs balistiques identiques à ceux utilisés avec les propergols homogènes ont été incorporés dans le liant 1. On observe (fig. 13) un effet de survitesse assez net (p entre 20 et 500 bars), mais incontestablement moins important que celui obtenu avec un propergol SD de potentiel voisin (courbe en pointillé):

Il est connu depuis les travaux d'AVERY [10] que l'introduction d'un sel de plomb dans les propergols homogènes modifie (pour un certain domaine de pression) la loi $v_c(p)$. Dans cette gamme de pression l'indice n augmente puis s'annule (effet plateau) ou même devient négatif (effet mesa). Au-delà de cette zone (en général < 200 bars) les deux lois sont à nouveau confondues. On peut noter que l'importance relative de l'effet de survitesse est d'autant plus marqué que le potentiel est moins élevé. L'addition de noir acétylène a pour effet d'accentuer le phénomène.

Le mécanisme proposé pour la première survitesse est lié à la présence d'une trame carbonée à la surface du propergol. Cette trame provient de réactions entre aldéhydes (issus de la phase condensée, en quantités d'autant plus importantes que le propergol est riche en nitrocellulose) et le résidu des sels de plomb. Cette trame a pour effet d'augmenter les réactions entre NO et carbone et, dans le cas où le résidu carboné est très important, de servir d'accroche flamme pour la flamme secondaire. Si l'on envisage un mécanisme analogue avec les liants énergétiques, l'intensité de la survitesse sera liée à l'aptitude de la partie polymère du liant à fournir au cours de sa dégradation du carbone, et éventuellement des aldéhydes susceptibles de réagir avec les sels de plomb. Dans l'immédiat on ne dispose pas d'analyses des produits de la dégradation en phase condensée du liant. Toutefois l'examen de la surface d'échantillons, éteints brutalement par une dépressurisation rapide et examinés au microscope électronique à balayage, montre clairement la présence de la trame carbonée pendant la survitesse, beaucoup plus importante pour le propergol SD que pour le liant 1 (fig. 14), ce qui est cohérent avec les résultats de la figure 13.

Les compositions à liant du deuxième type avec additifs n'ont pas encore été réalisées, mais compte tenu des observations précédentes (allure des résidus, lois de vitesse) on s'attend à ce que les additifs engendrent une survitesse voisine de celle obtenue avec le propergol SD.

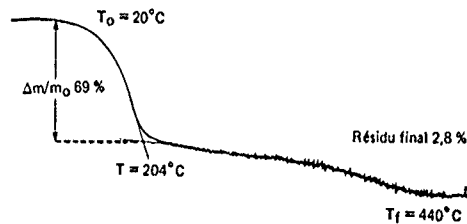


Fig. 10 - Thermogramme du liant 2 - Vitesse de chauffe $9^\circ\text{C}\cdot\text{mn}^{-1}$.

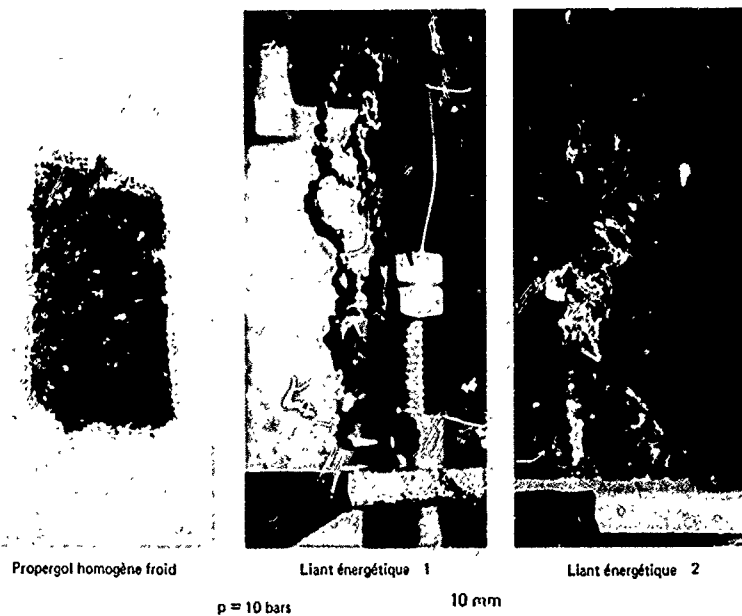


Fig. 11 - Résidus de combustion.

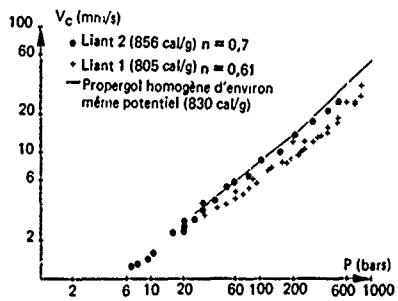
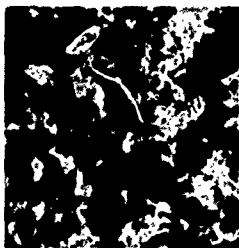
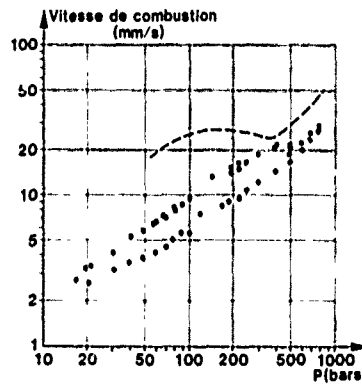
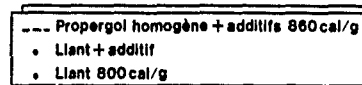
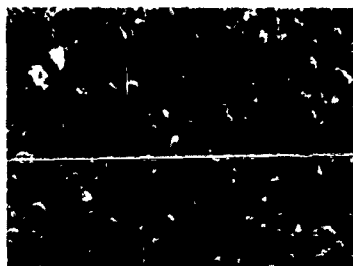


Fig 12 - Vitesse de combustion des liants nitrés.

Fig. 13 - Influence d'un catalyseur de type homogène sur le liant énergétique 1.



Propergol homogène
 Procédé sans solvant
 $p = 130$ bars



Liant énergétique 1
 $p = 100$ bars

Avec additifs spécifiques des propergols homogènes

Fig 14 - Structures de surface en combustion des liants

4 - COMBUSTION DES COMPOSITIONS OCTOGÈNE-LIANT

L'introduction d'octogène à un taux de 70 % dans le liant sans additif a un effet différent suivant la gamme de pression considérée (fig. 15). Aux basses pressions (<100 bars), la loi de vitesse est pratiquement confondue avec celle du liant. Aux pressions supérieures à 100 bars, la loi de vitesse se modifie : l'exposant de pression tend vers celui de l'octogène.

En présence d'additifs l'effet de survitesse obtenu est faible et disparaît vers 150 bars, c'est-à-dire lorsque la vitesse de régression est pilotée par l'octogène (fig. 16).

La difficulté d'obtention d'effets de survitesse significatifs, permettant par l'introduction d'additifs de moduler à la fois le niveau de vitesse et l'exposant de pression, peut conduire à introduire dans le propergol du perchlorate d'ammonium. La figure 17 est relative au liant seul dans lequel on incorpore 30 % de perchlorate d'ammonium à deux granulométries différentes (9 et 90 μm) :

- a pression donnée, le niveau de vitesse est d'autant plus important que la granulométrie est fine ;
- pour une granulométrie donnée l'exposant de pression est constant jusque 300 bars et d'autant plus faible que la granulométrie est fine. Au-delà de 300 bars les deux courbes sont confondues.

L'interprétation de ces résultats découle des considérations suivantes :

La combustion autonome du P.A. est caractérisée par la loi de pyrolyse de la figure 18, tenant compte des mesures les plus convaincantes, qui traduit une réaction exothermique productrice de O_2 importante (probablement 70 % du P.A.) dans la zone liquide superficielle, et par la cinétique $\text{NH}_3\text{-HClO}_4$ (portant sur les 30 % restant du P.A. sublimé) indiquée. La modélisation de cette combustion [11, 12], proche de celle de GUIRAO et WILLIAMS [13] mais plus simplifiée, permet de bien rendre compte des mesures (en particulier sur cristaux uniques de P.A.) de BOGGS, voir [9], ainsi que de l'évolution de la pression limite de combustion en fonction de la température initiale (20 bars à +25°C). L'introduction d'une faible quantité de P.A. permet de moduler le niveau de vitesse d'une composition à liant énergétique.

L'oxygène excédentaire de la flamme du P.A. réagit avec les gaz de flamme primaire du liant, voir figure 19, créant des flammes de diffusion d'autant plus efficaces sur le niveau de vitesse de combustion que la taille des particules de P.A. est faible.

Si on ajoute de l'octogène à la composition, en conservant constant le taux de perchlorate par rapport au liant plus perchlorate, on constate (fig. 20) une diminution des effets du perchlorate d'ammonium. Le niveau de vitesse est abaissé et l'exposant de pression passe de 0,5 à 0,7. La rupture de pente qui se produit vers 150-200 bars sans octogène s'effectue en sa présence à une pression inférieure à 100 bars. Dans la mesure où il s'avère difficile de créer des effets de survitesse suivis de plateaux avec niveaux de vitesse de combustion plus ou moins ajustables, comme dans le cas des propergols homogènes, l'utilisation d'une faible quantité de P.A. peut être une solution de repli, la discrétion des produits étant cependant légèrement affectée et l'atteinte de zones de plateaux à exposant de pression quasi nul n'étant pas réalisée.

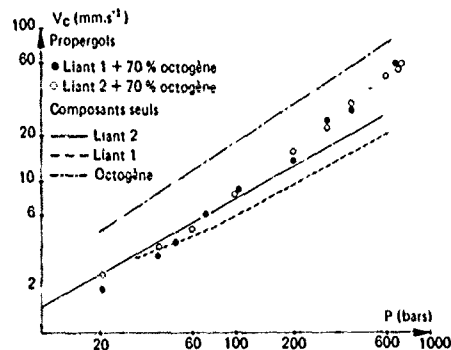
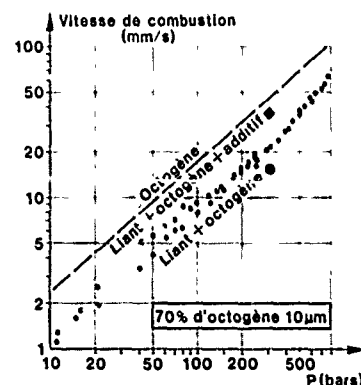
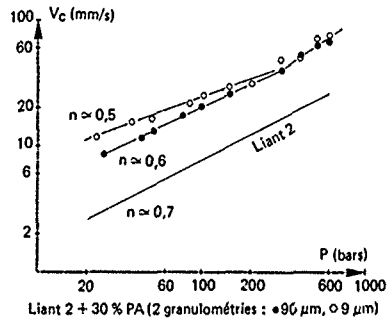


Fig 15 - Vitesses de combustion des compositions octogène - liant nitré

Fig 16 Influence d'un catalyseur de type homogène sur le propergol octogène-liant énergétique 1.





Liant 2 + 30 % PA (2 granulométries : \bullet 90 μ m, \circ 9 μ m)

Fig. 17 - Influence de la granulométrie du perchlorate d'ammonium sur la vitesse de combustion du liant.

Fig. 18 - Combustion autonome du perchlorate d'ammonium.

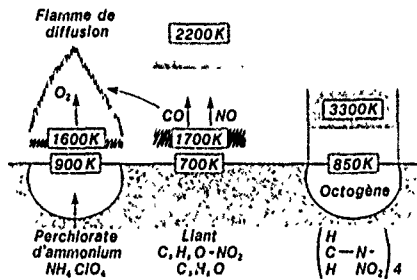


Fig. 20 - Influence de l'octogène à taux liant/P.A. constant.

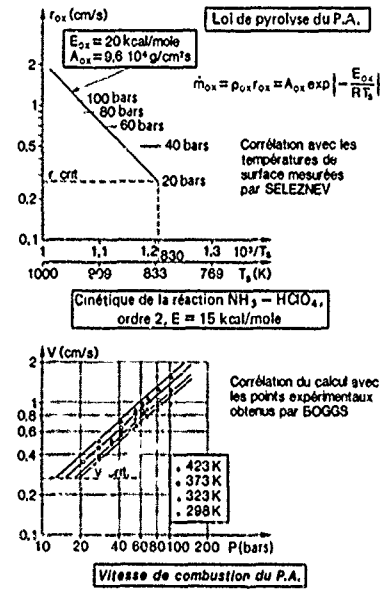
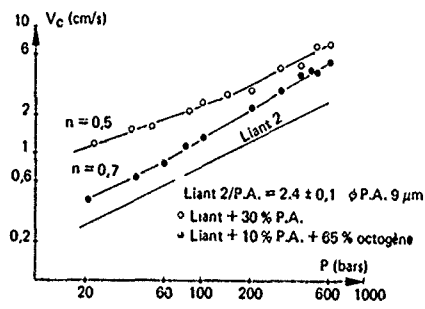


Fig. 19 - Combustion des compositions perchlorate d'ammonium-octogène-liant énergétique.



5 - CONCLUSIONS

L'étude de la combustion des composants seuls et des propergols à base d'octogène et de liant énergétique a permis d'établir un certain nombre de conclusions.

Le comportement en phase condensée de l'octogène, caractérisé par la cinétique de dégradation (déterminée par analyse enthalpique différentielle ou par allumage), l'énergie mise en jeu dans la transformation du solide en gaz, la loi de pyrolyse (relation vitesse de combustion-température de surface) et la nature des gaz, est maintenant assez bien connu.

La zone de flamme de l'octogène est comparable à basse pression à celle des propergols homogènes ; en effet on observe la présence de flammes primaire et lumineuse séparées ; cependant dès environ 10 bars les réactions se confondent en une seule flamme et la vitesse de combustion devient très sensible à la pression. Les additifs des propergols homogènes, un sel de plomb par exemple, n'ont une action qu'à très basse pression.

Les liants énergétiques (mélanges de nitroglycérine et d'un polymère) ont un comportement en combustion voisin de celui des propergols homogènes. Suivant la nature du polymère ils produisent une quantité plus ou moins importante de résidus de carbone. La présence de ce carbone intervient sur les réactions proches de la surface et donc sur l'évolution de la vitesse de combustion avec la pression. Par ailleurs, dans le cas des propergols homogènes, en présence d'additifs, ces résidus sont accrus et permettent un rapprochement de la flamme secondaire vers la surface et par là un effet de survitesse suivi d'effet de plateau. Cet effet est observé de manière modérée dans le cas des liants polyesters peu producteurs de carbone. Les liants polyéthers, de comportement plus proche des propergols homogènes, devraient être plus favorables aux effets de survitesse et de plateau ; ceci reste à être vérifié.

Les propergols à base d'octogène et de liant énergétique présentent une vitesse de combustion qui est un compromis entre les vitesses de chacun des composants. L'absence d'influence de la granulométrie de l'octogène confirme qu'octogène et liant brûlent côte à côte sans interaction. L'effet des additifs spécifiques des propergols homogènes, déjà modéré dans le liant seul, est faible dans le cas des compositions avec octogène. Dans un premier temps, un moyen permettant de moduler le niveau de vitesse et de réduire la sensibilité à la pression de la vitesse de combustion de ces propergols peut être l'introduction de faibles quantités de perchlorate d'ammonium. L'oxygène excédentaire de la combustion du P.A. réagit dans des flammes de diffusion avec les gaz de la flamme primaire du liant. En conséquence, il est possible d'obtenir une modulation des effets de l'addition de P.A. par le choix de sa granulométrie et de son taux de charge. L'introduction du P.A. n'est cependant pas favorable du point de vue de la discrétion des produits émis. Il reste donc à poursuivre l'étude des possibilités de créer, par l'emploi d'additifs, des effets de survitesse et de plateau largement modulables comme dans le cas des propergols homogènes.

Ces études sont menées grâce à la participation de MM. A. BIZOT, J. HOMMEL, J.F. TRUBERT, J.C. AMIOT et D. BENEVIDES, stagiaire à l'ENSTA.

REFERENCES

- [1] - J.E. SINCLAIR, W. HONDEE
The thermal decomposition of H.M.X.
7th Proc. Symp. Explos. Pyrotech. (1971), cité en [5].
- [2] - B. SURYANARAYANA, R.J. GRAYBUSH, J.R. AUTERA
Thermal degradation of secondary nitramines.
Chemistry and Industry, vol. 52, pp. 2177-2178 (1967).
- [3] - R.N. ROGERS
DSC determination of kinetics constants of systems that melt with decomposition.
Thermochemica Acta, vol. 3, pp. 437-447 (1972).
- [4] - A.J.B. ROBERTSON
The thermal decomposition of explosives. Part II : cyclotrimethylenetrinitramine and cyclotetramethylenetrinitramine.
Trans. Faraday Soc., vol 45, p. 85 (1949).
- [5] - T.L. BOGGS
The thermal behavior of R.D.X. and H.M.X.
Chapitre 3 de Fundamentals of Solid-Propellant Combustion, volume 90, AIAA Progress Series in Astronautics and Aeronautics, K.K. Kuo et M. Summerfield éditeurs (1984).
- [6] - G. LENGELLE, A. BIZOT, J. DUTERQUE, J.F. TRUBERT
Steady state burning of homogeneous propellants.
Chapitre 7 de Fundamentals of Solid-Propellant Combustion, op. cit.
- [7] - J.F. TRUBERT
Analyse des gaz dans l'étude de la combustion des propergols double base et de l'octogène.
66th Specialists' Meeting, Smokeless Propellants, Florence (Italie), Sept. 1985.
- [8] - N. KUBOTA
Combustion mechanics of nitramine composite propellants.
18th Symposium (International) on Combustion, p. 187, The Combustion Institute, 1981.

- [9] - C.F. PRICE, T.L. BOGGS, R.L. DERR
The steady-state combustion behavior of ammonium perchlorate and H.M.X.
AIAA Paper n° 79-0164, 17th Aerospace Sciences Meeting, Janvier 1979.
- [10] - W.H. AVERY
Burning rate studies in double base powder.
OSRD 5827, ABL/P/1, Janvier 1946.
- [11] - J.C. GODON
Modèle de combustion stationnaire du perchlorate d'ammonium.
La Recherche Aérospatiale n° 1982-2, 1982.
- [12] - J.C. GODON
Modélisation de la combustion normale et érosive des propergols composites.
Thèse de doctorat d'état, Université de Paris VI, novembre 1983.
- [13] - C. GUIRAO, F.A. WILLIAMS
A model of ammonium perchlorate deflagration between 20 and 100 atm.
AIAA Journal, vol. 9, n° 7, p. 1345, Juillet 1971.

ANNEXES

1 - THERMOGRAVIMETRIE, ANALYSE ENTHALPIQUE DIFFERENTIELLE

Un échantillon, de masses initiale M_0 et instantanée M , subit (uniformément dans sa masse) une montée en température $T = T_0 + v t$, suivant une vitesse de chauffage v programmable.

Avec $y = M/M_0$, la loi de dégradation s'exprime

$$\frac{dy}{dt} = -A_c e^{-E_c/RT} y^m, \quad (1)$$

$$\frac{dy}{dT} = -\frac{A_c}{v} e^{-E_c/RT} y^m. \quad (2)$$

Si l'on intègre cette relation entre conditions initiale et instantanée

$$g(y) = \int_1^y \frac{dy'}{y'^m} = -\frac{A_c}{v} \int_{T_0}^T e^{-E_c/RT} dT,$$

avec $\xi = E_c/RT$ (en fonction des résultats anticipés, on a $\xi \approx 49 \gg 1$)

$$g(y) = -\frac{A_c}{v} \frac{E_c}{R} \int_{\xi}^{\xi'} e^{-\xi'} \frac{1}{\xi'^2} d\xi'$$

(où l'on tient compte du fait qu'à T_0 la vitesse de réaction est nulle). Du fait que $\xi \gg 1$ le terme exponentiel domine très largement et

$$g(y) \approx -\frac{A_c}{v} \frac{E_c}{R} e^{-\xi} \frac{1}{\xi^2}, \quad (3)$$

soit

$$\ln[-g(y)] = \ln A_c \frac{E_c}{R} - \ln v - \frac{E_c}{RT} - 2 \ln \left(\frac{E_c}{RT} \right). \quad (4)$$

Si pour différentes vitesses de chauffe v on se place au même degré d'avancement y , on obtient une relation entre v et la température $T(y)$ atteinte à ce degré d'avancement

$$\frac{d \ln v}{d(1/T)} = -\frac{E_c}{R} \left[1 + \frac{2}{(E_c/RT)} \right]. \quad (5)$$

On peut donc utiliser un relevé comme celui de la figure 2, dont la pente est directement liée à l'énergie d'activation E_c (le terme en $1/(E_c/RT) \approx 0,02$ étant une correction). On obtient alors $E_c = 50$ kcal/mole.

En un point de la courbe de la figure 2, et en supposant une réaction de dégradation d'ordre $m = 1$, on a, à partir de l'équation (3),

$$A_c = v \frac{E_c}{RT^2} e^{E_c/RT} (-\ln y). \quad (6)$$

En analyse enthalpique différentielle il est difficile, en l'absence d'autre mesure, de connaître le degré d'avancement correspondant au départ du pic de dégagement exothermique. On peut estimer que 10 à 20 % du matériau s'est déjà dégradé. On obtient alors

$$A_c = 0,7 \text{ à } 1,6 \cdot 10^{17} \text{ s}^{-1},$$

reflétant la marge d'incertitude sur le degré d'avancement.

2 - ALLUMAGE PAR UN FLUX SUPERFICIEL

Un échantillon est chauffé en surface par un flux constant de densité ϕ_0 . L'évolution de la température en fonction du temps et de la profondeur x ($x < 0$ dans le matériau) est régie par la relation

$$\rho_p c_p \frac{\partial T}{\partial t} = \lambda_p \frac{\partial^2 T}{\partial x^2} + \rho_p \varphi_s A_c e^{-E_c/RT} \quad (1)$$

avec pour condition limite

$$\lambda_p \frac{\partial T}{\partial x} \Big|_s = \phi_0 \quad (2)$$

La température, pour un matériau inerte, est donnée par

$$T(x,t) = T_0 + \frac{\phi_0}{\lambda_p} \left[2 \left(\frac{d_p t}{\pi} \right)^{1/2} e^{-x^2/4d_p t} + x \operatorname{erfc} \left(-\frac{x}{2\sqrt{d_p t}} \right) \right] \quad (3)$$

et en surface

$$T_s = T_0 + 2 \phi_0 \left(\frac{t}{\pi} \right)^{1/2} \frac{1}{\Gamma} \quad (4)$$

avec $\Gamma = (\lambda_p \rho_p c_p)^{1/2}$ l'effusivité thermique, estimée pour $\rho_p = 1,9 \text{ g/cm}^3$, $c_p = 0,35 \text{ cal/gK}$ et $\lambda_p \approx 7,3 \cdot 10^{-4} \text{ cal/cm sK}$ à $\Gamma = 0,022$ (valeur correspondant à $d_p = 1,1 \cdot 10^{-3} \text{ cm}^2/\text{s}$).

Avant que la dégradation exothermique s'amorce les termes instationnaire et de conduction de l'équation (1) s'équilibrent. Un critère d'allumage (c'est-à-dire de première manifestation de réaction exothermique) est alors qu'au voisinage de la surface le terme de dégagement d'énergie devient égal ou supérieur au terme instationnaire

$$\rho_p c_p \frac{\partial T_s}{\partial t} \leq \rho_p \varphi_s A_c e^{-E_c/RT_s} \quad (5)$$

Si l'on tient compte de la relation (4) pour T_s on obtient

$$\rho_p c_p \phi_0 \frac{1}{\pi^{1/2} \Gamma t^{1/2}} \leq \rho_p \varphi_s A_c e^{-E_c/RT_s},$$

soit en fonction de la relation (4) t/T_s

$$T_{s,all.} = \frac{E_c}{2R} \frac{1}{\ln(A^*/\phi_0)} \quad (6)$$

$$A^* = \left[\lambda_p \rho_p \varphi_s A_c \frac{\pi}{2} (T_{s,all.} - T_0) \right]^{1/2} \quad (7)$$

Une description plus rigoureuse par un calcul numérique montre que l'équation (6) est une première approximation et qu'une expression qui permet de mieux représenter l'évolution de la température d'allumage est [1]

$$T_{s,all.} = \frac{E_c}{2R} \left[1 + 1,04 \ln(A^*/\phi_0) \right]^{-1} \quad (8)$$

[1] - A.D.BAER, N.W.RYAN

Ignition of composite propellants by low radiant fluxes, AIAA Journal, vol.3, n° 5, p. 884, mai 1965.

Les résultats de la figure 3 indiquant l'évolution du délai d'allumage en fonction du flux reçu peuvent être corrélés, d'une part, en calculant à partir de l'équation (4) la température $T_{s,all}$, atteinte au moment de l'allumage (à titre d'exemple à $\phi_o = 20 \text{ cal./cm}^2 \text{ s}$, $\tau_{all} = 0,104 \text{ s} \rightarrow T_{s,all} = 625 \text{ K}$) et, d'autre part, en ajustant l'énergie d'activation E_c et la constante A_c à partir de la relation (8). On peut ainsi obtenir

$$\begin{aligned} E_c &= 50 \text{ kcal./mole (valeur arrondie)} \\ A_c &= 1,1 \cdot 10^{17} \text{ s}^{-1}. \end{aligned}$$

3 - REGIME DE LA REGRESSION ETABLIE

En régression établie et dans un système (avec $\kappa > 0$ vers l'extérieur du matériau) lié à la surface régressant à la vitesse de combustion v_c , la loi $T(x)$ dans la phase condensée est régie par l'équation

$$\rho_p c_p v_c \frac{dT}{dx} = \lambda_p \frac{d^2T}{dx^2} \quad (1)$$

avec pour solution le profil, avec T_s à la surface et T_o en profondeur,

$$(T - T_o) / (T_s - T_o) = e^{-\kappa v_c x / \lambda_p} \quad (2)$$

L'épaisseur de matériau chauffé peut être définie conventionnellement pour l'atteinte d'une température T_e suffisamment proche de T_o

$$(T_e - T_o) / (T_s - T_o) = \frac{1}{10}$$

soit

$$e = \frac{d_p}{v_c} \ln 10. \quad (3)$$

La dégradation du matériau, pour une réaction d'ordre 1, est régie par l'équation

$$\rho_p v_c \frac{dY_p}{dx} = -\rho_p Y_p A_c e^{-E_c/RT} \quad (4)$$

avec Y_p la fraction massique du matériau en cours de dégradation (masse spécifique locale ramenée à la masse spécifique initiale ρ_p). L'épaisseur de réaction peut être définie par l'atteinte d'une température sous la surface pour laquelle le taux de dégradation s'est suffisamment atténué

$$e^{-\Sigma / (1 - \Delta T / T_s)} / e^{-\Sigma} = \frac{1}{10} \quad (5)$$

avec $\Sigma = E_c / RT_s$. On obtient

$$\Delta T / T_s = (1 + \Sigma / \ln 10)^{-1} \quad (6)$$

soit pour $T_s = 850 \text{ K}$, $\Sigma \approx 30$, $\Delta T = 60 \text{ K}$. Si l'on introduit cette expression pour ΔT dans l'expression du profil, équation (2), on obtient pour l'épaisseur dans laquelle la réaction de dégradation est active

$$e_{react} \approx \frac{d_p}{v_c} \ln 10 \frac{1}{\Sigma} \frac{T_s}{(T_s - T_o)} \quad (7)$$

Pour une vitesse de régression $v_c = 10 \text{ mm/s}$ par exemple l'épaisseur chauffée, équation (3), est de $e \approx 25 \mu\text{m}$ et l'épaisseur de réaction $e_{react} \approx 1 \mu\text{m}$. En dehors de cette zone réactive superficielle très fine le matériau est inerte (les températures atteintes sont encore trop peu élevées pour que la dégradation ait eu le temps de se produire). Le temps de séjour du matériau dans la zone chauffée est $\tau_c \approx e / v_c$ ($\approx 2 \text{ ms}$ pour l'exemple choisi) et dans la zone réactive $\tau_{react} \approx e_{react} / v_c$ ($0,1 \text{ ms}$). On conçoit qu'en fonction de ces temps de séjour extrêmement courts des températures de dégradation très élevées soient atteintes ($\approx 650^\circ\text{C}$ en régime établi pour $\approx 250^\circ\text{C}$ en A.E.D. pour des temps de séjour de l'ordre de dizaines de minutes).

L'équation (4) pour la conservation de la masse spécifique du matériau peut être intégrée au travers de la zone chauffée

$$\int_{-e}^0 \rho_p v_c \frac{dY_p}{dx} = - \int_{-e}^0 \rho_p Y_p A_c e^{-E_c/RT} dx$$

$$v_c \approx A_c d_p \frac{e^{-\Sigma}}{\Sigma} \ln 10 \frac{T_s}{(T_s - T_o)} \quad ,$$

où l'on a tenu compte de l'expression approchée pour l'épaisseur de réaction, équation (7). On a montré [1] qu'une expression plus rigoureuse est

$$v_c^2 = A_c d_p \frac{e^{-\frac{E_s}{RT_s}}}{\sum} \left[\frac{q_s}{c_p T_s} (1 + \ln Y_{p,s}) - \left(1 - \frac{T_0}{T_s}\right) \ln Y_{p,s} \right]^{-1}, \quad (5)$$

où $Y_{p,s}$ est la faible fraction de matériau restant à la surface (on a montré en [1] que la valeur précise a peu d'impact et qu'on peut adopter $Y_{p,s} \approx 0,01$). La loi de pyrolyse de l'équation (8) reliant la vitesse de régression à la température de surface a été utilisée pour la figure 6.

[1] - G. LENGELLE

Thermal degradation kinetics and surface pyrolysis of vinyl polymers.
AIAA Journal, vol. 8, n° 11, p. 1989, (1970).

4 - ZONE DE FLAMME

Les équations de conservation dans la phase gazeuse des espèces chimiques, de fraction massique Y_i , et de l'énergie s'écrivent

$$\dot{m} \frac{dY_i}{dx} - \frac{d}{dx} (\rho D \frac{dY_i}{dx}) = \dot{\omega}_i \quad (1)$$

$$\dot{m} c_p \frac{dT}{dx} - \frac{d}{dx} \left(\lambda_g \frac{dT}{dx} \right) = - \sum_i h_i^o \dot{\omega}_i \quad (2)$$

\dot{m} étant le débit masse unitaire ($= \rho_p v_c$ par conservation de la masse), $\dot{\omega}_i$ le taux de réaction en $g/cm^3 \cdot s$ et h_i^o l'enthalpie de formation de l'espèce i . Les conditions limites à la surface sont

$$\begin{aligned} \dot{m} Y_{i,c} & \text{(libéré par la dégradation du matériau, voir fig. 7)} \\ & = \dot{m} Y_{i,s} - \rho D \left. \frac{dY_i}{dx} \right|_s \end{aligned} \quad (3)$$

$$\dot{m} (c_{g,s} T_s - c_p T_0 - q_s) = \dot{m} q_c = \lambda_g \left. \frac{dT}{dx} \right|_s = q_s \quad (4)$$

L'intégration de (2) permet d'obtenir

$$\dot{m} (c_g T_f - c_g T_s) = -q_s + \dot{m} q_g \quad (5)$$

où

$$q_g = \sum_i (Y_{i,c} - Y_{i,f}) h_i^o$$

est la chaleur dégagée pour la réaction.

Si l'on représente la réaction chimique de la flamme par une réaction globale



on peut écrire $\dot{\omega}_i$

$$\frac{M_i}{M_{ox}} (\beta_i) \underbrace{C_{ox}^a C_{comb}^b}_{\dot{\omega}} e^{-E_g/RT} \quad (6)$$

ou $(-\alpha)$ pour le combustible
(-1) pour l'oxydant

où C est la concentration molaire, $C_i = \frac{Y_i}{M_i} \frac{p}{RT} M$. L'ordre de la réaction est $a + b$.

L'intégration de l'équation (1), compte tenu de (3), donne

$$\dot{m} (Y_{i,f} - Y_{i,c}) = \frac{M_i}{M_{ox}} \left[\begin{array}{c} \beta_i \\ -\alpha \\ -1 \end{array} \right] \underbrace{\int_s^f \dot{\omega} dx}_{\dot{R}} \quad (7)$$

En particulier pour l'oxydant

$$\dot{m} Y_{Ox,c} = \dot{R} \quad (8)$$

L'équation de l'énergie s'écrit, en tenant compte de (7) et (8),

$$\begin{aligned} \dot{m} c_g \frac{dT}{dx} - \frac{d}{dx} \left(\lambda_g \frac{dT}{dx} \right) &= \dot{\omega} \left[h_{Ox}^0 + \alpha h_{Comb}^0 - \sum_{P_i} P_i h_{P_i}^0 \right] \frac{M_i}{M_{Ox}} \\ &= \frac{\dot{\omega}}{R} \left[h_{Ox}^0 Y_{Ox,c} + h_{Comb}^0 Y_{Comb,c} - \sum_{P_i} Y_{P_i,c} h_{P_i}^0 \right] \\ &= \frac{\dot{\omega}}{Y_{Ox,c}} Q_g \quad (9) \end{aligned}$$

L'équation des espèces devient, en tenant compte de (7) et (8),

$$\dot{m} \frac{dY_i}{dx} - \frac{d}{dx} \left(D \frac{dY_i}{dx} \right) = \frac{M_i}{M_{Ox}} \left[\begin{array}{c} P_i \\ -\lambda \\ -1 \end{array} \right] \dot{\omega} = \dot{\omega} \frac{(Y_{i,f} - Y_{i,c})}{Y_{Ox,c}} \quad (10)$$

Du fait que $\lambda_g/c_g = f\lambda$, il y a similarité entre les équations pour T et pour Y_i de telle sorte que

$$c_g (T_f - T_i) / Q_g = (Y_{i,f} - Y_i) / (Y_{i,f} - Y_{i,c}) \quad (11)$$

Réaction du premier ordre, basse pression

A basse pression la flamme primaire, impliquant une réaction unimoléculaire de NO_2 [6], a seule une influence sur la régression de la surface (la flamme secondaire en est trop éloignée). On a alors, compte tenu de (9) et (11),

$$\begin{aligned} \dot{m} c_g \frac{dT}{dx} - \frac{d}{dx} \left(\lambda_g \frac{dT}{dx} \right) &= A_{g1} e^{-E_{g1}/RT} Y_{Ox} \frac{P}{RT} M \frac{Q_g}{Y_{Ox,c}} \\ &= A_{g1} e^{-E_{g1}/RT} \frac{P}{RT} M c_g (T_f - T) \quad (12) \end{aligned}$$

Si on pose $q(T) = \lambda_g \frac{dT}{dx}$ on obtient

$$\dot{m} c_g T - q \frac{dq}{dT} = \lambda_g A_{g1} e^{-E_{g1}/RT} \frac{P}{RT} M c_g (T_f - T)$$

En intégrant de surface à fin de flamme

$$\dot{m}^2 = \lambda_g \frac{P M}{RT_f} A_{g1} \int_{T_s}^{T_f} \frac{T_f}{T} \frac{c_g (T_f - T)}{Q_c} e^{-E_{g1}/RT} dT \left[c_g (T_f - T_s) F + \frac{Q_c}{2} \right]^{-1} \quad (13)$$

où on a tenu compte de (4) et où un "facteur de forme" du profil de température est défini par

$$F = \int_0^1 g(\theta) d\theta, \quad \theta = \frac{T - T_s}{T_f - T_s}, \quad g(\theta) = \frac{q}{q_s} \quad (14)$$

Il a été établi que $E_{g1} = 5$ kcal/mole [6] est représentatif. Une résolution numérique de l'équation (12) révèle que le facteur de forme F est plus évolutif en fonction de la pression et proche de 1. L'équation (13) indique alors que la vitesse de combustion $p v_c = \dot{m}$ évolue suivant $p^{1/2}$, évolution à laquelle s'ajoute l'influence de la variation modérée de $T_s, Q_c \dots$ Cette évolution est indiquée sur la figure A1 pour $p < 30$ bars.

Réaction du deuxième ordre, haute pression

Au-dessus de 30 bars on peut considérer qu'une flamme unique, dans laquelle réagissent NO_2, N_2O et NO avec $HCHO$ et HCN , représentée par une réaction bimoléculaire, influe sur la régression de surface. Compte tenu de l'équation (11) pour Y_{Ox} et Y_{Comb} , l'équivalent de l'équation (13) pour le débit masse devient

$$\dot{m}^2 = \lambda_g \left(\frac{P/M}{RT_f} \right)^2 A_{g2} \int_{T_s}^{T_f} \left(\frac{T_f}{T} \right)^2 \frac{[c_p(T_f - T)]^2}{\rho_c \rho_g} \frac{Y_{comb,c}}{M_{comb}} e^{-E_{g2}/RT} dT \left[c_g(T_f - T_s) + \frac{Q_c}{2} \right]^{-1} \quad (15)$$

Le calcul numérique montre que F est peu évolutif et ≈ 1.5 . L'équation (15) indique alors que la vitesse de combustion évolue suivant $P^{1.5}$, avec une légère modification apportée par la variation de T_s, ρ_c, \dots avec la pression. Cette évolution est indiquée sur la figure A.1. Sur cette figure, les constantes préexponentielles A_{g1} et A_{g2} ont été ajustées à 30 bars sur la valeur expérimentale, le reste du calcul se déroulant ensuite sans autre ajustement.

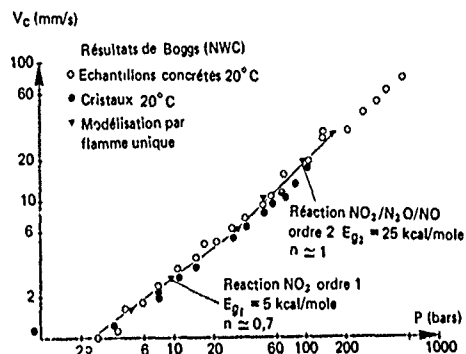


Fig A1 - Vitesse de combustion de l'octogène.

DISCUSSION

N.S.Cohen, US

It is interesting that the low pressure burning rate of the propellant is less than the individual burning rates of the HMX and binder ingredients (Fig. 6). I have also observed that with several propellants I have also observed the high pressure burn rate of the propellant to be higher than the ingredients in some cases. Thus the combination has a higher pressure exponent than the ingredients. I believe that this is due to an energy interaction by which the presence of the HMX reduces the net exothermicity of the solid at low pressure, and increases the rate of heat feed-back from the flame at high pressure, compared to the binder alone. But I agree that there is probably no chemical interaction between them. There is also controversy about whether the condensed phase of HMX is net endothermic or exothermic, whether HMX undergoes a vaporization that would be endothermic. It is difficult to deduce this from thermocouple measurements because it is much more difficult to measure the temperature gradients than the surface temperature. If the condensed phase of HMX is net exothermic, as you show, it must be less than for the binder because the pressure exponent is higher and the temperature sensitivity (σ_p) lower than for the binder. In any case, I feel that better catalysis of the propellant can be achieved through research that would match additive decomposition characteristics with particular combustion zone thermal environments, and some success in achieving plateaus through trial and error has been demonstrated.

Author's Reply

Although the thermocouple measurements are scattered, they show (Fig. 5) that the condensed phase decomposition is net exothermic, between 50 and 100 cal/g, in the case of HMX (this is in agreement with the gas analysis showing NO to be present. NO results from a beginning of the exothermic reactions in the condensed phase). A similar result (not shown in the paper) has been obtained for the (nitroglycerine and polymer) binder, that there is a net exothermic heat release in the condensed phase. Taking these results into account, and measurements of surface temperatures around 850K for HMX and around 650K for the binder, it is possible to extract, from the modelisation of the combustion of each component, temperature coefficients very compatible with experimental results, that is around 0.1% °C⁻¹ for HMX and around 0.5% °C⁻¹ for the binder.

With respect to additives, it is believed that one should try to obtain an interaction with the binder of the nature of that observed with double-base propellants; that is enhancement of the carbon residue on the surface and strengthening of the primary flame, to create super-rates followed by plateau effects. One has to try and find a polymer which gives an appreciable amount of carbon upon degradation, so that the additives are trapped in the carbon layer on the surface and can interact with the primary flame.

STABILITY OF NITROCELLULOSE PROPELLANTS ASSESSED VIA THERMAL
DECOMPOSITION AND ALTERATION OF THE STABILIZER COMPOSITION

Ir. P. van de Mey and Dr. A.H. Heemskerk
Prins Maurits Laboratory TNO
P.O. Box 45
2280 AA Rijswijk, The Netherlands

ABSTRACT

In the Netherlands the surveillance of propellants is performed by investigating the thermal behaviour of the propellant at a temperature of 358 K. This procedure is accepted to represent a degradation equivalent to a storage period of at least ten years at ambient temperatures.

To obtain additional information about the degradation of propellants thermal stability tests have been performed at various temperatures and under several environmental conditions. Both the thermal behaviour of the propellant and the chemical behaviour of the stabilizing amine compound have been determined during these experiments. The composition of the amine compounds has been analysed using HPLC-techniques developed for these experiments.

1. INTRODUCTION

Basically the surveillance of gun propellants is either performed by an investigation into the thermal behaviour of the propellant [1] or by the determination of its residual effective stabilizer content [2]. In most cases this surveillance is performed at elevated temperatures to reduce the time spent on investigation and to enable a prediction over a period of 5-10 years. In the Netherlands the thermal behaviour is investigated by following the isothermal heat generation of the propellant at 358 K for an aging period of one week. This procedure is accepted to be representative for a storage period of at least ten years at ambient temperatures.

Although generally agreeing in results the classic stability tests of the propellants and the above-mentioned heat generation tests occasionally lead to contradictory judgments.

Furthermore, the prediction method based on surveillance at elevated temperatures is only acceptable if the set of decomposition reactions involved in the degradation process of the propellant, the so-called "reaction pattern", remains approximately the same and more or less independent of temperature.

In this context the behaviour of the stabilizing compound is of major importance. This compound has been investigated intensively both qualitatively and quantitatively either as part of the propellant [2] or in its pure form exposed to nitrogen oxides [3]. However, none of these cases led to a definite link between the temperature and the behaviour of either the stabilizer composition in the propellant or the thermal decomposition of the smokeless powder.

In our current research programme the link between the thermal and chemical (viz. stabilizer composition) is being investigated as a function of temperature in the temperature range 300 - 390 K [4,5] applying various methods of investigation:

- investigations into the change in stability of propellants as a function of temperature (range 350 - 390 K) under various external conditions,
- investigations into the NO_x-generation during the slow decomposition at low temperatures (300 - 370 K) using chemiluminescence methods [5],
- investigations into the behaviour of the stabilizing compound exposed to nitrogen oxides in the temperature range between 300 and 350 K.

From these investigations both the existing pattern of reactions between the reactants as a function of time and the shift in this pattern as a result of temperature variation can be obtained.

In this paper we intend to show some of the results of the research programme obtained according to the first and the third method.

2. EQUIPMENT

The heat generated by the propellants has been measured with the help of the isothermal storage test (IST). At the end of the degradation period the stabilizer was extracted from the propellant and its composition determined using high performance liquid chromatography (HPLC). The IST has been developed in our laboratory to register small heat generations with considerable accuracy. The heat generated by reacting or decomposing substances at constant temperatures is measured as a function of time. Performance of these experiments at a number of temperatures leads to a quantitative understanding of the relation between the temperature and the heat generation of the substance under investigation.

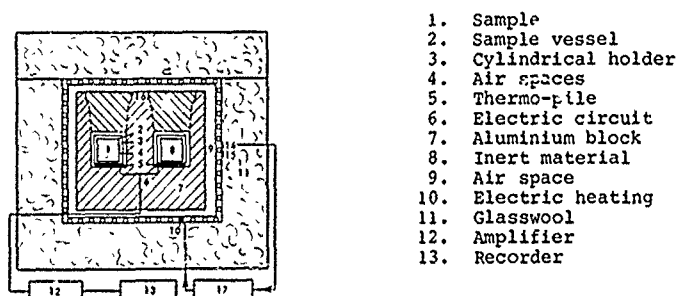


Figure 1. Construction of the Isothermal Storage Test.

The IST, shown in Fig. 1, consists of a large heat sink (an aluminium block) which is kept at the desired constant temperature. In the block are two wells with a heat flow sensor - a Peltier element - at the bottom. Holders are placed on the Peltier elements. Both holders are identical. One holder contains the sample, the other an inert substance. The heat generated by the sample results in a proportional voltage signal from the heat flow sensor. Random fluctuations in this signal are avoided by monitoring the voltage difference between both heat flow sensors. The minimum heat generation measured by the IST amounts to 5 mW per kg of sample with an accuracy of at least 30 percent for the very low heat generations.

The reactions of DPA or its derivatives were investigated by exposing the pure components to nitrogen oxides in a thermogravimetric balance, which is schematically shown in Fig. 2.

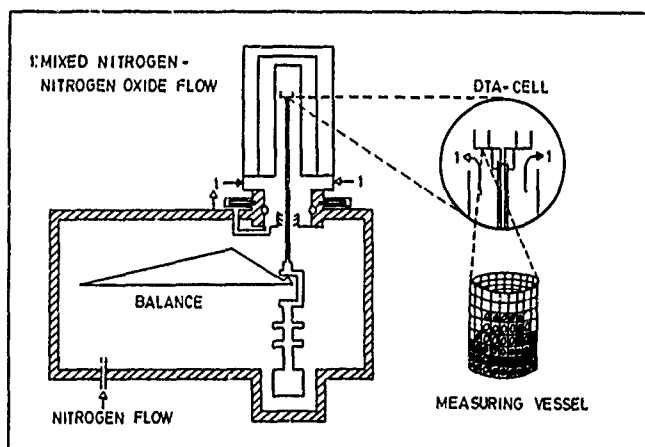


Figure 2. Thermogravimetric equipment adapted for investigations into diphenylamine + derivatives.

This balance basically combines thermogravimetric measurements with differential thermal analysis. The measuring cell of the thermographic equipment has been redesigned in the following way :

- An injection system was attached to the cell upstream of the sample vessel in order to introduce a nitrogen dioxide/nitrogen gas mixture to the sample. The injection system was designed in such a way that it caused no jumps in the weight signal and that it enabled well-defined, discrete, fast and accurate periods of exposure.
- The sample vessel was changed as well. In order to obtain an acceptably good mass transfer between the nitrogen dioxide and the stabilizer a wire-cloth sample vessel was constructed.

In order to prevent melting effects and to improve mass and heat transfer the DPA was deposited in thin layers on glass or steel balls.

The stabilizer composition was determined both qualitatively and quantitatively by HPLC. The resolution of the HPLC, shown in Fig. 3 appears to be remarkable good. The derivatives with equal retention times (5,7 and 10,11,12) hardly occur simultaneously in the stabilizer compounds investigated in practice.

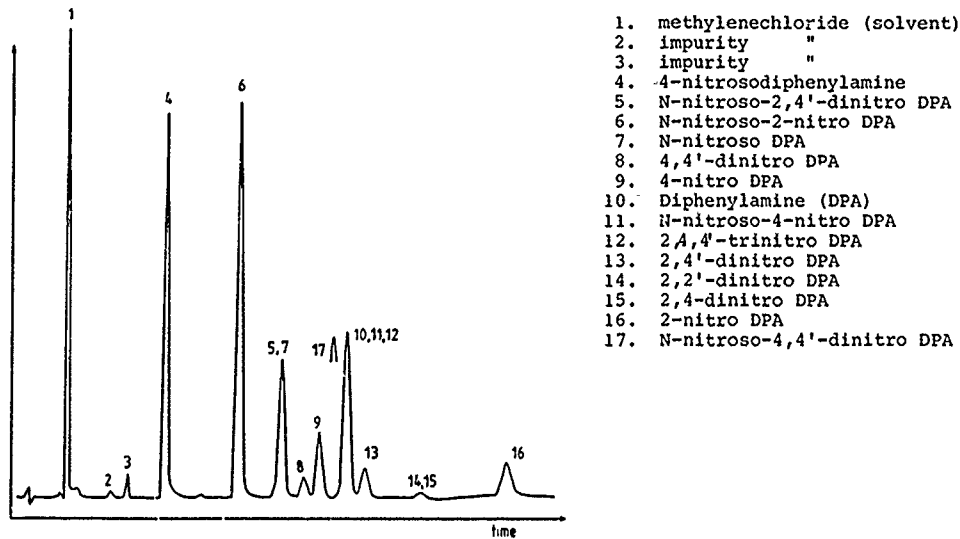


Figure 3. HPLC -chromatogram with 14 DPA-derivatives

3. RESULTS

Typical changes in the composition of DPA as a result of exposure to nitrogen dioxide are shown in Figures 4 and 5. In these Figures the time of exposure has been included on the z-axis. The time-dependent changes in composition at a temperature of 300 K are shown more clearly in Fig. 6.

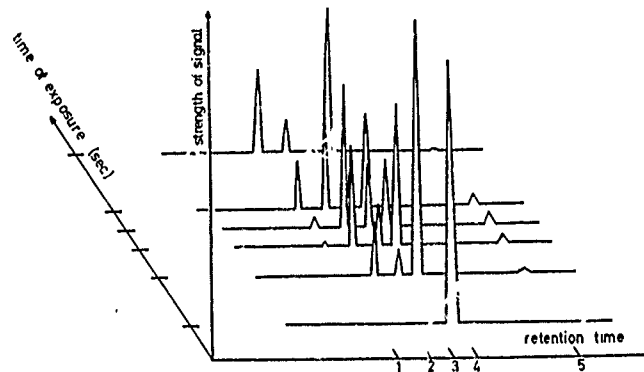


Figure 4. Series of HPLC-chromatograms showing the time-dependent behaviour of DPA-nitrodioxide at 300 K.

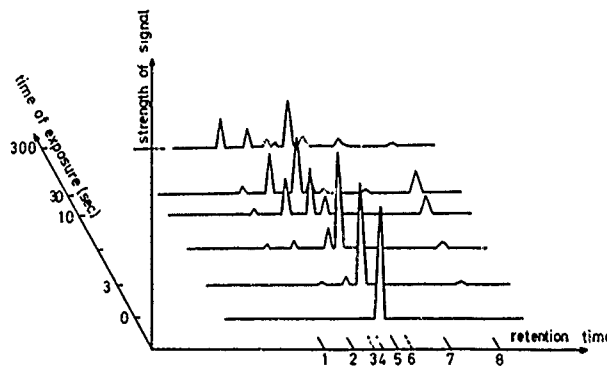


Figure 5. Series of HPLC-chromatograms showing the time-dependent behaviour of DPA + nitrodioxide at 350K.

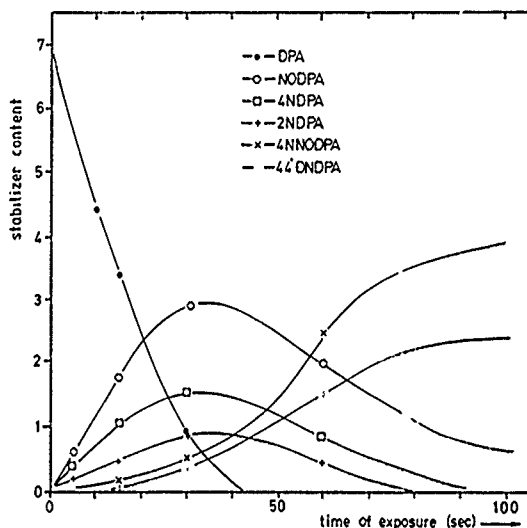


Figure 6. Fraction of DPA + derivatives as a function of time exposure to nitro dioxide at 300 K.

Considering the changes in composition in some detail we find that the DPA content initially decreases under the formation of nitrosodiphenylamine (NO-DPA) as main product, 4-nitrodiphenylamine (4-NDPA) as main by-product and a small amount of 2-nitrodiphenylamine (2-NDPA). The apparent increase in the peak of DPA (Fig. 4) following a sufficiently long period of exposure, is caused by the formation of nitroso-4-nitrodiphenylamine (NO-4-NPA Fig. 6), a compound with an equal retention time.

The concentrations of the primarily substituted DPA-derivatives show maxima and, as secondary substitution increases, decrease again. The main products become the DPA-derivatives NO-4-NDPA and NO-2-NDPA.

It appears that the second nitrogen oxide molecule starts to be substituted only after a substantial mono-substitution to the DPA has taken place. This secondary substitution leads to the formation of 2,2'-dinitrodiphenylamine (2,2'-di-NDPA), 2,4'-di-NDPA, 4,4'-di-NDPA, NO-4-NDPA and NO-2-NDPA in concentrations that strongly depend on the concentration of the nitrogen dioxide and on the temperature. At room temperature NO-2-NDPA and NO-4-NDPA appear to be the final products regardless of the concentration of nitrogen dioxide or the period of exposure. At elevated temperature the di-nitro-compounds appear to react further under the formation of nitroso-di-nitro compounds, which can be seen by the 350 K shown in Fig. 5. As indicated before the secondary addition of the nitrogen dioxide takes place at an earlier stage.

From the initial stages of each step in the addition process the relationship between the reaction rate and the nitrogen dioxide concentration can be obtained. In simplified form this relationship may be expressed by

$$\ln r = a + n \ln c$$

where the reaction rate r and the nitrogen dioxide concentration c are related by the order of the reaction n and constant a .

The order of the reaction n , which is represented by the slope of the lines in Figure 7, appears to be 0.8, 0.9 and 1.2 for the nitration and nitrosation to 2-NDPA, 4-NDPA and to NO-DPA, respectively. By performing this kind of experiment at various temperatures the activation energies of the individual reactions could be obtained. From these observations it appears that the nitrosation reaction dominates at lower temperatures, whereas the nitration reactions start to prevail at higher temperatures. This is illustrated by the changes in level of the lines in Fig. 7. The degradation of propellants is mainly affected by temperature. However, the oxygen concentrations and moisture contents appear to affect the degradation process as well. The influence of the oxygen concentration on the thermal degradation is illustrated in Figure 8. In Figures 9 and 10 typical changes in stabilizer composition due to variations in the oxygen concentration are shown with the other conditions remaining the same.

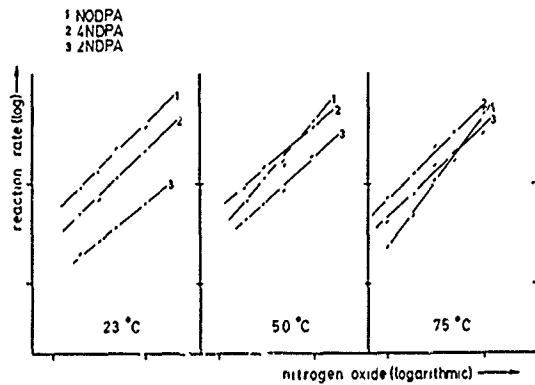


Figure 7. Relationship between reaction rate and nitrogen dioxide concentration as a function of temperature

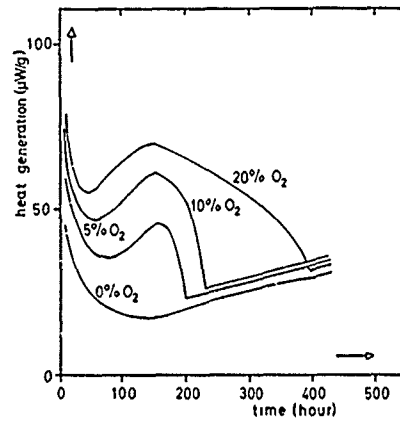


Figure 8. Heat generation in smokeless powder at 358 K.
Storage conditions: variable environmental oxygen concentration;
moisture contents : 1 w-%

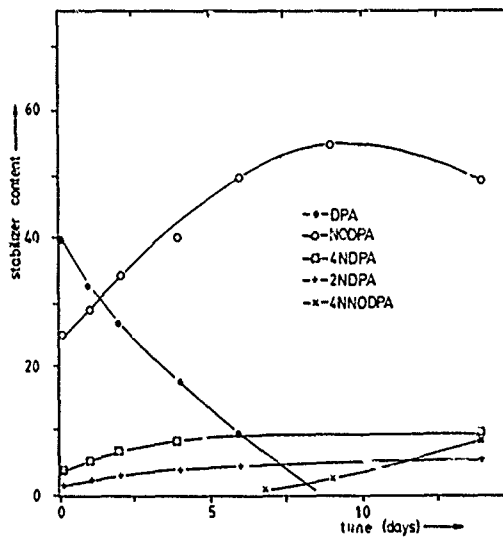


Figure 9. Changes of stabilizer composition in smokeless powder decomposing at 358 K.
Conditions : 100 % N₂ ; 0.0% moisture content

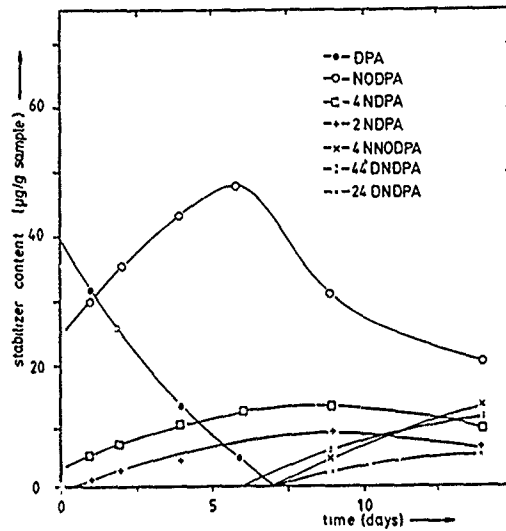


Figure 10. Changes of stabilizer content in smokeless powder decomposing at 358 K.
Conditions : 90 % N₂, 10 % O₂ ; 0.0 % moisture content.

In all experimental cases we observed that the oxygen concentration is potential to the excess heat generation obtained by subtracting the "zero oxygen" heat generation from the "oxygen rich". The activation energy of the degradation process appears to be independent of temperature. This indicates that oxygen affects only post-degradation reactions instead of the degradation process itself. The influence of moisture in the propellant has been investigated for a sequence of temperatures and environmental oxygen concentrations.

Typical results concerning the thermal behaviour and the changes in composition are shown in Figures 11, 12 and 13. In Figure 11 the characteristic effect of oxygen on the degradation process is encountered again. Moreover, an extra heat effect caused by the amount of moisture, appears to be superposed on the heat generation.

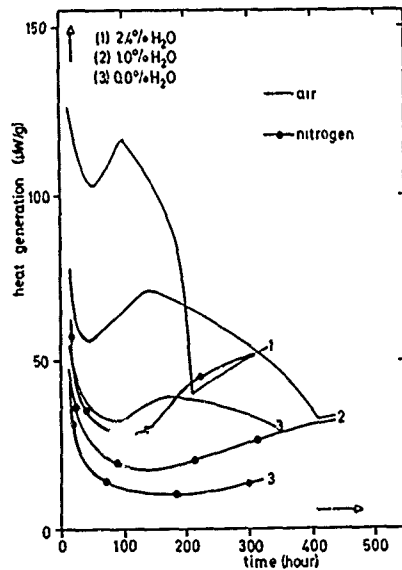


Figure 11. Relationship between heat generation and time as a function of moisture content and environmental oxygen concentration at 358 K.

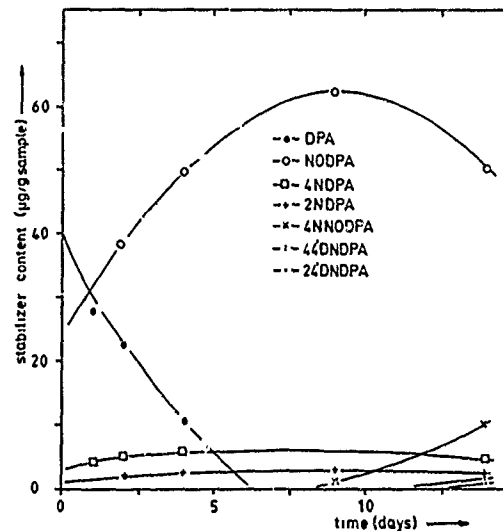


Figure 12. Changes of stabilizers content in smokeless powder decomposing at 358 K.
Conditions : 100 % N₂ ; 2,4 moisture content.

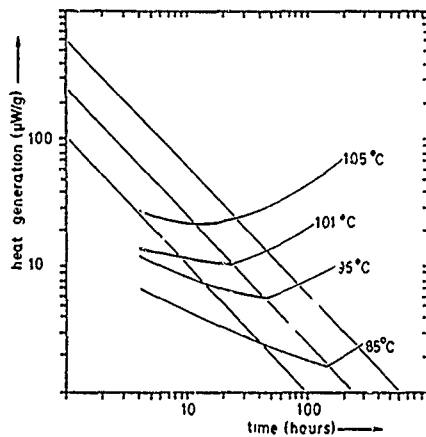


Figure 13. Heat generation vs. time curves obtained with a smokeless powder stored at various temperatures in the range 358 - 378 K. Conditions: 100 % N₂ ; 1.0 % moisture content

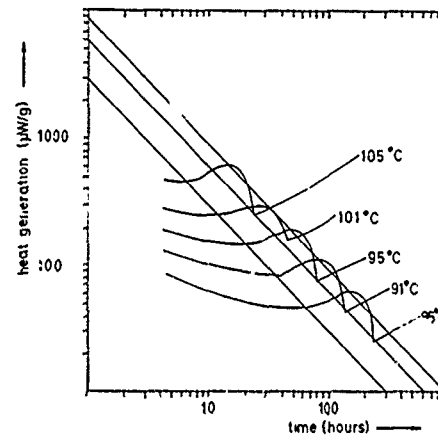


Figure 14. Heat generated by smokeless powder as a function of temperature and time. Conditions : 90 % N₂ , 10 % O₂ ; 1.0 % moisture content

Such an effect has been observed throughout the temperature range 330 - 370K. The "overall" activation energy of the degradation process, calculated for each water content, appeared to decrease with increasing content. Therefore, the amount of moisture affects the rate-determining steps of the decomposition itself. Possible explanations for this kind of behaviour may be found in different reaction mechanisms, increased acidity, obstructed mass transfer or combinations of these possibilities. The effect of the decreasing moisture content on the changes in stabilizer composition (Figures 9 and 12) reflect the observations of the thermal analysis. (Figs. 13 and 14).

4. DISCUSSION/CONCLUSIONS

Environmental storage conditions affect the stability of propellants. Increased moisture contents and increased oxygen concentrations stimulate the degradation process. The thermal behaviour (heat generation) and chemical composition (stability composition) of the propellant show similar tendencies with respect to the thermal degradation process. The strong influence of environmental conditions emphasizes that a comparison between experiments is only acceptable if similar conditions are used in the experiments.

The oxygen concentration appears to have no influence on the "overall" activation energy, thus indicating that the rate-determining step of the reaction mechanism is not affected.

Moisture in the propellant affects the rate-determining step of the reaction mechanism. This may be caused by an increase in local activity, changes in mass transfer, etc.

From the observations it may be concluded that the pattern of the reactions of nitrogen dioxide and DPA (and derivatives) only shows a small and gradual shift for increasing temperatures.

The thermal stability of the propellant is influenced by both the thermal effect and this small shift in pattern.

5. REFERENCES

1. J.L.C. van Geel and J. Verhoeff, 4th. Symp. on Chem. Problems connected with the stability of explosives, Sektionen för Detonik och Förbränning, Sweden, 1976
2. F. Volk, Prop. Expl., 1, (1976), 90
3. A. Alm, Chem. Probl. connected with the stability of explosives, Sektionen för Detonik och Förbränning, Sweden, 1968

4. J. Opschoor, A.H. Heemskerk, J. Verhoeff, H.J. Pasma,
14th. Int. Jahrestagung JCT, 1983.
5. R.U.E. 't Lam and A.H. Heemskerk,
7th. Symp. on Chem Problems connected with the stability of explosives,
Sektionen für Detonik och Förbränning, Sweden 1985.

BURNING STABILITY OF
DOUBLE BASE PROPELLANTS

by

L. De Luca, C. Zanotti, G. Riva, R. Dondé, A. Volpi, C. Grimaldi, and G. Colombo.
CNPM, Consiglio Nazionale delle Ricerche

and

Dipartimento di Energetica, Politecnico di Milano
32, Piazza Leonardo da Vinci, 20133 Milano, Italy.

SUMMARY

The nonsteady combustion and intrinsic burning stability of double base propellants are studied. Experimental results show that, over a large pressure range, the energetics and the dynamics of double base combustion is controlled by the fizz zone. This permits the classical quasi-steady gas phase assumption to be applied. However, a novel transient flame model is required, since the fizz zone, although thin in time, is thick in space. This novel transient flame model includes several previous models as particular cases; in addition it allows an already existing nonlinear burning stability theory to be immediately applied to double base combustion. Several analytical predictions are presented and some experimental validations discussed. In general, double base burning is found to be less stable than composite propellant burning, both statically and dynamically. This is due to the relatively little energy stored in the condensed phase and elongated fizz zone yielding a weak energy coupling at the burning surface.

LIST OF SYMBOLS

c	= specific heat, cal/g K
C	= c/c_{ref} , nondim. specific heat
d	= thickness, cm
E	= activation energy, cal/mole
$E(\cdot)$	= $E/\bar{Q}T(\cdot)_{ref}$, nondim. activation energy
$f(X,\lambda)$	= nondim. function depending on the optical properties of condensed phase and external radiation source
F_o	= I_o/ϕ_{ref} , nondim. external radiant flux
H	= Q/Q_{ref} , nondim. heat release
I_o	= external radiant flux, cal/cm ² s
k	= thermal conductivity, cal/cm s K
K	= k/k_{ref} , nondim. thermal conductivity
M	= parameter of a transient flame model (see Sec. 4)
n	= ballistic exponent
n_s	= pressure exponent in the pyrolysis law
p	= pressure, atm
p_{ref}	= 68 atm, reference pressure
P	= p/p_{ref} , nondim. pressure
q	= ϕ/ϕ_{ref} , nondim. energy flux
Q	= heat release, cal/g (positive exothermic)
Q_{ref}	= $c_{ref}(T_{s,ref}-T_{ref})$, reference heat release, cal/g
r_b	= burning rate, cm/s
$r_{b,ref}$	= $r_b(p_{ref})$, reference burning rate, cm/s
\bar{r}_λ	= average optical reflectivity of the burning surface, %
R	= $r_b/r_{b,ref}$, nondim. burning rate
t	= time, s
T	= temperature, K
T_{ref}	= 300 K, reference temperature
$T_{s,ref}$	= $T_s(p_{ref})$, reference surface temperature, K
u	= gas velocity, cm/s
w	= power of pyrolysis law
\bar{W}	= molecular weight of the gas mixture, g/mole
x	= space variable, cm

$X = x / (\alpha_{ref} / r_{b,ref})$, nondim. space variable

Greek Symbols

α = thermal diffusivity, cm^2/s ; also: parameter of a transient flame model (see Sec.4)
 β = parameter of a transient flame model (see Sec. 4)
 γ = parameter of a transient flame model (see Sec. 4)
 δ = $d / (\alpha_{ref} / r_{b,ref})$, nondim. thickness
 ϵ = nondim. reaction rate
 $\bar{\epsilon}_\lambda$ = average optical emissivity of the burning surface, %
 θ = $(T - T_{ref}) / (T_{s,ref} - T_{ref})$, nondim. temperature
 $T(\)$ = $T(\) / T(\),_{ref}$, nondim. temperature
 λ = wavelength, μm
 σ = 1.37×10^{-12} $\text{cal}/\text{cm}^2 \text{s K}^4$, Stefan-Boltzmann constant
 τ = $t / (\alpha_{ref} / r_{b,ref}^2)$, nondim. time
 \dot{q} = $Q_f \rho_g \tilde{e}_g$, heat release rate per unit volume, $\text{cal}/\text{cm}^3 \text{s}$
 \dot{q}_{ref} = $\rho_c c_{ref} r_{b,ref} (T_{s,ref} - T_{ref})$, reference energy flux, $\text{cal}/\text{cm}^2 \text{s}$

Subscripts and Superscripts

c = condensed phase
dz = dark zone
f = flame
fz = fizz zone
g = gas phase
out = out from the system
s = burning surface
c,s = burning surface, condensed phase side
g,s = burning surface, gas phase side
ref = reference
 λ = spectral
 $\langle \ \rangle$ = average value
- = steady state
o = at the burning surface
 $-\infty$ = far upstream
~ = dimensional value

Abbreviations

AP = Ammonium Perchlorate (NH_4ClO_4)
DB = Double Base
KTSS = Krier-T'ien-Sirignano-Summerfield
KZ = Kooker-Zinn
LC = Levine-Culick
MTS = Merkle-Turk-Summerfield
PDL = Pressure Deflagration Limit

1 - BACKGROUND

Double base (DB) propellants are still widely used in solid rocket propulsion, both as main component or in combination with more energetic ingredients. A particular advantage of DB propellants is that tailoring of the burning rate vs pressure is easily feasible by means of appropriate small amount of special additives called (burning rate) catalysts. Although this technology goes back to the '40s, the scientific understanding of transient burning and combustion stability of DB compositions (catalyzed or uncatalyzed) is poor.

Many factors can be invoked to excuse this lack of understanding, but of paramount importance appears the non availability of an appropriate transient flame model. It may be surprising that such models, instead, do exist for composite propellants, distinctly of much more complex structure in the condensed phase. The reason is the fact the flames associated with composite propellants are thin in space and time (compared with the corresponding condensed phase quantities) under most operating conditions. This allows the quasi-steady gas phase assumption to be implemented. A tacit corollary also follows: the specific space distribution of the gas phase heat release is inessential, since heat release occurs any way near the burning surface. Consequently, many researchers successfully followed the initial suggestion by Summerfield and coworkers (Ref. 1) of a uniform distribution of heat release in a spacewise thin layer adjacent to the burning surface (Refs.2-3).

Another line of modeling, based on Dirac function (Refs. 4-5), will be discussed later.

For double base propellants the physical picture is different. For standard compositions, up to 100 atm, the overall flame appears with a well defined structure (see Fig. 1) and rather thick both in space as well time. The frequent addition of catalysts makes even more complicated the microscopic structure of the issuing flame, especially very near the burning surface, but does not affect its overall look. What are the effects of such a complex and thick structure on the dynamic burning of DB propellants? How is their (intrinsic) combustion stability affected?

In order to answer these questions, the basic physical picture has to be understood and accounted for. Then, the main purpose of this paper is to predict dynamic burning and combustion stability features of DB propellants by properly modeling the associated transient flame. To reach this objective, first the steady flame structure of DB propellants shall be defined experimentally (Sec. 2), consequently assumptions and governing equations shall shortly be revised (Sec. 3), while a more detailed exposure shall be provided of the proposed new transient flame model (Sec. 4). At this point, the overall approach can rest on a firm ground (Refs. 6-12): a nonlinear burning stability theory, already reasonably well established for composite propellants, can easily be extended to DB propellants (Sec. 5). Numerical validation of this analytical procedure shall not be repeated here, since literally hundreds of tests were successfully performed by this research group in the past (Ref. 12). Experimental validation of dynamic stability, for a matter of time, is limited to fast depressurization tests (Sec. 6); other dynamic burning tests are in progress. Conclusions (Sec. 7) and Future Work (Sec. 8) will end this paper.

To avoid a misunderstanding commonly encountered in this line of research, it is emphasized that nonlinear burning stability analyses by definition require modeling of transient flames. Steady state combustion is incorporated in the transient flame model by means of experimental information. It is also emphasized that this research group (e.g., Refs. 6-12) for more than a decade has been putting forward a general nonlinear burning stability theory (including as special problems oscillatory combustion, pressure deflagration limit, dynamic extinction by depressurization or deradiation, and so on) based on fundamental thermokinetic processes, not ad hoc mechanisms for each specific problem.

2 - FLAME STRUCTURE OF DOUBLE BASE PROPELLANTS

The typical aspect of a DB propellant combustion wave, propagating under steady conditions, is well known: the qualitative sketch of Fig. 1 underlines the existence of a complex multi-zone flame structure. A large number of experimental investigations was carried out, over several decades, to define the relevant parameters of DB burning in a wide range of operating conditions; for a good summary, Ref. 13 is recommended. In spite of that, the comprehension of what are the really important aspects of DB flame structure is still unsatisfactory.

In this section, significant experimental data collected in this laboratory are summarized. The specific intent was to make available enough experimental information to formulate a transient flame model appropriate for DB burning. Several diagnostic techniques under steady burning were implemented. Steady burning rates were measured, in three different combustion chambers, over the pressure range 0.1 to 250 atm by nonintrusive optical methods. Steady thermal profiles were collected, over the pressure range 0.1 to 38 atm, by microthermocouples imbedded in the propellant sample. Steady gas velocities in the dark zone were measured, over the pressure range 10 to 35 atm, by means of a LDV system.

The solid propellant under examination was mainly a catalyzed DB composition of current production by a national manufacturer. Unfortunately, we are not permitted to publish its composition (unknown even to the authors) and the relevant quantitative data measured in this laboratory. However, our experimental results do not differ from others reported in the open literature. The important remark in our opinion is that properly analyzing and contrasting data sets, collected by different experimental techniques, substantially helps in locating where (and hopefully understanding how) controlling mechanisms occur.

Electrically welded Pt/Pt-Rh microthermocouples with a bead down to 5 μm were used; signals were digitally recorded. A typical output is shown in Fig. 2 (the associated curve will be discussed later). The gas phase thermal profiles were corrected by the radiative heat losses from the hot bead toward the cold surroundings. From microthermocouple recordings one can evaluate in particular the surface temperature T_s , the dark zone temperature T_{dz} , and the thickness of the relevant zones both in the condensed and gaseous phases. Although quite delicate, one can also estimate the thermal gradient at the gas phase side $(dT/dx)_{g,s}$ of the burning surface. From the ensemble of these steady

state measurements, one can reconstruct the detailed steady state energetics of the combustion wave within reasonable bounds. Since the dark zone features a constant temperature profile, the luminous zone is effectively filtered away from the burning surface up to at least 150 atm for the tested composition. This well known result (e.g., consult Ref.13) allows our attention to be focused on the fizz zone.

Nevertheless, the dark zone deserves some attention because, being isothermal and very thick in space, permits convenient experimental diagnoses. Of course, dark zone experimental data provide an upper or lower boundary (depending on the measured quantity) for the fizz zone experimental data. Typically, a LDV system, based on a 15 mW He-Ne laser emitting at 632.8 nm, produced significant results when probing in the dark zone but not in the fizz zone. Both the gas velocity in the dark zone (Fig. 3) and the actual thickness of the dark zone could be easily obtained in the pressure range 10 to 35 atm.

Combining burning rate, temperature, and gas velocity data, it is straightforward to obtain the characteristic times plotted in Fig. 4 for the condensed phase ($t_c = d_c / \bar{u}_b$), the fizz zone ($t_{fz} = d_{fz} / \langle u_{fz} \rangle$), and the dark zone ($t_{dz} = d_{dz} / \bar{u}_{dz}$). It should be noted that d_c and d_{fz} are the thicknesses of the condensed phase thermal layer and the fizz zone thermal layer, defined as the distance to travel away from the burning surface to recover 95% of the corresponding temperature excursion. On the contrary, d_{dz} is the actual thickness of the dark zone measured by LDV. The quantity $\langle u_{fz} \rangle$ is the average gas velocity in the fizz zone obtained as $(\bar{u}_s + \bar{u}_{dz})/2$, being \bar{u}_{dz} measured by LDV and \bar{u}_s the gas velocity just downstream of the burning surface computed from mass conservation combined with state equation.

The basic message contained in Fig. 4 is that the characteristic time of the fizz zone is orders of magnitude smaller than the characteristic time of the condensed phase. Since the fizz zone is the controlling sub-structure for the energetics of the overall combustion wave, the results of Fig. 4 allow the classical quasi-steady gas phase assumption to be applied to DB burning. This is a robust conclusion.

From this point on, only fizz zone will be dealt with. Dark zone and luminous zone will be put aside. Flame model for a DB actually means fizz zone model.

3 - ASSUMPTIONS AND GOVERNING EQUATIONS

Consider a strand of solid material burning, without velocity coupling, in a vessel at uniform pressure and subjected to a radiant flux originated exclusively from a continuous wave external source. Assume monodimensional processes, no radiation scattering, no photochemistry, and irreversible gasification at the burning surface. For nondimensionalizing take as reference values those associated with the conductive thermal wave in the condensed phase at 68 atm and adiabatic combustion. Define a cartesian x-axis with its origin anchored at the burning surface.

The nondimensional energy equation in the condensed phase ($X \leq 0, \tau \geq 0$) is:

$$(3.1) \quad C_c \left(\frac{\partial \theta}{\partial \tau} + R \frac{\partial \theta}{\partial X} \right) = \frac{\partial}{\partial X} \left(K_c \frac{\partial \theta}{\partial X} \right) + F_o f(X, \lambda)$$

$$(3.2) \quad \theta(X, \tau=0) = \bar{\theta}(X)$$

$$(3.3) \quad \theta(X \rightarrow -\infty, \tau) = \theta_{-\infty}$$

$$(3.4) \quad \left(K \frac{\partial \theta}{\partial X} \right)_{c,s} = \left(K \frac{\partial \theta}{\partial X} \right)_{g,s} + RH_s - q_{out}(\theta_s)$$

where $C_c(\theta)$ and $K_c(\theta)$ are arbitrarily assigned temperature dependent specific heat and thermal conductivity; $f(X, \lambda)$ is an arbitrarily assigned function depending on the optical properties of the condensed phase and nature of the (external) radiation source; $\bar{\theta}(X)$ is the initial steady temperature profile.

The heat release at the burning surface is:

$$(3.5) \quad H_s(P, \theta_s) = \bar{H}_s(P) - \int_{\bar{\theta}_s}^{\theta_s} C_c(\theta) d\theta + C_g (\bar{\theta}_s - \theta_s)$$

where $\bar{H}_s(P)$ is the nondimensional heat release at the operating pressure under steady conditions. The pressure dependent pyrolysis law at the burning surface is assumed as follows:

$$(3.6) \quad R = P^{n_s} \exp \left\{ -E_s \left(\frac{1}{T_s} - 1 \right) \right\} \quad T_s \geq T_K$$

$$(3.7) \quad R = P^{n_s} \left(\frac{T_s - T_m}{1 - T_m} \right)^w \quad T_k > T_s > T_m$$

$$(3.8) \quad R = 0 \quad T_m > T_s \geq 0$$

where E_s and n_s are determined by the best fitting of experimental data, under steady and adiabatic burning, over the available pressure range.

The term q_{out} in this report accounts only for radiative heat loss from the burning surface

$$(3.9) \quad q_{out}(\theta_s) = \bar{\epsilon}_\lambda \frac{\sigma (T_s^4 - T_\infty^4)}{\phi_{ref}}$$

Usually, the average emissivity of the burning surface was taken as $\bar{\epsilon}_\lambda = 0.75$. But analytical predictions and numerical results showed vanishing influences of the radiative heat loss even for $\bar{\epsilon}_\lambda = 1$. The heat feedback from the gas phase to the burning surface $(K \partial\theta/\partial X)_{g,s}$ will be discussed in Section 4.

4 - A FAMILY OF TRANSIENT FLAME MODELS

As a preliminary remark, recall that "flame" actually means fizz zone for DB burning (see Sec. 2). For any flame behaving according to the quasi-steady gas phase assumption, the nondimensional energy equation is:

$$(4.1) \quad \frac{\partial^2 \theta}{\partial X^2} - R \frac{C_g}{K_g} \frac{\partial \theta}{\partial X} + \frac{H_f}{K_g} \frac{\rho_g}{\rho_c} \epsilon_g = 0$$

where $\epsilon_g \rho_g / \rho_c$ is the mass reaction rate per unit volume. A formal integration provides the conductive heat feedback from the gas phase to the burning surface

$$(4.2) \quad q_{g,s}(P,R) \equiv (K \frac{\partial \theta}{\partial X})_{g,s} = \int_0^{X_f} H_f \epsilon_g \frac{\rho_g}{\rho_c} \exp(-\frac{C_g}{g} RX) dX,$$

where the usual assumption is made that

$$(4.3) \quad (\partial\theta/\partial X)_{g,s} \gg (\partial\theta/\partial X)_f \exp(-R^2 \langle \tau'_f \rangle).$$

The quantity $\langle \tau'_f \rangle$ is an average time parameter of the flame, conveniently defined (Ref.4) as

$$(4.4) \quad \langle \tau'_f \rangle \equiv \tau_f \frac{C_g}{K_g} \frac{\rho_c}{\langle \rho_g \rangle}$$

where τ_f is the residence time in the flame. Resorting to the quasi-steady mass conservation in the gas phase, one finds

$$(4.5) \quad \tau_f \equiv \frac{X_f}{\langle U \rangle} = \frac{X_f}{R} \frac{\langle \rho_g \rangle}{\rho_c} \quad \text{and}$$

$$(4.6) \quad \langle \tau'_f \rangle = \frac{C_g}{K_g} \frac{X_f}{R}.$$

It should be clear that the formal integration of Eq. 4.2 holds true for any integrable expression of the heat release rate $H_f \epsilon_g \rho_g / \rho_c$. How can this quantity be modeled? Looking back in the literature one can distinguish two main avenues: several models (notably KTSS, KZ, and LC respectively reported in Refs. 1-3) assume a spatially thin reacting region, of constant heat release rate, attached to the burning surface ("anchored flames"); other models (Ref. 5) assume a "flame sheet" (mathematically described by a Dirac function and therefore implying a reacting region of vanishing thickness)

located somewhere in the gaseous region. Other models, notably MTS (Ref. 4), assume a weighted combination of the two flames. Experimental evidence shows that both kinds of model yield a qualitatively wrong temperature distribution in the flame. In particular, a large collection of temperature profiles from this research group and a wealth of other laboratories (e.g., consult Refs. 13-14) consistently shows a convex temperature distribution, increasing more and more slowly while approaching the maximum value (see Fig. 2). Yet, anchored flame models essentially predict a linear temperature distribution, while flame sheet models predict a concave temperature distribution. In addition, if we conventionally define the flame thickness as the distance to travel from the burning surface to reach $0.95 (T_f - T_g)$, it turns out that the flame thicknesses experimentally evaluated are much larger than the values predicted by anchored flame models. In the case of flame sheet models, the reacting region is vanishingly small while, at least in principle, the maximum temperature point can be located anywhere (but usually is placed at a distance from the burning surface even shorter than for anchored flames).

To understand the reason of these obvious discrepancies between the experimental picture and the available transient flame models, the steady heat release distribution $\dot{q}(x) = Q_f \rho_g \dot{\epsilon}_g$ was worked back, according to Eq. 4.1, from several experimental temperature profiles, collected under steady burning of the tested propellant. It should be obvious that any transient flame model should recover steady state results as a particular case. An example of this exercise is shown in Fig. 2. The general trend of this and other heat release profiles is that, while a large fraction of the totally available energy is deposited very close to the burning surface, an equally important remaining fraction is delivered in a long tail elongating relatively far from the burning surface. This "comet effect" is totally missing in the current transient flame models: anchored flames overestimate the importance of the heat release near the burning surface by compressing the tail into the head of the comet, while flame sheets feature just the opposite effect than the comet picture (concentrated rather than distributed heat release).

Dramatic consequences of the implemented heat release profile can be perceived under most nonlinear dynamic burning conditions. In general, combustion stability is vigorous for anchored flames assuring a strong energetic coupling at the burning surface, whereas it is just fair for distributed flames with a long tail capable to assure only a weak energetic coupling at the burning surface; for flame sheets, combustion stability depends on where the Dirac function is located. For example, dynamic extinction by depressurization is much easier for flames with a long tail than for anchored flames.

The distinct feature of DB burning is that the fizz zone, although thin in time, is thick in space due to its long tail. How can we model flames with elongated tail? An overall mechanism will do it, as usual. Considering the nature of the experimental temperature profiles collected in this laboratory and some hints from the literature (of particular importance being an excellent contribution by Zenin in Ref. 15), the following nonuniform heat release distribution (see Fig. 5), containing the essential structure of elongated flames, is proposed:

$$(4.7) \quad H_f \epsilon_g \frac{\rho_g}{\rho_c} = \begin{cases} H_f M \left(\beta + \frac{1-\beta}{\alpha} \frac{X}{X_f} \right) & 0 < X < \alpha X_f \\ H_f M \left(\frac{1-X/X_f}{1-\alpha} \right)^\gamma & \alpha X_f \leq X < X_f \end{cases}$$

where M is the maximum value of the reaction rate, α gives the fraction of the flame thickness at which this maximum value occurs, β gives the reaction rate at the burning surface ($X=0^+$) as a fraction of the maximum value M , γ is a power describing quantitatively the tail of the heat release profile. By definition

$$0 \leq \alpha \leq 1 \quad \text{and} \quad 0 \leq \beta \leq 1,$$

while mass conservation requires

$$(4.8) \quad M(\tau) = \frac{\gamma+1}{1 + \alpha \frac{\beta(\gamma+1) + \gamma - 1}{2}} \frac{R(\tau)}{X_f(\tau)}.$$

Remark that for $\alpha=\beta=1$ (for this combination γ becomes irrelevant), the proposed transient flame model recovers the nonlinear versions of KTSS, KZ, and LC models as particular cases. Among the three parameters introduced (α, β, γ), γ is the most important; α and β will only occasionally be used in this paper to compare results with anchored flames. In general $\gamma = \gamma(P)$, in such a way that X_f follows the trend experimentally observed by microthermocouples. In this paper, $\gamma=3$ already gives results overall very satisfactory. Remark

that the flame thickness predicted by elongated flame models is $\gamma+1$ times larger than the thickness predicted by anchored flame models.

Substituting into Eq. 4.2 and integrating, one finds for the heat feedback

$$(4.9) \quad u_{g,s}(P,R) = \frac{H_f(P, \theta_{-\infty})}{X_f(\tau; P, \theta_{-\infty})} \frac{K_g}{C_g} \frac{\gamma+1}{1 + \alpha \frac{\beta(\gamma+1)+\gamma-1}{2}} F(\alpha, \beta, \gamma; R^2 \langle \tau'_f \rangle)$$

where

$$(4.10) \quad F(\alpha, \beta, \gamma; R^2 \langle \tau'_f \rangle) = \beta + \frac{1-\beta}{\alpha R^2 \langle \tau'_f \rangle} - \frac{(-1)^\gamma \gamma!}{(1-\alpha)^\gamma (R^2 \langle \tau'_f \rangle)^\gamma} \exp(-R^2 \langle \tau'_f \rangle) + \\ + \left[\sum_{i=1}^{\gamma} (-1)^i \frac{\gamma!}{(\gamma-i)! (1-\alpha)^i (R^2 \langle \tau'_f \rangle)^i} - \frac{1-\beta}{\alpha R^2 \langle \tau'_f \rangle} \right] \exp(-\alpha R^2 \langle \tau'_f \rangle)$$

Examples of steady temperature profiles computed according to Eqs 4.7-4.8 are shown in Fig. 6, contrasted with some profiles computed according to anchored flame models. The tail elongation can be adjusted closely to the experimental value, but for the sake of simplicity in this paper only $\gamma=3$ is used.

As to the characteristic time (or time parameter) of the flame, the usual approach is to consider only their pressure dependence, assumed to be the same (whatever this is) under steady or transient conditions. Actually, it is physically obvious that the characteristic time also will undergo dynamic effects, especially due to transient temperature effects on chemical kinetics. Only MTS model (Ref. 4) clearly recognized this and explicitly enforced pressure and temperature dependence for its relevant characteristic times (mass diffusion and chemical kinetics). In this work, first $\tau_f(P)$ was implemented and then $\tau_f(P, \theta)$: the overall effect is that $\tau_f(P, \theta)$ further reduces combustion stability, both statically and dynamically.

A gas phase working map can now be constructed easily, as shown in Fig. 7. A comparison with anchored flames is presented at 30 atm, suggesting that KTSS or KZ or LC flames for an identical set of data predict a larger (or smaller) heat feedback for the same decrease (or increase) of the burning rate from its steady value. This implies a stronger combustion stability for KTSS or KZ or LC flames rather than elongated flames with $\gamma=3$. As a further remark, note that reaching the static burning limit requires an heat loss of 149 cal/cm²s for elongated flames with $\gamma=3$, a value rather small compared with those obtained by implementing anchored flames (e.g., consult Ref. 12).

5 - NONLINEAR STABILITY

Having reduced the flame of DB propellants to the fizz zone only (in that, dark zone and luminous zone are in no way controlling steps for the tested DB composition up to at least 150 atm) and having modeled the elongated flame representative of the fizz zone, the nonlinear burning stability analysis of DB propellants is now a straightforward matter. The theory is exactly that already developed, under broad provisions, for unmetallized AP-based composite propellants (Refs. 6-7): the only essential assumption is that of quasi-steady gas phase (namely the fizz zone in the case of DB propellants).

An approximate analytical procedure, fully preserving the strong nonlinearity of the problem, allows the stability properties buried in the set of equations of Secs 3-4 to be unfolded. The mathematical technique and its numerical validation were extensively discussed in a recent report (Ref. 12) and will not be repeated here; the basic ideas can also be found in a bunch of published papers (e.g., see Refs. 6-11). It is only recalled that this analysis sheds light on both static burning stability (the capability of a given steady burning configuration to keep itself unchanged in time) and dynamic burning stability (the capability of a burning propellant to avoid unwanted extinction).

Results can be conveniently expressed by means of bifurcation diagrams, where the abscissa is the parameter of interest (pressure or heat release or activation energy and so on) and the ordinate is the surface temperature (taken as representative of the combustion event). A bifurcation diagram for the surface heat release Q_s is shown in Fig. 8, suggesting at 30 atm the existence of time-invariant steady solution for $Q_s < 117$ cal/g, self-sustained steady solution for 117 cal/g $< Q_s < 124$ cal/g and just no possible steady solution for $Q_s > 124$ cal/g. The special value $Q_s = 117$ cal/g, for which the steady solution bifurcates (i.e., changes its character from time-invariant to self-sustained oscillation).

tory) is called the bifurcation value of Q_S at 30 atm. The lower branch of the S-shaped curve defines the dynamic extinction boundary: when the surface temperature drops even momentarily below this boundary extinction necessarily follows for monotonic decreases of the forcing function (e.g., dynamic extinction by depressurization when pressure is the forcing function). Similar remarks hold true at 70 atm, with the only significant difference that the bifurcation value is larger (129 cal/g), implying a stronger static burning stability of the tested DB composition for increasing pressure.

Another bifurcation diagram is shown in Fig. 9 for the operating pressure p . This plot shows that the DB propellant under scrutiny is statically stable over a very large pressure range, including atmospheric pressure. Some limited static combustion instability is suggested only around 0.1 atm; however, the validity of the overall model in such a low pressure range is doubtful and in any event not sought for. On the contrary, the dynamic extinction limit (again given by the lower branch of S-shaped curve) is surprisingly large. This suggests a weak resistance to dynamic extinction, for example as compared to AP-based composite propellants.

A third bifurcation diagram is shown in Fig. 10 for the effects of the dark zone temperature (or end fizz zone temperature) at 30 and 70 atm. The surprising (perhaps) prediction is that, for T_{dz} values sufficiently low (below 1010 K at 70 atm or 965 K at 30 atm), steady burning becomes statically unstable and only the extinguished state is allowed as a steady solution. The reason of this dramatic effect is that, for T_{dz} decreasing, Q_{fz} decreases (being T_g and Q_S kept constant); therefore limiting lower values of T_{dz} are actually limiting lower values of Q_{fz} (respectively about 200 cal/g and 170 cal/g at 70 and 30 atm). The experimentally evaluated values of T_{dz} are around 1700 K. These analytical predictions were successfully confirmed by direct numerical integration of the governing set of equations.

For a matter of space, this section is not further developed. The basic message is that the broad theory reasonably established for heterogeneous thin flames (Refs. 6-12) is fully exploitable, once a proper flame model is implemented for the fizz zone of DB propellants. In particular, the effects on static and dynamic burning stability of any parameter of interest can be easily assessed, as shown in Figs. 8-10. Moreover, comparisons between different classes of solid propellants can be easily carried out (e.g., DB against AP-based composite propellants) if only the appropriate transient flame models and sets of thermophysical data are implemented.

6 - EXPERIMENTAL VALIDATION

Experimental validation of a burning stability theory is usually immediate for its static part, but quite complex for its dynamic part. For example, the sheer fact that steady combustion of the tested DB composition is time-invariant for a pressure range extending at least from atmospheric to 150 atm fully confirms the analytical predictions graphically shown in Fig. 9. In particular, steady combustion of the tested DB composition is time-invariant at 30 atm, just as expected from the analytical predictions of Fig. 8, being $Q_S = 91$ cal/g less than the bifurcation value (≈ 117 cal/g) at 30 atm. Likewise, at 70 atm $Q_S = 98$ cal/g is less than the bifurcation value (≈ 129 cal/g) at that pressure and therefore the steady combustion of the tested DB composition is expected to be time-invariant, just as experimentally observed. Similar remarks hold true for the analytical predictions of Fig. 10.

As to the static burning stability, another property that this theoretical approach is in principle capable to predict is the pressure deflagration limit (PDL) of a solid propellant (Refs. 10-11). For the tested DB composition, the analytical results graphically shown in Fig. 9 predict a PDL ≈ 0.03 atm. Although we are very skeptical about the applicability of the physical model (not of the stability theory) in such a marginal pressure range, it is however reassuring that the tested DB composition was burnt without problems down to 0.1 atm.

Testing dynamic burning stability is very difficult, because one should measure unsteady burning rate under widely changing operating conditions. An alternative experimental approach that this research group has found convenient to exploit over the years is the go/no-go depressurization test (Refs. 8-9). This procedure is relatively easy to perform, if well realized it yields unequivocal results (dynamic extinction or continued burning), is equally applicable to all propellants, probes the dynamic as well as static burning behavior over a large pressure interval, and finally is a direct test of a very sensitive result of the whole burning stability theory: the existence of a dynamic extinction limit as a property of the solid propellant. The analytical predictions for the tested DB composition are shown in Fig. 9 and were shortly discussed in Sec. 5. It is important to remark that the theory predicts the overall effect of the crossing of the dynamic extinction boundary (extinction or burning), but not the instantaneous values of burning rate.

Experimental results of go/no-go depressurization tests were collected with an apparatus similar to that fully described in Ref. 8. For the time being, available results include runs from an initial pressure 15 to 70 atm to final pressure 1 atm, as shown in Fig. 11. The experimental go/no-go boundary, separating an upper region of dynamic extinction from a lower region of continued burning, is a straight line. A similar result was found for unmetallized AP-based composite propellants (Refs. 8-9), but the maximum depressurization rate required for extinction was about twice as large that required for extinction of the tested DB composition. Numerical results, obtained by implementing an elongated flame model with $\gamma=3$ and a fizz zone characteristic time depending both on pressure and temperature, feature a good agreement. Other numerical results, obtained by implementing an elongated flame model with $\gamma=1$ and a fizz zone characteristic time depending on pressure and temperature according to a different formalism, feature a less satisfactory agreement especially for large values of the initial pressure.

It may be of interest to know that further numerical results, obtained by implementing a nonlinear version of KZ flame model with a fizz zone characteristic time depending only on pressure, gave bad results, as shown again in Fig. 11. As matter of fact, KZ flame model, although initially proposed specifically for DB propellants, is just a special case of anchored flame (constant heat release, attached to the burning surface). Consequently, the flame is spatially very thin but vigorous and the energetic coupling at the burning surface very strong. This in turn requires an excessively large depressurization rate to produce extinction.

7 - CONCLUSIONS

Flames of DB propellants are thick in space and time. However, for pressures up to at least 100 atm with standard compositions, the energetics of the heterogenous combustion wave associated with DB propellants is controlled by the fizz zone and its dynamics can be described by treating the fizz zone as quasi-steady. The fizz zone features complex chemical patterns yielding a reactive region with an elongated tail (comet-like flame, thin in time but not in space). After properly modeling this flame, the overall problem of DB burning stability is reduced to applying an already established mathematical approach.

A systematic predictive analysis at this point reveals that burning of DB is in general less stable than burning of composite AP-based propellants. At least two reasons conspire against DB burning stability: thermophysical properties are such that relatively little energy is stored in the condensed phase and the energy coupling at the burning surface is weak due to the elongated structure of the fizz zone. A third reason adding against DB burning stability is the probable presence of important chemical reactions distributed in the condensed phase; for a matter of time, the relative weight of this third factor has yet to be assessed.

The analytical predictions are fully supported by direct numerical integration of the governing set of equations and the experimental results so far collected.

8 - FUTURE WORK

Experimentally, a wide program is under progress to both define the steady state combustion properties and verify the burning stability of DB compositions.

Theoretically, several formalisms are under study to evaluate with some accuracy the pressure and temperature dependence of the fizz zone characteristic time.

Numerically, extension of the integration technique to two-dimensional configuration is under consideration.

REFERENCES

1. Krier H., T'ien J.S., Sirignano W.A., and Summerfield M., "Nonsteady Burning Phenomena of Solid Propellants: Theory and Experiments", AIAA J., Vol. 6, No. 2 pp. 278-285, 1968.
2. Kooker D.E. and Zinn B.T., "Numerical Investigation of Nonlinear Axial Instabilities in Solid Rocket Motors", BRL Contract Report No. 141, March 1974.
3. Levine J.N. and Culick F.E.C., "Nonlinear Analysis of Solid Rocket Combustion Instability", AFRPL TR-74-75, October 1974.

4. Merkle C.L., Turk S.L., and Summerfield M., "Extinguishment of Solid Propellant by Rapid Depressurization", Princeton University, AMS Report No. 880, 1969.
5. Cohen N.S. and Strand L.D., "Analytical Model of High Pressure Burning Rates in a Transient Environment", AIAA Journal, Vol. 18, No. 8, pp. 968-972, 1980.
6. De Luca L., "Nonlinear Burning Stability Theory of Heterogeneous Thin Flames", XVIII International Symposium on Combustion, University of Waterloo, Canada, 17-22 August 1980. Proceedings, pp. 1439-1450, 1981.
7. De Luca L., Riva G., and Bruno C., "Bifurcation in Heterogeneous Combustion", NATO Advanced Study Institute on Non-Equilibrium Cooperative Phenomena in Physics and Related Fields, Madrid, Spain, 1-11 August 1983. Proceedings, Plenum Press, pp. 339-348, 1984.
8. Dondé R., Riva G., and De Luca L., "Experimental and Theoretical Extinction of Solid Rocket Propellants by Fast Depressurization", XXXIII International Astronautical Federation Congress, Paris, France, 26 September-3 October 1982. IAF Paper 82-361. Acta Astronautica, Vol. 11, No. 9, pp. 569-576, 1984.
9. De Luca L., "Extinction Theories and Experiments", Progress in Astronautics and Aeronautics, Vol. 90, FUNDAMENTALS OF SOLID PROPELLANT COMBUSTION, Kuo K.K. and Summerfield M. editors, pp. 661-732, 1984.
10. Bruno C., Riva G., Zanotti C., Dondé R., Grimaldi C., and De Luca L., "Experimental and Theoretical Burning of Solid Rocket Propellants Near the Pressure Deflagration Limit", XXXIV International Astronautical Federation Congress, Budapest, Hungary, 10-15 October 1983. IAF Paper 83-367. Acta Astronautica, Vol. 12, No. 5, pp. 351-360, 1985.
11. De Luca L., Riva G., Zanotti C., Dondé R., Lapegna V., and Oleari A., "The Pressure Deflagration Limit of Solid Rocket Propellants", The Propulsion and Energetics Panel of AGARD, 63rd Meeting on Hazard Studies for Solid Propellant Rocket Motors, Lisse, Netherlands, 28-30 May 1984. AGARD Conference Proceedings No. 367, pp. 22/1-22/16, September 1984.
12. De Luca L., Riva G., and Zanotti C., "Nonlinear Burning Stability of Solid Propellants", Final Technical Report to European Research Office, Contract No. DAJA37-81-C-0215, Dipartimento di Energetica, Politecnico di Milano, December 1983.
13. Lengellé G., Bizot A., Dutergue J., and Trubert J.F., "Steady State Burning of Homogeneous Propellants", Progress in Astronautics and Aeronautics, Vol. 90, FUNDAMENTALS OF SOLID PROPELLANT COMBUSTION, Kuo K.K. and Summerfield M. editors, pp. 361-407, 1984.
14. Kubota N., "Determination of Plateau Burning Effect of Catalyzed Double-Base Propellant", XVII International Symposium on Combustion, The University of Leeds, England, 20-25 August 1978. Proceedings, pp. 1435-1441, 1979.
15. Zenin A.A., "Universal Dependence for Heat Liberation in the K-Phase and Gas Macrokinetics in Ballistic Powder Combustion", FGV, Vol. 9, No. 4, pp. 78-81, 1983.

ACKNOWLEDGMENTS

The authors wish to express their sincere gratitude to ing. M. Casarini and Mr. C. Liperi for help in reducing the experimental data. In addition, the senior author gratefully acknowledges the long discussions with and many suggestions by prof. M. Summerfield. The solid rocket propellant used for experimental tests was courteously provided by SNIA BPD.

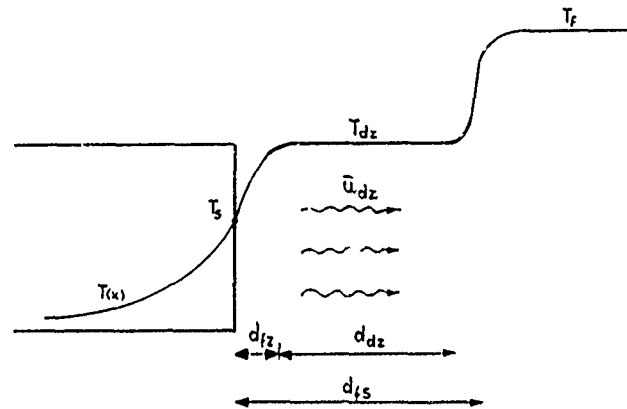


Fig. 1 - Qualitative sketch of the complex multi-zone flame structure associated with the combustion of double base propellants.

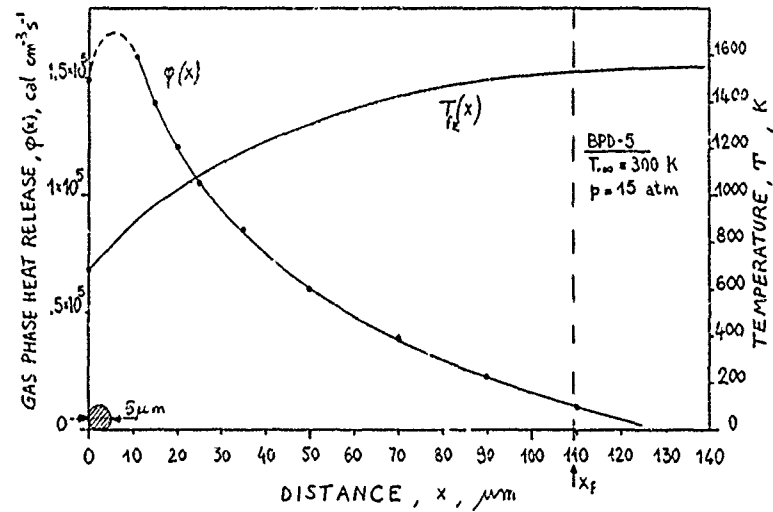


Fig. 2 - Steady temperature and heat release rate profiles in the fizz zone of the tested double base propellant at 15 atm. The long tail of the heat release rate yields a temperature profile growing smoothly in space.

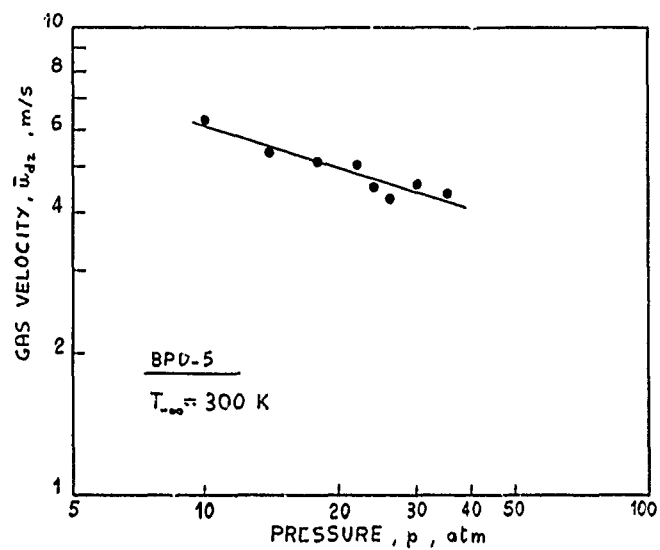


Fig. 3 - LDV measurements of steady gas velocity in the dark zone of the tested double base propellant in the pressure range 10 to 40 atm.

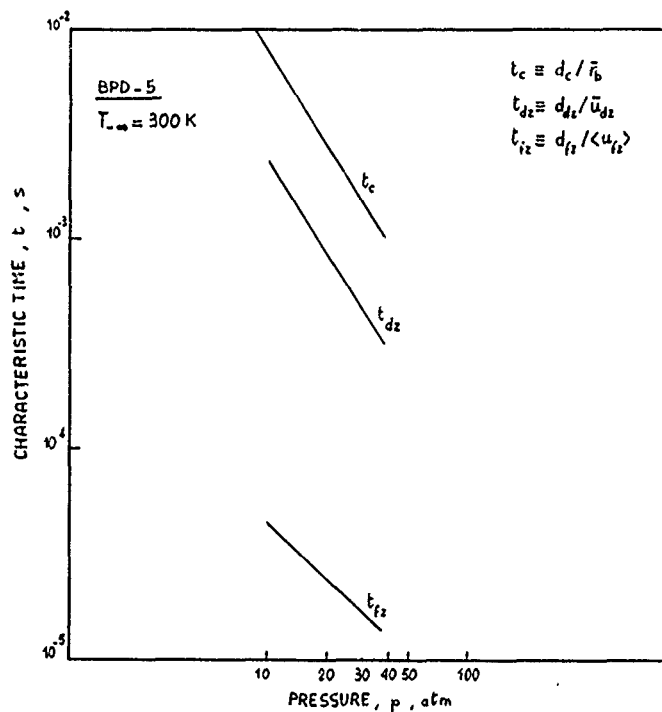


Fig. 4 - Measured characteristic times of the condensed phase, dark zone and fizz zone of the tested double base propellant in the pressure range 10 to 40 atm. The condensed phase characteristic time was found to be at least two orders of magnitude larger than the fizz zone characteristic time, allowing the assumption of quasi-steadiness for the fizz zone.

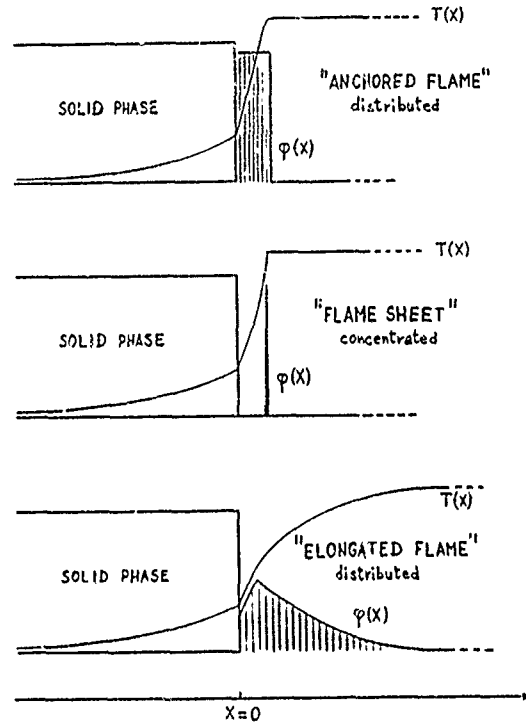


Fig. 5 - Qualitative sketch showing the structure of the three different transient flame models for the heat release rate in the fizz zone. The "elongated flame" model allows a more realistic shape of the resulting temperature profile.

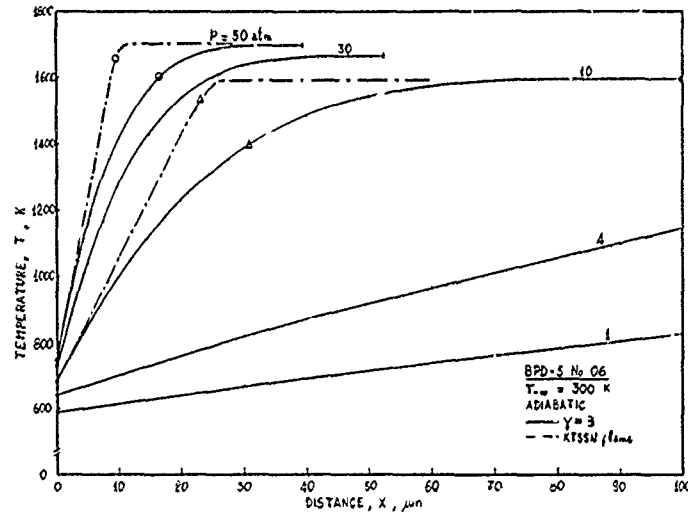


Fig. 6 - Computed temperature profiles in the fizz zone, in the pressure range 1 to 50 atm, by analytical integration of the energy equation. The "elongated flame" model was implemented with $\alpha=0.001$, $\beta=1$ and $\gamma=3$. Temperature profiles according to KTSS flame model are also reported at 10 and 50 atm.

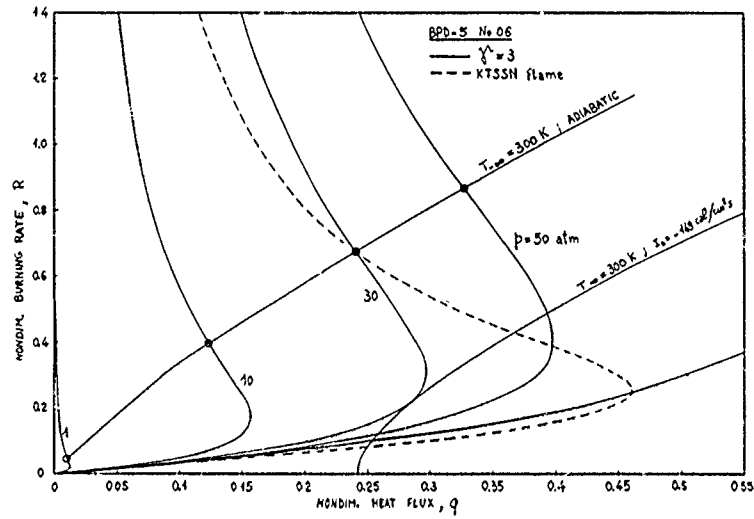


Fig. 7 - Gas phase working map for the "elongated flame" model in the pressure range 1 to 50 atm. The static burning limit at 30 atm is also shown. Comparison with KTSS flame at 30 atm suggests that "anchored" flames make the burning more stable, both statically and dynamically.

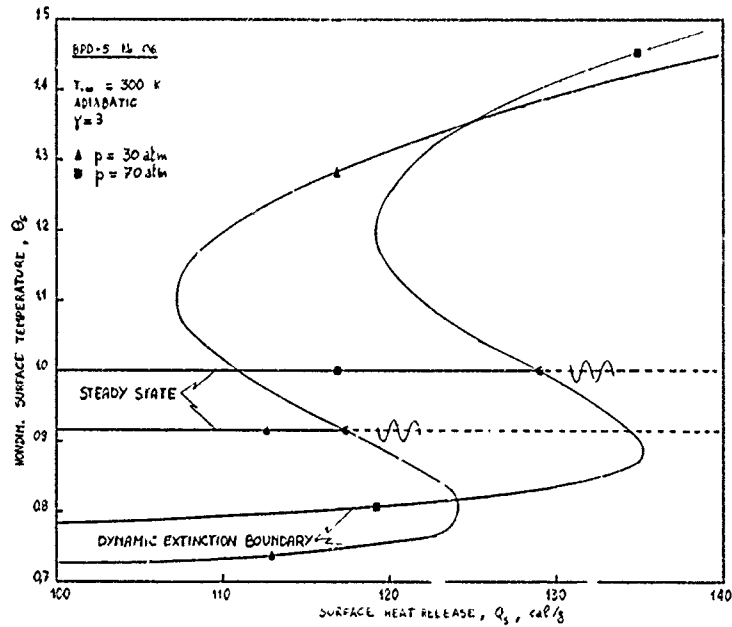


Fig. 8 - Bifurcation diagram for the surface heat release at 30 and 70 atm. Larger surface heat release is required at higher pressure to obtain bifurcation of the steady state solution from time-invariant to self-sustained oscillatory.

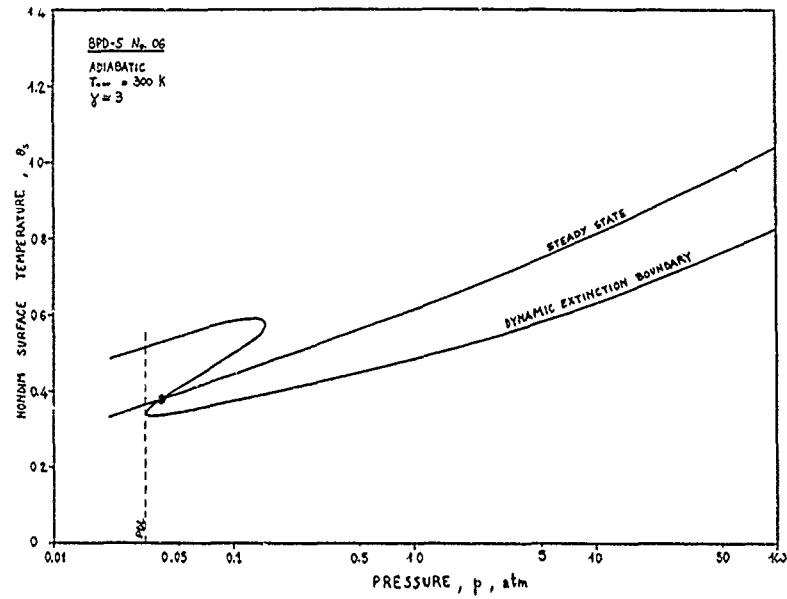


Fig. 9 - Bifurcation diagram for operating pressure p showing the existence of a stable time-invariant solution for $p > 0.04$ atm. A narrow region allowing self-sustained oscillations is expected between the bifurcation point and the pressure deflagration limit (PDL).

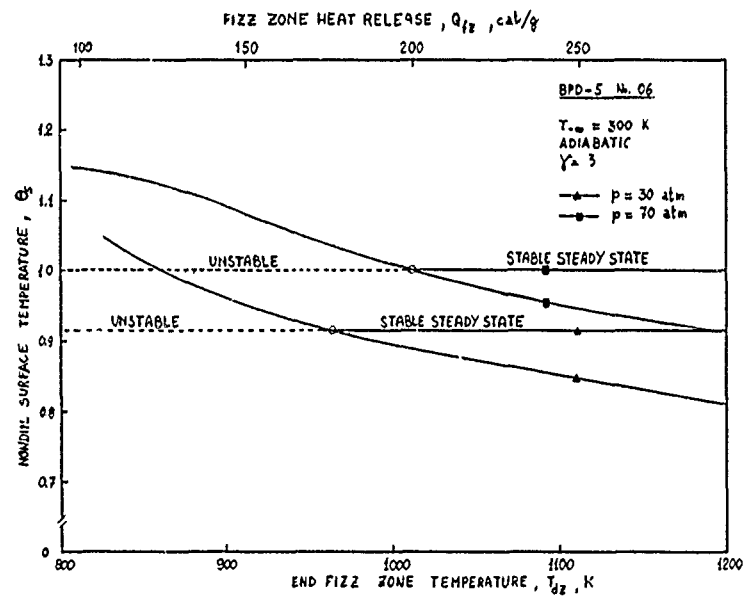


Fig. 10 - Bifurcation diagram for the end fizz zone temperature (or fizz zone heat release). For T_{fz} less than a critical value (about 965 K at 30 atm and 1010 K at 70 atm), the steady state reacting solution becomes statically unstable and only the unreacting state is allowed as a steady solution.

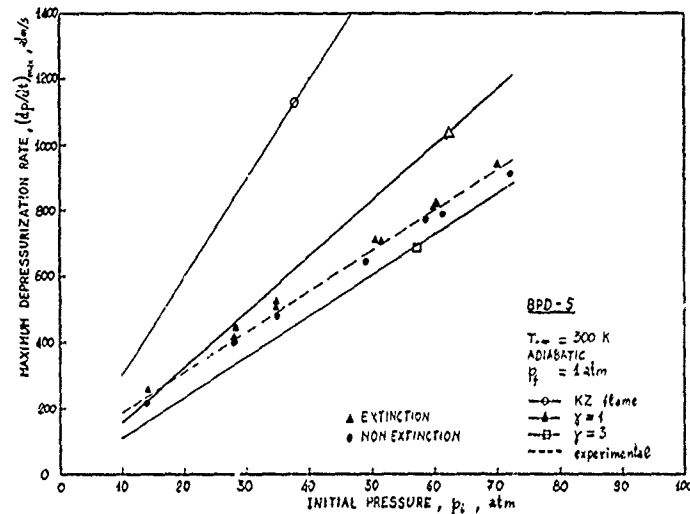


Fig. 11 - Experimental vs computed go/no-go extinction boundaries obtained by fast depressurization tests. "Anchored flame" models feature an excessively large dynamic stability, while a good agreement is found with "elongated flame" model with $\gamma=3$.

DISCUSSION

P.Ramette, FR

Pour les courbes de stabilité de combustion $\frac{dp}{dt}(P)$, vous comparez les résultats théoriques et expérimentaux pour une valeur de γ égale à 1, alors qu'une valeur de l'ordre de 3 pour γ semble plus appropriée. Comment se présenterait la comparaison théorie/expérience pour γ égal à 3?

Author's Reply

The answer is shown in Fig. 11, completed *later* only for a matter of time. You can see that $\gamma = 3$, as expected, decreases the pressure sensitivity of the boundary computed with $\gamma = 1$. The overall agreement between computed and experimental boundary is improved.

N.S.Cohen, US

This paper really deals with extinguishment boundaries resulting from rapid depressurization, and not 'stability' in the usual sense of the term. I disagree that existing steady-state models of double-base propellant combustion are unable to predict the flame height of the fizz zone. Several models, such as Kubota, Kistead and my own work, can do that and are consistent in predicting burn rate, pressure exponent, temperature sensitivity, surface temperature and condensed phase exothermicity reasonably well. I feel that it is unfortunate that you have used a *catalyzed* propellant for your data with which to develop a flame model that would be consistent for steady-state and non steady-state. The catalytic additives introduce additional complication phenomena which you are not addressing, and in particular would have a significant effect upon the extinguishment mechanism. So it is not surprising that existing theory would not agree with your data.

Author's Reply

Probably my poor English made unclear the presentation. It is perhaps useful to state the following points:

- (1) The precise connection between extinguishment from rapid depressurization and burning stability has been investigated by this research group for over 10 years. For a reasonable summary you may consult Ref.9, for example.
- (2) I did *not* make any remark whatsoever concerning steady-state models, since we model transient flames.
- (3) Before invoking any special mechanism, one should first wonder whether the usual extinguishment mechanism (based on fundamental thermophysics) suffices to explain experimental results. The answer is clearly given by the plots of Fig. 11.

- (4) To the best of my knowledge, no other theory exists capable of reproducing numerically or predicting analytically *transient* burning data of double-base propellants.

M.Summerfield, US

This is a very significant paper. The fact that Prof. DeLuca can show fairly close agreement between theoretical predictions of depressurization extinguishment and experimental results for a nitrocellulose propellant, by postulating that the thin fizz zone alone is quasi-steady and not the entire flame, is encouraging. To my knowledge, this is the first time that a theory of non-steady burning has been developed that takes account of the complexity of the nitrocellulose propellant burning process, instead of routinely applying the quasi-steady analysis of Zeldovich to the problem. The Zeldovich analysis (equivalent to the Summerfield analysis) has been shown to be applicable to ammonium perchlorate propellants in rapid depressurization extinguishments, but the success in that case rested on experiments on flame structure that showed clearly that the quasi-steady postulate is valid for the entire solid propellant flame, i.e., that the entire flame was "thin" in the non-steady sense. It may be expected that, as more complete information emerges from such experiments as Dr Trubert's, it will be possible for Prof. DeLuca to refine his analyses, with better numbers at each combustion pressure, so as to improve the agreement between his predictions and his experimental extinguishments. An additional remark: the method of decoupling the fizz flame from the rest of the flame employed by Prof. DeLuca is probably valid for his experimental combustor, but for a gun-type combustor or a practical rocket motor, other modes of decoupling may be advisable, depending on the geometry. His paper may well be a landmark paper, the first of many on so-called thick flames of solid propellants.

Author's Reply

Thank you for your comment. I do share every bit of it.

ELASTOMER MODIFIED CAST DOUBLE BASE PROPELLANTS

by: G I Evans
D Facer

IMI Summerfield
(Operated by IMI Kynoch Limited on behalf of
Royal Ordnance plc)
Kidderminster, Worcs
United Kingdom

Summary

Cast double base propellants have many attractive features for tactical missile systems, not least where plume signature transparency is at a premium. However, such propellants are limited in mechanical properties, particularly strain capability at low temperatures of -40°C or less.

The paper describes the development of a new class of CDB propellants utilising an elastomer in the binder. The advantages, properties and performance of these EMCDB propellants are given. The field of candidate polymer systems is explored with test results and chemistry of the binder together with the criteria leading to the selection of suitable elastomer binders.

Introduction

This paper deals with the development of a new class of propellants based on elastomer modified cast base double binders (EMCDB). The classical CDB process is based on two main components, namely casting powder and casting liquid or solvent. The powder in fact takes the form of granules typically 1 mm dia and 1 mm length for which the binder is nitrocellulose or nitroglycerine plasticised nitrocellulose. Various additives and filler ingredients may be incorporated into the granule binder to impart desired properties to the final propellant.

The casting powder is added to the casting powder mould to form a dry packed bed of granules with a voidage fraction of typically 0.3. The casting liquid is then introduced into the mould to displace the air and fill the voids. The liquid is nitroglycerine normally desensitised with an inert plasticiser, which is miscible in the nitroglycerine.

Under the influence of heat and pressure the casting powder granules partially dissolve in the liquid by a process of gelatinisation of the nitrocellulose. As a result the granules swell and coalesce to form a monolithic block of propellant.

There are a number of attractions to this process since it is readily adaptable from the small to the very large propellant castings. It lends itself to the manufacture of more complicated and varied charge geometry than extrusion processes. By two stage powder filling of the mould it imparts dual thrust boost/sustain capability in a single casting. Techniques have been developed to enable casting of the propellant to final dimensions and shapes without the necessity of expensive machining. The double base composition enables platonisation of burning with suitable catalysts i.e. rendering burning rate independent of pressure over large regions. This latter feature is obtained over a spread of burning rates of 3 mm/s to 42 mm/s.

The base grain CDB process has attractive production planning features. Powder increments made in sequence can be tested in sub-lots and cleared sub-lots blended into final lots of any desired size, say from 1 ton to 40 tons. Such powder blend lots may be stored for prolonged periods of many years without significant change. Thus a propellant production lot may be cleared in advance without committing motors. This is not true of propellants manufactured and cast from mixers due to pot life considerations and each mix is an individual production lot.

Similarly such pre-cleared powder lot blends facilitate flexibility in production insofar that manufacture rates may be varied at will, as circumstances demand, from single motors to multiples of motors. Production manufacturing rates tied to propellant mixers are constrained by mixer minimum/maximum capability and scale effects on quality.

An important advantage is the facility of blending several individual powders of differing properties to obtain an infinite range of intermediate properties. This blending feature is valuable in utilising propellant ingredients or additives which in a homogeneous mix would chemically react or mutually inhibit their desired effect.

Since CDB propellant is derived from gelated and coalesced granules the latter retain their identity in the propellant such that fillers and ingredients are spatially fixed in the propellant. The contents of one granule type in the blend are physically separated from those in other granule types of the blend.

Thus platonised burning rate features are retained more readily in CDB propellants which contain additives for secondary flame suppression, acoustic combustion instability suppression, high loadings of fillers such as RDX and HMX.

By the latter means higher energy smokeless propellants are produced compared to those originally envisaged in the CDB process. Where rocket exhaust smoke is not a constraint then filler loading of AP (ammonium perchlorate) and Al (aluminium) enable higher density, specific impulse propellants to be achieved. All the foregoing propellants can be case bonded as a result of the casting process.

Binder Aspects of CDB

The original classical CDB process envisaged large cartridge loaded charges for rocket motors. The propellant had hard relatively inelastic binders, similar to EDB propellants. The binder NC:plasticiser ratio was typically 1.5:1 or greater.

In the 1960's case-bonded CDB systems were developed at IMI(S) with joint casting powder formulation research involving Nobel's Explosives Co Ltd. To impart more elasticity to the propellant for these purposes, propellant binders of NC:plasticiser ratio of 1:1.25 were utilised and a large class of compositions emerged. Such binders, largely NC/NG, are temperature dependent like all thermoplastics characterised by rapid softening at temperatures approaching 60°C. Thus the lower limit on NC:plasticiser ratio was the high temperature modulus constraints involved in highly loaded case bond motors.

Such case bonded CDB propellant systems have been in-service since the 1960's for both Naval and Land Service deployments. Fig 1 illustrates such systems where volume loading fractions in the motor in excess of 96% are typical. In the case of Land Service systems with environmental requirements in the range -40 to +60°C then ingenious mechanical stress relief devices have been incorporated into the propellant charge design.

The latter devices are necessary because of the low strain capability of such CDB propellants with brittle points or Tg in the region -20 to -30°C. The standard JANNAF tensile test at -40°C at the standard rate of 50 mm/mm/min gives elongation to break of approximately 1% compared to 30% or more for cast composites based on CTPB or HTPB.

Elastomer Modified CDB (EMCDB)

Because of the limitation in low temperature strain capability a new class of double base propellants was developed in the 1970's. An elastomer was introduced into the binder. The nitrocellulose content is markedly reduced to minimise the temperature dependent effect of the thermoplastic NC/NG binder. The binder NC:plasticiser ratios are typically between 1:3 and 1:4 although occasionally slighter stiffer modulus with ratios of 1:2.5 are employed. The elastomer is introduced via the casting liquid in which the desensitiser is partly or wholly replaced with monomers or prepolymers which are cross-linked during propellant cure. Thus there is no reduction in energy compared to conventional CDB, in fact there is a gain since the reduced NC content is replaced with nitroglycerine.

The lower limit to the NC:plasticiser ratio is determined by the casting powder process and the binder needs of the casting powder granule. Thus typical EMCDB compositions for tactical applications are:

Unfilled:	NC/NG/Plasticiser/Additives/Elastomer	
	20/68/ 4.5 / 4.5 / 3	parts per 100
Filled:	NC/NG /Plasticiser/Additives/RDX Filler/Elastomer	
	12.37.5/ 4.5 / 3 / 40 / 3	

Mechanical Properties of EMCDB Propellants

Table 1 shows the comparison of tensile properties with conventional CDB, EMCDB and cast composite propellants. As can be seen the limitations in low temperature strain capability of conventional CDB systems are evident. The % elongation to break is typically 1% with Tg approx -20 to -30°C.

In contrast EMCDB propellants retain elastic properties with low temperature strain capability comparable to the cast composite propellants and Tg of -60°C.

Fig 2 and Fig 3 exemplify the change in strain capability compared to conventional CDB at alternative strain rates typical of rocket motor application. Fig 2 utilises a strain rate equivalent to that seen in shock temperature cycling between low and high temperature regimes in a typical service case-bond motor with a 96% volume loading of the combustion chamber ($4.8 \times 10^{-5} \text{ min}^{-1}$). Fig 3 utilises a strain rate equivalent to the rapid pressurisation of such a motor on ignition.

Fig 4 shows the inner conduit strain measurements of such a motor measured as the motor was taken down in temperature in 5°C steps. Conduit strains of 70% at -55°C were measured with no defects resulting in the propellant charge.

A motor designed for an in service application has been subjected to extensive testing. A 125 mm diameter dual thrust boost/sustain motor with a volume loading fraction of 96% in the case bonded radial proportion was tested. Shock temperature cycling across the regime -55 to $+60^\circ\text{C}$ was successfully demonstrated with test firing at the extreme temperatures.

The above results are critically dependent on the choice of elastomer for the binder and are typical of the first generation EMCDB systems described hereafter. The above given compositions without the elastomer binder possess no significant cohesive solidity. A block of such propellant stored at $+60^\circ\text{C}$ would collapse into a pool of liquid gel and when strained at any temperature is permanently deformed with no elasticity. The elastomer imparts a tough elastomeric consistency, resistance to high strain in torsion, shear, compression and tension. It is tolerant to repeated stress/strain to levels close to the UTS.

The elastomer requires to be nitroglycerine philic to a high degree to avoid plasticiser exudation and loss. The EMCDB systems based on caprolactone polymer systems, described later, possess these features to a high degree. Table 2 summarises the findings. Volatile loss and dimensional stability on prolonged exposure to elevated temperatures ($60, 70, 80^\circ\text{C}$) is excellent and compares more than favourably with conventional case bondable CDB. Chemical stability is equivalent to CDB and dependent on the behaviour of the nitric esters NC and NG. With modern nitric ester chemical stabilisers the chemical life as defined by full depletion of these stabilisers is of the order of 50+ years at $+20^\circ\text{C}$. Propellant gas crack life for similar compositions is less than conventional CDB. This result is because of the lower tensile strength of EMCDB compared to the harder CDB but this may be compensated for by the higher gas solubility and diffusion properties of the highly plasticised propellant.

Ballistic Properties of EMCDB

Fig 5 illustrates 6 classes of CDB propellant developed at IMI(S) based on two main groups, namely conventional CDB and EMCDB. Each group has three sub-groups of unfilled smokeless high energy filled smokeless (RDX, HMX etc) and high energy filled high smoke propellants (aluminium/AP).

Table 3 illustrates the main ballistic properties of these classes of propellants. Of particular note are the specific impulse and density impulse of the filled smokeless EMCDB now developed for tactical missile applications. These are significantly higher than was thought feasible in the early 1970's. For tactical missile applications such EMCDB systems not only require to possess the advantages described for CDB in the preamble of this paper. Such systems also require to be amenable to burning rate catalysis to achieve platonisation and good temperature coefficient across the regime -40 to $+60^\circ\text{C}$ (i.e. $\frac{\Delta V_k}{V_k} < 0.25\%$ per $^\circ\text{C}$).

In joint research with Nobel's Explosives into such catalysis platonised burning rates have been achieved across the range 3 mm/s to 42 mm/s. Fig 6 illustrates typical pressure-burning rate curves obtained.

The achievement of such catalysed platonisation is based on the presence of nitrocellulose in the propellant intimately incorporated with the metal salt catalysts. Thus the levels of NC in the EMCDB propellant as typified in the example are essential to these effects. The utilisation of the base grain CDB features in EMCDB is unique in that the NC is introduced into the motor, via the powder granules, prior to casting.

This feature contrasts with the alternative cross-linked slurry cast double base process in use elsewhere. Here the nitrocellulose is introduced perforce, into the propellant composition in the mixer prior to casting. As such the NC contents in the propellant are limited to 1% to 2% since higher levels result in highly viscous gels with consequent casting transfer constraints. Such low levels of NC limit the catalysis/platonisation possibilities - particularly in the boost burning rates.

Rocket Exhaust Plume Properties

A particular merit of the higher energy RDX filled EMCDB propellants are the smokeless properties of the exhaust. The products of combustion are essentially gaseous with no condensed phase apart from some of the minor additives deployed. By applying the principles and materials described in ref 6, considerable advances have been developed in the last decade and typically 90% transmission of incident intensity at visible and infra-red wavelengths are obtained through the axis of the plume.

Of particular note are substantial advances made in secondary flame suppression in the exhaust by means of selective additives incorporated into the RDX filled high energy propellants. Flame suppression with nozzle exit plane temperatures as high as 1700°C with obstruction of the exhaust by TVC devices has been achieved. Apart from absence of visible flame the consequent cooling of the exhaust results in reduction in signature emission in the near and far infra-red by factors of 10 to 15 and similar results in radar attenuation of the plume. These features are described in ref 6.

Elastomer Chemistry

As indicated earlier the polymer materials are introduced via the casting liquid. The screening research into candidate material involved laboratory scale tests for chemical compatibility with nitric esters (NC and NG), miscibility with nitroglycerine, mechanical safety sensitivity of the casting solvent by impact and friction tests, viscosity of the casting liquid.

Miscibility of the polymer in nitroglycerine is paramount and the stability of the solution in storage and in excursions down to -30°C have to be examined. Since the polymers partially replace the desensitiser plasticiser in the casting solvent (typically triacetin) alternative plasticisers were examined as mutual solvents for NC and polymer to enhance miscibility. A total of 16 plasticisers soluble in NG were examined for each system ranging from triacetin, phthalates from dimethyl to dioctyl, dioctyl sebacate, tri-ethyl citrate, tri-butyl formal etc.

The viscosity of liquids selected from such plasticisers and polymers requires to be similar to traditional casting liquids. Acceptance of systems was based on a minimum pot life of 8 hours defined as a viscosity less than 100 cps at 20°C, following from the addition of the part B cross-link agents.

Since the systems examined were mainly catalysed reactions requiring heat input to initiate reactions the viscosity constraint proved to be no serious problem in virtually all the systems described in this paper. Typically viscosities were in the range 40 to 70 cps at 20°C.

Following the above tests, laboratory scale casting powder gelation tests are carried out since this facility is crucial to the CDB propellant process. Some polymers inhibit gelatinisation. The comparative rates of powder gelation are observed. These features in conjunction with elastomer cross-link reaction rates are mutually opposed. Too rapid a polymer cross-link rate will inhibit powder gelation resulting in poor cohesion of the propellant and possibly shrinkage voids in the inter-granule interstices.

The final stage of the screening investigations involved casting sheets of plasticised polymer from the cross-linked nitroglycerine casting solvent system. This enabled study of the ability to form satisfactory elastomers, the reaction rate, exotherm and cure conditions in polymer to plasticiser ratios ranging from 1:3 to 1:9. Modifications to the cross-link agents, catalysts, plasticiser and cure conditions can be rapidly and conveniently examined by this technique prior to full cast propellant studies.

Elastomer Systems Examined

In the search for a new class of propellant binder the potential polymer field to be screened is large. In practice the constraints of project timescale and resources dictated choices at each stage to narrow the field for fuller development. Accordingly many promising binder systems emerged which effort did not permit full examination. A summary of the main results from the survey of potential polymer systems is given.

Field 1

A range of potential polymer systems was investigated (Ref 1).

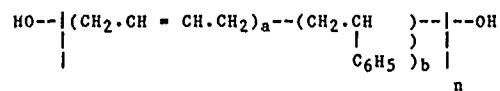
1. Polyether Polyols

A total of 15 polyether polyols were examined, with molecular weights from 400 to 4500 of di and tri-functional types. Mixed aromatic/aliphatic isocyanates with selected catalysts used as cross-link agents.

2. Styrene and Acrylonitrile Modified HTPB Systems

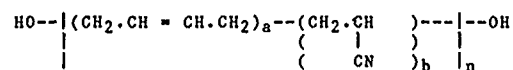
HTPB is an excellent low temperature binder but the basic polyol is immiscible in nitroglycerine. On the other hand acrylonitriles and styrene polymers have a high affinity for nitroglycerine but have poor low temperature binder properties. Co-polymers of these could provide an optimum solution. Those examined of most promise were:-

(a) Styrene Modified HTPB



$$a = 0.75, b = 0.25, n = 54.$$

(b) Acrylonitrile Modified



$$a = 0.85, b = 0.15, n = 78-87.$$

Since both modified types are long chain diols they were cross-linked to elastomers with catalysed mixed isocyanates.

3. Acrylonitrile Modified CTPB and Mercaptan terminated Acrylonitrile Modified CTPB

These pre-polymers contained variously 15 to 25% nitrile for NG affinity and molecular weights of 1 700 to 3 200 with functionality 1.8.

Using dioctyl phthalate as mutual plasticiser with NG various cross-link systems were examined such as (i) di- and tri-acrylates, (ii) metal di and peroxides, (iii) isocyanates.

4. Polytetramethylene Ether Glycols (poly tetrahydrofuran derivatives)

These take the form:-



Various molecular weights in the range 700-2000 were examined. As diols they can be cross-linked with isocyanates. As the structure implies, very attractive low temperature elastomeric properties are obtained.

5. Reinforced Organic Phase Dispersions in Liquid Polymers

The main polymer medium used was polyether polyols as previously. The dispersed phase took the form of suspended fine droplets (800-2000 Å size) of either styrene-methyl methacrylate or acrylonitrile-methyl methacrylate. The polyol medium was cross-linked with isocyanates and the dispersed phase by catalysed free radical polymerisation under heat to give a reinforcement.

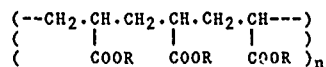
The systems 1 to 5 above gave promising elastomer binders in plasticised ratios of 1:9. However, in general the most promising showed reduced polymer miscibility or reduced cross-link density as the NG content of the liquid was progressively raised at the expense of inert plasticiser (NG contents of 76 to 80% in the liquid are desired for propellants).

Thus pursuit of these polymers was stopped in favour of other more promising systems described below.

Field 2Acrylate Polymer Binder Systems

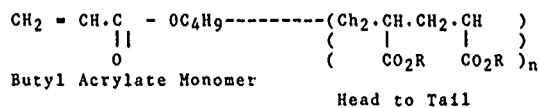
Acrylates form excellent thermoplastic rubbers and a successful development of such systems was taken to an advanced stage of cast propellant evaluation (ref 2).

The acrylate monomers were found to be chemically compatible with nitric esters and in most instances readily miscible in nitroglycerine liquids and excellent gelatinising agents for NC. The monomers are polymerised by free radical initiators activated during the cast propellant curing process at elevated temperatures. Elastomers of the structure below are obtained:-

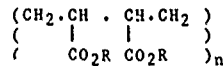


However, the choice of acrylate is crucial to achievement of good elastomeric properties and in particular good low temperature strain capability. Fig 7 shows the structural relationship to low temperature brittle point from which it can be seen that polymers based on methacrylic are less suitable than acrylics and the best results are obtained with 8 carbon atoms in the monomer unit giving elastomer Tg of -65°C. Thus it would be predicted that polybutyl acrylate and poly 2-ethyl hexyl-acrylate would be the most suitable candidates. Testing confirmed this.

Thus



or



Head to Head

(R = C₄H₉)

A mixture of head to head and head to tail configurations occurs during polymerisation. In the EMCDB process a solution polymerisation is employed where the acrylate monomer is dissolved in the casting liquid. The reaction rate is first order with respect to monomer concentration and the square root of the initiator concentration. At approximately 20-25% monomer conversion the reaction becomes autocatalytic and the rate increases rapidly until high levels of conversion and then drops rapidly to a limiting conversion level.

Fig 8 illustrates a typical reaction rate/monomer conversion level profile. The period of high reaction rate is critical to the EMCDB process because the polymerisation is exothermic. The monomer concentration and thermal mass of the propellant and casting mould influence the temperature rise. Of particular importance is the choice and concentration of initiator. The latter were chosen to have an activation temperature for free radical initiation intermediate between the casting temperature of 16 to 22°C and the normal propellant curing temperature of +65°C. For the favoured initiator an activation temperature of 43°C was involved. Thus polymerisation to high levels of conversion can be achieved with temperature rise within the body of the propellant peaking well below 65°C. Final propellant and polymer cure was completed in a cure oven at +65°C. Propellant masses from 1 kg to 20 kg were cast/cured by this technique during evaluation.

The choice of free radical initiator catalyst is constrained by the variety and complexity of propellant compositions which can inhibit free radical release. A large investigation into catalysts was necessary to establish suitable materials. Basically AZO nitriles and cyclohexyl perdicarbonates were found most suitable.

EMCDB propellants evaluated had binders based on NC:plasticiser ratios of 1:4 and 8% of the propellant composition as acrylate elastomer. Typical mechanical properties are given in Table 4.

This propellant binder system development was stopped prior to the full scale motor evaluation and compositional development for range of burning rates. This decision was taken because of the results of the parallel development of polycaprolactones described below and the programme timescale/ effort needs to concentrate on a single choice qualification programme.

Because of the promising results the choice was to a large degree subjective but the following considerations influenced the choice:-

- (i) The reaction chemistry for EMCDB acrylates is more complex than the simpler chemistry of the caprolactone system. Propellant compositions have wide variety and complexity to tailor desirable properties e.g. burning rate catalysts, flame suppressant and acoustic stability additives etc.

Many chemical ingredients inhibit free radical changes in free radical initiator concentration or even type. Thus there is a possibility of the need to tailor the reaction chemistry for variations in propellant composition.

- (ii) Unlike the caprolactone systems the acrylate polymerisation reactions are exothermic. Whilst this feature is controlled at the scale described here (up to 20 kg), the use of more massive propellant castings is an uncertain area which may perforce result in further changes and developments in the reaction chemistry.

- (iii) The acrylate monomers involved have a significant vapour pressure at 20°C. Whilst toxicity is not a major problem nevertheless the vapour odour is pungent, penetrating and persistent in work-shop areas. This renders closed equipment and exhaust stations necessary which are less operationally flexible than both conventional CDB and caprolactone EMCDB require.

Field 3

Polyester Polyurethane EMCDB Binders

This family of propellant binders was developed to an advanced stage of cast propellant evaluation and were attractive systems (ref 3).

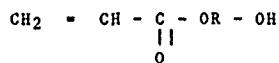
Essentially polyester polyols are dissolved in the casting solvent and a part B cross-link system based on selected isocyanates/catalyst added within 1 hour of casting.

A large range of polyester polyols was examined, basically a large family of polyester adipates variously derived from dibasic acids (adipic, phthalic). These were mixed with/without short chain diols or triols to modify cross-link density. In general the short chain (low mol wt), branched polyols, produce highly cross-linked, rigid products. Thus the linear long chain polyester polyols of mol wt in the range 2000-3000 and hydroxyl functionality just above 2.0, were found as expected to give the best results. The limiting mol wt of 3000 is governed by solubility in nitroglycerine liquids.

Polyethylene glycol adipate - toluene di-isocyanate (PGS-TDI) has been reported elsewhere as used in slurry XLCDB systems - these were not found to be the most suitable elastomer binders for EMCDB. To form the best low temperature rubbers it is considered structurally preferable to have copolymer polyols of dissimilar groups in the chain. This would minimise the tendency of regular groups to form crystalline centres or high brittle point via strong hydrogen bonds between chains.

In this work it was found that copolymers of polyethylene-butylene adipates gave superior low temperature elastomer extensibility than the mono-polyols of ethylene, propylene or butylene adipate. With the appropriate isocyanate/catalyst combination this system gave optimum strain/modulus properties and no advantage was found in using a range of either multifunctional polyols (penta erythritol, sucrose, inositol, mannitol, sorbitol) or multifunctional isocyanates to improve cross-link density.

A particular variant which shows significant interest was the use of acrylate polyols such as hydroxy ethyl methacrylate viz:-

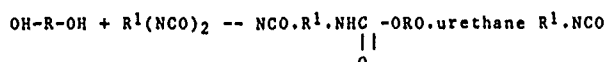


Acrylate mixture of HEMA with the polyester adipates were reacted with suitable isocyanates. Urethane links with the -OH group of the HEMA are followed by free radical polymerisation of the acrylate. Thus a binder based on a polyurethane-polyacrylate resulted. However, the chemistry is more complex and the competitive reaction rates of urethane-acrylate:NC gelatinisation were not optimised within this programme.

Field 4

Quasi Pre-polymers

A parallel investigation (Ref 4) researched pre-polymers based on pre-reaction of long chain diols with isocyanates under controlled reaction conditions. The objective is to end-cap the diols with free isocyanate groups thus:-



The pre-polymer is subsequently dissolved in the casting solvent and so has to be a moderate mol wt liquid or low melting point solid.

Just prior to casting the propellant a mixture of diols/triols are added to the casting solvent to chain extend and cross-link via the end-capped isocyanates.

An advantage is the ability to use more complex isocyanates than may otherwise be immiscible in the casting solvent. Thus polymer chains with long, linear flexible polyester segments may intersperse with stiff urethane segments e.g. 1,5-naphthalene di-isocyanates may be used in lieu of low molecular weight isocyanates.

The most successful variant was found to be a difunctional co-polymer polyester adipate of mol wt 2000 pre-reacted with di-cyclohexyl di-isocyanate in 1:6 molecular equivalents. Cross-link diols/triols were not wholly successful since in the main they were not soluble in NC, but hydroxy ethyl methacrylate with free radical initiator gave promising binder results.

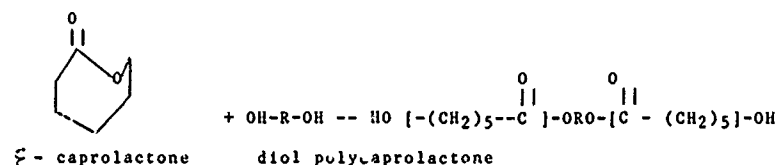
The binder systems previously described i.e. polyacrylates, polyester polyurethanes, pre-polymers were examined to an advanced stage at the laboratory and pilot scale (5-20 kg propellant). Processing and properties were evaluated and shown to give good prospects as practical propellant binders.

However, full scale development to project application was devoted to the polycaprolactone systems.

Field 5

Polycaprolactone Systems

The polymer binder is based on poly ϵ caprolactone diol reacted with suitable isocyanates and catalysts. The polycaprolactone is formed by reaction of ϵ caprolactone with reactants such as alcohols, diols, triols etc.



In our case the preferred diol is neo-pentylene glycol i.e. $\text{OH}-(\text{CH}_2)_5\text{-OH}$.

It is important to reduce the predominance of the thermoplastic plasticised NC binder influence. Accordingly in EMCDB, NC:plasticiser ratios of 1 to 4 or less are used compared to conventional CDB ratios of 1:1 or greater. A minimum NC content is required for (a) casting powder binder (b) to effect burning rate platonisation.

Within these parameters a lower NC:plasticiser ratio whilst benefiting low temperature capability also results in a trade-off in lower high temperature modulus. The addition of fillers to this standard propellant also affects strain/modulus through filler/binder adhesion. The nitramine (RDX/HMX) fillers appear more prone to dewetting under stress than AP/AL fillers. Table 8 summarises the above mentioned parameters on the standard EMCDB propellant.

Accordingly avenues of improvement of the second generation of EMCDB propellant have been investigated. Thus the NC/plasticiser ratio requires to be tailored according to application and in accordance with the filler loading. Normally fillers would be expected to stiffen the modulus of the propellant. However, RDX/HMX have relatively poor binder/filler adhesion and there is some tendency to dewetting of the filler at high loading and high stress. Resin coating of the RDX to enhance filler/binder adhesion is a promising avenue. Table 9 illustrates the effect on modulus of such techniques using some of the most suitable resins evaluated. Significant improvements are seen in the mechanical properties by this route.

Further alternatives to improve the binder property are being developed and the results to date are illustrated in Table 10. Table 10.1 shows the beneficial effect of increasing the isocyanate to caprolactone polyol ratio significantly over stoichiometric. A similar but more marked effect is obtained by changing the desensitiser/phlegmatiser plasticiser in the casting solvent. Table 10.2 illustrates the effect. Triacetin is an excellent gelatiniser for NC (significantly better than the phthalates or nitroglycerine). Thus the plasticised NC thermoplastic binder is more dominant than is the case with phthalate plasticiser. The latter appears to result in a greater proportion of ungelatinised NC fibres in the binder, acting as fibre fillers rather than binder.

Table 10.3 illustrates the effect of increasing the proportion of caprolactone elastomer in the propellant in increasing modulus. The above mentioned parameters in tables 9 and 10 do not suffer in trade-off of low temperature extensibility.

Returning to the first generation EMCDB propellants prior to the Table 9 investigations, such propellant systems have been fully developed for in-service project application. Safety sensitivity testing, chemical stability and ageing stability of mechanical properties in prolonged storage at 60°C/100% RH are comparable to conventional CDB. Since the combustion products of such propellants are almost wholly non-condensable, gaseous the propellants are truly smokeless.

The pot life of such casting solvents is indefinite prior to the addition of catalyst/cross-link agents and 4 to 6 hours thereafter. The cure period for full cross-linking is approximately 6 days at 65°C. Due allowance in the reaction rates for the competing gelatinisation process has to be made in selecting catalysts.

Table 11 illustrates two rocket motors which have been tested to service project technical requirements.

References

1. IMI(S) Technical Report 76/21 - Investigation of Miscellaneous Polymer Systems for EMCDB Propellant Application by G I Evans, D Facer, M J Ruston.
2. IMI(S) Technical Report 76/24 - The Development and Evaluation of Acrylate Based EMCDB Propellant by G I Evans, D Facer, M J Ruston, K Sanders.
3. IMI(S) Technical Report 76/20 - The Evaluation of Polyester Adipate Elastomers in EMCDB Propellants by G I Evans, D Facer, M J Ruston, K Sanders.
4. IMI(S) Technical Report 77/9 - Urethanes Formed from Quasi-Prepolymers for EMCDB propellants by G I Evans, D Facer, M Ruston, K Sanders
5. IMI(S) Technical Report 76/23 - Interim Report on the development of Polycaprolactone based EMCDB Propellant by G I Evans, D Facer, M Ruston, K Sanders
6. AGARD Paper Florenc 1985 - Reduction of Exhaust Signature in Solid Propellant Rocket Motor by G I Evans and P K Smith

TABLE 1 TENSILE PROPERTIES: STANDARD JANNAF TENSILE TEST

Strain Rate 50mm/min	-40°C		+20°C		+60°C	
	MN/m ²	%	MN/m ²	%	MN/m ²	%
1 Classical CDB	>32.5	<1	10.5	30	2.35	44
NC:Plast = 3.2						
2 Case Bondable CDB	12.8	<1	3.3	58	0.73	65
NC:Plast = 11.25						
3 HTPB	1.75	37	0.32	41	0.62	36
4 EMCDB unfilled	8.2	35	0.57	100	0.17	80
5 EMCDB 40% RDX Filler	9	10	0.73	55	0.17	80

Break Point - To
 Conventional CDB = -20 to -30°C
 EMCDB = -60°C
 HTPB = -60 to -80°C

TABLE 2

	EMCDB	Conventional CDB
1 Storage 6 months at 60°C	0.8	0.8
1.1 % Volatile loss	0.8%	0.7%
1.2 Dimensional stability shrinkage		
2 Chemical Stability*		
2.1 Time to stabiliser depletion to 60°C	94 weeks	92 weeks
2.2 Equivalent depletion time at 20°C	100 years	100 years +
3 Gas Crack Life 50mm Cube at 80°C	8 days	15 days

*Percentage of stabiliser type and content as propellant.

TABLE 3 PROPELLANT BALLISTIC PROPERTIES

Class	Smoke	Specific Impulse	Density	Density/Impulse
		Ns/kg	Kg/m ³	MN/m ²
CDB	Minimum	2190 - 2250	1610	3.52 - 3.62
Filled CDB	Minimum	2300 - 2400	1650	3.80 - 3.97
Filled CDB	Smoke	2530	1770	4.48
EMCDB	Minimum	2370	1580	3.77
Filled EMCDB	Minimum	2450	1650	4.05
Filled EMCDB	Smoke	2530 +	1770	4.48 +

Impulses at theoretical full expansion from 70 bar.

Conventional high energy smokeless } Burning Rates 3mm/s to
 EMCDB high energy smokeless } 42 mm/s at $\tau_x < 0.2\%$ °C

TABLE 4 ACRYLATE BASED EMCDB PROPELLANTS TENSILE PROPERTIES BY JANNAF

Test Method and Strain Rate 50mm/min/min	-40°C		+60°C	
	UTS MN/m ²	% Elongation	UTS MN/m ²	% Elongation
Conventional CDB	12.8	<1	0.73	65
Acrylate Based EMCDB	6.9	29	0.11	15
Ditto at Strain Rate 160mm/min/min*	9.0	12	-	-

*Rapid strain applicable to the igneous phase of a grain project motor.

TABLE 5 COMPARISON OF ELASTOMERS (UNPLASTICISED)

Polyol 2 000 Mol Wt	Physical Properties of MDI Urethanes/20°C		
	Shore Hardness	UTS kg/cm ²	Tear Elong. Strength
Polycaprolactone	90	548	590 121
Polyethylene Adipate	92	648	670 131
Polyethylene Butylene Adipate	92	700	680 —
		Cold Flex °C*	Relative Hydrolysis Resistance**
Polycaprolactone		-41	68%
Polyethylene Adipate		-25.3	7%
Polyethylene Butylene Adipate		-31	35%

*Standard polymer Test

**Retention of UTS after 24 hour immersion in boiling demineralised water

TABLE 6 HYDROLYSIS RESISTANCE OF URETHANES

Urethane From:	% Retention of UTS after Immersion in H ₂ O at 100°C					
	Initial	2 days	4 days	6 days	10 days	30 days
Polyethylene Adipate	100	7	0	0	0	0
Polyethylene Butylene	100	16	10	0	0	0
Polycaprolactone	100	64	35	32	30	30

TABLE 7 ISOCYANATE VAPOUR PRESSURES

Type	Vapour Pressure mm HG
Toluene di-isocyanate TDI	0.05 at 25°C
Hexamethylene di-isocyanate HDI	0.05 at 25°C
Trimethyl Hexamethylene di-isocyanate TMDI	0.0007 at 20°C, 0.015 at 50°C
Triphenyl methane tri-isocyanate	0.00009 at 25°C

TABLE 8 EFFECT OF BINDER NC: PLASTICISER RATIO
ON CAPROLACTONE BASED EMCDB

	-40°C		+60°C	
	UTS MPa/psi	Elong %	UTS MPa/psi	Elong %
1 Unfilled EMCDB	10	35	0.16	65
NC: Plast 1/3.5				
2 Unfilled EMCDB	13	13	0.26	80
NC: Plast 1/2.4				
3 30% AP/AL filled EMCDB	15	20	0.35	45
NC: Plast 1/2.4				
4 40% AP/AL filled EMCDB	16	10	0.45	30
NC: Plast 1/2.4				
5 30% BDX filled EMCDB	9	10	0.20	60
NC: Plast 1/2.8				
6 30% BDX	13	6	0.27	60
NC: Plast 1/2.8				
7 40% BDX	5	14	0.15	90
NC: Plast 1/4.3				
Commercial CDB	23.5	<1	2.35	24
NC: Plast 3/2				
Commercial CDB	12.8	<1	0.73	6.5
NC: Plast 1/1.3				

TABLE 10 EFFECT ON MODULUS/ELASTICITY OF EMCDB PROPELLANTS - STRAIN RATE 50mm/min
 M.I. Variation of Incompressible Poisson Ratio over Stoichiometric

Charge No.	Propellant	%RDX	MOI, DE Trade	% Elong	Modulus Below elastic limit
837/BL	A	0	1.051	33	0.14
837/BL	A	0	1.81	31	0.14
837/BL	A	0	1.221	31	0.25

10.2 Replacement of Trisoclon Plasticizer with Dibutyl Phthalate

Charge No.	Propellant	%RDX	MOI, DE Trade	% Elong	Modulus Below elastic limit
817/1	B	0	7A	33	0.23
817/1	B	0	DST	35	0.58
817/1	C	20	7B	29	0.20
817/1	C	20	DST	21	0.51
867/1	D	20	7A	25	0.46
817/1	D	20	DST	14	1.20

10.3 Increasing Diameters Level in Propellant

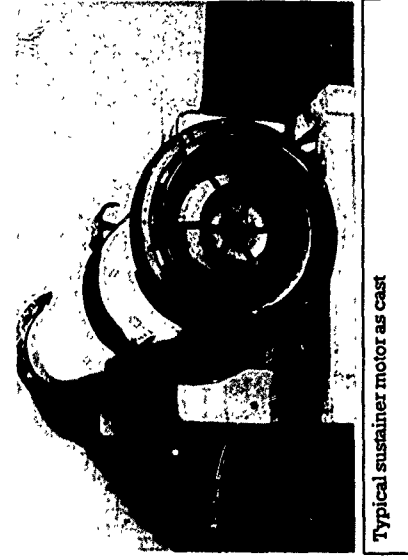
Charge No.	Propellant	%RDX	MOI, DE Trade	% Elong	Modulus Below elastic limit
830/1	E	40	3% Elast	45	0.14
72	E	40	4%	40	0.15
73	E	40	5%	37	0.50
867/1	F	20	3	9.5	0.48
817/1	F	20	4	10.7	0.60
72	F	20	5	10.9	0.60
73	F	20	6	9.0	0.58

TABLE 9 EFFECT OF RESIN COATING RDX FILLER
 RDX SIZE 5 - 2,000cm⁻¹

Charge No.	Propellant	Resin	% Elong	MIN/Mr	Modulus
843/1	A	None	33	7.4	0.13
839/1	A	A	39.5	6.8	0.27
7/2	A	B	37.0	7.1	0.23
7/3	A	C	38	6.7	0.20
840/1	A	E	36	7.3	0.31

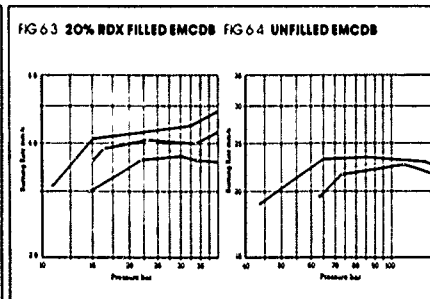
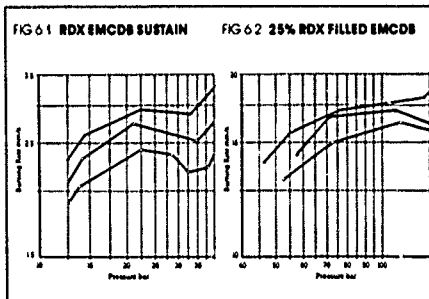
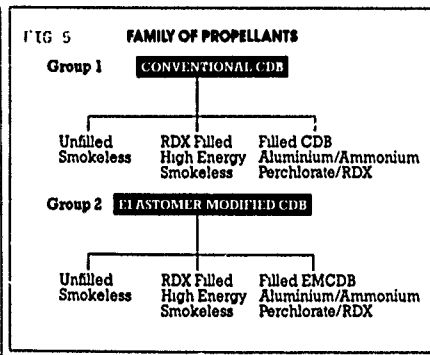
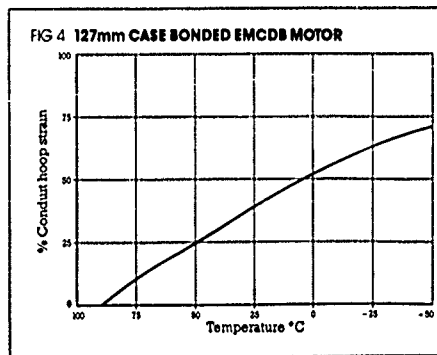
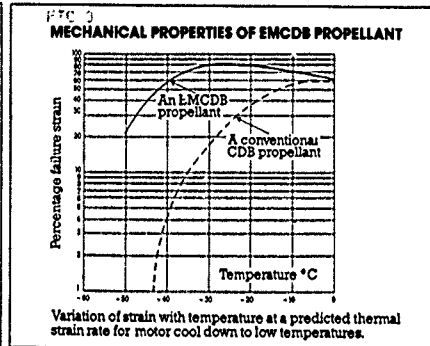
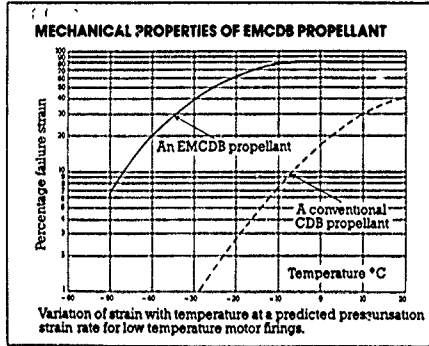
TABLE 11 PROJECT MOTOR DEMONSTRATION

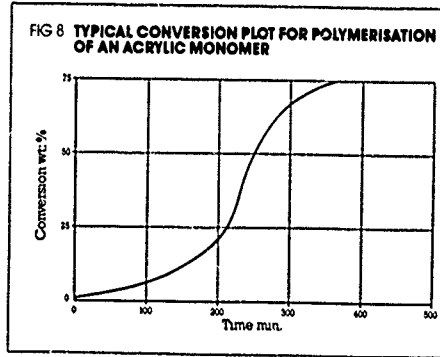
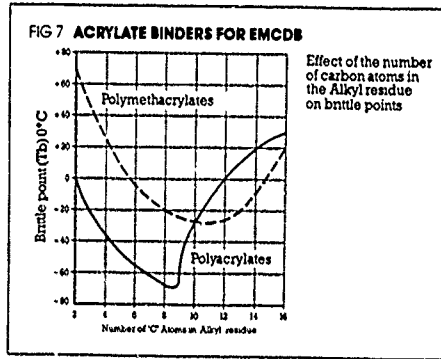
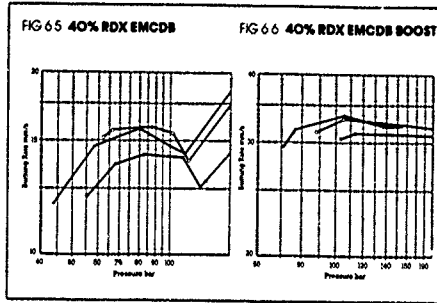
	Motor A	Motor B
Motor diameter mm	127	169
Case Bonded	V	V
Thrust	Boost/Sustainer	Single Thrust
Propellant Mass kg	17.6	29.5
% RDX Filler	20/25	NJ
Delivered SI (20°C)Ns/kg	2100	2000
Volume Loading Fraction %	96	93
Radial Portion Propellant	70%/ -50°C	40%/ -55°C
Propellant Conduit Strain %	-50/+60°C	-55/+60°C
Tested Shock Cycling	-40/+60°C	-55/+60°C
Firing Regime	-40/+60°C	-55/+60°C



Typical sustainer motor as cast

FIG 1





DISCUSSION

G.Malescot, FR

I want to ask a question outside the frame of your presentation. You obtained a propellant with burning rate of 40 mm/s. The curves you showed gave a 40% RDX propellant with 33 mm/s. At 40% RDX loading what burning rate can you achieve?

Author's Reply

With the unfilled EMCDB propellants the burning rate range achieved, which is platonised, extends from 2 mm/s to as shown on the slide 42 mm/s -- in fact nowadays up to 45 mm/s. When RDX is introduced the platonisation becomes more complex. To date the burning rate range, which we could consider usable with 40% RDX extends from 2.5 to 33 mm/s. We are working on increasing this further currently but cannot claim that above 33 mm/s they are of acceptable temperature coefficients for tactical missile applications.

G.Malescot, FR

What temperature coefficients of burning rate do you obtain for burning rates of 40 mm/s?

Author's Reply

I must emphasise here that when referring to all these burning rates then we are talking of platonisation burning rates defined as temperature coefficients of burning of 0.2% per °C or less.

I should add that these are determined by the technical requirements for rocket motors for tactical missiles.

THE REDUCTION OF EXHAUST SIGNATURE
IN SOLID PROPELLANT ROCKET MOTORS

by: G.I. EVANS
P.K. SMITH

IMI SUMMERFIELD, KIDDERMINSTER
WORCESTERSHIRE, UK.
(OPERATED BY IMI KYNOCH LIMITED
ON BEHALF OF ROYAL ORDNANCE PLC).

Abstract

An important feature of Cast Double Base propellants is that during combustion the propellant itself produces extremely low levels of exhaust smoke. Developments in insulation material and, in particular, charge inhibitors have allowed the low smoke potential of the propellant to be fully realised in rocket motor firings.

A further dramatic reduction in exhaust signature has been obtained by suppressing secondary combustion in the rocket motor. This has been achieved over a wide range of typical propellant charge and motor configurations using propellant additives.

Flame suppressed plumes offer the desirable property of low exhaust emissions both in the visible and IR regions of the electromagnetic spectrum. Similarly missile communications both at optical and radio frequency wavelengths are improved by the absence of secondary combustion.

This paper reviews the inhibitor and propellant developments concerned and quantifies the reductions in exhaust signature which are obtained by the optimised use of secondary flame suppression.

Introduction

The principal starting point for suppression of secondary flame and low signature rocket exhausts is smokelessness of the plume. The nature and sources of smoke in rocket exhausts is dealt with in detail in Ref. 1. Smoke is a cloud of condensed phase particles suspended in gas which can be of a range of particle sizes, shapes, density, refractive index and reflective/absorptive properties which determine the optical properties of the cloud. The particles may be present in the gas leaving the nozzle exit plane or formed by condensation from the vapour downstream. Coagulation of the particles occur by collision and the size, density and dilution affect the persistency, dispersion and fall-out from the plume.

The smoke cloud particles may be organic in nature (hydrocarbon soots, organic mists) or inorganic condensed phases. The former provide additional fuel for secondary flame and can depress the ignition point. Both types of particle can form local hot spots by thermal lag for re-ignition. Importantly clouds of particles will interfere, by collision, with exhaust secondary flame additives which are normally alkali metal ions.

Thus smoke laden exhausts render secondary flame suppression more difficult, requiring higher concentration of suppression additives, or ultimately make suppression impossible.

The design of rocket motors for low smoke is described in detail in Ref. 1, 2, 3. The formulation of the propellant is a core feature but double based and EMCDB propellants with or without Nitramine fillers (RDX/HMX) as shown in Table 1, are particularly suitable. However fillers such as aluminium and/or ammonium perchlorate as used in EMCDB or composite propellants render optically dense smoke clouds inevitable. Even levels of 1 to 2% aluminium in the propellant give rise to serious obscuration of incident radiation.

With smokeless propellants the principal sources of smoke in rocket exhausts are the inert parts consumed such as insulants and inhibitors. These require to be formulated to eliminate inorganic sources of condensed particles by pyrolysis or erosion of the inert parts. Where total elimination is not possible dilute clouds, defined as single particle as opposed to multiple particle scattering of incident beams, are required. The particle size needs to be minimised to avoid the peak in the scattering coefficient versus particle size characteristic.

Organic source smoke can be eliminated by certain formulation rules to minimise pyrolysis reactions giving rise to primary hydrocarbon species which polymerise to higher molecular weight condensed phase hydrocarbons. Dehydrogenation of the latter produce hydrocarbon soots. The technology for the above is described in Refs. 1, 2, 3 and smokeless rocket motors are now an established technology on these principles.

It is the objective of this paper to describe suppression of secondary flame in rocket exhausts whilst retaining smokelessness. The benefits are low signature from visible flame and emission in the near to far infra-red spectrum and further reductions in attenuation of radar frequencies and laser transmission.

Flame suppression is achieved by use of additives giving rise to alkali metal ions in the exhaust, for example potassium. Clearly these alkali metals form condensed phase species in the exhaust and thus contribute to smoke.

Accordingly the most efficient additive (i.e. lowest mass fraction to effect suppression) is most important.

The use of the optimum type, amount and mode of incorporation of the additive in the propellant is particularly important with the more demanding higher energy propellants now being developed.

Table 2 shows typical properties of such currently available propellants illustrating specific impulse, density and burning rates now available. Using such propellants and materials rocket motors have been designed with in excess of 95% transmission of the incident intensity in wavelengths from the visible to the far infra-red, directed through the axis of the exhaust plume.

Secondary flame suppression

With smokeless propellant rocket motors the fuel for secondary flame is hydrogen and carbon monoxide. Mixing with air in the recirculation region at the nozzle exit results in a flammable mixture. Shock waves in the plume result in regions of pressure shock and temperature rise followed by ignition. Nozzle design is significant in reducing shock wave formation. Full expansion with a parallel flow nozzle profile is particularly advantageous.

Nevertheless high energy propellants, high thrust motors with nozzle exit plane temperatures in the 1200 to 1700°K+ region inevitably give rise to secondary flame.

The reaction in the flame is propagated by free radicals such as H and OH. Combustion of hydrogen in air results in the formation of such free radicals thus



Research has shown that the incorporation of certain additives, in particular alkali metal compounds and more particularly potassium can suppress the flame reaction. The probable mechanism is by free radical combination thus



Where the reaction rates for (2) and (3) are fast in relation to (1).

With secondary flame the temperature recovery in the exhaust plume approaches that of the flame temperature of the propellant. As a result emission in the infra-red spectrum is high from such species as CO_2 , H_2O and condensed phase matter. By flame suppression a much cooler plume results and as the results in this paper show the emission intensity can be reduced by an order of magnitude. Similarly transparency of the plume to lasers in the near and far infra-red is markedly increased since significant defraction and dispersion of the incident laser beam occurs in hot plumes.

Furthermore, radar attenuation by the exhaust plume is substantially reduced by secondary flame suppression. Attenuation of microwave frequencies largely arises from the presence of free electrons in the plume, produced from ionisation of metallic species at high temperature. Absorption of the incident beam power arises from the acceleration of the electrons by the beam and the energy absorbing collisions with molecules in the gaseous exhaust. Minor levels of alkali metals such as potassium can, by ionisation in the flame, result in an increase in the electron concentration. However once the threshold concentration of potassium is reached to achieve flame suppression the cooler plume temperature results in a marked reduction in ionisation and electron concentration.

However a trade-off for the above features can be an increase in exhaust smoke arising from the condensed phase potassium. Accordingly the most efficient, lowest mass fraction of potassium metal compatible with effecting flame suppression is important. To this end attention has to be given to minimising organic and inorganic smoke in the plume; optimum nozzle design; selection of the most effective potassium salt and the most effective means of incorporating the salt into the propellant. The latter two aspects have been found most important in effect on efficiency and appears to be related to the proportion of vapourised/condensed potassium species at the nozzle exit plane.

Type of suppressant additive

The detailed work has largely been reported in Ref 4. An ideal flame suppressing additive would be able to suppress secondary combustion in rocket motors whilst maintaining the chemical, physical and ballistic properties of the propellant. Further certain features of any additive would make it potentially attractive. For example the additive should contain the highest possible mass fraction of the flame suppressing metal to minimise the energy losses associated with the non-reactive part of the molecule. In addition the salt should not contain anything which in itself could be a potential source of smoke e.g. possible sulphate induced hydrocarbon smoke from potassium sulphate.

A large number of different additives were investigated but the work reported here concentrates on various Potassium Salts which were known to have good flame suppressing properties.

The traditional flame suppressing additive for use in gun propellants was Potassium Sulphate. However this additive had been used at high levels which although successful as a flame suppressant gave excessive amounts of smoke. The work undertaken at IMI Summerfield was aimed at optimising the type and amount of additive necessary to suppress flame in a given configuration and so minimise smoke effects.

Although the effective agent in suppressing the flame chemistry in the exhaust is the potassium ion K^+ , nevertheless the type of potassium salt influences the effectiveness. This may be due to variations in the potassium combustion products and the properties of potassium present in the vapour as opposed to condensed phase together with the particle size of the latter resulting from the rapid expansion through the nozzle.

Figure 1 compares several potassium salts incorporated in a standard propellant and standard test motor. The figure illustrates the variable effectiveness in terms of the minimum level of additive necessary to suppress flame. The levels refer to the potassium metal equivalent (not salt).

Method of additive incorporation

The effect of these various salts on propellant chemical stability, propellant gassing, propellant burning rate and the inherent chemical stability of the additive have been investigated (Ref. 4) to characterise systems for in-service propellant applications. Some potassium salts are chemically reactive with nitric esters and effect stability but in the majority of instances stability is satisfactory.

For the purposes of this paper it may suffice to state that the variety of ingredients that may be used in propellants is extensive. Some of these ingredients, in particular some burning rate catalysts, may chemically interact with some potassium salts to destroy or degrade the burning rate platonisation. Fortunately the CDB process is based on the use of powder granules in casting. Blends of two or more different powders may be used. The casting process is characterised by partial solution, gelation of the granules in the casting solvent. The granules swell and coalesce into monolithic blocks of propellant but the gelated granules retain their individual density. Thus insoluble ingredients/additives in one powder granule are physically separated and spatially fixed in the propellant areas. Mutually reactive ingredients are kept apart. The powder blending process thus permits the use of ingredient formulations which would not otherwise be possible in propellant systems based on homogeneous mixing prior to casting or extrusion.

This effect is illustrated in Fig. 2. This shows a given propellant A with a burning rate catalyst manifesting platonisation. Propellants B, C, D are exactly the same as A except for the addition of a potassium salt. The percentage level of burning rate catalyst is the same in all four propellants. In the case of propellant D the potassium salt is uniformly distributed throughout the propellant in a single powder blend. Chemical interaction has destroyed the platonisation. In propellants B & C a two part powder blend is used where the burning rate catalyst and potassium salt are incorporated in separate powders. Platonisation effects are retained in the latter case.

The method and distribution of potassium salt in the propellant also influences its efficiency in flame suppression and there is an optimum level and distribution. Reduced efficiency i.e. the necessity for higher levels of additive has a penalty in increased exhaust smoke.

Predictive models for the level of additive necessary to suppress flame in given rocket designs are available but there are significant uncertainties in the input data. The models generally predict significantly higher levels of potassium additive than the experimental work given here demonstrates. The models do not allow for the effects of the type and method of physical incorporation on the efficiency. However an extensive experimental programme has examined the main design parameters to establish practical predictive guidelines. These have been used regularly at IMI(S) with a large degree of success. The use of the powder blending technique available in the CDB/EMCDB process enables rapid adjustment/optimisation of the motor from the preliminary experimental test firing.

Nozzle Design

Full and optimum expansion in the nozzle is desirable and the RAO or preferably parallel flow nozzles are superior to conical nozzles. In general it is desirable to minimise shock formation in the plume downstream of the nozzle exit plane.

Figure 3 illustrates the effect on experimental motors of various nozzle designs in terms of nozzle exit plane temperature and pressure versus additive level (selected additive and mode of incorporation) necessary to suppress secondary combustion.

Motor Thrust Level

Figure 4 illustrates the effect in a standard motor of varying the thrust level by varying the propellant burning rate and charge configuration. In each case the nozzle is designed for optimum expansion. The two boundaries shown represent the minimum and maximum additive level for absence or presence of flame. The additive level increases with thrust level to achieve flame suppression. The propellant energy level is essentially constant in Figure 3. Such data enables interpolation to estimate with reasonable accuracy the level required for a given design.

Propellant Energy Level

In general the amount of additive necessary increases with propellant energy level. Assuming optimum nozzle expansion in all instances, this result is to be expected in line with the higher nozzle exit plane temperature accompanying the higher energy propellant.

With the higher energy/density smokeless propellants derived from RDX/HMX filler loading levels the additive level is slightly less than that predicted from the nozzle exit plane temperature. It may be that this results from the higher proportion of inert nitrogen in the exhaust gas arising from the chemical structure of the Nitramines.

Figure 5 illustrates the effect of a selected potassium additive on flame suppression versus RDX level. A standard 150 mm heavyweight re-usable motor has been used as the test vehicle. Two nozzle configurations have been used, namely either a single nozzle or a twin nozzle side venting arrangement. The thrust per nozzle is thus varied. As can be seen the required additive level is significantly lower in the twin nozzle case (compare Trial No. 258 and 226) and the additive level increases with increasing RDX level in the propellant, although not as much as expected.

Motor Velocity

The above comments refer to static test firings. In flight theoretical modelling of the plume would be expected to give a more collimated tendency with less rapid mixing with surrounding air until the plume has cooled substantially. Accordingly it is considered that flame suppression should be more readily achievable i.e. at slightly lower additive levels.

This effect has been examined extensively but more economically by means of test firings on a sledge track at PEE Pendine. Motor velocities are relatively low; typically 60 - 100 metres/sec. However the effect has been noticeable in that slightly lower levels of additive are required compared to static test firings.

(Table 5 illustrates the effect).

Properties of Flame Suppressed Plumes

The suppression of secondary combustion in solid propellant rocket motors has a number of significant advantages. These are concerned mainly with the reductions in motor emissions at various wavelengths giving reduced detectability of a missile together with the reduced attenuation for command links involved in active guidance systems.

For non flame suppressed motors the possibility of detection of the missile and for the launch site is greatly increased, due to the secondary flame emitting much higher amounts of energy in both the visible and infra-red regions of the spectra, than the remainder of the body. Similarly the secondary combustion region can strongly attenuate missile communication systems operating at both Optical frequency and Radio frequency regions of the electromagnetic spectrum.

Trials have been carried out at IMI(S) and in some cases in collaboration with other establishments, using IMI(S) supplied motors, to quantify some of the advantages obtained from flame suppression. (Ref. 5, 6, 7, 8).

Optical emissions from flame suppressed plumes

Flame suppressing additives incorporated into propellants produce a dramatic change in the Optical emission from the plume in the visible light region.

Fig. 6 illustrates two high energy sustainer propellant motors of identical 2kN thrust. One motor has 0.28% flame suppression additive in the propellant. Fig. 7 is a similar illustration of high energy smokeless boost motors of 12kN thrust. One motor has 0.56% additive in the propellant.

Fig. 8 illustrates a high energy smokeless boost motor, where the propellant contains 35% RDX, of 5kN thrust. One motor has 0.42% additive in the propellant. It is noticeable in Fig. 8 that the flame is firmly attached to the nozzle whereas in Figs. 6 and 7 it is detached. This arises from the higher nozzle exit plane temperature with the RDX filled propellant.

Table 4 shows the effect of additive level for flame suppression versus nozzle exit plane temperature, thrust level and smoke for a recent motor design. The table also shows the effect of a thrust vector spoiler resulting in a 37% nozzle area blockage. The latter device creates a shock wave in the exhaust gases to produce thrust vectoring. The recovery temperature at the shock would normally create reignition of the exhaust. The ability to suppress such flames is a substantial advance in the state of the art.

Emission Signature in the Infra-red

Trials were carried out in conjunction with other establishments to measure motor emission in the infra-red region of the spectra and to determine the effects on these emissions on flame suppression. A number of motors supplied by IMI(S) were fired over a range of thrust levels both with and without flame suppression. Short range whole plume emissions at two IR wavelengths were determined using a Scanning Radiometer.

Fig. 9 shows data from the firing of two identical motors of 8.5 kN thrust. In one motor the propellant contains a flame suppression additive. The data shows plume contours of emission intensity in the far infra-red spectrum (7.5 - 12.9 micron wavelength). The reduction in the size of the plume is evident and in particular the maximum intensity is reduced by a factor of 10. Fig. 10 shows data for the same pair of motor firings but in this case presented as an isometric projection. The emission signature in this example is in the near infra-red (4.0 - 5.0 micron wavelength). The effect is evident with a reduction in the peak intensity by a factor of 7 for the flame suppressed motor.

The motors were viewed from 26m range at an angle of 90°. The spectral coverage of the short wave camera is 4.1 to 5.0 micron and the long wave camera 7.5 to 12.9 micron (50% points).

Fig. 11 illustrates long range irradiance measurements which were made on flame suppressed and unsuppressed motors operating at three thrust levels: 1.5 kN, 8.5 kN and 12 kN. The radiometer used operated over the 4.49 - 5.04 μ m spectral range and had standard Cassegrain type optics using a cooled In-Sb infra-red detector. Measurement range and aspect were, 707 m and 155°, (zero aspect, head on) respectively. The radiometer field of view at the plume encompassed the whole of the 1.5 kN and 8.5 kN thrust rounds but with the 12 kN thrust round up to 25% could have been outside the field. The quantity plotted, irradiance is the radiant power per unit area at the measurement instrument. Fig. 11 shows the detailed results for the 8.5 kN thrust motor and it can be seen that the irradiance falls by at least one order of magnitude in the case of flame suppression of the exhaust.

Optical laser transmission through flame suppressed plumes

Some work has been carried out on the propagation of visible light wavelengths through suppressed and unsuppressed plumes. The beam was produced by a Helium-Neon Laser operating at 0.63 micron wavelength in the visible region. The results show that for the 8.5 kN thrust motor transmission levels in excess of 85% were obtained with flame suppressed motors. Difficulties arose with unsuppressed rounds due to rocket plume emissions influencing the laser detector and it was difficult to obtain a reliable transmission level for the unsuppressed motors.

Trials were carried out to examine the affect of flame suppression on the propagation of carbon dioxide laser beams through exhaust plumes. The trials were carried out in conjunction with the optical emission trials using suppressed and unsuppressed motors at three thrust levels. The laser used on the trials was a tunable carbon dioxide laser (Edinburgh Instruments Type PL2) operating on selected lines in the 9-11 micron band, with a nominal power output of two watts continuous wave at 10.6 micron. The laser beam was directed through the plume at 90° to the motor axis and intercepted the plume on centre line at a distance of 25 nozzle diameters from the expansion cone. Detection of the beam was achieved using a multi-element mechanically scanned thermal imager (IR 18 MK 1) which employed time domain integration detectors operating over the 8-12 micron band.

Comparisons of the transmission properties of suppressed and unsuppressed rounds were made and in each case the beam profile in the "No Fire" conditions immediately before and after each firing was measured to enable beam steering and attenuation effects to be determined.

Fig. 12 shows the results obtained for the 12 kN thrust motor with the laser tuned to the 10.59 micron P20 line. It can be seen that during the firing of an unsuppressed round considerable broadening and attenuation of the laser beam occurs. Comparison with the flame suppressed round shows that in this case significantly less broadening occurs with the beam profile becoming much closer to the "No Fire" condition. Calculations performed for these two firings yield transmission figures of approximately 60% for the unsuppressed motor rising to approximately 87% for the flame suppressed round.

Radar transmission through flame suppressed plumes

Measurements of the attenuation of an X-band beam traversing both suppressed and unsuppressed plumes have been carried out both at IMI(S) and other establishments. The trials arrangement at IMI(S) was for an X-band transmitter situated close to the nozzle on the centre line of the motor axis. The beam was arranged to intercept the plume at a shallow angle some 25 nozzle diameters from the exit plane. This was calculated as being the hottest region of the burning plume. The beam was detected by a suitable receiver situated approximately 1.5 metres downstream from the nozzle. Flame suppressed and unsuppressed motors were fired over a range of thrust levels.

An example of the results obtained is given in Fig. 13.

It can be seen from this result that burning plumes produce a high level of attenuation. The level of attenuation increases with thrust level. Flame suppression however dramatically reduces the level of attenuation and over a range of thrust levels the attenuation becomes effectively zero if ignition and burnout effects are neglected.

A further series of trials was conducted whereby the motors were fired on a tower 9 metres above ground level with the detector placed on an adjacent tower. The object of the trial was to eliminate any possible ground reflections of the radar beam. The results obtained on this trial were identical to the IMI(S) trials showing that radar attenuation for a burning round effectively falls to zero when the plume is fully flame suppressed.

Radar attenuation determinations have only been carried out for X-band. However, there is no reason to believe that similar results should not be obtained for J and K band wavelengths.

Effect of Flame Suppression on Smoke in Rocket Plumes

The use of Potassium Salts as flame suppressing additives has the inevitable effect of adding to the amount of smoke produced by motor firings, due to the formation of condensed phase Potassium derivatives appearing as a white smoke downstream of the motor. However, by minimising the amount of additive required for a particular configuration smoke effects can be kept within acceptable limits, associated with minimum smoke propellants.

Throughout the development programme smoke evaluation was carried out for the various additives and methods of incorporation. The major test vehicles for this programme were 150 mm coned cigarette burning charges. The charges were either fired statically, usually in heavyweight reusable motors using fully expanded conical nozzles, or fired down the long sledge track at PEE Pendine using production standard lightweight equipment. In each case the smoke produced was compared with two standard charges with no additive. The first of these was a charge cast in the smoke free inhibition system described previously. The second standard was a charge cast in an elastomeric inhibitor which produces a slightly higher smoke level, but one which is known to be acceptable on flight firings for an in service missile. The potassium containing charges were cast in the smokeless inhibitors and it was reasoned that if the smoke levels emitted did not exceed the standard of the charges cast in the elastomeric inhibitor then an acceptable standard of low smoke had been achieved.

The levels of smoke obtained were assessed by means of a photometric technique with the incident beam traversing the axis of the plume at a narrow angle, and by trained visual observers. An example of the results obtained is presented in Fig. 14.

These show that when assessed by the photometric technique a small smoke penalty is obtained. However the results produced by visual observers show a larger smoke penalty which rises as the potassium level increases.

This is not an isolated result; the same trend has occurred on numerous other occasions. The explanation for these results appears to be connected with the nature of the smoke produced. Potassium Hydroxide is formed in the exhaust cloud and as evidenced by the persistence of the cloud in still conditions the particle size of the smoke is extremely small, probably sub micron. The absorption and scattering coefficients of dilute clouds of sub micron particles are extremely small and therefore a collimated light beam would be expected to suffer little attenuation whilst traversing the plume. However, the visual smoke signature seen by an observer is caused by reflected light from the individual particles. Although the reflection coefficient for each particle is very small the source of illumination, in this case the sky, is extremely large and so an appreciable total amount of reflected light is received by the observer. The reflected component will increase as the source illumination increases and certainly the visual observations suggest that the smokes are apparently thicker and whiter under bright or sunny conditions whereas photometer readings remain unchanged.

As a further demonstration of the effect of the additive on smoke evolution, charges were fired along a 1 000 meter sledge test track at PEE Pendine.

Control rounds were fired in the two inhibitor standards and again the smoke levels produced were assessed by trained observers both visually and from cine records taken at the time of firing.

The results of these firings are presented in Table 5 and it can be seen that fairly high levels of Potassium can be incorporated into the propellants before the smoke level rises above that produced by the elastomeric inhibitor.

Conclusion

Significant advances have been made over the last decade in propellants of properties suitable for tactical weapons. Higher energy/density CDB/EMCDB propellants are available which are smokeless. Specific impulses under standard conditions of 2 400 Ns/kg with density increases of 7% are achievable by Nitramine filler loading.

Equally substantial advances in the state of the art have been demonstrated in secondary flame suppression of high energy propellant boost motors with minimum smoke penalty. Flame suppression has been achieved at low additive levels for nozzle exit plane temperatures up to 1 700°C. Flame suppression has been efficiently achieved with significant nozzle exit area blockage by thrust vector control spoiler devices, with minimum smoke performance. This has been a significant development for tactical missile applications.

The consequential beneficial effects of flame suppression has been reduced signature and improved transparency of the cooler plumes. Visible flame is eliminated and signature in the infra-red spectrum or reduced radar attenuation have been improved by an order of magnitude.

References

1. Minimum Smoke Solid Propellant Rocket Motors
G.I. Evans
AIAA/SAE 8th Joint Propulsion Specialist Conference.
AIAA Paper No. 72-1192
2. Methacrylic Co-polymers:
The Development of a Smokeless General Purpose Inhibitor System
G.I. Evans : D. Facer : M. Ruston : R. Westwood
SRS Technical Report No. 73/20
3. Dox-Mix Systems
A Smokeless Inhibitor for Potting Applications
G.I. Evans : D. Facer : M. Ruston
SRS Technical Report No. 74/2
4. The Suppression of Secondary Combustion in Solid Propellant Rocket Motors
P.K. Smith : G.I. Evans
SRS Technical Note 82/5
5. Spatial Resolved Radiometric Measurement in the 4-5 and 7.5-13 μ m Spectral Bands on Solid Propellant Rocket Motors with and without Secondary Combustion
J.M. Ridout : S. Cockle. PERME Tech Report 237 (1982)
6. Radiometric and Spectrometric Investigation of the Effects of Flame Suppression on the Infra Red Radiation Emitted by a Series of Cast Double Base Propellant Rocket Motors
J.A. Donovan : J.M. Ridout. PERME Tech Report 239 (1983)
7. Measurements of the Effects of a Rocket Motor Efflux on Laser Beams
A.M. Newton. British Aerospace Technical Report ST 26119
8. Additives for the Chemical Modification of Rocket Exhaust Plumes
PERME(W) - IMI Collaboration Trial at Westcott 16-17 May 1978
R.E. Lawrence : J.M. Ridout : B.C. Webb. PERME Memorandum 66

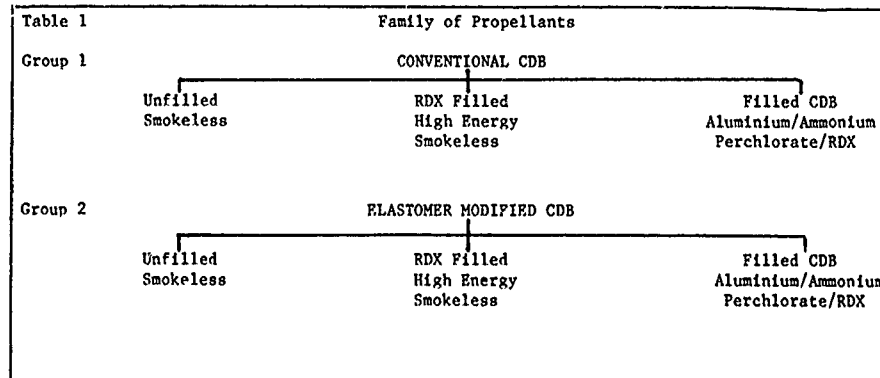


Table 2

PROPELLANT BALLISTIC PROPERTIES

Class	Smoke	Specific Impulse Ns/kg	Density kg/m ³	Density/Impulse MN/m ²
CDB	Minimum	2190-2250	1610	3.52-3.62
Filled CDB	Minimum	2300-2400	1650	3.80-3.97
Filled CDB	Smokev	2530	1770	4.48
PMCDR	Minimum	2370	1580	3.77
Filled EMCDB	Minimum	2450	1650	4.05
Filled EMCDB	Smokev	2530+	1770	4.48+

Impulses at theoretical full expansion from 70 bar

Conventional high energy smokeless) Burning Rates 3mm/s to
EMCDB high energy smokeless) 42mm/s at $\bar{T}_K < 0.2\%/^{\circ}C$

Table 3

POTASSIUM LEVEL FOR FLAME SUPPRESSION
STATIC AND TRACKED FIRINGS

Round	Percentage Potassium in Propellant	Firing Method	Flame
1	0	Static	Continuous
2	0.1	Static	Flashes
3	0.1	Static	Flashes
4	0.2	Static	Out
5	0.2	Static	Out
6	0	Tracked	Continuous
7	0.1	Tracked	Out
8	0.1	Tracked	Out
9	0.2	Tracked	Out
10	0.2	Tracked	Out

Round	Percentage Potassium in Propellant	Average Transverse Transmission %			Axial Smoke Transmission %	Flame	
		0.5 μ m	0.9 μ m	10.6 μ m		Without Deflection	*Full Deflection
1	0	88	91	95	99	CONTINUOUS	CONTINUOUS
2	0.28	88	96	94	96	FLASHES	CONTINUOUS
3	0.42	84	87	96	92	OUT	FLASHES
4	0.56	88	90	93	90	OUT	OUT

MOTOR EXIT PLANE TEMPERATURE 1690°K ; * TVC DEVICE OBSTRUCTING 37% OF NOZZLE EXIT PLANE AREA; RECOVERY TEMPERATURE 2850°K

Round	Percentage Potassium In Propellant	Exhaust Smoke Visual Scale 1-5	Flame
1	0	1	CONTINUOUS
2	0*	2	CONTINUOUS
3	0.14	2	FLASHES
4	0.14	2	FLASHES
5	0.28	2	OUT
6	0.28	2	OUT
7	0.56	3	OUT
8	0.56	3	OUT

* Higher Smoke Elastomeric Inhibitor: Remaining Charges in smokeless Inhibitor

Figure 1. Potassium Level Required for Flame Suppression with Various Potassium Salts

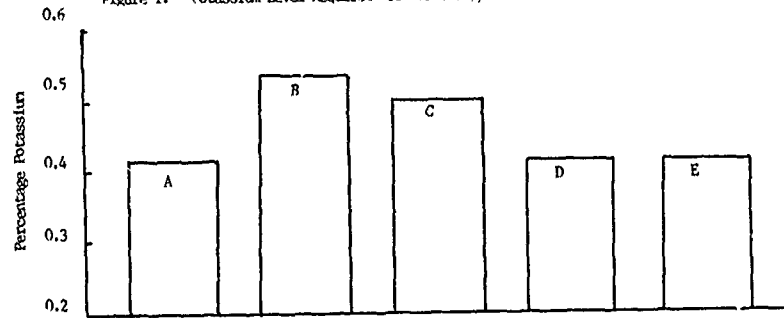


Figure 2. Effect of Incorporation Method of the Flame Suppressing Additive on Propellant Platonisation and Burning Rate

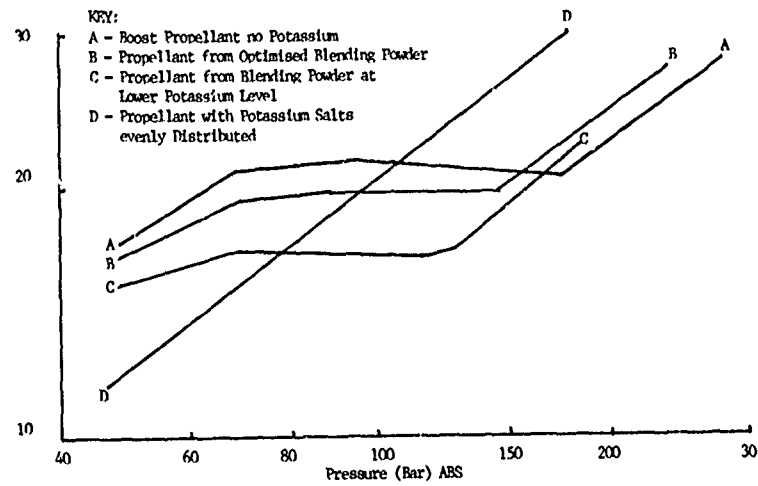


Figure 3. Potassium Level Required for Flame Suppression with Varying Nozzle Expansion Ratio

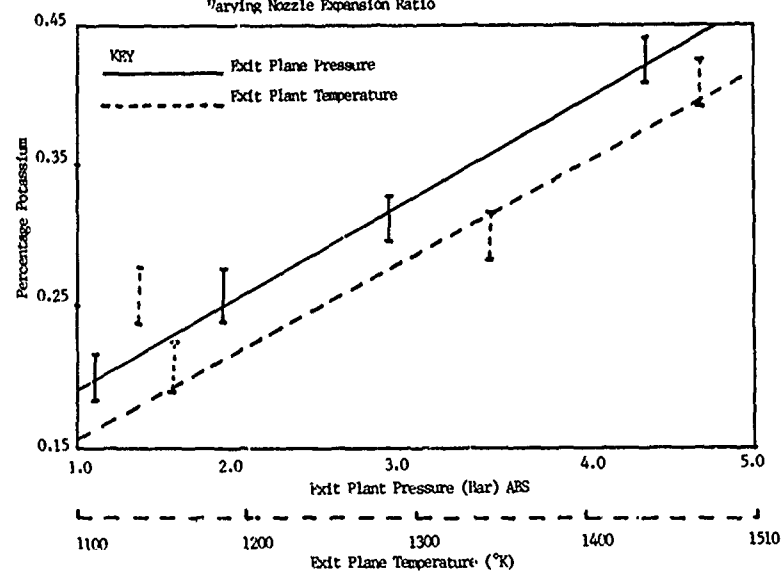


Figure 4 Potassium Level Required for Flame Suppression at Various Thrust Levels

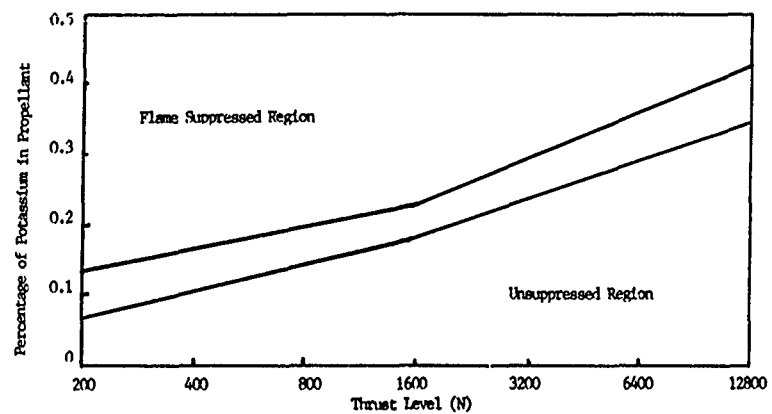


Figure 5 Potassium Level Required for Flame Suppression in RDX Filled Propellant

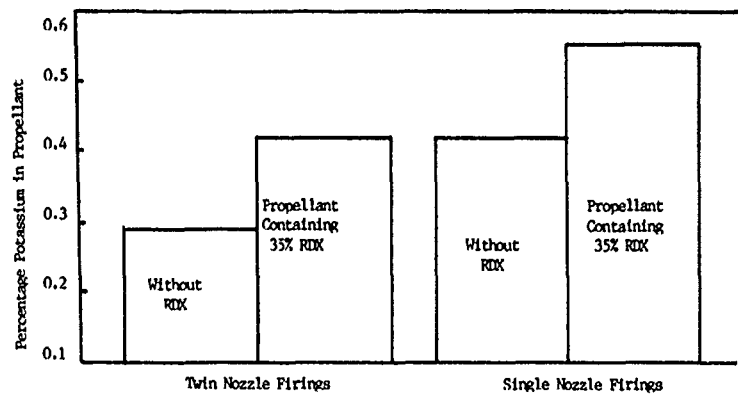


Figure 6 Sustain Motor 2 KN Thrust



Figure 7 Boost Motor 12 KN Thrust

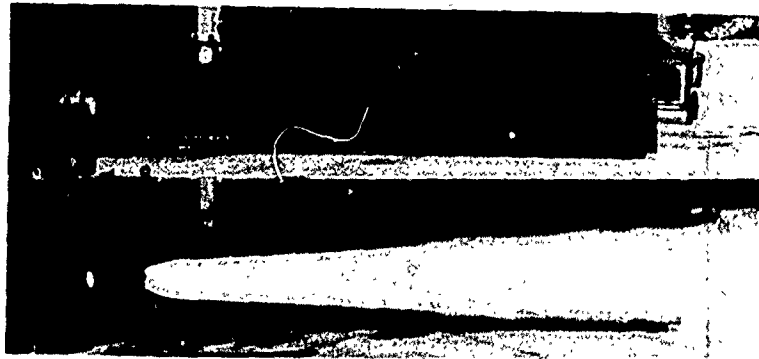


Figure 8 Nitramine Filled Boost Motor 5 KN Thrust

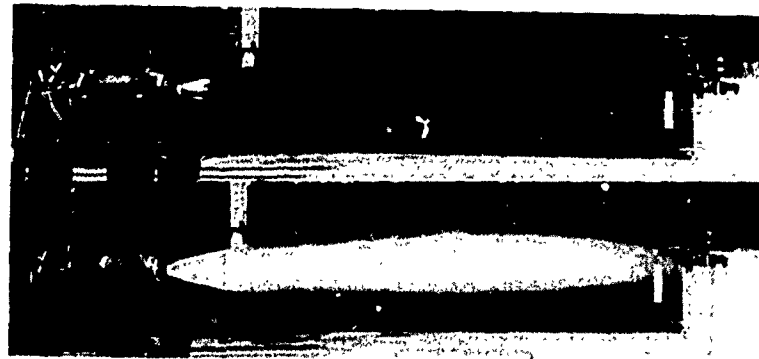


Figure 9 Effect of Plane Suppression on Infra-red Emission

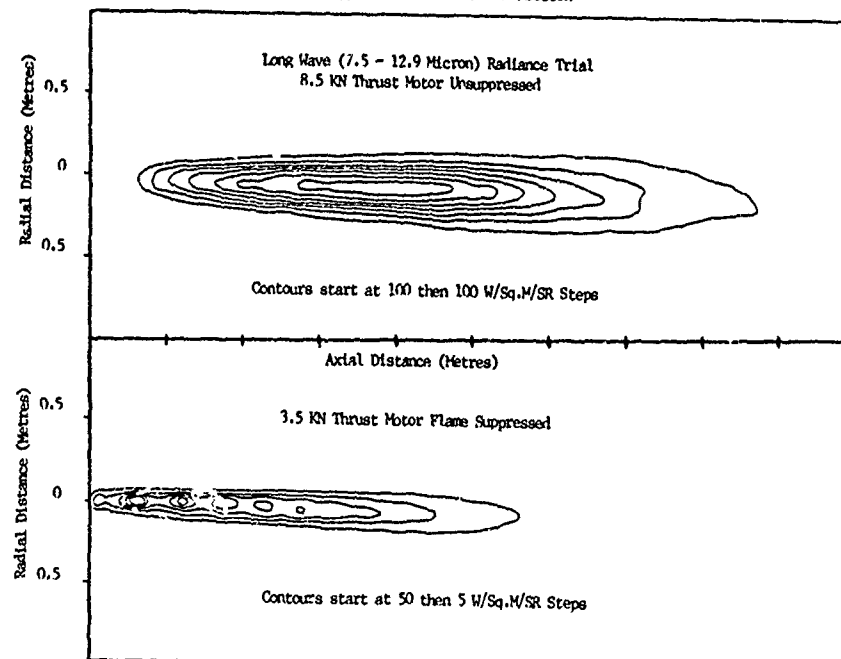


Figure 10 Effect of Flame Suppression on Infra-red Emission

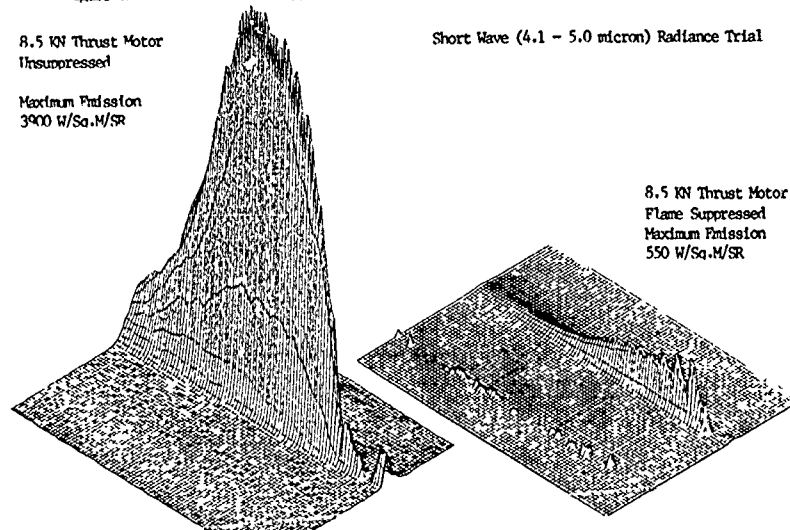


Figure 11 Effect of Flame Suppression on Infra-red Emission

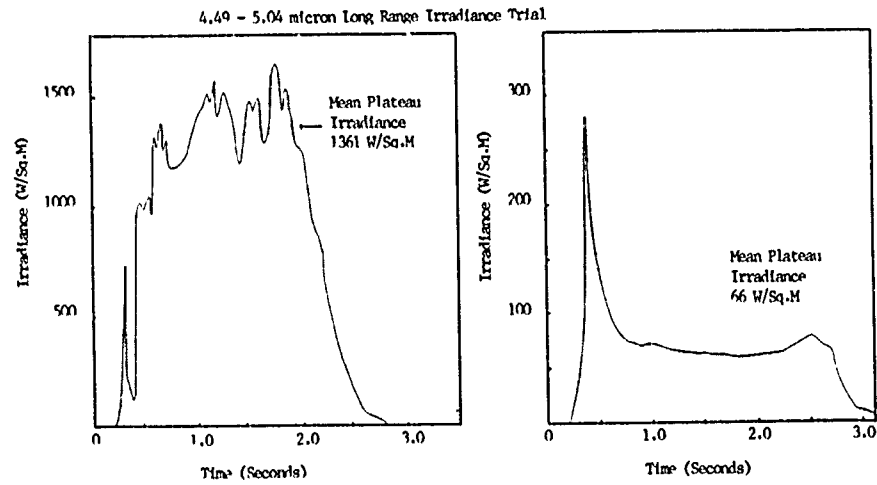


Figure 12 Effect of Flame Suppression on Laser Transmission

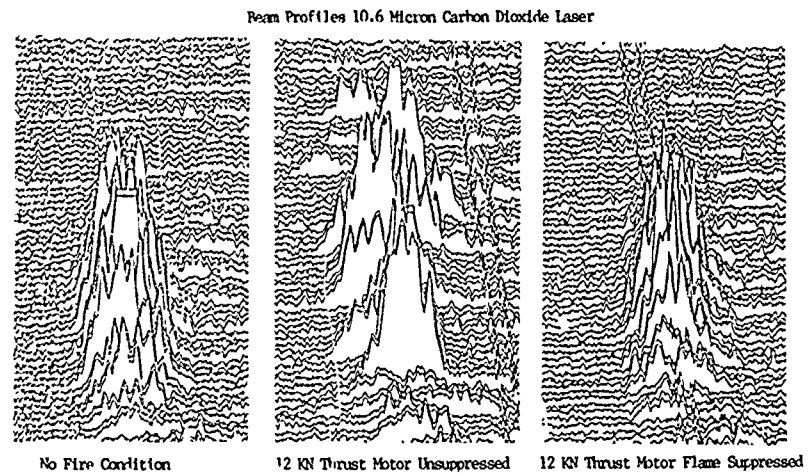


Figure 13 Effect of Flame Suppression on Radar Transmission

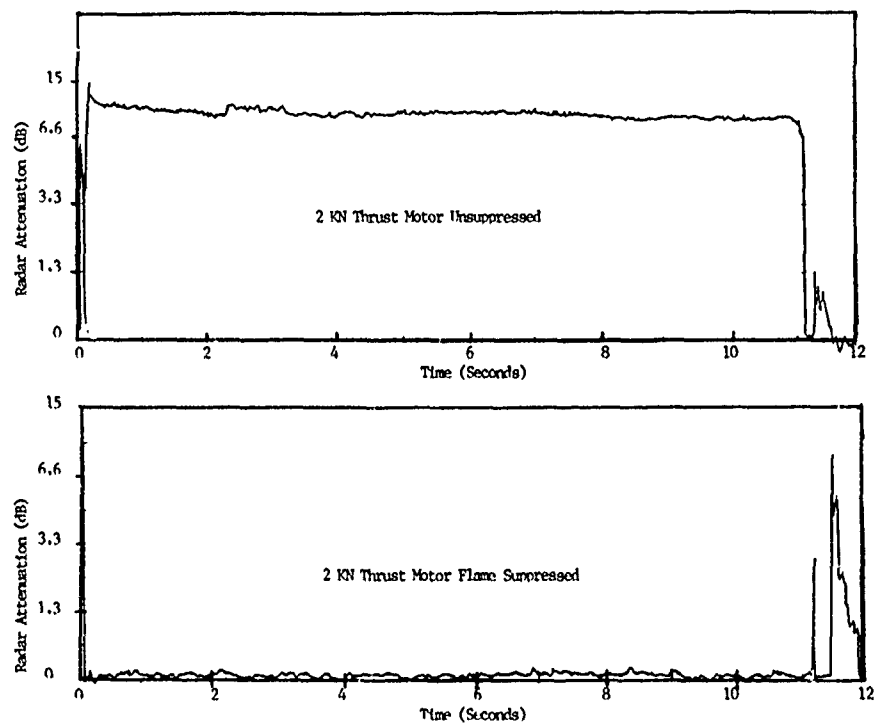
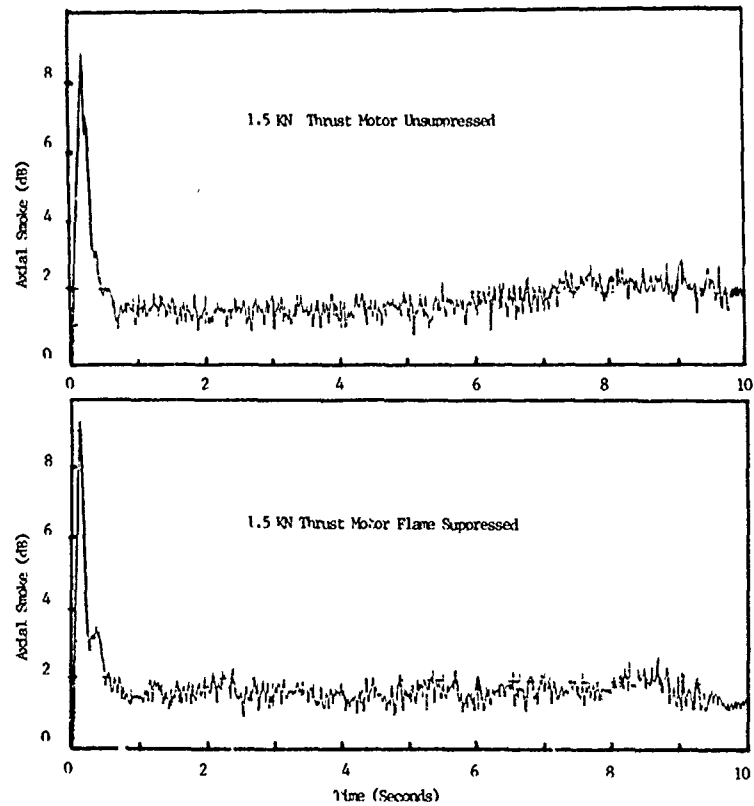


Figure 14 Effect of Flame Suppressing Additive on Smoke Emission



DISCUSSION

N.S.Cohen, US

From what you have presented is it possible that the mechanism of flash suppression by potassium salts is an alteration of the thermochemistry of the propellant combustion zone rather than ionic suppression of plume reactions? If so would this not lead to a different model of flash suppression?

Author's Reply

You could conclude that. I think you are referring to the type of potassium salt and mode of incorporation having a pronounced effect. Most workers in this field seem to rely on the plume gas phase ionisation of the potassium and interruption of the flame chemistry free radical chain reaction as the sole model. I have no information or evidence on how it would function in the propellant combustion zone. However, I firmly believe that the interaction of the potassium salt with the lead salt platonising agent to destroy catalysis takes place in the condensed phase fizz zone interface.

N.S.Cohen, US

My thinking is that the potassium salts promote a thermochemical equilibrium in the propellant combustion zone that does not otherwise exist in minimum smoke propellants. This could be helpful to flash and stability but perhaps detrimental to plateau ballistics. A common thread is the extent to which carbonaceous residues are produced. HMX and RDX also have an influence on this. Did those motor firings shown comparing with and without flame contain stability additives?

Author's Reply

Yes. In the trials shown the higher thrust examples used a radial burning propellant charge. The latter usually requires an instability additive. These additives are chosen to be both refractory and chemically inert in the solid and gas regions. This enables us to control the particle properties and tune the size and density of the instability additive to the acoustic frequency and minimise mass fraction necessary. The amount varies between 0.5% and 1% by weight.

N.S.Cohen, US

Did you look at the use of potassium in these motors without instability additive?

Author's Reply

Yes. If there is no instability, that is no irregular burning, the effects are as shown in the presentation. If irregular burning is present then the variable thrust affects the efficiency of the potassium salt suppression i.e. the minimum mass fraction of potassium salt required to suppress flame.

N.S.Cohen, US

Does the potassium salt itself act as an instability additive in your work?

Author's Reply

We have looked at that to see if the condensed phase potassium, although the mass fraction was small, would contribute to acoustic combustion instability suppression. Its effect was found to be minor. It is a very inefficient form of dampening and so we could not rely on potassium alone.

J.Heimerl, GE

For the record, is the potassium ion suppression mechanism referenced in the paper?

Author's Reply

The postulation mechanism is covered in a number of reports by D.Jensen and his team, of which Chris Mace is a colleague. These reports are referenced in the paper. I should point out, however that, the predictive model predicts levels of potassium required for suppression much higher than we have found necessary in practice.

J.Heimerl, GE

I understand the Jensen reports involve a potassium atom not ion mechanism.

Author's Reply

My reading of the postulation mechanism was of a potassium ion involved in 3 body collisions recombining radicals. If an atom is involved it implies a vapour phase which at the exit plane and shock wave temperature will be largely ionised and in progressively approaching the threshold of flame suppression via unstable flame then such high secondary flame temperatures imply a very high degree of ionisation of the potassium vapour. The vapour phase as opposed to condensed phase potassium is assumed to be the more efficient suppression state.

A.C.H.Mace, UK

There is an element of semantics but the postulated mechanism involves potassium atom and hydroxide species through two chemical reactions. $K + H_2O \rightleftharpoons KOH + H$ and $K + OH + M \rightleftharpoons KOH + M$. The net effect is to accelerate free radical $H + OH$ recombination.

E.Ajdari, FR

I note that in order to fix or predict the level of potassium additive you take account of the nozzle exit plane temperature, and thrust level and the percentage RDX in the propellant. Do you think the RDX has a specific chemical action or does it act by modification of the level of CO and hydrogen in the gas exiting from the nozzle?

Author's Reply

It is correct that we take the nozzle exit plane temperature and thrust to arrive at additive level. It is also true that when RDX is present we require significantly less potassium than this empirical model, based on experiment would predict. I do not know the mechanism but it appears to be chemical because it significantly affects the optical properties of the smoke cloud beneficially i.e. at the same potassium mass fraction, exit plane temperature and thrust, the smoke properties differ significantly if RDX is present.

E.Ajdari, FR

Would you estimate that the attenuation of a laser beam in presence of secondary combustion would be sufficient to prevent functioning of the guidance system by laser?

Author's Reply

I hope the presentation made clear that when secondary flame is present the plume is hotter. This results in more diffraction, dispersion, broadening of the laser beam and the attenuation is greater. I showed you two test firings where the transmission of a 10.6 μm beam was 60% with secondary flame present and 87% when the flame is suppressed. I cannot give a threshold of an acceptance because this depends on the missile guidance but in general a missile designer will always ask for the maximum transmission or minimum attenuation.

T.Vaillant, FR

You showed diagrams illustrating interaction of potassium additives and burning rate catalysts to destroy platinisation. You also showed method of incorporation to prevent this interaction. Would you not have this chemical interaction occurring on ageing?

Author's Reply

This is a very relevant question. The paper describes that where such additives can react these are incorporated in separate granules which are blended. These granules retain their individual identity in the propellant so that the ingredients are spatially separated. Thus, providing the ingredients are not soluble in the matrix and do not migrate, then stability with ageing is obtained.

This is the case with the work presented here. Our normal practice in qualifying these propellants is to store them continuously at 60°C for 24 weeks and to monitor the platinised burning rate at 4 week intervals to demonstrate stability of burning features.

T.Vaillant, FR

You have shown diagrams of the effect of thrust level on the minimum amount of potassium necessary and you say the diagrams use optimum nozzle expansion. Do you mean that optimum nozzle expansion is critical or do you mean the nozzle has been specially adapted?

Author's Reply

The diagrams you refer to involved trials utilising full expansion with conical nozzles. Full expansion minimises shock waves and standardises the comparative trials. Nozzle shape design is covered elsewhere in separate trials and is important. Parallel flow designed nozzles are superior to conical nozzles in reducing shock waves and reducing the amount of potassium to suppress flame. Does that answer the question?

T.Vaillant, FR

Yes.

THE CHEMICAL INTERACTION OF
BALLISTIC MODIFIERS IN CDB PROPELLANT
- ITS EFFECT UPON BALLISTICS AND STABILITY

By

J D M PEARSON, A C J SHEDDEN AND I A DUNCAN

DEFENCE AND AEROSPACE RESEARCH

DEFENCE AND AEROSPACE GROUP, NOBEL'S EXPLOSIVES COMPANY LIMITED, ICI,
STEVENSTON, Ayrshire, SCOTLAND, KA20 3LN

SUMMARY

During the development of a platonised cast double base propellant it was noted that a spread of burning rates from batch to batch was obtained. Subsequently batches of the propellant persistently showed a marked decrease in gas crack lifetime, on accelerated ageing, compared with earlier satisfactory results.

Extensive work showed the stability problem to be associated with a chemical reaction between the ballistic modifiers. This reaction was reproduced in the laboratory, while at the same time the ballistic variability of the propellant was under investigation. It became apparent that the chemical interaction between the modifiers affected the propellant platonised burning rate and that the by-products of this reaction cause the accelerated ageing problem. This understanding allowed a new ballistic modifier to be developed which helped solve the stability problem while at the same time give much more reproducible ballistics.

1. INTRODUCTION

Ballistic modifiers have been used in nitrocellulose, based propellants since their discovery and exploitation in the 1950's. They modify the burning rate - pressure relationship of a propellant so that the pressure exponent 'n' is reduced over a useful pressure range - this region is called a plateau when $n = 0$.

Platonised propellants offer considerable advantages over unplatonised formulations in reducing the variability in motor performance over the temperature range of operations.

Work in the area of ballistic modifiers has tended to concentrate on two topics:

- (i) studying and modelling of propellant burning rates to understand the mode of action ballistic modifiers (1, 2 and 3)
- (ii) investigating propellant processing aspects and ingredient dispersion with respect to plateau development and burning rate control (4, 5).

This paper explores one example from an area which has not received the same amount of attention in the past, namely the chemical interactions of ballistic modifiers in propellant either during or after manufacture. It is often assumed that ballistic modifiers are added to propellant during manufacture and remain in the propellant, essentially as they were added, until required to catalyse combustion processes. Here an example of the chemical interaction between two ballistic modifiers is described with its resultant effect upon propellant ballistics and stability.

2. EXPERIMENTAL OBSERVATIONS

During the development of a Lead B Resorcyate (LBR) Basic Copper Salicylate (BCS) modified propellant formulation it became apparent, as ballistic data from a number of batches were collected, that a spread of platonised burning rates was obtained. The spread of values was up to $\pm 3\text{mm/sec}$ on the mean burning rate. Further, the reproducibility of the plateau character also displayed some variability. These phenomena are shown in Figure 1. The spread of burning rates and plateau shapes was wider than expected from the usual experience of batch to batch variations in casting powder manufacture. It might be argued that such a spread of ballistics merely demonstrated variability in the casting powder mixing schedule. Conventionally, by achieving good ingredient blending and a satisfactory processing record (ie. sufficient work on the casting powder dough) a well platonised propellant formulation is obtained. A poor processing record on a propellant dough gives only a partly developed plateau. A descriptive illustration of this is given in Figure 2. However such an explanation did not seem to fit the experimental observations in this case. Further, work done at one of the Government Research Establishments - PERME Waltham Abbey - suggested that plateau development in this propellant type was a function of the solvent system used.

The original evaluation of the long term propellant stability as determined by the Silvered Vessel Test and the Crack Cube Test showed it to be satisfactory. Crack life values obtained for the early powders are shown at the top of Table 1. The crack cube test, which determines the gas crack lifetime of the propellant, is considered acceptable if the propellant has a crack life in 2" cubes stored at 80°C of greater than 10 days (equivalent to 20 years or greater at 20°C).

With these early results work on the propellant development continued, with the main emphasis on tightening and improving the batch to batch variability of the ballistics.

However during routine batch testing of casting powder lots for ballistics and stability, it was observed that the propellant crack life in 2" cubes stored at 80°C had dropped markedly to between 2 and 5 days, compared with the previous figures of 14 days and above, as can be seen from Table 1. Another observation made was that some of these casting powders had a grey bloom on the surface of the granules which had not been observed previously. Repeated manufacturing of batches of casting powder all showed poor propellant crack life results. All the powders showed good absolute and bulk densities and gave satisfactory powder liquid ratios, so these parameters had not changed.

However the propellant was now suffering from a gassing phenomenon, presumably due to nitric ester breakdown, which was not evident in the earlier batches. Vacuum stability results on chopped propellant stored at 80°C for 7 days showed that about 1ml of gas (at STP) was evolved per gram of propellant.

3. FURTHER WORK - RESULTS AND DISCUSSION

(a) Propellant Stability

The work done on the propellant stability problem may be presented under the headings given below:

- (i) Observations and analysis
- (ii) An examination of the individual ingredients and formulation variations
- (iii) A re-examination of the old powder batches
- (iv) Casting powder processing

This follows rather loosely the chronological order in which the work was carried out.

(i) Observations and Analysis

A grey/white bloom was often noted on samples of this casting powder formulation when it was more than a few months old. The bloom growth continued as a function of time. It was found to be water soluble, was washed off, recovered and analysed. Results from x-ray diffraction, melting point and IR analysis showed it to be B resorcylic acid obviously from the lead salt modifier in the propellant. An examination of a range of powder batches showed differing degrees of blooming, and although it appeared that in some powder batches the LBR was undergoing hydrolysis, this did not appear to correlate with the poor propellant crack life.

The propellant rheology between good and bad batches was not considered to be significant in this work as it was shown that even substantially increasing the propellant tensile properties had little effect upon the propellant gas crack life.

As propellant gassing or nitric ester breakdown generally occurs after stabiliser consumption, samples of cracked propellant were examined for stabiliser content. This showed that the propellant contained significant quantities of stabiliser when gas cracking occurred. It was therefore obvious that the gassing reaction in the propellant was fairly vigorous and not contained by the stabilisers.

(ii) An Examination of Individual Ingredients and Formulation Variants

One of the first thoughts in this work was to check the efficacy of the propellant stabilisers. A number of batches of casting powder were made with different batches of stabilisers and using double quantities of stabilisers, but without increasing the gas cracklife of the propellant - see Table 2.

Initially all the analysis records of batches of ingredients used in 'good' and 'bad' stability batches of casting powder were examined against their specifications, and nothing significant was observed.

However it was observed during this exercise that the 'good' batches of casting powder had all been made from one lot of Nitrocellulose (NC). This NC batch had a higher chalk level at 0.44% compared with powders made subsequently which gave poor crack lives and had chalk levels of 0.3 to 0.33%. Yet all the NC batches gave similar heat test and Bergmann and Junk's Test values. This prompted the manufacture of casting powder from low medium and high chalk content NC, the results of which are shown in Table 2. These show that the chalk level has little effect on the propellant stability. Nitroglycerine (NG), a further raw material in this propellant, was not suspected of contributing to the stability problems as it fully met its specification and in the wide range of NEC casting powders no other stability difficulties had been observed.

Although the ingredients met their respective specifications, items like a material's 10% w/v pH, specific surface or moisture content were believed might affect their reactivity and thereby their compatibility. Results here suggested that the carbon black used, which showed acidic behaviour with its low 10% w/v pH and the copper salicylate, which could have high specific surface areas, might be reactive ingredients. This prompted an examination of various ingredients from alternative suppliers, where possible. The results are shown in Table 2. They demonstrate that although a range of NC's of different Nitrogen contents, stabilisation cycles, sizes and from different manufacturers were used; carbon blacks from different batches and sources with both acid and basic pH's were tested; and copper salicylates from different batches and sources were employed none of these markedly improved the propellant crack life.

'Maglite', (synthetic calcined magnesite) an acid acceptor, was used in an experiment to counter the acidic pH of the carbon black in case this was affecting the propellant stability. The propellant crack life improved to 7 days (see Table 2). However this result was difficult to explain as the original good casting powder had been made using the same carbon black having the same 10% w/v pH as that used in poor batches.

The various minor casting powder ingredients were then checked in two series of vacuum stability tests. In the first of these the dry ingredients - Lead B Resorcyate, Basic Copper Salicylate and Carbon black were mixed with chopped samples of the propellant base matrix i.e. NC, NG, plasticisers and stabilisers immediately prior to testing, as in a typical compatibility test. The gassing results gave the following order of reactivity:

Carbon Black (CB) >> Basic Copper Salicylate (BCS) > Lead B Resorcyate (LBR) which tended to suggest that the carbon black might be expected to cause gassing problems in the propellant. This experiment was followed up by one in which small scale batches of the CDB propellant formulation were made incorporating the various minor ingredients at the correct levels either on their own or in combinations. The chopped propellant was again submitted for vacuum stability testing and the results are shown in Table 3. These results show that the ranking order for gassing is now:-

BCS + CB > BCS + LBR + CB > BCS alone > other ingredients.
This suggests that it is the Basic Copper Salicylate in the final incorporated formulation either on its own or with carbon black or with LBR and carbon black that gives rise to propellant gassing. All other combinations liberate considerably less gas.

In order to test this hypothesis batches of casting powder were made in an omission of ingredients experiment. The stability results are shown in Table 4 and plainly show that it is the Basic Copper Salicylate which is implicated in the gas cracking reactions. This suggested an avenue of approach to solving the problem by studying formulations without any Copper Salicylate. However the presence of Basic Copper Salicylate is required to give the required platonised ballistics.

The effect of doubling the stabiliser content or changing the stabilisers or their respective ratios however had no effect on reducing the propellant gassing in which the Basic Copper Salicylate was implicated.

At this point, since the Basic Copper Salicylate in recent batches was the source of the propellant gassing problems, it was decided to 'look back at the older 'good' stability powders to try to understand why they gave good crack lives.

(iii) A Re-examination of the Old Powder Batches

One of the previous good casting powders was submitted to both analytical and crack life testing. The powder had a good heat test result, acceptable stabiliser content and showed evidence of slight blooming not observed previously. This was shown to be 2,4 dihydroxybenzoic acid as described above. The vacuum stability test on the powder gave a value similar to that seen in recently manufactured poor crack life batches. After casting the propellant it was found to have a crack life of only 3 to 4 days and not 14 days as seen previously (see Table 1).

This was a baffling result which was not immediately explainable.

(iv) Processing

Work in this area tended to overlap with the studies of the ballistic variability, however only the aspects of processing not directly affecting the ballistic modifiers are described here.

The need to tailor the solvent systems and their quantities to the type of casting powder being made in order to give adequate processing has long been recognised. So it was postulated that the processing solvents and their quantities might have had some effect upon the casting powder and hence the propellant.

A number of solvent ratios were investigated initially with the normally employed solvent system. These had no effect upon the propellant crack life, see Table 5. Predissolving the casting powder stabiliser in processing solvent prior to incorporation had no effect either on the propellant crack life. The platonised ballistics observed lay within the usual spread. A number of less gelatinising solvent systems were also examined. These solvents tend to have a lower moisture content. Although they showed poor plateau quality ballistics (Figure 3) they did give a crack life of 7 days. The poor ballistic quality

seen was ascribed to the 'dryness' of the solvent, as it was already known from PERME Waltham Abbey work that moisture in the processing solvents was required to allow plateau development.

The casting liquid used to cast the propellant was also subject to examination. The addition of larger quantities of stabilisers, plasticisers and nitrocellulose cross linking agents were investigated but none of these improved the crack life of the propellant.

(b) Propellant Processing

The casting powder processing work commenced with a view to improving the ballistic reproducibility of the propellant about the same time as the onset of the stability problem. The importance of the processing findings to the stability problem became apparent as the work progressed.

The work may be split under the following headings:

- (i) Pretreatment of the ballistic modifiers
- (ii) Laboratory trials and the importance of water
- (iii) The effect of water on the casting powder
- (iv) Formation and testing of a mixed Pb Cu organometallic complex

(i) Pretreatment of the Ballistic Modifiers

It was known from reported work at PERME Waltham Abbey that the presence of moisture helps develop the plateau in Lead B Resorcyate Basic Copper Salicylate modified propellants. As the solvent used during casting powder incorporation has a minor but significant water content the lead and copper salts were submitted to vigorous mixing in the ratios used in the casting powder. Similar experiments were also tried by increasing the water level in the solvent. Also examined was the predispersion of all the minor ingredients. The moisture level was observed to be critical in allowing the formation of a good plateau while allowing normal propellant processing to occur. Results show a well developed plateau with a narrow spread of platonised rates (with one exception). Some typical plots are given in Figure 4. Other forms of pretreatment of the modifiers involved adding them during the NC/NC wet mixing process and again a well platonised propellant of essentially the same rate as those above was obtained - see Figure 4. These results confirmed the suggestion from Waltham Abbey that water was important to the plateau development.

When these powder batches were examined for their propellant crack life stability, they showed a general improvement over those normally seen - see Table 6.

This was the first direct suggestion that the reaction between the lead and copper salts affected the propellant stability as well as the ballistics.

This work led to the laboratory examination of the reactions involved between Lead B Resorcyate and Basic Copper Salicylate.

(ii) Laboratory Trials and the Importance of Water

The compounds Lead B Resorcyate and Basic Copper Salicylate were investigated singly and together in a range of polar and non polar organic solvents, as well as water, under different conditions of mixing and temperature. The reaction products were examined in each case.

The conclusions of this work were that a reaction took place between the lead and copper salts to form a mixed lead and copper organometallic complex of the two acid anions with the liberation of some of the resorcyate and salicylate as free acids.

There was no significant hydrolysis of either LBR or BCS unless forcing conditions were employed.

The reaction between the lead and copper salts was shown to require the presence of a protic solvent for it to occur with any marked reaction rate. Water is a good protic solvent and the need for such a solvent is explained by the fact that part of the thermodynamics driving this reaction might appear to be the formation of the free acids B Resorcylic and Salicylic.

A postulated route to the formation of the complex is given in Figure 5. This allows the observed reaction to take place at an appreciable rate, which would be unlikely between two solid particles, and explains the importance of solvents and water.

(iii) The Effect of Water on the Casting Powder

Whilst the above work was progressing, and after the importance of water had been demonstrated, trials to generate the complexation reaction between LBR and BCS in situ in casting powder were undertaken. The process used was water steeping of the powders. This was found to help develop the plateau and increase the platonised burning rates - see Figure 6. It was observed that a fairly tight spread of ballistics is obtained over all the trials with rates almost identical to the work reported above when the modifiers were pretreated prior to being incorporated. The crack lifetimes were tested on the propellant and are reported in Table 7. These values of 7-14 days show a big improvement over the

unsteeped powders. So steeping not only allows complexation to improve the ballistics it also benefits the propellant stability, presumably by removing the acidic by-products of the reaction.

However with powder steeping a balance had to be struck to allow complexation to occur between the modifiers as well as removing the acidic impurities on the one hand and not leeching out propellant stabiliser on the other.

(iv) Formation and Testing of a Mixed Lead & Copper Organometallic Complex

Having made and isolated a reaction product between Lead B Resorcylic and Basic Copper Salicylate it was characterised and a number of repeat preparations of the material were carried out. This showed that a specific characterised material could be reproducibly made.

The material was incorporated into propellant, making a small adjustment to the old formulation. The new casting powder formulation was made and cast into propellant which gave a well platonised propellant of reproducible ballistics - see Figure 7 - with the same burning rate as the old formulation.

This propellant also showed good accelerated ageing stability with a crack life of 14 days, a Silvered Vessel Test of 84 days and a Vacuum Stability Test of about 0.2 mls gas/g propellant.

Obviously the gassing reactions in the propellant are now much reduced as instanced by the vacuum stability data and this is reflected in the satisfactory crack life figure. Repeated powder manufacture gives propellant with a well developed plateau (see Figure 7) and a spread of burning rates of ± 1 mm/sec or better about the mean value, and a crack life range from 14-17 days.

In a deliberate attempt to age the new casting powder formulation, following experience related above, a sample was stored at 43°C for 2 months. The powder stability and heat test were still satisfactory and on casting the propellant showed no change in its ballistics or stability characteristics (see Figure 7).

(c) Synthesis and Conclusions

Having demonstrated that making and using the Lead B Resorcylic Basic Copper Salicylate complex in casting powder both solved the stability problems of the propellant as well as giving reproducible ballistics all the other observations made during this study fall into place. The explanation of these early observations is given below:

In the initial casting powder batches, which gave good crack lives, processing had obviously not allowed the formation of the modifier complex with release of free acids, so the propellant stability was satisfactory. However upon standing in the casting powder the two modifiers had obviously started to react together, releasing incompatible free acids causing powder bloom and reducing the propellant crack life.

The bloom seen on casting powders was identified as B Resorcylic acid which had been shown to be a by-product of the modifier complexation reaction. The extent of powder blooming was always rather variable and no doubt depended upon the rate of reaction of the lead and copper modifiers and the diffusion rate of any acid to the granule boundary.

The addition of Maglite D to the casting powders improved the propellant stability. It was added originally to counter any acidity of the carbon black, however it no doubt acted by countering the acidity of the free B resorcylic and salicylic acids from the complexation reaction.

The removal of ECS from the casting powder formulation greatly improved the propellant stability not because of any incompatibility of the material but because no modifier complexation would then occur with the subsequent release of the free acids.

Using dry solvent systems during casting powder processing improved propellant crack life and gave rather poor quality ballistics. This can be explained in that to form the modifier complex the presence of moisture or water is required, so without it the lead and copper salts had not reacted, so little incompatible free acids would be released. The poor quality ballistics are probably due to two effects - poor processing of the propellant dough on account of the solvent system used and a lack of the active modifier complex to promote platonised burning.

In the initial trials using water or moist solvents to process the modifier salts the stability of the propellant improved but not to a satisfactory level. This is thought to be due to the fact that the free acids from the complexation were not being carefully enough removed and there was no guarantee that the reaction between the modifiers was complete.

Casting powder steeping was a way of forming the modifier complex in situ as well as washing out the free acids. Hence its success in raising the crack life and giving good ballistics. The drawback of powder steeping was the leeching out of stabilisers.

The separate manufacture and assessment of the complex tied together the two strands of this work - ballistic variability and propellant stability and allowed many observations which seemed, at the time, rather unrelated to fit well together.

References

1. D Hewkin, J A Hicks, J Powling and H Watts,
"The Combustion of Nitric Ester Based Propellants : Ballistic Modification by Lead Compounds",
Combustion Science and Technology, 2, 1971, 307-327.
2. N Kubota,
"The Mechanism of Superate Burning of Catalysed Double Base Propellants", Aerospace and Mechanical
Sciences
Report No 1087, Princeton University, N J, USA.
3. T J Lewis
"The Interpretation and Simulation of Burning Rate Curves for Platonised and Unplatonised Double
Base Propellants"
PERME, Waltham Abbey, Technical Report 270.
4. R J Ayerst
"The Influence of Size and Dispersion of Particulate Ingredients on the Ballistics of Double Base
Propellants"
ICT Internationale Jahrestagung, Karlsruhe 1978, 73-77
5. I A Duncan
"Production Control in Cast Double Base Powder Manufacture for Rocket Motors"
ICT Internationale Jahrestagung, Karlsruhe 1983, 91-92.

Acknowledgements

The authors would like to thank Mr D Facer and Mr N Veton of IMI Summerfield Research Station and
Mr E Baker of Royal Ordnance, Explosives Division, Waltham Abbey for collaboration and discussions during
this work.

TABLE 1

GAS CRACK LIFETIMES FOR EARLY AND SUBSEQUENT BATCHES OF CASTING POWDER

POWDER BATCH	FORMULATION	PROPELLANT CRACK LIFE, DAYS AT 80°C
Early batches	Standard	14
	"	30
	"	35
Subsequent batches	"	5
	"	5
	"	2
	"	3
Early batches recast later	"	3-4

TABLE 2

GAS CRACK LIFETIMES OF VARIOUS FORMULATION VARIANTS

FORMULATION	PROPELLANT GAS CRACK LIFETIME* DAYS AT 80°C
CHANGED STABILISER BATCHES	4
DOUBLE STABILISER 1	5
DOUBLE STABILISER 2	5
CHALK FREE NC	3
STANDARD CHALKED NC	5
HIGH CHALK NC	4
VARIATIONS IN MINOR INGREDIENT LEVELS	3-4
MINOR INGREDIENTS FROM DIFFERENT SOURCES	3-5
NC FROM ALTERNATIVE SOURCE	3
STANDARD NC	3-5
BLASTING SOLUBLE NC	3
NEW BATCH NC	5
DIFFERENT GRADES OF CARBON BLACK	3-7
ADDITION OF MAGLITE	7
DIFFERENT PLASTICISER	3

* The figures given are representative of a much larger collection of results

TABLE 3
VACUUM STABILITY RESULTS
MINOR INGREDIENTS INCORPORATED INTO THE BASIC MATRIX

BASIC MATRIX	MINOR INGREDIENT INCORPORATED	GAS EVOLVED ml PER GRAM OF PROPELLANT
NC/NG/PLASTICISER	None	0.62
NC/NG/PLASTICISER/STABILISERS	None	0.20
"	LBR	0.20
"	BCS	1.69
"	Carbon Black	0.27
"	LBR + Carbon Black	0.32
"	BCS + Carbon Black	3.62
"	LBR + BCS	0.26
"	LBR + BCS + Carbon Black	2.96

LBR = Lead R Resorcyate BCS = Basic Copper Salicylate

TABLE 4
THE EFFECT OF SINGLE INGREDIENT OMISSION
ON GAS CRACK LIFE OF THE PROPELLANT

FORMULATION VARIANT	GAS CRACK LIFETIME, DAYS AT 80°C
OMITTING CARBON BLACK	4-7
OMITTING BCS	18
OMITTING LBR	3

BCS = Basic Copper Salicylate

LBR = Lead B Resorcyate

TABLE 5
THE EFFECT OF PROCESSING SOLVENT
UPON PROPELLANT GAS CRACK LIFE

FORMULATION	PROCESSING	CRACK LIFETIME OF PROPELLANT IN DAYS AT 80°C
Standard	Normal solvents	3
	Normal solvents increased level	4
	Normal solvents stabiliser dispersed in solvent	3
	Dry solvent system	7

TABLE 6
THE EFFECT OF PRETREATMENT OF THE BALLISTIC MODIFIERS
ON PROPELLANT GAS CRACK LIFE

FORMULATION VARIANT	CRACK LIFETIME OF PROPELLANT IN DAYS AT 80°C
Modifiers predispersed in solvent + water	6
Modifiers predispersed in wet solvent	6
Wet incorporation	7
Modifiers added at NC/NG wet mixing	7
All minor ingredients in alcohol before incorporation	3

TABLE 7

EFFECT OF POWDER STEEPING ONGAS CRACK LIFE OF THE PROPELLANT

FORMULATION	GAS CRACK LIFE OF PROPELLANT IN DAYS AT 80°C	
	UNSTEEPED	STEEPED
Standard	3	10
Standard	3	14
Different NC	3-5	7
Chalk Free NC	3	7
Different BCS	5	10
Different Carbon Black	4	10
Double Stabiliser	2	6-10

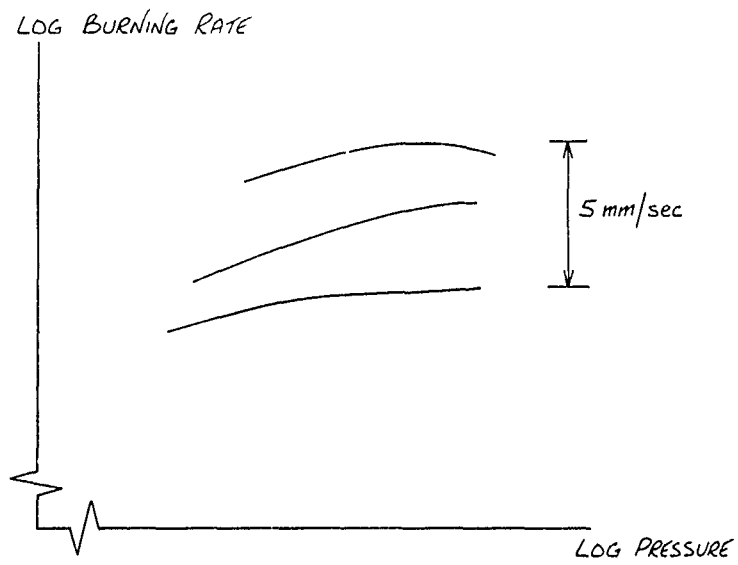


FIGURE 1
SPREAD OF BURNING RATES AND PLATEAU SHAPE

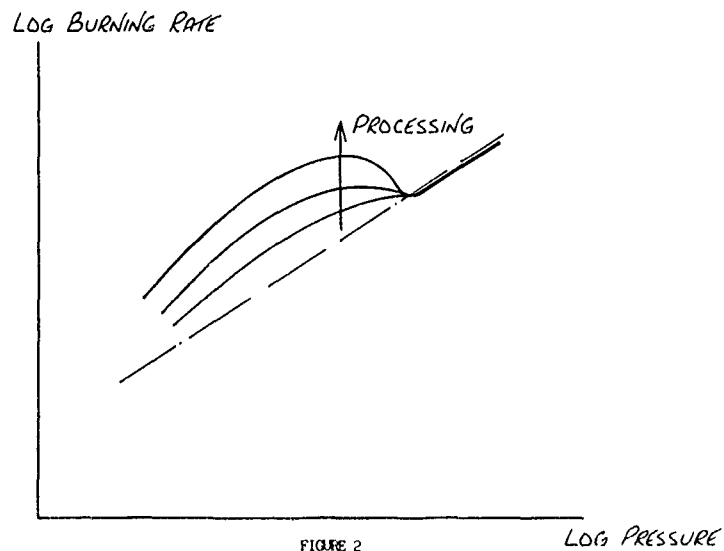


FIGURE 2
EFFECT OF PROCESSING ON PLATEAU DEVELOPMENT

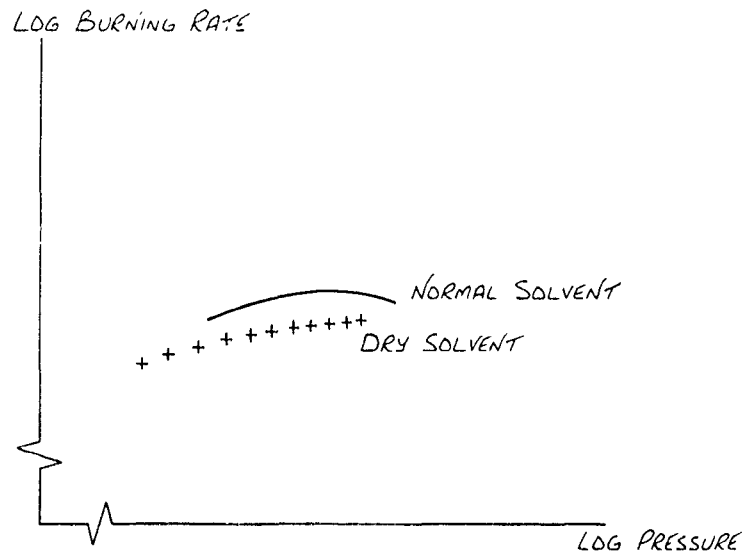


FIGURE 3
EFFECT OF PROCESSING ON BALLISTICS

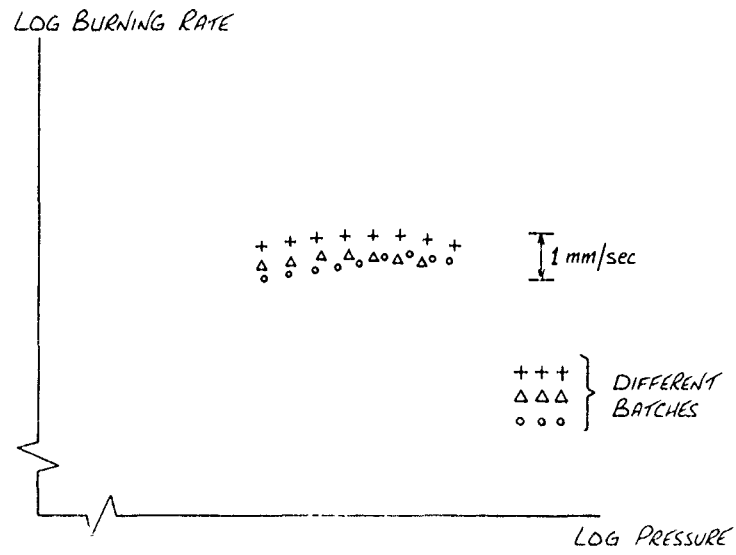


FIGURE 4
EFFECT OF PREPARATION METHODS ON BALLISTICS

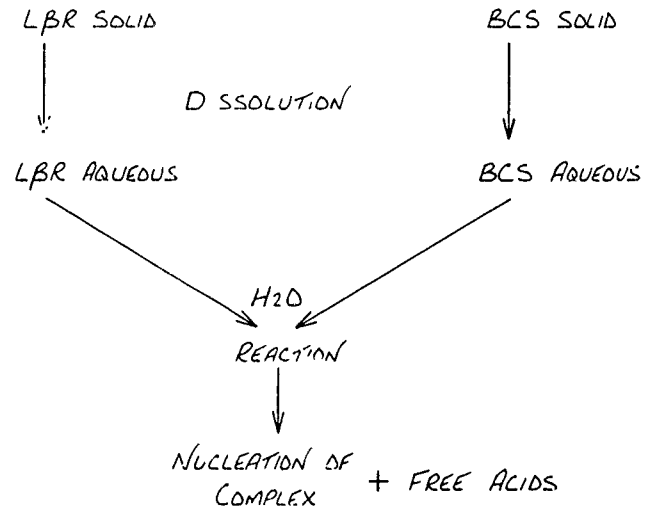


FIGURE 5
REACTION SCHEME

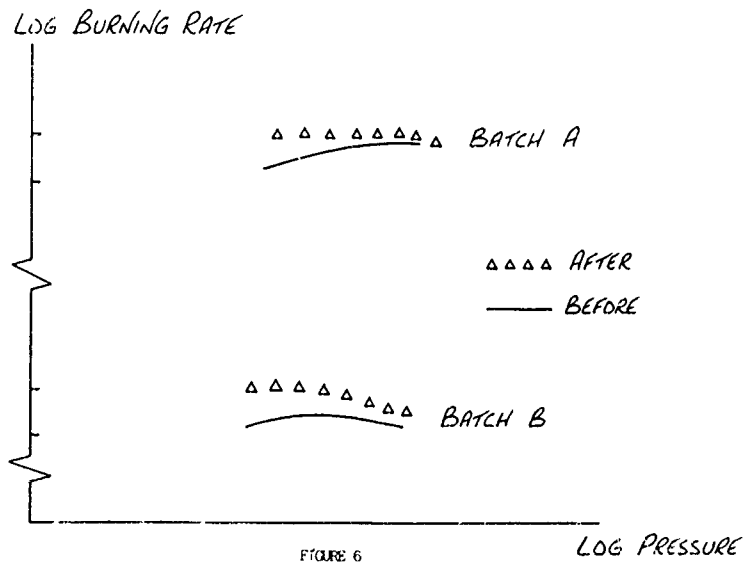


FIGURE 6
BALLISTICS OF WATER STEEPED POWDERS

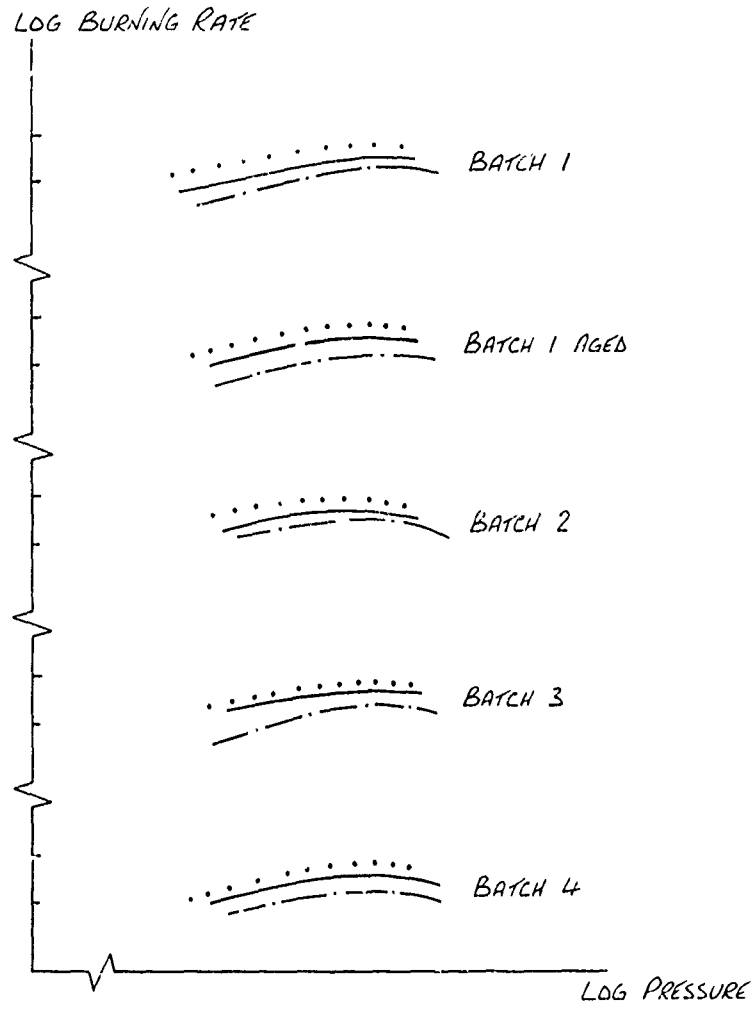


FIGURE 7
BALLISTICS OF NEW POWDER FORMULATION

KEY

- HOT FIRING
- AMBIENT FIRING
- — — COLD FIRING

DISCUSSION

R.Lanteri Minet, FR

Is the copper salicylate in your composition basic or neutral? Is it the salicylate with one copper atom for two acids with free phenol functions? I ask because in treating neutral copper salicylate with ether or ether alcohol you can convert it to the basic form with release of free salicylic acid. I demonstrated this equilibrium 30 years ago, which affects stability.

Author's Reply

The copper salicylate used was the basic form with one salicylate entity to one copper atom. We were aware of the work with ether solvents but in our case we were not using ether solvent systems.

H.Austruy, FR

You have presented results with two salts namely lead β resorcyate and copper salicylate. Do you have other experience of the formation or utilization of other complexes resulting from other salts? Are they specifically for rate of burning purposes?

Author's Reply

The short answer is that there are such other instances of complexes formed in casting powder from the use of two individual burning rate ingredients. We can discuss this outside the meeting.

DIRECT EROSION BURNING MEASUREMENTS OF A
REDUCED-SMOKE SOLID PROPELLANT ROCKET BY
FLASH X-RAYS

by
T. Constantinou, Defence Scientist
Defence Research Establishment Valcartier
P.O. Box 8800, Courcellette
Quebec, Canada GOA 1R0
and
D. Greatrix, Researcher
Institute for Aerospace Studies
University of Toronto
4925 Dufferin St., Downsview
Ontario, Canada M3H 5T6

SUMMARY

Despite the multitude of models available, proper erosive burning modelling continues to be a difficult task in the internal ballistic prediction of solid-propellant rockets with high volumetric loading. The majority of models have been based on erosive burning measurements using small motors, window motors and with such techniques as imbedded probes or interrupted burning. Such methods however are not believed to exhibit the real combustion process. The flash X-ray technique using full-size motors gives a more realistic measurement of burning rates. This technique can be used to evaluate the different erosive burning models and estimate their coefficients. Furthermore, using an internal ballistic code with different erosive burning models, a pressure-time record can be obtained and compared to experimental data. A comparison and evaluation of the different models, is thus possible. Data based on static firings of reduced-smoke motors have been analyzed by the above method and the results are presented.

NOMENCLATURE

A	Kreidler's experimental erosion coefficient
A_t	Core cross-sectional area
A_1	Core cross-sectional area at the left position of a core segment
A_2	Core cross-sectional area at the right position of a core segment
B	Kreidler's experimental erosion coefficient
C	Burning rate constant
C_1	Kreidler's erosion constant
C_2	Kreidler's erosion constant
C_p	Effective specific heat of the combustion products at the flame
C_s	Specific heat of the solid propellant
CP	Cylindrically perforated
DREV	Defence Research Establishment Valcartier
d	Diameter of port
E	Kreidler's erosion coefficient
f	Darcy-Weisback friction factor
q	Mass flow velocity
G-G	Greatrix-Gottlieb model
Q_{tv}	Threshold mass flow velocity
Q^*	Mass velocity required for Mach 1 conditions in the same channel
h	Effective convective heat transfer coefficient
h_0	The convective heat transfer coefficient under zero transpiration
HPTB	Hydroxyl-terminated polybutadiene
k	Effective thermal conductivity at the flame
k_e	Green's experimental erosion coefficient

L	Distance measured from the motor head end
L-R	Lenoir-Robillard
M	Molecular weight of the propellant gases
M	Mach number
\dot{m}	Mass flow rate
n	Burning rate exponent
n_0	Experimental constant in Green's equation
P	Pressure
P_0	Head pressure
Pr	Prandtl number of combustion products at the flame
R	Gas constant
Re_d	Reynolds number based on diameter
r_b	Total burning rate
r_0	Nominal pressure-dependent burning rate
r^2	Correlation coefficient
S	Segment wall surface area
T	Gas temperature
T_f	Propellant flame temperature
T_1	Initial propellant temperature
T_s	Propellant surface temperature
u	Gas-flow velocity
α	Erosion coefficient in Lenoir-Robillard law
β	Parameter in Lenoir-Robillard law
γ	Ratio of specific heats of combustion gas
c	Propellant roughness height
μ	Absolute viscosity of the combustion products at the flame
ρ_{pr}	Propellant density

1.0 INTRODUCTION

Erosive burning of the rocket propellant grain refers to the sensitivity of the burning rate to the gas-flow velocity parallel to the burning surface. The resulting erosive effect is most pronounced in the early stages of combustion when the ratio of the port cross-sectional area to the nozzle throat area is smallest. It is particularly evident in rockets with high propellant loading and large length/diameter ratios.

This phenomenon can cause significant variations in the performance of the rocket motor, arising from variations in mass burning rate and thus in operating pressure, since the grain is prevented from burning in parallel layers as is generally assumed in performance calculations. The erosive effect could be diminished by increasing the initial port cross-sectional area, but the volumetric loading factor and motor performance are consequently compromised. In most practical applications the ratio of the port cross-sectional area to the nozzle throat area lies between 2 and 4. Thus the effect of erosive burning cannot be eliminated and must be taken into account in the design calculations. Consequently, a knowledge of the erosive burning characteristics of a particular propellant is crucial to the elimination of the aforementioned problems through proper modification of the motor and/or grain design. Thorough knowledge can even lead to improvements in rocket performance by proper use of the erosive burning characteristics to obtain a particular pressure-time profile desired.

To improve the understanding of erosive burning, many experimental investigations have been carried out and several empirical and semi-empirical theories have been developed. The aim of these studies was to determine the dependence of the burning rate on mass flow rate and on other flow characteristics in the central port. Although sometimes the theories agree well with the experimental results shown by the author, they

do not have a universal character. Furthermore the semi-empirical models make use of a certain number of constants that have to be determined from experimental data. Therefore, these models are of no use in predicting the erosion function of a new propellant since numerous experiments would be required in order to accurately determine the constants which describe these erosive functions.

The objective of this paper is to provide an experimental evaluation of the various empirical and semi-empirical expressions for erosive burning. It is essential that the various models be judged on the merit of comparison to accurate experimental data, with as little ambiguity due to the apparatus as possible. It was thought that the radiographic technique can provide the means for this analysis. A new model is also described that does not rely on any arbitrary constants. Experimental data obtained with the X-ray technique show good agreement with this model and the Lenoir-Robillard law. However further data comparisons from different sources are needed to build confidence in this new model.

2.0 THEORETICAL MODELS OF EROSIVE BURNING

Literature reviews on erosive burning studies have been reported by several authors (Refs. 1, 2). Razdan and Kuo (Ref. 2) in their most recent review group the theoretical models in four major categories, according to the physical basis of each model. These are: (i) the phenomenological heat transfer theory, (ii) integral boundary layer analysis, (iii) modification of the propellant combustion mechanism and (iv) chemically reacting boundary layer analysis. Most of the early models fall in the first category. These models are not only relatively simple but also produce satisfactory results. They could also be easily incorporated into large internal ballistic codes and used for motor performance prediction. Since these models are of prime importance to internal ballisticians for simulation studies, this paper focusses on them; their capability to accurately predict erosive burning is also assessed.

2.1 Lenoir-Robillard (L-R) Model

Lenoir and Robillard (Ref. 3) were the first to develop a promising model to describe erosive burning based on the heat-transfer theory. This has become the most popular model amongst users because of its inherent simplicity, easy coding characteristics and adequate motor performance accuracy that resulted. They postulated a reciprocal relationship between local convective heat transfer to the propellant surface and an additive erosive burning rate component in the form:

$$\begin{aligned} r_b &= r_0 + r_e \\ &= C_p^n + \frac{h(T_f - T_s)}{\rho_{pr} C_s (T_s - T_1)}, \end{aligned} \quad (1)$$

where r_b is the total burning rate, r_0 is the pressure-dependent burning rate, r_e is the erosive burning rate, h is the effective convective heat transfer coefficient, T_f is the propellant flame temperature, T_s is the propellant surface temperature, T_1 is the initial propellant temperature, ρ_{pr} is the propellant density and C_s is the specific heat of the solid propellant. Evaluation of h is critical to the Lenoir-Robillard model. They assumed (Ref. 3) an X -dependent flow development along the propellant grain, and used an empirical expression developed by Rannie (Ref. 4) for h under transpiration. The erosive burning equation is generally given as

$$r_e = \frac{\alpha G^{0.8}}{L^{0.2} \exp(\beta r_b \rho_{pr}/G)} \quad (2)$$

where α and β are generally determined from experimental data, G is the mass flow velocity rate, and L is the distance as measured from the motor head end.

For many motor geometries, the Lenoir-Robillard model compares well with the available experimental data. Of course, since the model is semi-empirical with two free constants in the general case, this agreement can be considered at least partly fortuitous.

2.2 King's Modification to the L-R Law

Some authors have attempted modifications to the L-R equation to remove some of the empiricism with marginal success for general applicability (Refs. 5, 6). As studies in erosive burning continued, criticisms emerged in the literature on the validity of the L-R model. Some researchers opted for more complicated modeling of this phenomenon resulting in some very extensive models (Ref. 2). These will not be treated here. However King (Ref. 5) suggested a simple modification to the L-R law by claiming that the L-R model failed to account for the fact that increased burning rate, caused by erosive feedback at constant pressure, results in the propellant flame being pushed further from the surface, decreasing the heat feedback rate, and thus decreasing the propellant burning rate back toward the base rate. King derived the following modified equation to account for the above mentioned deficiency:

$$r = \frac{\alpha}{L} + \frac{\alpha G^{0.8}}{L^{0.2} \exp(\beta r \rho / G)} \quad (3)$$

Other researchers (Refs. 7, 8) developed similar relations and came to the conclusion that the L-R model overpredicts the burning rate especially in large motors.

2.3 Kreidler's Model

Kreidler (Ref. 9) derived a different equation for erosive burning based on partial motor firings and the use of cineradiographic techniques. His results showed that the erosion ratio (r/r_0) is a simple function of local mass velocity and pressure above a threshold velocity G_{tv} , and that this limit, G_{tv} , varied directly with pressure.

$$\frac{r}{r_0} = 1 + \frac{E}{Pn_0} (G - G_{tv}) \quad (4)$$

where $G = \frac{\dot{m}}{A_t}$ = average mass velocity in the grain port, $G_{tv} = A + BP$ and A , B , E and n_0 are experimental erosion coefficients.

2.4 Green's Equation

Green (Ref. 10) in an earlier study had presented a relationship correlating erosion ratios in terms of a reduced mass velocity

$$\frac{r}{r_0} = 1 + k_e \frac{G}{G^*} \quad (5)$$

where k_e is an experimental erosion coefficient, $G = \frac{\dot{m}}{A_t}$ = average mass velocity in the grain port and G^* = mass velocity required for Mach 1 conditions in the same channel

$$G^* = \frac{\gamma}{\gamma - 1} \frac{P_0}{2 \frac{R}{M} T} \quad (6)$$

where γ is the ratio of specific heats of the gas, P_0 is the head pressure, R is the gas constant, M is the molecular weight of the propellant gases and T is the gas temperature.

2.5 Greatrix-Gottlieb Model

In searching for a generally applicable but practical model for erosive burning of composite propellants, Greatrix and Gottlieb (Ref. 11) have developed a theoretical model based on the convective heat transfer postulate of Lenoir and Robillard. Modifications to the general postulate include an assumption of fully-developed flow along the long, small-diameter grain, surface roughness effects and an alternative expression for the convective heat transfer coefficient. The pertinent equations for the Greatrix-Gottlieb model are summarized below:

$$r_b = C_p^n + \frac{h (T_f - T_g)}{\rho_{pr} C_s (T_s - T_1)} \quad (7)$$

where

$$h = \frac{\rho_{pr} r_b C_p}{\exp \left(\frac{\rho_{pr} r_b C_p}{h_*} \right) - 1} \quad (8)$$

$$h_* = \frac{k}{d} Re_d Pr^{1/3} f \quad (9)$$

$$r^{-1/2} = -2 \log_{10} \left[\frac{2.5}{Re_d r^{1/2}} + \frac{\epsilon/d}{3.70} \right] \quad (10)$$

$$Re_d = \frac{Gd}{\mu} \quad (11)$$

where C_p is the effective specific heat of the combustion products at the flame, h_* is the convective heat transfer coefficient under zero transpiration, k is the effective thermal conductivity at the flame, Pr is the Prandtl number of the combustion products at the flame, f is the Darcy-Weisback friction factor, ϵ is the propellant roughness height, Re_d is the Reynolds number based on diameter, and μ is the absolute viscosity of the combustion products at the flame. It should be noted that the Greatrix-Gottlieb model does not require an evaluation of a free constant for the erosive burning rate.

3.0 EXPERIMENTAL MEASUREMENT OF EROSIIVE BURNING

Most experimental methods make use of indirect measuring methods where a sample of propellant is placed downstream of the principal motor in a device equipped with windows to permit observation of the effects of flow velocity on the burning rate of the sample. Difficulties arise when the results are applied to real motors. Early direct methods (Ref. 1), on the other hand, have not met with much more success. Measurements from quenched grains were not very accurate. Data obtained with probes buried in the grain to detect the passing of the flame front were also left with the problem of introducing foreign elements into the rocket motor environment and their unknown interaction with the combustion process. The radiographic technique, however, overcomes these problems since

an X-ray picture of the actual motor chamber is taken at some precise instant of time. Our initial experiments, which employ current technology in X-ray image production show that this method holds considerable potential and more accurate measurements should be possible in the near future.

3.1 Experimental Procedure

Several 70-mm solid rocket motors with reduced-smoke composite propellant and with cylindrically perforated (CP) grains were fired at DREV to study erosive burning via radiography. The propellant formulation consisted of 12% HTPB binder, 0.55% Fe_2O_3 catalyst and 87.45% ammonium perchlorate oxidizer. The motors were fired vertically in the static firing facilities at DREV. A single flash X-ray of the motor was taken during each firing at some predetermined time after ignition. A Field Emission flash X-ray unit model 180 kvolts was used for this purpose. The time was different for each firing and thus a burning history of the rocket motor was obtained. With a CP grain, the port remains cylindrical to a high precision and the problem is reduced to determining the inner and outer diameter of the propellant. This is done by making a diametral scan across a radiograph with a microdensitometer. Figure 1 presents an intensity/distance profile obtained by traversing the rocket motor through a narrow X-ray beam. The accuracy can vary depending on the quality of the X-ray film; it is expected that accuracies better than 0.05 mm can be achieved by this method. This process was carried out for about 20 points along the rocket motor.

Once the inner and outer diameters were determined, the data were converted into forms such as propellant web distance burned and weight of propellant burned between measurement stations. Using the computed value of propellant web burned as a variable, the variable versus burning time relationship was determined by fitting a third-order polynomial to the data points. Differentiation of this curve then yields the instantaneous burning rates. The total mass flow rates through the grain port can be determined in a similar manner by differentiating the polynomial fitted through the points of weight of propellant burned versus burning time. However, a more elegant method was chosen for the evaluation of the local flow variables pressure P, local mass velocity G and local Mach number M along the grain at a given time. It should be noted at this point that the nozzle throats of the rocket motors used in these experiment were eroding during firing. Therefore a calculation of the throat size at each time an X-ray picture was taken is necessary.

The general one-dimensional hydrodynamic conservation equations for both steady and unsteady gas-particle core flow in the motor are readily derived (Ref. 11). These equations may include the effects of friction, heat transfer to and from the motor walls, radial dilatation, axial area change, offset and direct mass, enthalpy and kinetic energy addition from the propellant, particle drag and heat transfer. For the present work, most of the above effects are very weak and can be neglected. Assuming a gas phase only for the core flow, the hydrodynamic equations can be reduced to a quasi-steady, finite-difference scheme as denoted below for a given segment from the motor core:

$$\rho_1 A_1 u_1 + \rho_{pr} r_{b1} S_1 = \rho_2 A_2 u_2, \quad (12)$$

$$\rho_1 A_1 u_1^2 + p_1 \left(\frac{A_1 + A_2}{2} \right) = \rho_2 A_2 u_2^2 + p_2 \left(\frac{A_1 + A_2}{2} \right), \quad (13)$$

$$\begin{aligned} \rho_1 A_1 u_1 \left(C_p T_1 + \frac{u_1^2}{2} \right) + \rho_{pr} r_{b1} S_1 C_p T_f \\ = \rho_2 A_2 u_2 \left(C_p T_2 + \frac{u_2^2}{2} \right), \end{aligned} \quad (14)$$

where the subscripts 1 and 2 denote the left and right positions of a core segment of length dx, A is the core cross-sectional area, and S is the segment wall surface area ($\pi d \cdot dx$). Equations [12]-[14] are respectively the continuity, momentum and energy equations of the gas flow. The equation of state is also required to complete this scheme:

$$p = \rho RT \quad (15)$$

where R is the specific gas constant of the combustion products. The above 4 equations are a closed system which give an algebraic solution to the unknown flow variables (p_2 , ρ_2 , u_2 , T_2), with the local r_b given from experimental measurements. It should be noted that this approach is more accurate than that presented by Kreidler (Ref. 9), which neglects the effect of mass addition and area on the governing hydrodynamic equations.

4.0 DATA REDUCTION

Once the local variables P, G and M are determined, plots of the associated burning rate versus the various erosive related functions were made to determine the empirical constants. All erosion models were considered in this fashion except the Greatrix-Gottlieb model which does not rely on any empirical constants. The nominal burning rate was reduced from small ballistic motor firings and for the particular propellant used in these experiments, St-Robert's law $r = cP^n$, can be expressed as

$$r = 0.000417 P^{0.363} \text{ m/s} \quad (16)$$

where P is expressed in kPa.

4.1 Lenoir-Robillard Law

Equation (1) may be rewritten as

$$r - r_0 = \alpha \frac{g^{0.8}}{L^{0.2} \exp(\beta r \rho / G)} \quad (17)$$

or

$$r - r_0 = \alpha f(\beta) \quad (18)$$

$$\text{where } f(\beta) = \frac{g^{0.8}}{L^{0.2} \exp(\beta r \rho / G)}$$

Lenoir and Robillard found β to be apparently independent of propellant identity and having a value around 53. Some subsequent authors (Refs. 6, 9 and 12) have used different values for β according to their derivation from first principles and obtained good agreement between theoretical and experimental results. For the DREV propellant considered here the values $\beta = 78.9$ and $\beta = 110$ also resulted in satisfactory motor performance predictions in the past (Ref. 12). Therefore a parametric study was carried out for these three different values of β (53, 78.9, 110) and plots of $r - r_0$ versus $f(\beta = 53)$, $f(\beta = 78.9)$ and $f(\beta = 110)$ were drawn up to obtain the corresponding values of α by linear regression (Figures 2-4). These appear in Table I. The correlation coefficient r^2 is also shown to indicate the measure of linear correlation between the two variables.

TABLE I Constants in the L-R Law

α	β	Correlation Coefficient r^2
0.00002776	53	0.74
0.0000396	78.9	0.73
0.00005825	110	0.71

4.2 King's Modification to the Lenoir-Robillard Law

King's modification to the L-R law can be rewritten as $r - \frac{r_0^2}{r} = \alpha \left[\frac{g^{0.8}}{L^{0.2} \exp(\beta r \rho / G)} \right]$.

Figures 5-7 show a plot of $r - \frac{r_0^2}{r}$ versus $\frac{g^{0.8}}{L^{0.2} \exp(\beta r \rho / G)}$ using the three different values for β . The corresponding erosion coefficients α are shown in Table II.

TABLE II Constants in King's Modification to L-R Law

α	β	Correlation Coefficient r^2
0.00004386	53	0.63
0.00006179	78.9	0.61
0.0000898	110	0.59

4.3 Kreidler's law

Kreidler's law can be rewritten as $r - r_0 = \frac{r_0 E}{p n_0} (G - G_{tv})$ and with $n = n_0$ and $G_{tv} = A + BP$ where $B = 0$ for these experimental measurements, the law reduces to

$$\begin{aligned} r - r_0 &= CEG - CEA \\ &= C_1 + C_2 G. \end{aligned}$$

After a plot of $r - r_0$ vs G (Fig. 8), these constants were determined by linear regression.

$$\begin{aligned} C_1 &= -0.1858 \times 10^{-2} \\ C_2 &= 0.4065 \times 10^{-5} \\ E &= 0.00974 \\ A &= 457.1 \end{aligned}$$

with a correlation coefficient $r^2 = 0.80$.

4.4 Green's Law

With some manipulation Green's law can be reduced to $r - r_0 = k_1 \frac{G r_0}{P_0}$ where k_1 is an empirical constant. Figure 9 presents a graph of $r - r_0$ vs $\frac{G r_0}{P_0}$ and the slope of the line going through the origin (k_1) is determined. Thus $k_1 = 34254$ and Green's constant $k_e = 0.005884$ with a correlation coefficient $r^2 = 0.80$.

5.0 DISCUSSION OF RESULTS

Once the empirical constants of these models were determined then points of measured burning rate versus the theoretical burning rate described by the various models were plotted to see the agreement obtained (Figs. 10-18). A good correlation would have the points fall on top of a line 45° to the horizontal.

As can be seen for all models, the points are scattered around this 45° line. Since a proper choice of the constants was made in all cases, the 45° line passes through the middle of these points. However, it is the degree of scatter that gives an indication as to how much the model digresses from the actual results. It is seen that King's modification to the L-R law results in greater scatter tending to indicate that King's modification is rather inappropriate (Figs. 13-15). Green's and Kreidler's model seemed to do rather well as the smaller scatter might indicate (Figs. 16, 17). However, other considerations such as fully empirical constants in the equations would tend to make such apparently good performance seem insignificant.

The Greatrix-Gottlieb model seems to predict burning rate as well as any of the other models, although the 45° line is a little off center (Fig. 18). This is to be expected since the model is not normalized with empirical constants.

Figures 19 and 20 depict the burning rate profiles along the propellant grain for two specific times during the firing of the test motor. Due to technical circumstances, experimental recording of grain dimensions between 0 and 15.3 cm, and between 43.2 and 65.5 cm, did not take place. These gaps resulted in a slight aberration of the theoretical curves, since they are based on the finite-difference data reduction code's estimation of local flow variables. Nevertheless, the curves predicted by the Greatrix-Gottlieb and Lenoir-Robillard models compare well to the experimental data. The coefficients α and β ($2.89 \times 10^{-7} \text{ m}^{2.8} \text{ kg}^{-0.8} \text{ s}^{-0.2}$ and 78.9 respectively) for the Lenoir-Robillard equation were selected from a curve-fit of previous motor firing data (Ref. 12).

Differences between the predictive models are small in this case, though the general pattern of the Lenoir-Robillard model predicting stronger erosive burning near the head end and weaker erosive burning with greater distance as compared to the Greatrix-Gottlieb model is quite evident. The "negative erosion" effect was not observed either experimentally or theoretically near the test motor head end.

As a final test the Grain Design and Internal Ballistics Evaluation Program (Ref. 13) was used to predict the motor operating pressure based on some of these models. Figures 21 and 22 show the results of this study. The Lenoir-Robillard model with $\beta = 53$, $\alpha = 0.0000278$ came closest to the measured internal pressures. This would tend to signify that the claim that the value of $\beta = 53$ tends to hold true in this case. The curves of the other models with $\beta = 78.9$ and $\beta = 110$ were off the experimental curve by a noticeable amount. Green's and Kreidler's models were off quite a bit from the experimental points and it seemed that the curves were not very sensitive to the empirical constants.

Although this particular performance prediction code can handle linear eroding throat functions, it is thought that non-linearities in throat erosion exist that tend to alter the real results from the simulation study. Thus these errors have not been eliminated in the present study.

6.0 CONCLUDING REMARKS AND RECOMMENDATIONS

The radiographic technique can provide researchers with the added capability to carry out accurate erosive burning rate measurements in order to predict the actual burning rate during motor firings.

As was expected all empirical models can predict erosive burning accurately enough if the constants are chosen properly for the particular case. Green's model, in particular, seems to give a good agreement between theory and experiment as the narrow spread of points might indicate. However, such agreement is really fortuitous and the empirical model might break down for a slightly different motor.

The internal ballistic code seems to be geared towards the semi-empirical L-R model because of its relatively sound derivation and more general applicability. An improvement to this popular model has been shown in this paper with the Greatrix-Gottlieb equation as the model does not depend on any empirical constants for the erosive burning calculation. This new model would be of great utility to researchers especially when the performance of a new propellant motor is desired.

The apparent agreement between the experimental data and the predictive model of Greatrix and Gottlieb, and the model of Leroir and Robillard, is encouraging. Nevertheless, further experiments are necessary to provide more conclusive evidence of the viability of these predictive models. Experiments contemplated at DREV include rocket motors with non-eroding nozzle throats and pressure transducers along the grain length to eliminate any errors from the calculation of these two parameters. A double exposure radiograph will be attempted since it will tend to remove film to film variations and increase the data output per test at least threefold, if the flash X-ray unit can be pulsed with sufficient rapidity.

REFERENCES

1. Williams, P.A., Barrère, M. and Huang, H.C., "Fundamental Aspects of Solid Propellant Rockets", AGARD 116, Oct 1969, pp. 395-456.
2. Kuo, K.K. and Summerfield, M., "Fundamentals of Solid Propellant Combustion, AIAA Vol. 90, Oct. 1984, pp. 515-598.
3. Lencir, J.M. and Robillard, G., "A Mathematical Method to Predict the Effects of Erosive Burning in Solid-Propellant Rocket", Sixth Symposium (International) on Combustion, Reinhold, New York, 1957, pp. 663-667.
4. Rannie, W.B., Progress Report 4-50, Jet Propulsion Laboratory, Pasadena, California.
5. King, M.K., "A Modification of the Composite Propellant Erosive Burning Model of Lencir and Robillard", Combustion and Flame, Vol. 24, pp. 365-368, 1975.
6. Jovic, B. and Blagojevic, D.J., "Theoretical Prediction of Erosive Burning Characteristics of Solid Rocket Propellant Based on Burning Rate Dependence of Pressure and Initial Temperature and Its Energetic Characteristics", AIAA/SAE 12th Propulsion Conference, Palo Alto, California, AIAA Paper No. 76-697, July 26-29, 1976.
7. Parkinson, R.C., Penny, P.D., "A Transpired Boundary-Layer Model of Erosive Burning", AIAA/SAE 14th Joint Propulsion Conference, Las Vegas, July 25-27, 1978, AIAA Paper 78-980.
8. Parkinson, R.C. and Penny, P.D., "Boundary Layer Models of Erosive Burning", AGARD Conference Proceedings No. 259, Solid Rocket Motor Technology, Oslo, April 1979.
9. Kreidler, J.W., "Erosive Burning: New Experimental Techniques and Methods of Analysis", AIAA Solid Propellant Rocket Conference, Palo Alto, California, Jan. 29-31, 1964, AIAA No. 64-155.
10. Green, L., "Erosive Burning of Some Composite Solid Propellants", Propulsion, Journal of the American Rocket Society, Jan.-Feb. 1954, volume 24, No. 1, p. 9.
11. Greatrix, D.R. and Gottlieb, J.J., "A Study of Quasi-Steady Flow Behaviour in Solid-Propellant Rocket Motors", U.T.I.A.S. Report to be published, University of Toronto Institute for Aerospace Studies, Downsview, Ontario, Canada.
12. Reitsma, H.J. and Hughes, P.M., "A Status Report on the Investigations of Erosive Burning of Propellants", DREV Memorandum 2589/82, January 1982.
13. Barron, J.G., Cook, K.S. and Johnson, W.C., "Grain Design and Internal Ballistics Evaluation Program", Program No. 64101, Hercules Incorporated, Magna, Utah, June 30, 1967.

ACKNOWLEDGMENTS

The authors wish to give credit to P. Hughes and H.S. Reitsma for initiating the present investigation and planning and executing the first erosive burning flash X-ray experiments at DREV.

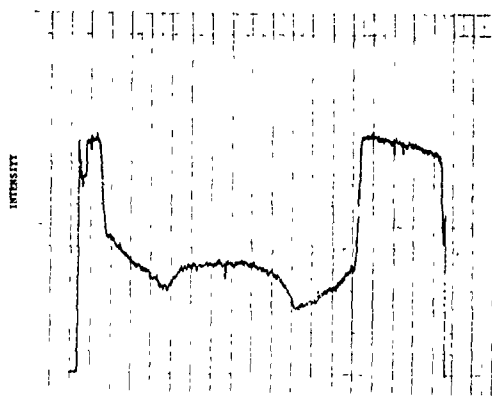


FIGURE 1 - Dimetral scan across a radiograph with a microdensitometer

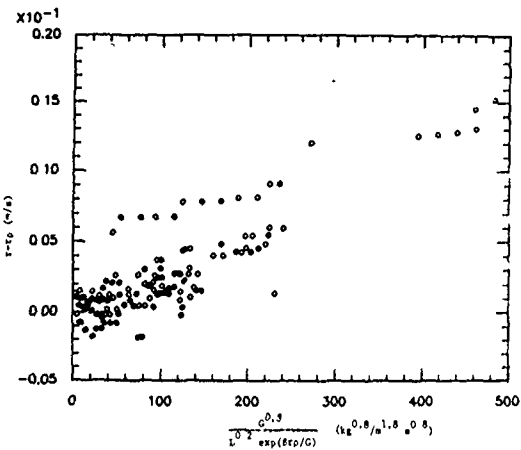


FIGURE 2 - Erosive burning, $r - r_0$, versus $\frac{C^{0.8}}{L^{0.2} \exp(\beta r_0/C)}$ with $\beta = 53$ (L-R model)

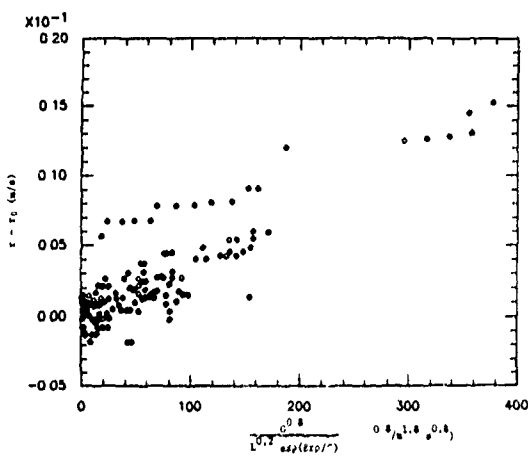


FIGURE 3 - Erosive burning, $r - r_0$, versus $\frac{C^{0.8}}{L^{0.2} \exp(\beta r_0/C)}$ with $\beta = 78.9$ (L-R model)

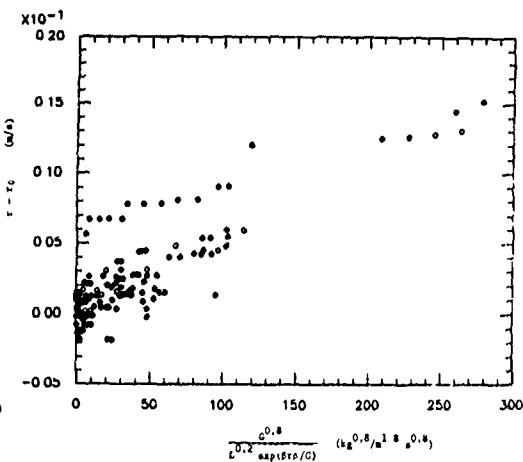


FIGURE 4 - Erosive burning, $r - r_0$, versus $\frac{C^{0.8}}{L^{0.2} \exp(\beta r_0/C)}$ with $\beta = 110$ (L-R model)

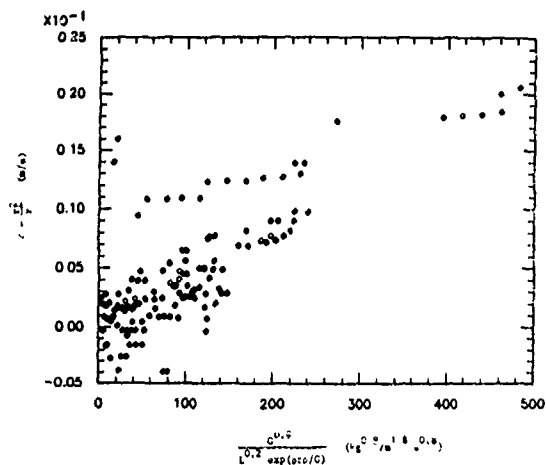


FIGURE 5 - King's burning rate related quantity, $(r - \frac{r_0}{2})$, versus $\frac{C^{0.8}}{L^{0.2} \exp(\beta r_0/C)}$ with $\beta = 53$

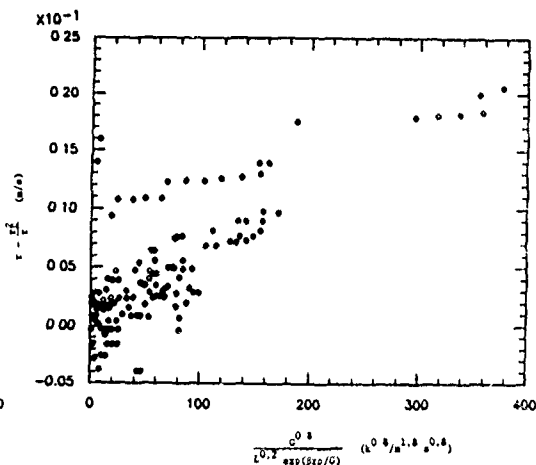


FIGURE 6 - King's burning rate related quantity, $(r - \frac{r_0}{2})$, versus $\frac{C^{0.8}}{L^{0.2} \exp(\beta r_0/C)}$ with $\beta = 78.9$

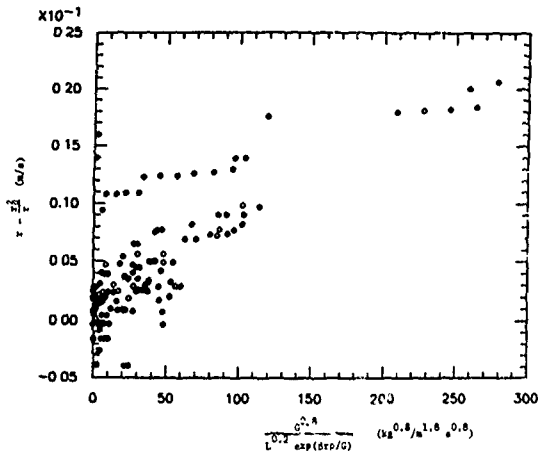


FIGURE 7 - King's burning rate related quantity, $(r - r_0) \frac{G^{0.8}}{\exp(870/G)}$ with $\beta = 110$

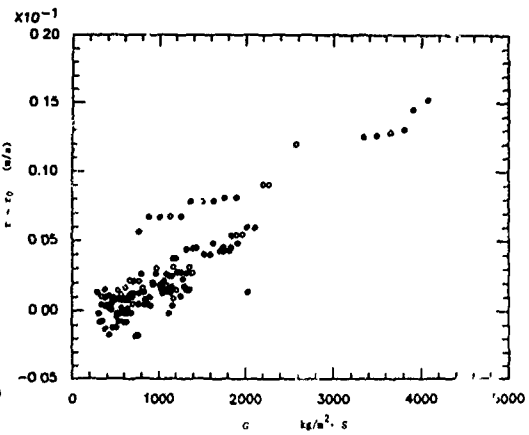


FIGURE 8 - Reactive burning, $r - r_0$, versus cross-sectional mass velocity G for Koeller's Law

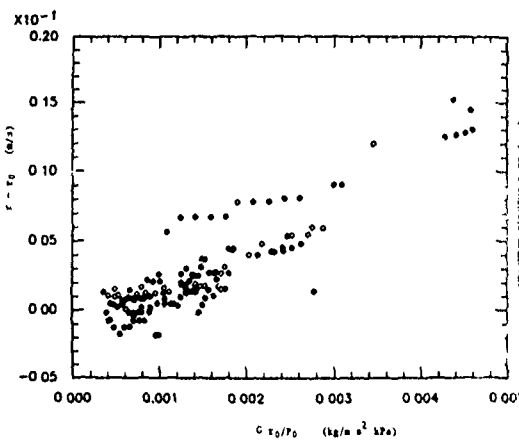


FIGURE 9 - Reactive burning ($r - r_0$), versus Green's expression $G r_0 / P_0$

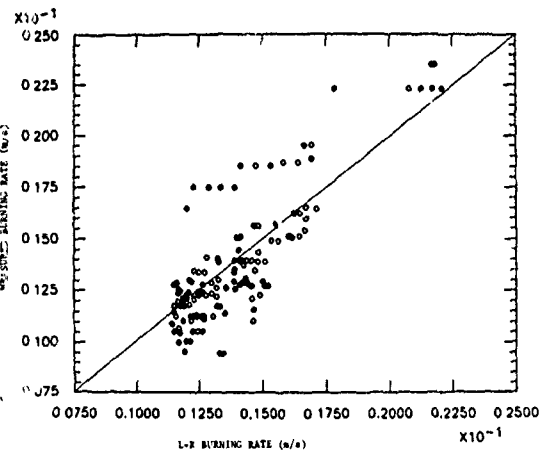


FIGURE 10 - Measured and theoretical burning rate based on L-R model with $\beta = 53$

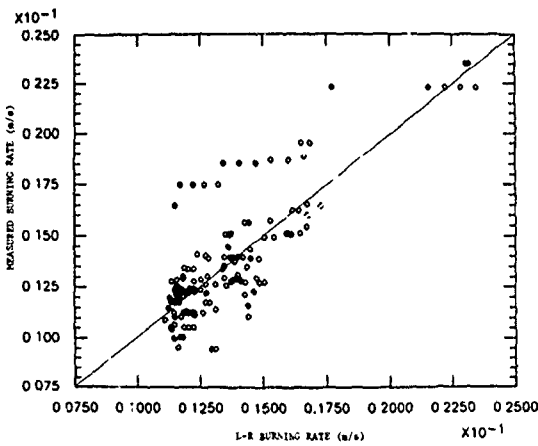


FIGURE 11 - Measured and theoretical burning rate based on L-R model with $\beta = 8.9$

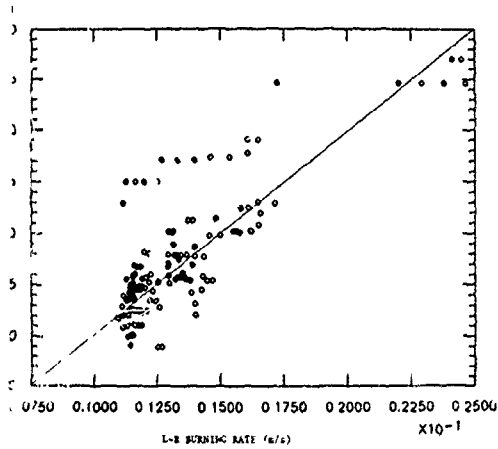


FIGURE 12 - Measured and theoretical burning rate based on L-R model with $\beta = 110$

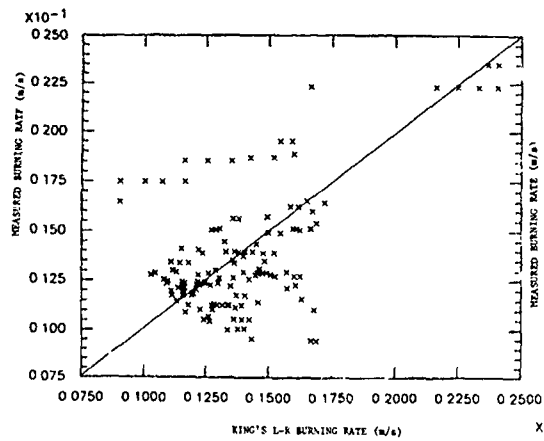


FIGURE 13 - Measured and theoretical burning rate based on King's modification with $\beta = 53$

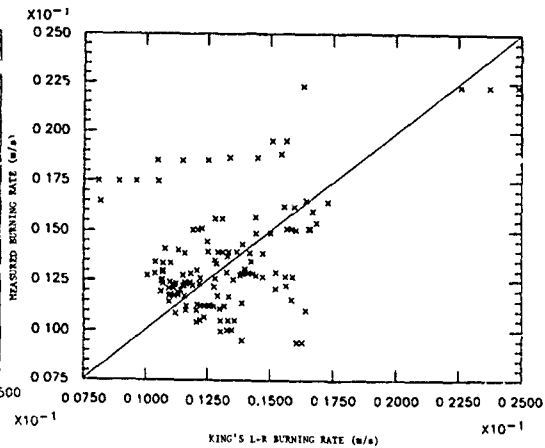


FIGURE 14 - Measured and theoretical burning rate based on King's modification with $\beta = 78.9$

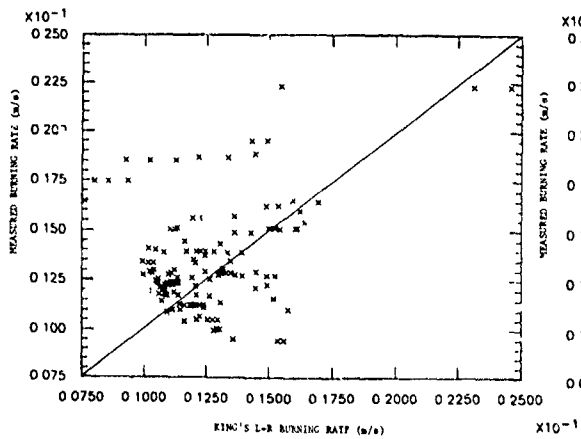


FIGURE 15 - Measured and theoretical burning rate based on King's modification with $\beta = 110$

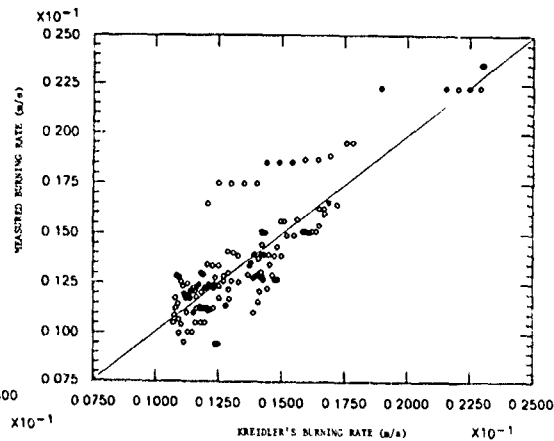


FIGURE 16 - Measured and calculated burning rate based on Kreidler's model

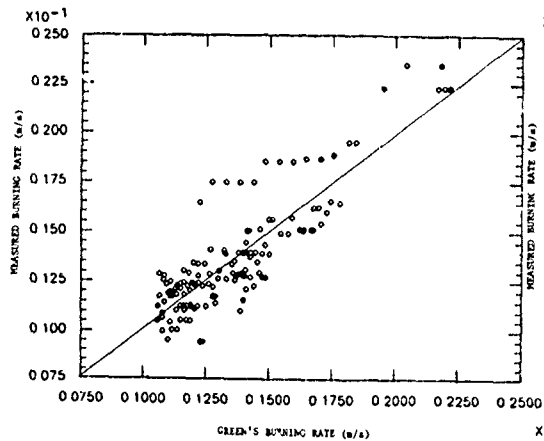


FIGURE 17 - Measured and calculated burning rate based on Green's model

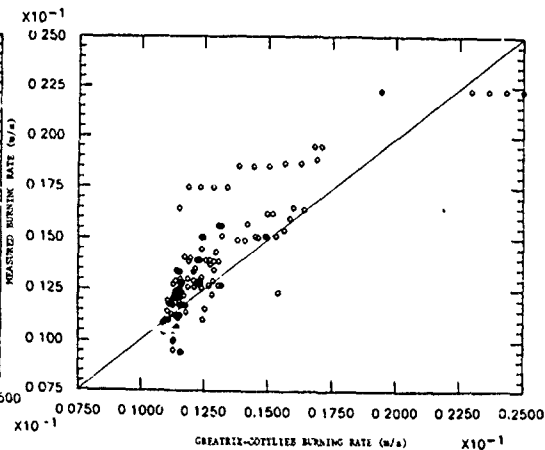


FIGURE 18 - Measured and calculated burning rate based on Green's-Gottlieb Model

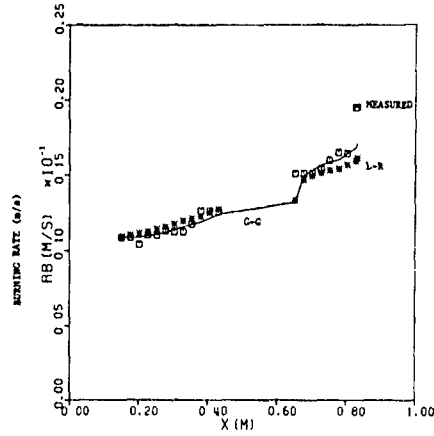


FIGURE 19 - Burning rate profile along the propellant grain, $t = 0.248$ s

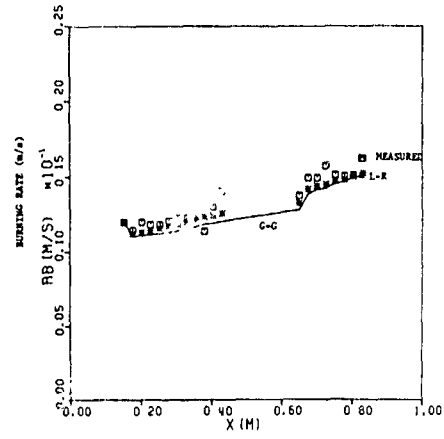


FIGURE 20 - Burning rate profile along the propellant grain, $t = 0.422$ s

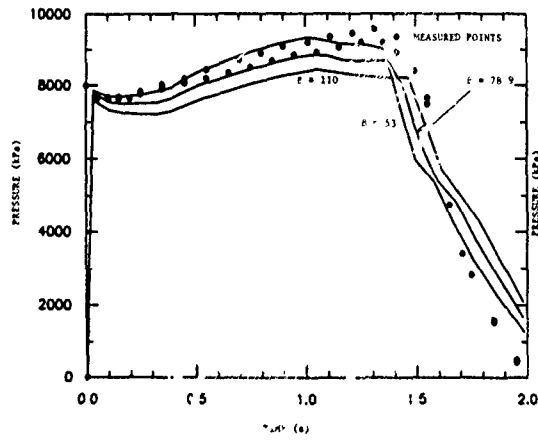


FIGURE 21 - Pressure-time trace comparing experimental points with L-R model.

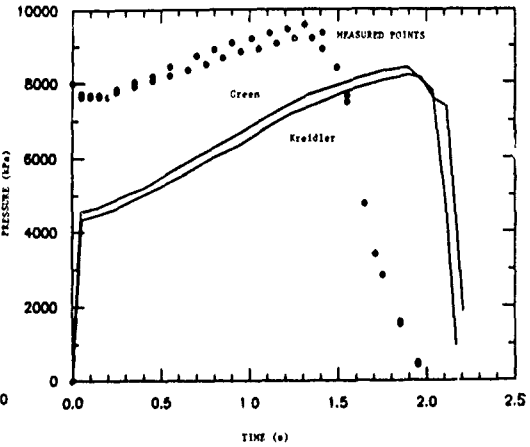


FIGURE 22 - Pressure-time trace comparing experimental points with Kreidler's and Green's models

DISCUSSION

N.S. Cohen, US

King has developed a reduced smoke propellant, erosive burning, combustion model that is in the direction of meeting your objective of having a better predictive model that accounts for changes in propellant formulation. I am using a model similar to that in an erosive burning study that is similar to yours. Leon Strand at JPL is using a plasma capacitance gauge technique for direct measurement of burn rate in a cylindrical grain motor. I use the model to generate a table of burn rate as a function of pressure and local velocity, and I input this table into a simple ballistics code for a cylinder with the measured data. I also take the 'measured' burn rate as a function of time and position, and input that to the code, and that gives me a second calculated pressure-time curve so that I may evaluate the accuracy of the 'measured' burning rates. I suggest that you do the same in your own work, so as to have a better combustion model and to check your measured burning rates.

Author's Reply

As I pointed out, this was not an exhaustive study of erosive burning models but rather a study of certain erosive burning models that are presently used in the big international ballistic codes like the Hercules and SPP programs.

The method you have described is certainly a good check on the accuracy of the measured burning rates. However I would be very hesitant in altering these measured rates to fit the pressures obtained since it would tend to hide any unexplained phenomena, if all the variables were included in the analysis. To treat any such discrepancies I would rather try to obtain more accurate measurements which can be compared directly with theoretical predictions.

T. Vaillant, FR

Does your technique of flash x-rays enable frequent and systematic measurements of burning rate for routine chemical characterisation of propellants? Does the technique require a lot of precautions making it more suitable for basic studies of model validation?

Author's Reply

Our purpose was comparison of models and we took an x-ray photograph at a given time and compared it with a sequence of others. It was a 'one-off' thing. It is not a cinematic method.

EXPERIMENTAL TECHNIQUES FOR OBTAINING PARTICLE BEHAVIOR
IN SOLID PROPELLANT COMBUSTION

by

David W. Netzer and John P. Powers

Naval Postgraduate School
Monterey, California 93943
USA

SUMMARY

A continuing investigation is being conducted to develop techniques to obtain quantitative data that can be used to relate solid rocket propellant composition and operating environment to the behavior of solid particulates within the grain port and exhaust nozzle. The techniques employed are high speed motion pictures of propellant strand burners and slab burners in a cross-flow environment, SEM analysis of post-fire residue (strand, slab, and motor), determination of D_{32} across the exhaust nozzle using measurements of scattered laser light, and holograms of burning propellant strands, slabs and motors. In addition, techniques are being studied for automatic retrieval of particle size distributions from holograms taken of the combustion of solid propellants.

Actual particle sizes of burning aluminum particles were obtained in high speed motion pictures by using high intensity rear illumination of the burning propellants to eliminate the flame envelopes surrounding the burning particles.

Measurements of diffractively scattered light have been made for determination of changes in D_{32} across a solid propellant rocket motor exhaust nozzle.

Two-dimensional motors have been employed to obtain holograms of propellant burned in a cross-flow environment. Other efforts have been directed at reduction of speckle in the recorded holograms and optimization of techniques for minimizing excessive smoke in the recorded scenes.

A computer controlled Quantimet 720 is being used in an effort to obtain particle size distributions from reconstructed holograms.

INTRODUCTION AND OVERVIEW

Aluminum is added to solid propellants to increase performance and to suppress high-frequency combustion instabilities. A small amount of a variety of additives in addition to aluminum (aluminum oxide, zirconium, etc.) are also used in reduced-smoke propellants for acoustic stabilization. Although the delivered specific impulse of metallized propellants is higher than that of the base propellants, the specific impulse efficiency is lower. This results from the presence of condensed metal oxides in the nozzle flow and from unburned metal within the motor port. Some particles, upon reaching the burning surface, depart immediately while others agglomerate on the surface before passing into the gas flow. Most of the metal combustion is thought to occur in the gas phase, resulting in small (typically less than two microns) metallic oxide particles. In addition, particle burnout also can result in the break-up of a metallic oxide cap or layer. This can result in larger (greater than five microns) particles. The larger particles are more important in the determination of two-phase flow losses in the exhaust nozzle flow since they can lag the gas flow and, in principle, could be affected through propellant changes. There are several rather complex computer codes [Ref. 1] which attempt to model the important processes of momentum and thermal energy exchange between the solid, liquid, and gaseous phases as well as particle collisions, break-up, and wall collisions. However, these models remain semi-empirical and are generally based upon particle size distributions which were obtained from collected nozzle exhaust flows [Ref. 2]. Particle histories from the surface of the propellant to the nozzle exit remain largely unknown, due to the difficulty of making direct measurements within the motor and nozzle. Prediction of performance losses due to the presence of the original metal and the metal oxides are very sensitive to the assumed particle size distribution, and essentially no data are available that give this distribution as a function of position throughout the motor and nozzle.

Collecting exhaust products is feasible only for small rocket motors. Even then, the techniques employed result in considerable variation in the measured sizes [Ref. 2]. Dobbins [Ref. 3] and Dobbins and Strand [Ref. 4] attempted to use an optical technique for measuring exhaust particle size and to compare the measurements with tank collected exhaust results. The optical technique used was a three-wave-length transmission measurement. This technique requires knowledge of particle index of refraction and the standard deviation of the particle size distribution. The collected exhaust particles indicated that the exhaust particle size was not influenced significantly by either the propellant weight fraction of metal or the chamber

pressure. The optical measurements generally yielded sizes which were too small and the results were inconsistent with the collected exhaust data. It was speculated that this discrepancy resulted from a bi-modal exhaust particle distribution.

Light transmission measurements have the advantage of being applicable to dense concentrations where multiple scattering occurs [Ref.5]. However, the method works best for small particles (on the order of the wavelength of the illumination source) and requires a-priori knowledge or the particle characteristics.

Light scattering measurements can also be used to determine particle size [Refs. 6-15]. If the scattering angles used are specifically selected, the technique can be used to look almost entirely at one lobe of a bi-modal size distribution. Ratioing intensities obtained at two forward scattering angles can be used to further reduce the complexity of the method. However, scattering techniques are generally thought to be applicable only to systems where the transmittance is greater than approximately 90% in order to satisfy single scattering requirements.

A combination of light transmission and light scattering measurements [Ref.13] appears to be well-suited for many solid propellant rocket motor exhaust flows. However experimental efforts are first needed to determine under what conditions (metal loadings, operating pressure, propellant ingredients, etc.) light scattering measurements can be effectively made in this difficult environment.

The goal of the investigation to date has been to develop and compare experimental techniques that can be used for obtaining quantitative data on the effects of propellant properties, operating pressure, and nozzle geometry on the behavior of metallized particulates within the grain port and nozzle of solid propellant rocket motors. These data are needed in order to (1) improve solid propellant performance predictive capabilities, (2) provide needed input to current steady-state combustion models which include oxidizer-metal interactions, (3) provide data on the effects of motor and propellant conditions on exhaust signature and (4) provide in-motor particle size distributions which will allow more accurate predictions of damping in stability analyses. The techniques employed have been high speed motion pictures of strand burners and slab burners in a cross-flow environment, SEM analysis of post-fire residue (strand, slab, and motor), determination of changes in D_{32} across the exhaust nozzle using measurements of scattered laser light, and holograms of burning propellant strands and slabs. In addition, considerable effort has been directed toward development of automatic data retrieval methods for obtaining particle size distributions from holograms taken of the combustion of solid propellants. The holographic effort is a two-part problem. Techniques must be developed for obtaining good quality holograms in a realistic solid propellant combustion environment. However, these holograms are of limited value unless the particle size data can be obtained from them in a reasonable time period. This requires development of computer-aided image analysis techniques.

In previous efforts [Ref.16] the motion picture and holographic techniques were successfully demonstrated using propellant strands with up to 15% aluminum. Fourteen micron resolution was obtained in the high speed motion pictures with a 1.12X magnification (and very small depth of field). In addition, initial determinations of D_{32} were made using measurement of scattered laser light at the exhaust of a small rocket motor. Apparatus modifications were then made to expand and improve the obtainable data. Subsequent results are reported herein.

The high speed motion picture investigation of burning propellant strands was continued using a combination of monochromatic and white-light illumination. The final illumination method used either intense white-light rear illumination or two side/front illumination sources during one test, a 2500 watt white-light and a 0.8 watt laser at 488 nm. With the latter illumination method a rotating filter disc was placed between the combustion bomb window and the camera lens. This provided alternating frames with high intensity white-light illumination and filtered 488 nm illumination. The camera was mounted on a mill bed to provide both stability and precise focusing. An example of the ability to eliminate the recording on the film of the flame envelopes surrounding burning aluminum particles through the use of intense (2500 watt) rear illumination is shown in figure 1.

A dual-beam apparatus for measuring scattered light was developed to simultaneously measure particle size (D_{32}) at the entrance and exit of an exhaust nozzle of a small solid propellant rocket motor. The diameters were determined using 1024 element linear photodiode arrays to measure diffractively scattered laser light. He-Ne illumination was used at the nozzle exhaust but significant 632.8 nm radiation within the motor combustion zone required the use of 488 nm illumination in that region. Early measurements were successful at both locations. However, the presence of char agglomerates and the use of a short motor with small residence times (less than 5 msec) significantly affected the "measured" D_{32} and produced large amounts of condensate on the converging section of the exhaust nozzle. Several improvements were then made. The motor was lengthened to increase residence time to approximately ten msec, multiple sweeps of the diode arrays were made to improve the statistical validity of the data and the Air Force Rocket Propulsion Laboratory fabricated GAP propellants to replace the HTPB propellants which were originally used in an attempt to provide "cleaner" exhaust products. In addition, the optics and data acquisition

methods were modified to improve accuracy. Transmitted light is now blocked with a "stop" so that the non-deflected laser beam can be positioned directly on the first diode of the array if desired. Interactive graphics have also greatly improved the speed and accuracy of the data reduction. A cylindrically perforated, aft-end uninhibited grain is currently being used in an attempt to further eliminate inhibitor char in the exhaust gases while providing a nearly neutral burning grain.

Efforts have been directed at improvement of the quality of the holograms which are obtained in the 2-D motor in the presence of cross-flow. The propellant slabs are bonded between borosilicate glass side plates and burned within a combustion bomb. Currently, efforts are being directed at obtaining holograms from within a small rocket motor.

Various techniques have been suggested for the automatic retrieval of particulate diameter data from reconstructed holograms; ranging from complete digitization to man-in-the-loop optical methods. A reasonable near-term solution appears to be a combination of both optical and digital methods. Digital methods appear to be needed to reduce non-uniform background illumination and speckle, whereas analog techniques (such as the Quantimet 720) appear to be well suited for rapidly obtaining particle size data from holograms which have improved uniformity in background illumination.

DETERMINATION OF PARTICULATE SIZE USING MEASUREMENTS OF SCATTERED LIGHT

Introduction

The method used in the present effort is the diffractively scattered light technique. The diffraction patterns of light scattered by particles are analyzed to determine the volume-to-surface mean diameter (D_{32}). This method has the disadvantages that size distributions cannot be easily determined and particles larger than some threshold size will not be detected due to the exceedingly small angles at which they scatter light. However, it has the advantage that it is non-intrusive and, in theory, can be used in the internal motor environment. Propellant composition can limit the application of the technique by producing large particulates and/or very dense particle clouds.

The completely general theory of scattering was developed by Mie and is presented by Van de Hulst [Ref.15]. The light scattering characteristics for spherical particles of any size are fully described and the phenomena of reflection, refraction, diffraction and extinction are considered. For particle sizes much smaller than the wavelength of the illuminating light source the Mie equations simplify to what is called Rayleigh scattering.

The size of the particles of interest in solid propellant rocket motor combustion depends upon the application. Most applications are concerned with particles having diameters much greater than the wavelength of visible light. Scattering by these larger particles is described by Fraunhofer diffraction. Measuring the particle size for a monodispersion can be accomplished by measuring the angular position of a dark or bright ring in the diffraction pattern. This method is not used for polydispersions since the discrete rings are not observed. However, Dobbins, et al [Ref.7] found that the volume-to-surface mean diameter of a polydispersion (D_{32}) defined by

$$D_{32} = \frac{\int_0^{D_{\max}} N_r(D) D^3 dD}{\int_0^{D_{\max}} N_r(D) D^2 dD} \quad (1)$$

(where $N_r(D)$ is a distribution function describing the proportion of particles with diameter D in the sample), could be accurately measured. The value of D_{32} was shown to be quite insensitive to the form of $N_r(D)$. In addition, since the ratio of forward scattered light at two angles is dominated by Fraunhofer diffraction, it is insensitive to the particle refractive index and the particle concentration [Ref.13]. To evaluate the integrated intensity over all particle sizes requires specification of $N_r(D)$. Dobbins, et al [Ref.7] used the Upper-Limit-Distribution-Function developed by Mugele and Evans [Ref.9] and this approach was followed in the present investigation.

For $\pi D_{32} \theta / \lambda$ (where θ is the scattering angle and λ is the wavelength) less than 3.0, a Gaussian curve [Ref.14] can be used which closely matches the theoretical intensity profile obtained by integrating the Fraunhofer diffraction expression together with the Upper-Limit-Distribution-Function [Ref.7]. This Gaussian expression has been presented by Buchele [Ref.14] and is given by

$$I_{\theta} / I_{\theta=0} = \exp - (0.57 \pi D_{32} \theta / \lambda)^2 \quad (2)$$

Equation (2) can be used to obtain the intensity ratio between two (within the apparatus limits) forward scattering angles:

$$I_2/I_1 = \exp - D_{32} \left[\left(\frac{\theta_2^2}{\theta_1^2} - 1 \right) / (0.57 \pi / \lambda)^2 \right] \quad (3)$$

Experimental Apparatus and Procedures

Figure 2 is a photograph of the complete apparatus including the exhaust collection tube. The light scattering equipment was mounted on two optical benches; one for measurements in the nozzle exhaust and one for measurements within the motor cavity. The light sources employed were eight milliwatt helium neon and argon lasers for the exhaust and motor paths respectively.

Each beam passed through the appropriate test volume and was then intercepted by a physical stop located in front of the receiving optics. The further the stop was placed from the test section, the smaller was the angle at which scattered light could be measured. The upper limit of scattering angle is determined by the diameter and focal length of the focusing lens, the distance between the focusing lens and the particles, the diameter of the motor window, or the height/position of the diode array. In the present apparatus scattered light could be measured within an angle increment of approximately 0.05 radians. The minimum possible scattering angle was approximately 0.008 radians and the maximum approximately 0.07. These angles can be changed by changing one of the above limits. The presently employed angle limits introduce some bias in the collected data as illustrated in figure 3.

The scattered light passed through a laser line filter and a 50cm focal length lens which focussed the light onto the linear diode array. The arrays each contained 1024 silicon photodiodes on a single chip with 25 micron spacing. The accompanying circuits provided a "sampled and held" output which was essentially analog except for switching transients. The actual sampling time of the array was about 34 msec with a delay between scans of about 6 msec. Currently the system is being improved to permit sampling in approximately 4 msec.

Raw data was plotted on the CRT where any obviously erroneous scans could be excluded from further data reduction. The valid scans were averaged to obtain a mean scattering profile. The mean intensity profile taken before particles were introduced was then subtracted from that taken with particles present. This corrected for the characteristics of individual photodiodes and extraneous light which was independent of the particles.

A symmetric moving-average-type of digital filter was then applied to the profile to achieve smoothing. This type of digital filter was chosen for simplicity and because it does not have the phase lag of analog filters. Smoothing of the data has been found to be necessary if good results are to be obtained using the two-angle methods when only a few scans of the array are possible (as in time-dependent combustion).

Several data reduction techniques have been investigated for obtaining D_{32} from the measured intensity profiles. The initial method required the comparison of the experimentally obtained intensity profile with that produced using equation 2. This required the profile to be normalized using the "unknown" (since the transmitted light dominates at small angles) forward scattered intensity at $\theta=0$. This quantity and D_{32} for the theoretical profile were adjusted using interactive graphics until the theoretical and experimental profiles provided the best match. This technique provided reasonably good results but required considerable user interpretation of the "best fit".

The method currently being used minimizes both data reduction time and "user interpretation". A minimum value of θ is chosen from the filtered profile (where beam stop effects or diode position begin to influence the data). This yields I_1 and θ_1 for use in equation (3). D_{32} is then varied, each value resulting in a curve for I_2 vs. θ_2 . The "best fit" to the experimental profile is then found, without the need to estimate the $\theta=0$ scattering intensity.

The two-angle method is also used. The data is scanned using many values of θ_1 together with several angle ratios to determine θ_2 . D_{32} is then found from equation (3) and displayed as D_{32} vs. v_1 for each value of θ_2/θ_1 .

Calibration of the apparatus was accomplished by measuring D_{32} of various particles of known size distribution. Polydispersions of glass or polystyrene spheres and aluminum oxide powder were suspended in water within a Plexiglas or glass container. A scanning electron microscope (SEM) was also used to photograph each particle sample.

Some of the calibration results (using the original method discussed above) are summarized in Table I. Figures 4 and 5 present typical calibration results.

TABLE I CALIBRATION RESULTS FOR LIGHT SCATTERING APPARATUS

PARTICLE MATERIAL	SAMPLE PARTICLE SIZE RANGE (microns)	CALCULATED D ₃₂ (microns)	MEASURED D ₃₂ (microns)
Polystyrene	3-6	4.7**	4.5
Polystyrene	6-16	10.2**	10.0
Polystyrene	15-30	21.6**	21
Glass	37-44	38*	40
Glass	53-63	54*	54-58
Glass	1-37	25*	28-30

* From SEM photographs ** From Manufacturers Data

The results of the calibration tests showed that the apparatus is capable of accurately measuring mean particle size for a broad range of mean diameters providing that size range is not too wide (per figure 3).

If the larger sizes in a bi-modal distribution of actual motor products includes a wide range of particle sizes, then care must be taken in the selection of the forward scattering angles so as to not bias the measurements to the larger or smaller particle sizes. Another concern about the measurement technique is the effect of the index of refraction of the exhaust gases in which the particles are present. To examine this, the 6-16 micron polystyrene sphere data was used to find D₃₂ with varying assumed values for the index of refraction. The result was that a 10% increase in the index of refraction increases the "measured" D₃₂ by approximately 10%. This could present difficulties if the present technique were attempted to be applied to a wide range of propellants/operating conditions where the unknown exhaust index of refraction could vary significantly from test-to-test. In the present effort similar propellant compositions are used with varying solids size and loading and with varying nozzle geometries. Variations in the index of refraction should be small in this case.

A further concern, especially for the "in-motor" measurement, was the maximum attenuation of the transmitted beam which would allow the scattering measurements to be properly made. Measurements have generally been assumed to require less than 10% attenuation in order to insure single scattering. Calibrations using the 6-16 micron polystyrene beads were conducted with transmittances varying from 85% down to 30%. The two-angle method results are shown in Table II.

TABLE II TRANSMITTANCE EFFECTS ON SCATTERING MEASUREMENTS

TRANSMITTANCE, %	D ₃₂ , MICRONS
85	10
70	10
60	9.5
50	9.5
30	9

These results indicate that a significant attenuation of the transmitted beam did not prohibit use of the single-scattering theory for obtaining D₃₂. However, very low "in-motor" transmittance values are often encountered in highly metallized systems. Fortunately, minimum smoke propellants often have less than 2% metal and, therefore, may often be studied using this diagnostic technique.

Results and Discussion

In this initial investigation, two solid propellant compositions were used. One propellant was non-metallized and used a GAP binder with AP. The other was an HTPB/AP propellant with 2%, 40 micron aluminum and 0.25% Fe₂O₃.

The non-metallized propellant was used to determine the effects of apparatus design, exhaust gas opacity and thermal and velocity gradients on the laser beam transmittance and scattering characteristics. Significant attenuation (greater than 20%) and broadening at small angles occurred in the nozzle exhaust beam. The measurement location was located very close to the exhaust plane of the converging nozzle. This indicated that future tests should be conducted with the measurement location further aft; where jet spreading will both reduce opacity and minimize velocity and thermal gradient effects. The "in-motor" measurement revealed the necessity for very careful alignment of the windows. If the windows are not very nearly perpendicular to the laser beam, changes in the index or refraction of the gas when the motor is fired can cause the transmitted beam to deflect either off of the array or below the beam stop.

When the metallized propellant was fired, the two-angle method yielded a D₃₂ in the exhaust products of approximately 8 microns (Fig. 6) for the larger scattering angles (greater than 0.020 radians). SEM photographs of a small portion of the collected exhaust products (Fig. 7) showed particles as large as 20 microns, a few between 5 and 10 microns and many (as expected) in the one micron range. At the nozzle entrance the measured D₃₂ using the two-angle method was between 8 and 10 microns (Fig. 8). Residue collected from the combustor wall near the viewing location is shown in figure 9. Particles in the 9 to 10 micron range were evident with many having diameters less than 3 microns.

These limited initial results indicate that the diagnostic method can be used to determine the change in D₃₂ across the exhaust nozzle if care is used in window alignment and exhaust measurement location. In addition, the angle limits of the apparatus must not unduly bias the data toward the larger or smaller particles. Little change in D₃₂ was observed to occur across the exhaust nozzle in this initial test.

HOLOGRAPHIC INVESTIGATION

One of the diagnostic techniques available for studying particulate behavior in solid propellant rocket motors is holography. For the exposed scene a hologram provides both amplitude and phase information. The latter characteristic enables a 3-D image to be reconstructed so that particles within in the entire depth of field of the scene may be recorded. Flame envelopes surrounding the burning particles are readily eliminated from the recorded scene through the use of narrow pass laser line filters. Single pulsed holography provides a means for effectively stopping the motion. However, it only provides information during a single instant of the combustion process.

Smoke generation (i.e., small Al₂O₃ and binder products, etc.) during the combustion process presents a major obstacle to obtaining good holograms, and consists of two distinct, but related, problems. The first is that a laser can only penetrate a finite amount of smoke, and the second involves the required reference beam to scene beam illumination ratio. To obtain a high-resolution hologram, the illumination ratio reaching the holographic plate should be between 5:1 and 10:1. Test-to-test variation in the amount of smoke in the beam path can significantly affect this ratio. To achieve an optimum combination of low levels of combustion chamber smoke and well-developed propellant burning requires experimental determination of the most suitable propellant composition and dimensions and the optimum time for taking of the hologram during the burn.

Initial efforts utilized strand burners within a nitrogen-purged combustion bomb. Subsequent to these initial strand burner tests it was desired to obtain holograms in flow environments which more nearly approached that in an actual motor. Small two-dimensional, windowed motors were used next. Currently, efforts are being directed at obtaining holograms within a small rocket motor. Additionally, holograms have been recorded of resolution charts for calibration purposes. Investigations into changing the recording and reconstruction geometries have also been conducted.

The laser holographic system uses a pulsed ruby laser (Ref. 18) together with a holocamera (Ref. 19). The operating wavelength is 694.3 nm with a beam diameter of approximately 3.2 cm. A one joule pulse with a 50 nsec pulsewidth was used for this investigation.

The 2-D motor employed two opposed propellant slabs with ends and sides inhibited with a very thin coating of GE Hi-temp gasket (red RTV) material. The 1 cm x 4 cm slabs were placed between two borosilicate glass slides and the inhibitor was then allowed to cure. Propellant thickness was varied from 1 to 3 mm.

All holograms were recorded with diffuse illumination from the laser in order to minimize the presence of schlieren interference fringes produced by temperature and density variations of the combustion gas products during the burn. This diffuse illumination introduces speckle into the reconstructed images as discussed later. The primary problem in sizing the particles in the reconstructed image is interference from this speckle which can have a maximum size that is comparable to the particles at the lower end of the expected particle size distribution.

The resolution limits of the holographic system were determined by placing a 1951 USAF resolution target in the 2-D motor at the propellant location. Fourteen micron resolution was readily attained through the microscope. With very careful alignment and cleaning of all optical components, together with the use of a rotating mylar disc (discussed below), 9 micron resolution has been achieved.

Holographic recordings have been made successfully using propellant strands burned at pressures of 34 and 68 atm and with various concentrations of aluminum up to 15%. Figure 10 is a photograph taken at one plane within a reconstructed hologram. The propellant and strand dimensions are the same as shown in figure 1 for the high speed motion pictures. It is apparent that the flame envelopes and schlieren effects are readily eliminated from the recorded picture.

A representative photograph of a reconstructed hologram obtained using the 2-D motor is shown in figure 11. Good quality holograms were obtained with all propellants containing less than 5% metal additive to pressures of approximately 59 atm (the maximum attempted). A good quality hologram was also obtained with 10% aluminum at approximately 33 atm. No holograms could be obtained with 10% aluminum at pressures of 53 atm or with 15% aluminum. The 2-D motor construction method has proven to provide good results within the above limits. Impingement of the particulates on the glass walls and a high inhibitor-to-propellant mass ratio have provided the upper limits in metal content and propellant thickness in the tests. Holograms may actually be more easily obtained in a 3-D motor. In that case, although the scene depth is greater, both of the above limitations can be significantly reduced.

During reconstruction, the geometry shown in figure 12 is used. The real image of the hologram was focused onto a spinning mylar disk, introduced to reduce speckle effects in the observed image. The spinning disk changes the speckle pattern at a rate faster than the response time of the imaging system, causing a reduction in the contrast of the speckle pattern. A variable power microscope was used to view the reconstructed image either by eye or with the image scanner of the image processing system.

With the successful recording and reconstruction of the holograms, an effort has begun to automatically locate particles against the background, and to size the particles using a computer-controlled image processing system. The Quantimet 720 image processor used in this investigation is a general purpose, television-type image analyzer that is capable of elementary shape recognition and various physical measurements of objects by distinguishing differences in grey levels in the image and performing various logical tests on measured dimensions.

Several problems have been identified in this application of data reduction, and potential solutions are being investigated. The problems can be divided into two parts: those that exist without image speckle being present and those that exist with speckle being present.

The first problem is to compute the number of locations that must be investigated in the hologram. For example, for a nominal depth of interest in the hologram of 2 mm, calculations show that for larger (200 microns) particles only one plane is required by the microscope's depth of focus of 6.18 cm, while for 1 micron particles the depth of focus of 1.54 microns will require 1300 planes to be imaged.

The Quantimet also has limitations which can lead to inaccurate results. One technique of separating particles from background is to accept for measurement only those pixels that are darker than a specified threshold. Once the particle has been isolated, the particle size is measured. The Q720 locates an edge of a particle by noting regions where there is a sharp change in grey level. The edge location is determined by finding the pixels with the greatest and least grey levels and locating the edge midway between these two locations. This technique is consistent only for particles with the same extremes in grey levels. For frames that include particles of differing grey levels, the edge location is variable. Uneven illumination is the primary cause of differences in particle grey level. The illumination problems can occur in the hologram recording (i.e., laser nonuniform beam pattern, smoke), in the development of the hologram leading to a plate with variable transmissivity (bleaching the plate can help this problem), and in the reconstruction process (i.e., uneven laser illumination, nonuniform spatial response of the image tube). Additionally, electronic noise in the various modules and quantization noise can corrupt the image signal leading to measurement errors.

Having speckle present, as in our hologram reconstructions (due to the diffuse illumination required to eliminate the schlieren fringes in the reconstruction as previously described), we wish to reduce the maximum size of the expected speckle

to the smallest value possible. The speckle can have two effects on the image. It produces black spots in the background which cannot be readily distinguished from real particles. The second effect is that the speckle can give the perimeter of the particle a "swiss cheese" appearance where the speckle overlaps the edge. This alters any calculated measurements of the particle, such as area or perimeter. The Quantimet usually ignores any holes within the measured area, but significant error is introduced when the perimeter is altered.

Generally, to reduce the speckle size, large aperture optics are desirable. Once the speckle is smaller than the typical particle size the logic test based on the feature size can be implemented in the Quantimet to extract particle information from the background.

If the speckle size cannot be made negligible compared to the particle size, other techniques must be used to reduce the contrast level of the speckle relative to the particle. These techniques are based on the fact that the speckle pattern will shift if one or more of many variables are changed while the object position remains fixed. By averaging N images with differing speckle patterns, a reduction in the speckle contrast on the order of $(N)^{-1/2}$ is expected.

Variables that can be changed to cause a shift in the speckle pattern are (a) changing the random phase of the diffuse illuminating wave, (b) changing the image aperture, (c) changing the object position (or, equivalently, changing the image screen position or changing the imaging lens position) and (d) computer superposition of images with different diffuse illumination. Each of these techniques introduces complexity into the processing of the image. The first is the easiest to implement with a spinning diffuser in the image reconstruction. While the image is dramatically improved when the disk is spinning compared to the image on a motionless disk, the image quality is not dramatically improved with increased rotation rate. The techniques other than computer processing appear to present insurmountable problems, leaving computer processing of the images the most likely solution. Work has begun on implementing the computer-controlled configuration in an effort to explore this technique.

An example of an initial effort to use the Quantimet 720 in the manual mode is shown in figure 13. This histogram was taken from a photograph of a reconstructed hologram shown in figure 14. Recently, the Q720 has been operated in the computer controlled mode. A particle calibration reticle (Laser Electro-optics LTD. No. RR-50-30-0.08-102-CF-#154M) was viewed directly by the Q720 television camera through a microscope and the particle diameter distribution was determined. Figure 15 presents a comparison between the measured particle size distribution and that specified by the manufacturer of the reticle.

SUMMARY AND CONCLUSIONS

High intensity white-light and monochromatic light have been used to eliminate the flame envelopes that surround burning aluminum particles from the recorded images in high speed motion pictures.

Light scattering measurements have been used to measure the change in D_{32} across the exhaust nozzle of a small solid propellant rocket motor. The diagnostic technique is sensitive to alignment and must be used with caution in order to ensure that particle size biasing is not severe.

The holographic techniques have been successfully used to record particles from strand burner and 2-D motor combustion of solid propellants. The image particle count and sizing from a hologram has successfully been done in the manual mode but automatic techniques that have been recently initiated are preferred. The diffuse illumination required in the recording process to avoid phase fringes due to thermal effects has led to the presence of speckle in the images. Efforts have been made to analyze the size of the speckle and to reduce the maximum speckle diameter. The remaining speckle is reduced by using a spinning diffuser in the reconstruction process. The computer-processed images appear to have the most likelihood of further reduction of the speckle contrast. This method is currently under investigation.

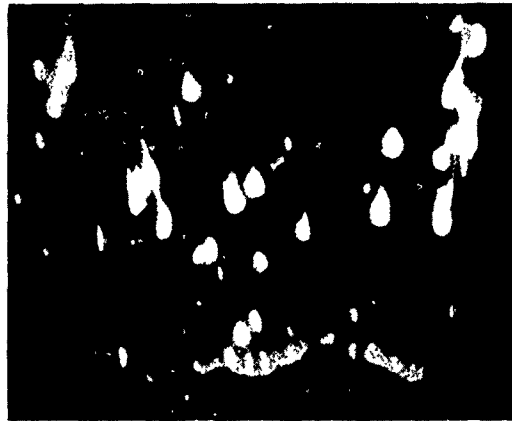
REFERENCES

1. D. George, "Recent Advances in Solid Rocket Motor Performance Prediction Capability", AIAA Paper No. AIAA-81-033, 19th Aerospace Sciences Meeting, Jan 12-15, 1981.
2. R.W. Hermsen, "Aluminum Oxide Particle Size for Solid Rocket Motor Performance Prediction", AIAA 19th Aerospace Sciences Meeting, Jan 12-15, 1981.
3. R.A. Dobbins, "Remote Size Measurements of Particle Product of Heterogeneous Combustion", Eleventh Symposium (International) on Combustion, The Combustion Institute, 1967, p.921.
4. R.A. Dobbins and L.D. Strand, "A Comparison of Two Methods of Measuring Particle Size of Al_2O_3 Produced by a Small Rocket Motor", AIAA J. Vol.8, 1970, pp 1544-1550.
5. K.L. Cashdollar, C.K. Lee, and J.M. Singer, "Three Wavelength Light Transmission Technique to Measure Smoke Particle Size and Concentration", Applied Optics, Vol. 18, No.11, June 1979, pp 1763-1769.

6. R.O. Gumprecht and C.M. Sliepcevich, "Scattering of Light by Large Spherical Particles", J. Physical Chem., Vol. 57, Jan 1953, pp 90-94.
7. R.A. Dobbins, L. Crocco and I. Glassman, "Measurement of Mean Particle Size of Sprays from Diffractively Scattered Light", AIAA J. Vol 1, No. 8, 1963, pp 1882-1886.
8. J.H. Roberts and M.J. Webb, "Measurements of Droplet Size for Wide Range Particle Distributions", AIAA J., Vol. 2, No. 3, 1964, pp 583-585.
9. R.A. Mugele and H.D. Evans, "Droplet Size Distribution in Sprays", Ind. and Eng. Chem., Vol. 43, 1951, pp 1317-1324.
10. R.A. Dobbins and G.S. Jizmagian, "Optical Scattering Cross-Sections for Polydispersions of Dielectric Spheres", J. Optical Soc. of Am., Vol. 56, No. 10, 1966, pp 1345-1350.
11. R.A. Dobbins and G.S. Jizmagian, "Particle Measurements Based on Use of Mean Scattering Cross-Sections", J. Optical Soc. of Am., Vol. 56, No. 10, 1966, pp 1351-1354.
12. J.R. Hodgkinson, "Particle Sizing by Means of the Forward Scattering Lobe", Applied Optics, Vol. 5, No. 5, 1966, pp 839-844.
13. E.A. Powell, R.A. Casanova, C.P. Bankston and B. Zinn, "Combustion Generated Smoke Diagnostics by Means of Optical Measurement Techniques", AIAA Paper No. 76-67, AIAA 14th Aerospace Sciences Meeting, Jan. 1976.
14. D.R. Buchele, "Particle Sizing by Measurement of Forward Scattered Light at Two Angles", NASA TP 2156, May 1983.
15. H.C. Van de Hulst, Light Scattering by Small Particles, John Wiley and Sons, Inc. New York, 1957.
16. S.G. Karagounis, et.al., "An Investigation of Experimental Techniques for Obtaining Particulate Behavior in Metallized Solid Propellant Combustion" Air Force Rocket Propulsion Laboratory Report AFRPL-TR-82-051, July 1982.
17. R.G. Cramer, et.al., "An Investigation of Experimental Techniques for Obtaining Particulate Behavior in Metallized Solid Propellant Combustion", Air Force Rocket Propulsion Laboratory Report AFRPL-TR-84-014, Feb. 1984.
18. R.A. Briones and R.F. Wuerker, "Instruction Manual for the Improved Ruby Holographic Illuminator", AFRPL-TM-78-11, Edwards AFB, CA, July 1978.
19. R.A. Briones and R.F. Wuerker, "Operation Manual for the Lens Assisted Multipurpose Holocamera with Reflected Light Option", AFRPL-TM-78-12, Edwards AFB, CA, July 1978.

ACKNOWLEDGEMENTS

This paper summarizes work which has been directed by the authors but which has been conducted primarily by graduate students and Naval Postgraduate School engineering technicians. The most recent contributors have been J.M. Glenn, K.J. Graham, R.K. Harris, P.J. Hickey, A. Kertadidjaja, L.A. Klooster, J. Rosa, Y. Lee and P. Shook. This work has been sponsored by the Air Force Rocket Propulsion Laboratory, Edwards AFB, California, USA.



1000 μm

(a) Self-Illumination



1000 μm

(b) 2500 Watt White-Light Rear Illumination

Figure 1. High Speed Motion Pictures of Propellant Strands Burned at 34 atm. Pressure (83% AP, 12% HTPB, 5% Al, 45-62 micron)



Figure 2. Photograph of Small Rocket Motor With Light Scattering Measurement Apparatus.

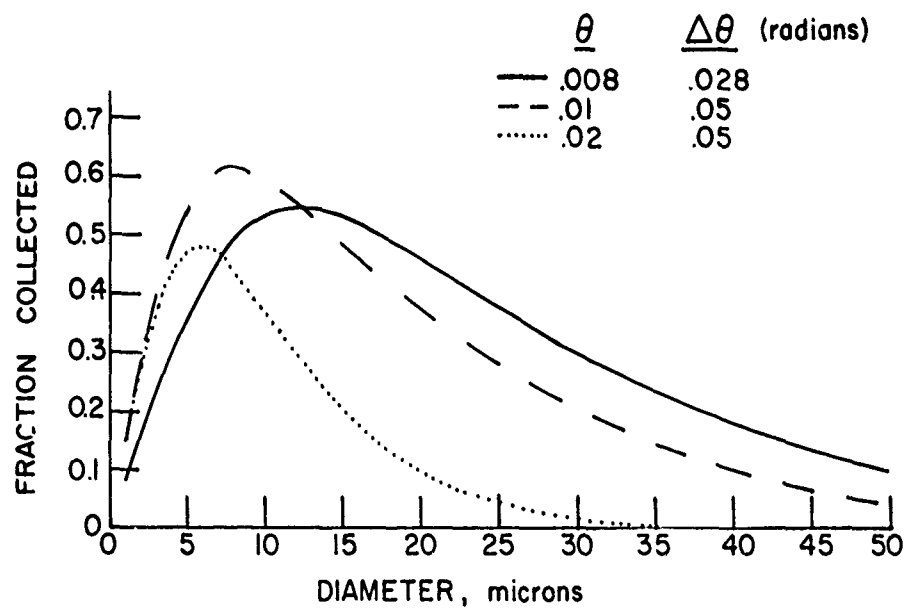


Figure 3. Fraction of Total Normalized Scattered Light Collected as a Function of θ_1 and $\Delta\theta$.

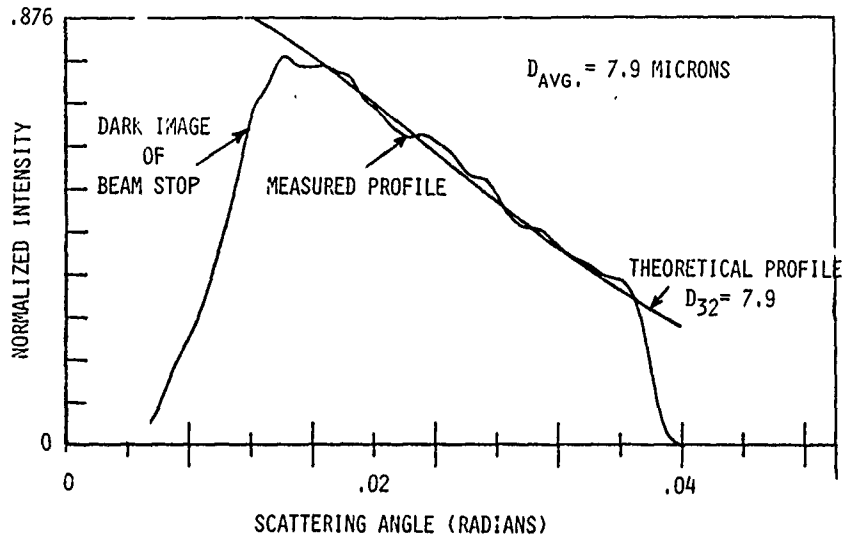


Figure 4. Measured Mean Particle Diameter Using 6-16 Micron Polystyrene Spheres With Curve-Fit Method.

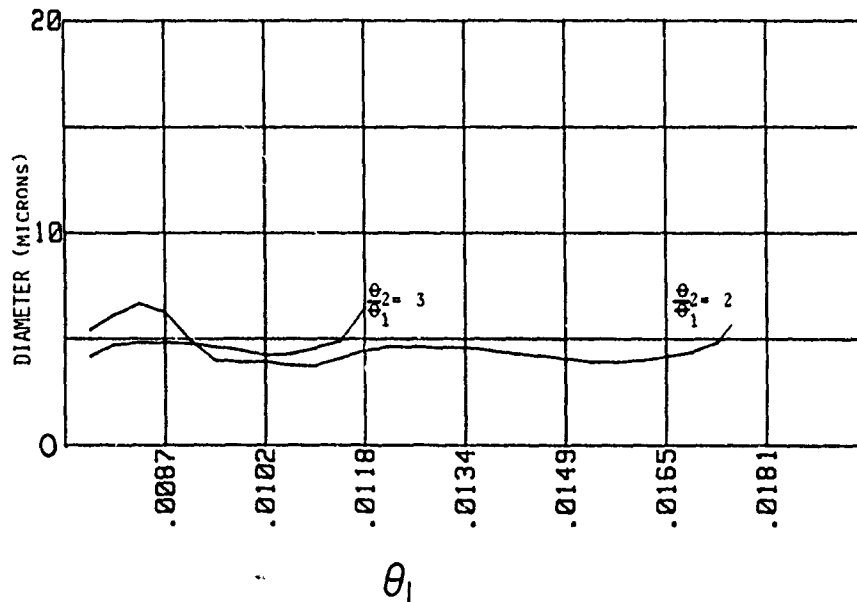


Figure 5. Measured Mean Particle Diameter Using 3-6 Micron Polystyrene Spheres With Two-Angle Method.

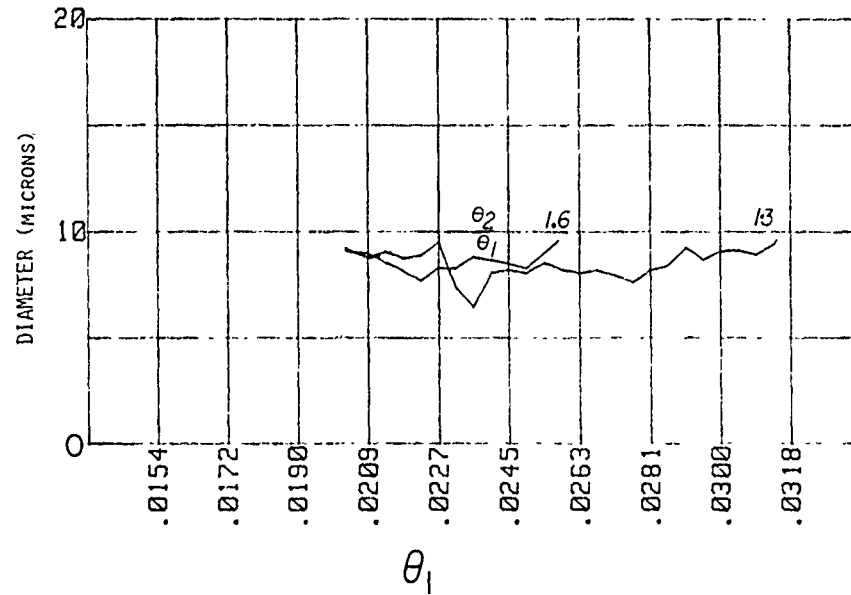


Figure 6. Measured Mean Particle Diameter in Exhaust Flow Using the Two-Angle Method, HTPB/AP Propellant With 2%, 40 Micron Aluminum and 0.25% Fe_2O_3 Burned at a Nominal Pressure of 10 atm.

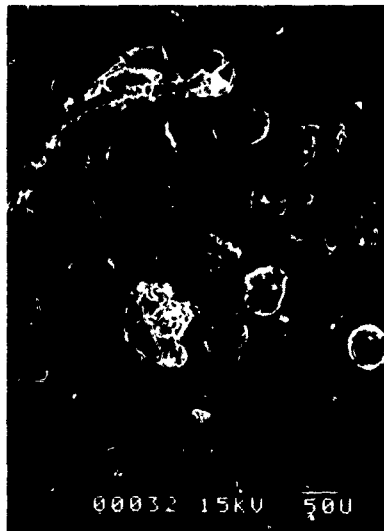


Figure 7. SEM Photograph of Residue From Exhaust Products, HTPB/AP Propellant With 2%, 40 Micron Aluminum and 0.25% Fe_2O_3 Burned at a Nominal Pressure of 10 atm.

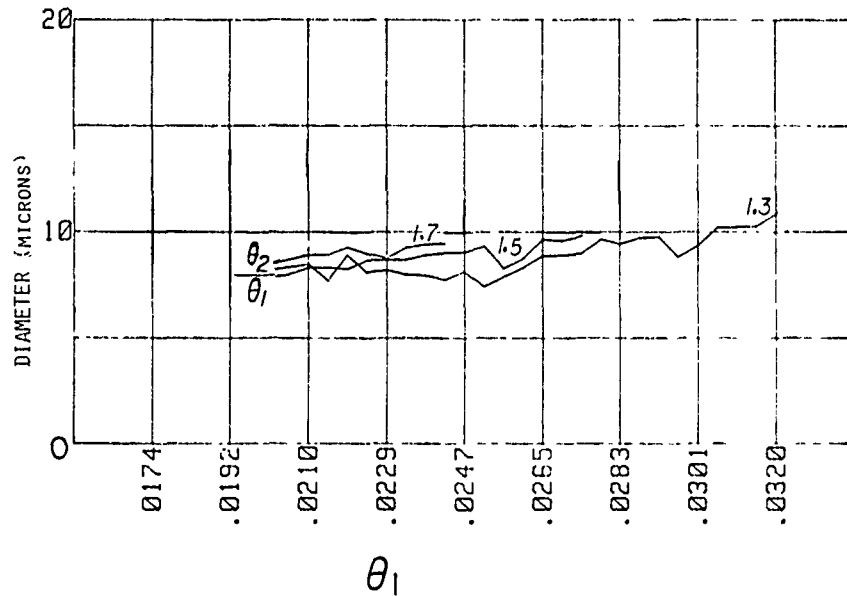


Figure 8. Measured Mean Particle Diameter at Nozzle Entrance Using the Two-Angle Method, HTPB/AP Propellant With 2%, 40 Micron Aluminum and 0.25% Fe_2O_3 Burned at a Nominal Pressure of 10 atm.

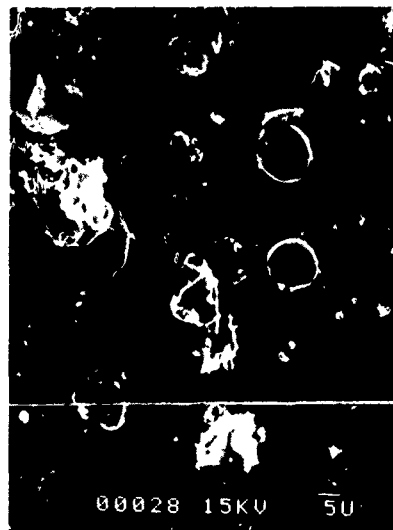


Figure 9. SEM Photograph of Residue From Motor Cavity Wall, HTPB/AP Propellant With 2%, 40 Micron Aluminum and 0.25% Fe_2O_3 Burned at a Nominal Pressure of 10 atm.

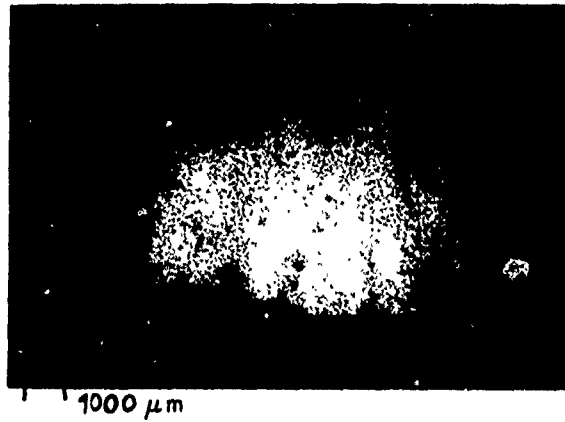


Figure 10. Photograph of Reconstructed Hologram of Strand Burner at 34 atm Pressure (83% AP, 12% HTPB, 5% Al, 45-62 Microns).



Figure 11. Photograph of Reconstructed Hologram of 2-D Motor Combustion at 28 atm Pressure (83% AP, 12% HTPB, 5% Al, 45-62 Microns).

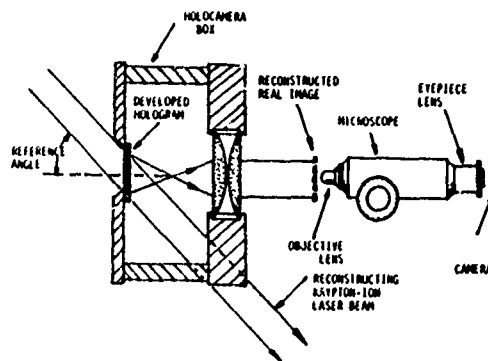


Figure 12. Schematic of Hologram Reconstruction and Viewing Method (Ref. 20)

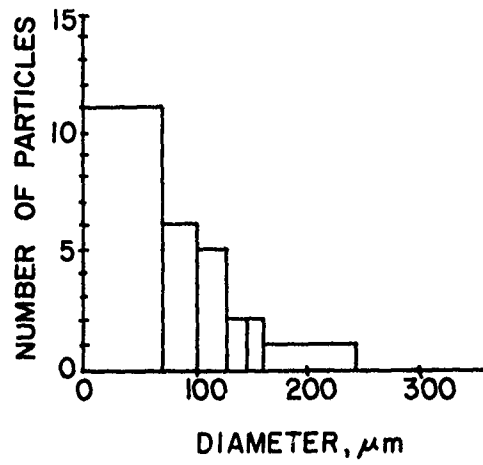


Figure 13. Particle Size Histogram Obtained From Photograph of Figure 14 Using Quantimet 720 in Manual Mode.

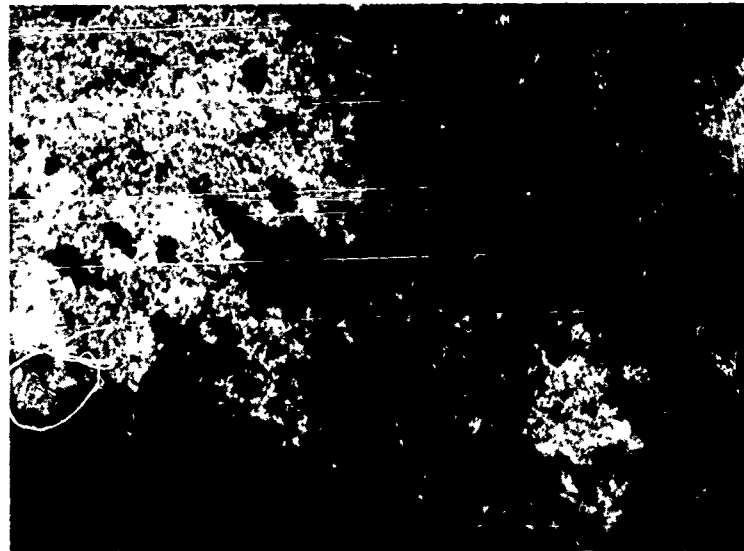


Figure 14. Photograph of Reconstructed Hologram From Propellant Strand Combustion With Stability Additive.

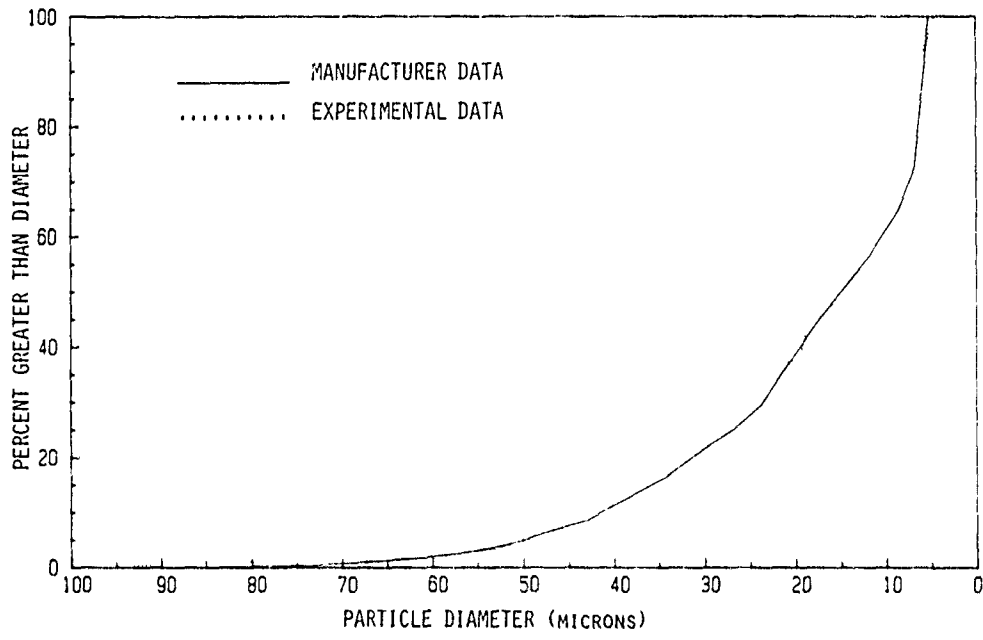


Figure 15. Particle Size Distribution Obtained Using the Quant'met 720 in the Computer-Controlled Mode With a Calibration Reticle.

ANALYSE DES GAZ DANS L'ETUDE DE LA COMBUSTION
DES PROPERGOLS DOUBLE BASE ET DE L'OCTOGENE

par Jean-François TRUBERT

Office National d'Etudes et de Recherches Aérospatiales
29, avenue de la Division Leclerc
92320 CHATILLON (France)

Résumé

La méthode de pyrolyse linéaire sous vide par conduction ou rayonnement, avec analyse par spectrométrie de masse, permet de déterminer la composition des gaz issus de la dégradation des propergols solides en phase condensée, en minimisant les réactions secondaires et dans des conditions proches du fonctionnement réel.

Cette méthode a été mise au point sur des propergols double base de référence et en présence d'additif. On obtient d'importantes quantités de formaldéhyde, glyoxal et dioxyde d'azote. La présence minoritaire de monoxydes d'azote et de carbone, de dioxyde de carbone et d'eau témoigne de la qualité naissante des gaz. Le peu de différence entre les compositions quantitatives montre que l'additif n'agit pas en phase condensée.

Cette méthode a été appliquée à l'octogène. L'analyse fait apparaître de fortes proportions de divers oxydes d'azote (NO_2 - NO - N_2O), de formaldéhyde et d'acide cyanhydrique et de faibles quantités d'eau, d'azote et d'oxydes de carbone.

GAS ANALYSIS FOR THE INVESTIGATION OF THE COMBUSTION
OF DOUBLE-BASE PROPELLANTS AND HMX

Summary

The linear pyrolysis method under vacuum by conduction and radiation, with analysis by mass spectrometry is used to obtain the composition of the gases produced by the solid propellant condensed phase degradation, while minimizing the secondary reactions and under conditions close to actual burning.

This method has been elaborated with reference double-base propellants, then in presence of additives. Important quantities of formaldehyde, glyoxal and carbon dioxide are obtained. The presence in low amounts of nitrogen and carbon monoxides, carbon dioxide and water indicates that the gases result mostly from the degradation. The small difference between the quantitative compositions shows that the additive does not act on the condensed phase degradation.

This method has been applied to HMX. The analysis shows large amounts of several nitrogen oxides (NO_2 , NO , N_2O), formaldehyde and cyanhydric acid and small quantities of water, nitrogen and carbon oxides.

1 - INTRODUCTION

Dans le but d'améliorer les performances, les mécanismes de combustion des propergols solides ont déjà fait l'objet de nombreuses études. En particulier, on a souvent cherché à préciser la nature et la concentration des gaz issus de la pyrolyse (dégradation en phase condensée) sous l'effet des flammes et au cours de la combustion. Toutefois, la plupart des analyses réalisées à la sortie de la zone superficielle de dégradation et dans la zone d'induction ont été menées dans des conditions :

- n'assurant pas vraiment l'absence de réactions secondaires (expériences en vase clos, temps de séjour élevés, sous vide partiel...);
- ne cherchant pas à reproduire les conditions réelles de fonctionnement (échantillons de petite taille, vitesses de dégradation mal connues...).

La méthode de pyrolyse linéaire sous vide, par conduction ou par rayonnement et avec analyse par spectrométrie de masse, mise en oeuvre à l'ONERA permet de déterminer la composition des gaz issus de la dégradation en phase condensée, en minimisant considérablement les réactions secondaires et dans des conditions proches du fonctionnement réel.

Le prélèvement des gaz dans la zone d'induction au cours d'une combustion réelle sous faible pression fait apparaître les évolutions de composition dues aux réactions chimiques dans la flamme primaire.

La méthode de pyrolyse linéaire sous vide avec analyse par spectrométrie de masse est également appliquée à d'autres produits, entrés plus récemment dans la fabrication des propergols solides, en particulier l'octogène. La bibliographie fait apparaître de grandes divergences dans les analyses réalisées de ses gaz de dégradation.

2 - COMBUSTION DES PROPERGOLS HOMOGÈNES DOUBLE BASE

L'analyse des gaz aux différentes étapes de la combustion des propergols solides homogènes de référence a déjà fait l'objet de publications précédentes [1, 2]. Cet exposé présente les analyses de gaz réalisées lors de la dégradation en phase condensée de propergol homogène, en présence d'additif et au cours de la combustion par prélèvement dans la zone d'induction.

2.1 - Gaz résultant de la dégradation en phase condensée2.1.1 - Principe

Le mécanisme de régression des propergols homogènes, le plus communément admis, propose la rupture de la liaison CO/NO_2 comme étape initiale de la dégradation. Elle conduit à la formation de NO_2 et d'espèces combustibles telles que des aldéhydes supposées réagir très rapidement au niveau de la flamme primaire, cette dernière entretenant le mécanisme de pyrolyse par conduction thermique.

On désigne par "gaz naissants", les gaz issus de la dégradation thermique (pyrolyse) en phase condensée avant réaction dans la flamme primaire. De nombreuses précautions sont nécessaires pour assurer ce caractère. Elles conditionnent très impérativement les techniques mises en oeuvre.

Les espèces chimiques émises étant effectivement très réactives, il est indispensable d'opérer cette pyrolyse sous très basse pression. Or, la diminution de pression, en figeant les réactions entre gaz naissants, élimine la flamme primaire. Absente, celle-ci n'entretient plus la pyrolyse. Il faut fournir un flux de chaleur auxiliaire pour la simuler. Dans le propergol en cours de combustion, en cigarette, l'élévation de température (de 20 à 300-400°C) conduisant à la pyrolyse s'effectue en un temps très court : de l'ordre de 20 ms, dont seulement 1 à 2 ms dans la zone réactionnelle à :

$$300^\circ\text{C} < T < 400^\circ\text{C} \text{ ([2] et tableau 1).}$$

La simulation de la combustion implique donc de mettre en oeuvre une technique de chauffage rapide (dans le cas contraire, le risque d'observer des phénomènes ne se produisant pas réellement en combustion n'est pas négligeable). Sous vide, cette simulation peut être réalisée de deux manières : par conduction ou par rayonnement.

2.1.2 - Dispositifs expérimentaux

Les expériences sont menées sur des échantillons de propergol chaud $\text{PC} \approx 1100 \text{ cal.g}^{-1}$ dans une enceinte en verre démontable placée sur un bâti de vide primaire assurant une pression minimale de 10^{-2} mbars et un débit de $15 \text{ m}^3\text{h}$. Cela est suffisant pour maintenir une pression inférieure à 1 mbar en cours de régression. Cette enceinte d'un volume de 20 l est pourvue de deux capteurs de pression à jauge de contrainte, insensibles à la nature des gaz (gamme de mesures : 10^{-2} à 100 mbars et 1 à 2000 mbars).

Pour simuler l'apport thermique, deux montages totalement réalisés à l'ONERA ont été utilisés :

Le montage de pyrolyse par conduction est présenté sur la figure 1. Le flux de chaleur est fourni à l'échantillon par un ruban chauffé par effet Joule, perforé pour faciliter l'évacuation des gaz et éviter de créer une surpression locale compromettant leur caractère naissant. Un thermocouple chromel-alumel sert dans l'un des trous pour mesurer la température du ruban. Un système à contre-poids assure le contact permanent de l'échantillon avec le ruban.

Ce montage, déjà employé lors des expériences précédemment citées [1, 2], ne fonctionne correctement que pour le propergol de référence. En effet, en présence d'additif, une couche de carbone s'interpose progressivement entre l'échantillon et le ruban chauffant. A l'intérieur de cette couche isolante se produisent des réactions chimiques incontrôlées. L'analyse des gaz révèle alors une composition chimique déjà partiellement brûlée.

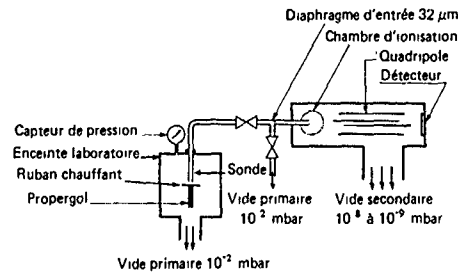


Fig. 1 - Montage de pyrolyse par conduction.

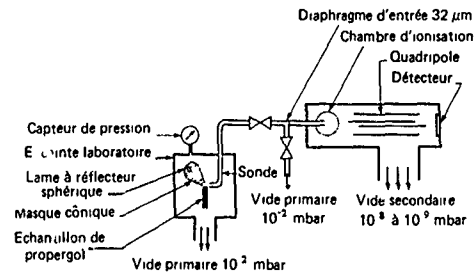


Fig. 2 - Montage de pyrolyse par rayonnement d'une lampe à filament de tungstène

Le montage de pyrolyse par rayonnement est présenté sur la figure 2. Sous vide et en l'absence de conduction, seul le rayonnement permet de réaliser un apport de chaleur à un matériau ; soit par exemple : le flux de rayonnement d'une source infrarouge. Celle-ci peut être une lampe de 150 W à filament de tungstène placée à l'intérieur de l'enceinte laboratoire, figure 2. Un réflecteur sphérique focalise le rayonnement sur l'échantillon. Un masque conique entourant le faisceau lumineux diminue le contact entre les gaz de dégradation et l'ampoule chaude. Il permet également de positionner facilement l'échantillon au point de focalisation. La surface de régression est maintenue à hauteur constante, à l'aide d'un fil métallique tendu en travers de l'échantillon. Un capteur de déplacement permet de déterminer la vitesse de dégradation obtenue.

Dans les deux cas, la pyrolyse de l'échantillon, en cigarette, est nette et rapide, et une sonde de prélèvement de grand débit est positionnée de manière à aspirer préférentiellement les gaz s'échappant directement de la surface en régression.

2.1.3 - Analyse des gaz de dégradation des propergols homogènes

L'identification des espèces chimiques résultant de la dégradation est réalisée par spectrométrie de masse, à l'aide d'un piège cryogénique à -180°C intercalé sur le circuit de prélèvement. Après une expérience, le réchauffement progressif du piège libère les différentes espèces chimiques par petits groupes de 2 ou 3. La dégradation des propergols homogènes en phase condensée conduit à la formation de NO , NO_2 , CO , CO_2 , HCHO , HCN , $(\text{CHO})_2$, H_2 et H_2O .

Le tableau 1 résume les conditions de pyrolyse pour les deux montages et les données que l'on peut en tirer, à partir de la modélisation établie en [2] pour le même propergol. Elles permettent de produire des gaz de pyrolyse dans le cas où le propergol subit un front thermique de faible épaisseur.

Tableau 1

Source de chaleur	flamme primaire	conduction ruban chauffant	Rayonnement lampe tungstène à miroir sphérique
Pression de l'échantillon sur le ruban		$5 \cdot 10^{-2} \text{ Nmm}^{-2}$	néant
Puissance de chauffage		repérée par $T_{\text{r}} \approx 600^{\circ}\text{C}$	150 W
Température de surface, T_3	650 K	320°C ou 590 K	inconnue
Pression dans l'enceinte laboratoire, P_E en début	25 bars	10^{-2} mbar	10^{-2} mbar
en fin de régression		1 mbar	1 mbar
Vitesse de régression, V_r	5 mms^{-1}	$0,6 \text{ mms}^{-1}$	$0,5 \text{ mms}^{-1}$
Épaisseur chauffée, x_c ($T_c < T < T_3$) $x_c = \frac{a_p}{V_r} \left \ln \frac{1}{100} \right $ avec $a_p = 1,3 \cdot 10^{-3} \text{ cm}^2 \text{ s}^{-1}$	$120 \mu\text{m}$	$1000 \mu\text{m}$	$800 \mu\text{m}$
Temps de séjour dans la zone chauffée, $t_c = \frac{x_c}{V_r}$	24 ms	1,7 s	1,6 s
Écart de température correspondant à l'épaisseur de réaction, ΔT $\Delta T = \frac{T_3}{1 + \frac{E_p}{RT_3 \ln 100}}$ avec $E_p = 40 \text{ kcal/mole}^{-1}$	84 K	70 K	inconnu
Épaisseur de réaction, x_r ; ($T_3 - \Delta T < T < T_3$) $x_r = \frac{a_p}{V_r} \left \ln \left(1 - \frac{\Delta T}{T_3 - T_c} \right) \right $	$7 \mu\text{m}$	$60 \mu\text{m}$	inconnue
Temps de séjour dans la zone de réaction, $t_r = \frac{x_r}{V_r}$	1,4 ms	0,1 s	inconnu

Le tableau 2 fait apparaître les compositions (Xi et Yi %) des mélanges gazeux naissants :

- en pyrolyse par conduction et rayonnement pour le propergol de référence,
- en pyrolyse par rayonnement seulement, en présence d'additif.

Tableau 2

Pyrolyse par conduction et rayonnement - Propergols référence et additif

Fractions molaires Xi % et massiques Yi %

Espèces chimiques		(CHO) ₂	CO ₂	HCN	HCHO	NO ₂	NO	CO	H ₂	H ₂ O	C***
Précision (%)		± 25	± 20	± 18	± 18	± 22	± 22	± 11	± 26	± 13	-
Propergol référence											
Pyrolyse conduction et rayonnement	X	7,0	7,1	0,8	20,0	24,5	13,4	13,5	0,73	12,9	-
	Y	11,7	9,0	0,6	17,2	32,3	11,5	10,9	0,04	6,7	(6,8)
Propergol additif	X	7,8	8,6	0,9	22,3	22,3	13,7	11,8	0,81	11,8	-
Pyrolyse par rayonnement	Y	12,9	10,8	0,7	19,1	29,3	11,7	9,4	0,05	6,1	(4,7)
Commentaires		b*	L**	b	b	b	b	L	b	b	

* bon ** limite *** déduit du bilan élémentaire

La première ligne correspond à l'estimation de l'erreur commise sur la détermination en fonction de la reproductibilité de l'échantillon de gaz.

Le tableau 3 fait ressortir le bon accord des bilans de ces compositions avec le propergol initial.

Tableau 3

Bilans élémentaires C.H.O.N

	C	H	O	N
Propergol initial	24,6	2,8	58	14,5
Propergol référence	19,1	2,4	63,0	15,6
Pyl. cond. et ray.	17,8	2,2	58,7	14,5
Propergol additif	20,3	2,2	62,5	14,7
Pyr. rayonnement	19,9	2,1	61,5	14,5

2.1.4 - Discussion des résultats

Le caractère naissant des gaz peut être apprécié simplement en faisant ressortir les différentes espèces chimiques naissantes (n), intermédiaires (i) ou non réactives (f) composant le mélange dit "naissant".

		Référence (X %)	Additif
n	(CHO) ₂ HCHO NO ₂ H ₂ HCN	53 %	54,1 %
i	NO CO	26,9 %	25,5 %
f	CO ₂ H ₂ O	20 %	20,4 %

La part des espèces véritablement naissantes est la plus importante (≈ 53 %). La part des espèces non réactives peut paraître également importante (≈ 20 %), toutefois CO₂ ne résulte pas en totalité de réactions chimiques entre les espèces naissantes mais peut également provenir directement de la dégradation de la nitrocellulose.

Il est possible d'illustrer concrètement l'avancement de la combustion en considérant l'évolution de la fraction molaire de CO₂, par rapport à celles de toutes les espèces carbonées du mélange ((CHO)₂, HCHO, CO, CO₂, HCN, C_xH_y) et en tenant compte du nombre d'atomes de carbone contenu dans chacune (n) :

$$\text{soit : } \mathcal{X} = \frac{\sum n_i X_{CO_2}}{\sum n_i X_i}$$

Ce rapport est normalement nul au niveau de la phase condensée :
$$\mathcal{Z} = \frac{X_{CO_2}}{X_{CO_2} + X_{\text{propergol}}}$$

et il augmente constamment au cours de la combustion (la température finale de combustion des propergols homogènes n'est pas suffisante pour conduire à une dissociation importante en CO).

En fin de combustion, il ne tend pas vers 1 mais devient maximum (les propergols homogènes étant trop pauvres en oxygène, une partie du carbone reste sous forme de CO). L'indice maximum en fin de combustion peut être estimé à partir des résultats de Heller et Gordon [3] ou d'un calcul à l'équilibre (tableau 4).

Tableau 4

Composition des gaz en fin de flamme secondaire - Heller-Gordon [3] et résultats cités en [2]

Espèces chimiques	CO	CO ₂	N ₂	CH ₄	H ₂	H ₂ O	P.C. cal.g ⁻¹	\mathcal{Z}
[3] X _i %	30	38	21	0,2	10	-	1 330	0,557
(gaz secs)	38,8	33,2	20,6	0	7,7	-		
[2] X _i %	27,5	23,7	14,7	0	5,5	29,0	800	0,463

On a ainsi, en surface, pour le propergol de référence $\mathcal{Z} = 0,13$

avec additif $\mathcal{Z} = 0,15$

Cette valeur et la présence de NO, CO, H₂O et CO₂ (dans une moindre mesure) dans les gaz témoignent d'un début de réaction chimique. Ceci est en bon accord avec le fait que la fraction massique de NO₂ dans les mélanges gazeux analysés ($Y_{NO_2, Ref} = 0,323$ et $Y_{NO_2, Add} = 0,293$) est plus faible que celle théoriquement disponible dans le propergol initial ($Y_{NO_2, P} \approx 0,466$).

J. Gobbo FERREIRA [4] a récemment montré que l'énergie libérée par ces réactions correspond bien à l'exothermicité de la dégradation en phase condensée, et que leur intensification explique la variation de la température de flamme primaire lorsque la pression s'élève.

La faiblesse des différences de composition des gaz de pyrolyse des deux propergols et de l'écart des indices de combustion montre bien que les additifs n'ont pas d'action sur la dégradation en phase condensée.

2.2 - Gaz issus de la flamme primaire

La flamme primaire est la seconde étape importante de la combustion. D'après les recherches menées précédemment [1, 2], c'est à ce stade que les additifs interviennent dans le processus de combustion.

La composition des gaz dans cette zone a déjà fait l'objet d'investigations [4 ; 5], mais soit seulement sur un propergol de référence [4], soit sur des compositions assez différentes des propergols homogènes [5].

2.2.1 - Principe

Les flammes primaire et secondaire des propergols homogènes sont séparées par une zone (zone d'induction) où la température et la concentration des espèces chimiques évoluent peu. C'est un point de prélèvement particulièrement intéressant.

Sous pression normale de fonctionnement (20 à 100 bars), l'épaisseur de cette zone est très faible (quelques dizaines de microns). Cependant il est possible de la dilater, sans modifier sensiblement les réactions chimiques, en abaissant la pression. Une sonde de prélèvement refroidie peut alors y être facilement introduite.

2.2.2 - Dispositif expérimental

Le propergol choisi PC ≈ 1100 cal.g⁻¹ présente un effet de survitesse (pas très important) entre 10 et 30 bars. La combustion est réalisée en bombe sous pression d'argon à 6, 11, 16 et 21 bars, pour les deux propergols (référence et référence + additif). Les vitesses de combustion varient de 2,2 à 4,2 mms⁻¹, et de 2,2 à 5,5 mms⁻¹ respectivement.

Un échantillon de propergol de 5 x 4 x 35 (mm) est placé verticalement sur une nacelle mobile. Un fil de résistance chauffé par effet Joule permet d'allumer l'échantillon qui brûle en cigarette. Un système électrique de rattrapage asservi par une photodiode et un faisceau lumineux maintient la surface de combustion à une hauteur constante. Il permet de positionner assez précisément, au-dessus de la surface (≈ 3 mm), une sonde refroidie à l'eau et munie d'un col, qui assure un figeage efficace des gaz. Le schéma de ce montage est donné figure 3.

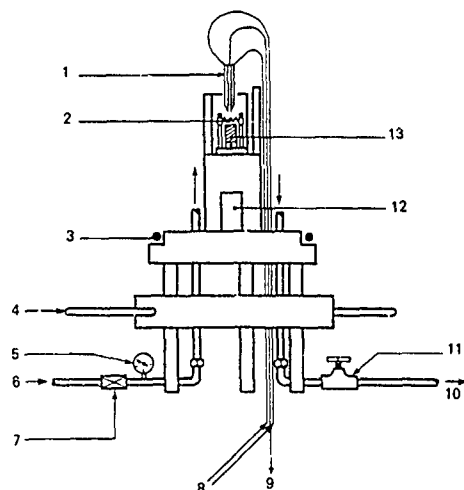


Fig. 3 — Montage pour le prélèvement et l'analyse des gaz de la flamme primaire.

- | | |
|---------------------------|--|
| 1 Sonde de prélèvement | 8 Circuit de refroidissement |
| 2 Résistance d'allumage | 9 Vers la capacité d'air prélèvement ou le spectromètre de masse |
| 3 Joint | 10 Evacuation des gaz brûlés |
| 4 Couronne de serrage | 11 Vanne de détente |
| 5 Manomètre | 12 Moteur de rattrapage de la position de l'échantillon |
| 6 Arrivée d'argon | 13 Echantillon de propergol |
| 7 Vanne électromagnétique | |

2.2.3 - Analyse des gaz

L'identification a été réalisée par chromatographie et confirmée par spectrométrie de masse. Les espèces chimiques présentes sont CO , CO_2 , NO , N_2 , H_2 , CH_4 , C_2H_4 , C_2H_6 , H_2O , ainsi que HCN et N_2O à l'état de traces.

Le tableau 5 contient les compositions sèches obtenues en fonction de la pression pour les deux propergols.

Tableau 5 : Fraction molaire sèche (%)

Propergol	CO_2	C_2H_4	C_2H_6	NO	CH_4	HCN	N_2	CO	H_2
pression (bars)									
Référence									
Précision (%)	± 3	± 8	± 13	± 3	± 5	-	± 35	± 6	± 25
6	12,3	0,9	2,1	27,6	2,5	0,4	4,0	37,9	12,3
11	12,9	1,2	1,8	27,3	2,5	0,4	4,1	38,0	11,8
16	13,0	1,4	1,4	26,4	2,6	0,3	4,3	38,8	11,8
21	12,1	1,5	1,1	26,8	2,6	0,2	4,8	38,9	12,0
Avec additif									
Précision (%)	± 3	± 8	± 13	± 3	± 5	-	± 43	± 7	± 50
6	17,1	2,7	2,5	29,6	3,5	0,4	3,6	34,8	5,9
11	16,7	3,3	1,5	28,7	3,7	0,3	3,7	36,0	6,0
16	19,0	3,5	1,1	27,8	3,7	0,1	4,2	35,1	5,5
21	19,2	4,0	0,8	29,0	3,9	0,2	4,6	36,2	2,2

Seul le résultat sec est présenté ; en effet, quoique la ligne de prélèvement soit thermostatée à 70-80°C, l'eau n'est pas correctement prélevée. Elle n'apparaît de manière substantielle ($X_{\text{H}_2\text{O}} \approx 20\%$) que pour $P = 6$ bars. Au-delà, plus la pression augmente, plus le pic 18 paraît petit dans le spectre de masse des gaz.

Les tableaux 6 et 7 font apparaître les bilans élémentaires obtenus dans chaque cas. Toutefois, pour les obtenir, il a fallu estimer l'eau à partir des résultats à $P = 6$ bars.

Tableau 6

Propergol de référence				
Bilans	C	H	O	N
Propergol	24,6	2,8	58	14,5
initial				
6 bars	22,19	3,32	58,73	15,76
(recalé)	20,42	3,06	54,04	14,5
11 bars	22,63	3,10	58,39	15,88
(recalé)	20,66	2,83	53,30	14,5
16 bars	22,77	3,09	58,52	15,63
(recalé)	21,12	2,87	54,29	14,5
21 bars	22,43	3,08	58,31	16,18
(recalé)	20,11	2,76	52,26	14,5

Tableau 7

Propergol avec additif				
Bilans	C	H	O	N
Propergol	24,6	2,8	58	14,5
initial				
6 bars	22,2'	3,40	59,77	14,59
(recalé)	22,10	3,38	59,40	14,5
11 bars	22,81	3,22	59,38	14,6
(recalé)	22,65	3,19	58,97	14,5
16 bars	23,42	2,87	58,92	14,80
(recalé)	22,95	2,81	57,74	14,5
21 bars	23,34	2,66	58,81	15,19
(recalé)	22,29	2,54	56,16	14,5

2.2.4 - Discussion des résultats

Les résultats du tableau 5 sont directement comparables à ceux de Heller et Gordon [3] (tableau 8).

Tableau 8

Gaz issus de la flamme primaire
Résultats de C.A. Heller et A.S. Gordon [3]
Fractions molaires, %

GAZ	CO ₂	C ₂ H ₄	C ₂ H ₆	NO	CH ₄	HCN	N ₂	CO	H ₂	O ₂	N ₂ O	C ₂ N ₂
*(1)	11,5	1,3	-	32	0,9	0	4,3	41	8,9	-	-	0
11,5 bars (2)	10,9	1,3	-	30,9	1,1	0,13	4,7	42	-	-	-	0,08
(3)	12	1,1	-	30	0,9	0,1	9	38	9,3	-	-	0
15 bars (4)	13	0,6	-	28,6	1,0	0,5	6	40	10	-	-	0,09
(5)	12,9	0,7	-	30	1,1	0,2	4,4	40	10,1	-	-	0,07

(*) - pour différentes hauteurs de la sonde au-dessus de la surface

(1)	4 mm	(3)	6 mm
(2)	5 mm	(4)	14 mm
		(5)	16 mm

- analyse par spectrométrie de masse

On peut remarquer que le propergol de référence conduit à une composition très proche de celle de Heller et Gordon. En revanche, en présence d'additif, le taux de CO₂ s'élève, tandis que celui de CO baisse, ce qui amène à reprendre l'indice d'avancement de la combustion déjà utilisé pour l'étude des gaz naissants.

Soit, pour le propergol de référence et en présence d'additif :

P = 6 bars	$\bar{X} = 0,208$	0,258	} 0,255
11 bars	0,214	0,252	
16 bars	0,216	0,283	} 0,2A1
21 bars	0,205	0,278	

$$\bar{X}_{\text{moyen}} = 0,211$$

et pour Heller et Gordon $\bar{X} = 0,2$.

Les résultats obtenus montrent bien un renforcement de la flamme primaire en présence d'additif. Ce renforcement semble agir plus sur la cinétique chimique du carbone que sur celle de l'azote. Le taux global d'hydrocarbures est un peu plus élevé en présence d'additif (10 → 13 %) et les proportions de CO et CO₂ sont modifiées, tandis que les taux de NO et de N₂ varient très peu d'un propergol à l'autre.

Les différences observées ne sont cependant pas très importantes. Ceci est probablement dû au choix du propergol chaud qui était imposé par la position de la sonde en fonction de la pression et par une production minimum de carbone déjà bien gênante au niveau de l'entrée de la sonde.

3 - COMBUSTION DE L'OCTOGÈNE

En raison de sa température de flamme particulièrement élevée, l'octogène permet d'améliorer les performances ($I_s \sim \sqrt{\frac{R T_c}{M}}$) des propergols solides homogènes, tout en conservant leur caractère discret.

La bibliographie fait apparaître de nombreux travaux concernant la détermination des constantes physico-chimiques et les mécanismes de décomposition [réf. 6 à 15]. Cependant, l'analyse des produits de décomposition, pourtant importante, y est bien souvent abordée de manière peu précise, entraînant quelquefois des interprétations des phénomènes totalement opposées [6-10-13-14-15-16-17].

La pyrolyse linéaire sous vide avec analyse par spectrométrie de masse assure les conditions de dégradation les plus proches de celles d'une combustion réelle et les plus propres à éviter les réactions chimiques, avant analyse, entre les espèces produites. Cela permet de préciser la composition chimique du mélange réactif mis en jeu dans la flamme.

3.1 - Principe

KUBOTA [13] a montré que l'octogène brûle avec une flamme étagée comme les propergols homogènes. Cependant, son épaisseur est si faible même à basse pression (P ≈ 1 bar) qu'il est exclu d'y réaliser un prélèvement. Au-delà de 10 bars, les deux flammes sont totalement confondues (il faut atteindre 300 bars avec les propergols homogènes pour obtenir ce résultat). Seuls les gaz de dégradation en phase condensée sont donc accessibles, leur caractère naissant étant défini et assuré de la même manière que dans l'étude précédente.

3.2 - Dispositif expérimental

Seule la pyrolyse par conduction peut être mise en oeuvre. Il est difficile, en effet, d'utiliser une source de rayonnement placée à l'intérieur ou à l'extérieur de l'enceinte laboratoire. Lors du passage du front thermique, une partie de l'octogène se vaporise et se recondense (sans décomposition : $P \approx 1$ mbar, T chute brutalement à 25°C) en une poudre blanche très fine sur toutes les parois froides, tapissant ainsi le miroir réfléchissant le rayonnement ou le hublot d'entrée. Cette fraction n'est donc finalement pas prélevée.

Le montage utilisé (pyrolyse par conduction) a été expérimenté pour l'étude des gaz naissants des propergols homogènes (figure 2). Il est inchangé. Seule la puissance de chauffage du ruban a dû être relevée pour obtenir la régression des échantillons. Les mêmes sondes de prélèvement et spectromètre de masse sont utilisés pour l'analyse des gaz.

3.3 - Spectre d'évaporation de l'octogène

L'évaporation partielle de l'octogène lors de la dégradation impose de s'assurer du spectre propre de cette molécule. Il est réalisé en introduisant directement un petit échantillon dans la chambre d'ionisation du spectromètre, à très basse pression (environ 10^{-8} mbar) et en élevant lentement la température à partir de 25°C (≈ 2 à 3°C/mn). Dans ces conditions, l'octogène s'évapore notablement et sans dégradation à partir de 170°C.

Le spectre inscrit au tableau 9 ci-après et représenté figure 4 est obtenu entre 190 et 230°C.

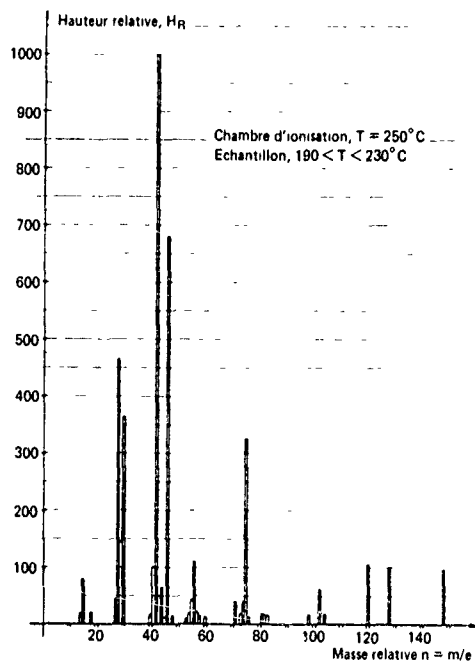


Fig. 4 - Spectre d'évaporation de l'octogène

Tableau 9

Spectre de masse de l'octogène évaporé

m/e:	42:	46:	2C:	30:	75:	29:	56:	120:	128:	41:	148:	15:	44:	102:	43:	27:	55:		
Hr:	1000:	681:	465:	363:	325:	144:	110:	105:	99:	99:	96:	78:	64:	61:	49:	45:	43:		
	71:	74:	57:	18:	73:	54:	14:	81:	104:	98:	40:	82:	83:	48:	58:	60:	76:	45:	53:
	40:	30:	22:	20:	19:	19:	18:	18:	17:	17:	17:	17:	15:	15:	14:	13:	12:	12:	11:

Ce résultat concorde très bien avec les travaux de Bulusu [19], Stals [20] et Volk et Schubert [21]. Ces auteurs ont obtenu une bonne similitude quant aux fragments obtenus, certains les ont même identifiés. Cependant, [20] ne donne pas vraiment le spectre et [19] a fait disparaître tous les fragments de masse relative $m/e < 30$.

3.4 - Analyse des gaz de dégradation

L'identification des espèces chimiques résultant de la dégradation est réalisée de la même manière que précédemment (2.1.3). L'octogène conduit ainsi aux espèces de dégradation suivantes :

NO_2 , N_2O , NO , N_2 , CO , CO_2 , HCN , H_2O , NH_3 , HCO_2H et HCHO .

Les conditions de production des gaz de pyrolyse de l'octogène sont les suivantes :

- la température de contact ruban-échantillon s'établit à 297 - 300°C. Elle est stable pendant toute la durée de l'expérience et notablement plus élevée que la température de fusion (276°C) ;
- la vitesse de régression est de 0,40 mm.s⁻¹ ;
- une fraction importante de l'échantillon est évaporée et recondensée sur les parois de l'enceinte et de la sonde (non prélevée : absence du pic à la masse relative 42 correspondant à un fragment important de la molécule d'octogène dont il serait caractéristique) ;
- la pression, de l'ordre de 10⁻² mbars au départ, s'élève à 1,5 mbar en cours de pyrolyse.

Le tableau 10 ci-dessous résume ces conditions et les données qu'il est possible d'en tirer à partir des relations établies en [2]...

Tableau 10

: Température de surface	300°C ou 570 K :
: Pression enceinte	10 ⁻² à 1,5 mbar :
: Vitesse de régression	0,4 cm.s ⁻¹ :
: Epaisseur chauffée :	$x_c = \frac{\alpha_p}{V_r} \left \ln \frac{1}{100} \right = 0,1 \text{ cm}$ soit 1000 μm :
(avec $\alpha_p \approx 10^{-3} \text{ cm}^2.\text{s}^{-1}$)	
: Temps de séjour dans la zone chauffée :	$T_c = \frac{x_c}{V_r} = 2,5 \text{ s}$:
($T_c < T < T_s$)	
: Ecart de température correspondant à l'épaisseur de réaction :	$\Delta T = \frac{T_s}{1 + \frac{E_p}{RT_s \ln 100}} = 51 \text{ K}$:
(avec $E_p \approx 53 \text{ kcal.mole}^{-1}$ [6])	
: Epaisseur de réaction :	$x_r = \frac{\alpha_p}{V_r} \ln \left(1 - \frac{\Delta T}{T_s - T_c} \right) = 0,0046 \text{ cm}$ soit 46 μm :
: Temps de séjour dans la zone de réaction :	$T_r = \frac{x_r}{V_r} = 0,12 \text{ s}$ soit 120 ms :
($T_s - \Delta T < T < T_s$)	

Toutes ces valeurs sont proches de celles obtenues pour les propergols homogènes. Cependant, la pyrolyse de l'octogène est réalisée à une température supérieure à celle du point de fusion, 276°C [22]. Il existe donc une zone fondue dont il n'est pas possible de déterminer l'épaisseur (l'échantillon est pressé contre le ruban chauffant).

Le tableau 11 et la figure 5 présentent le spectre moyen ainsi obtenu sur 4 expériences :

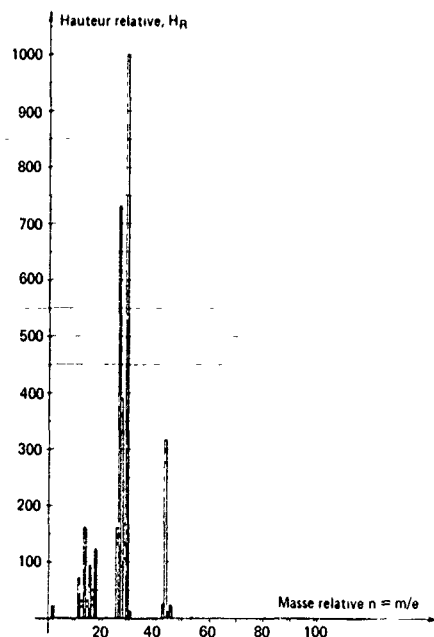


Fig. 5 - Spectre de pyrolyse de l'octogène.

Tableau 11

Spectre de masse des gaz
de pyrolyse de l'octogène

m/e :	30	27	28	44	29	14	26	18	16	:
Hr :	1000	706	361	297	137	159	144	100	88,9	:
	12	17	13	15	46	14	2	31	45	22
	60,7	34,7	24,5	23,7	18,9	18,8	16,9	8,6	6,3	0,6

La composition des gaz de dégradation obtenue est présentée au tableau 12. La première ligne de celui-ci donne une estimation de l'erreur commise sur chaque espèce en fonction de la reproductibilité de l'échantillon gazeux. Pour les autres espèces chimiques, NH₃, CO₂, HCOOH, N₂ et CO qui sont déduites du spectre dans de mauvaises conditions, il n'est pas possible de déterminer sérieusement l'erreur commise.

Tableau 12

Calcul de la composition du mélange de
gaz issu de la pyrolyse de l'octogène

Espèce	HCN	H ₂ O	H ₂	CO ₂	N ₂ O	HCOOH:NH ₃	NO ₂	HCHO	NO	N ₂	CO
chimique	27	18	2	44	44	46	17	46	30	30	28
Erreur %	+ 4	+ 20	+ 24	-	+ 8	-	-	+ 26	+ 23	+ 19	-
% fraction molaire	20,4	6,7	1,2	1,1	14,2	0,2	0,7	15,8	15,4	19,1	3,5
% fraction massique	16,8	3,7	0,1	1,4	19,1	0,2	0,3	22,2	14,1	17,5	3,0

A partir de cette composition, il est possible de recalculer le bilan élémentaire C.H.O.N, et l'on constate alors un bon accord avec la composition élémentaire d'origine.

Tableau 13

Bilans élémentaires

	B I L A N	C	H	O	N
octogène de départ		16,2	2,7	43,2	37,8
gaz analysés		14,2	2,1	44,6	39,0

3.5 - Discussion des résultats

Le caractère naissant des gaz est assuré par les conditions des expériences (température, pression, temps de séjour : tableau 10) et de l'analyse (SM). Si l'on reprend l'indice d'avancement de la combustion défini lors de l'étude des propérgols homogènes 2.1.4, il vient :

$$\alpha = \frac{\sum n X_{CO_2}}{\sum n X_i} = \frac{1,1}{20,4 + 1,1 + 0,2 + 15,4 + 1,9} = \frac{1,1}{39} = 0,03$$

(limité aux espèces chimiques carbonées)
(n nombre d'atomes de carbone contenu dans chacune)

Le caractère naissant des gaz apparaît également en établissant les sommes des espèces naissantes et finales :

- espèces réactives issues directement de la dégradation

HCN	}	67 %
H ₂		
N ₂ O		
NO ₂		
HCHO		

- espèces partiellement brûlées mais susceptibles de réagir encore :

NO	}	21,2 %
CO		
HCOOH		

La somme de ces espèces est faible par rapport à celles n'ayant pas du tout réagi.

- espèces de fin de combustion :

N ₂	}	11,3 %
CO ₂		
H ₂ O		

La somme de ces espèces est faible par rapport à la somme des deux autres catégories.

Bien que présentant des limites dues aux recouvrements de spectre de masse des gaz analysés, les résultats acquis apportent quelques précisions :

- ils montrent l'importance équivalente des ruptures initiales des liaisons R-N-NO₂ et R-N-NO₂ entraînant la formation simultanée de NO₂ et N₂O ;

- ils montrent que seule une analyse des gaz dans la zone inter-flamme pourrait apporter d'autres renseignements pour compléter les connaissances actuelles. Devant les difficultés du prélèvement à réaliser, on peut se demander si une telle expérience possède un réel intérêt, d'autant qu'à la pression réelle de fonctionnement (P < 100 bars), les deux flammes sont totalement confondues.

Les réactions chimiques en phase gazeuse seront plus complexes que dans le cas des propergols homogènes, du fait de la présence de trois oxydants et deux combustibles :

NO ₂	HCHO
N ₂ O	HCN
NO	et très peu de ()

Comme dans le cas des propergols homogènes, le NO peut provenir d'un début de réaction en phase condensée correspondant à un dégagement de chaleur qui rend la dégradation globalement exothermique.

La présence de N₂ dans les gaz de dégradation peut avoir une origine semblable : un début de réduction de N₂O.

Comparaison avec les résultats publiés [16] et [17]

Il est difficile de comparer complètement les résultats obtenus à l'ONERA avec ceux de Beyer [17]. Ce dernier donne un spectre des gaz de pyrolyse très incomplet. Cependant, il a travaillé dans des conditions très proches de celles décrites précédemment. Il a décelé la présence d'une quantité notable de NO₂, ce qui montre que la rupture de la liaison N - N se produit bien.

Il est plus facile de faire la comparaison avec les résultats de Suryanarayana et Graybush [16], mais ils ne précisent pas toutes les conditions de la dégradation. Il apparaît des différences importantes pour les espèces suivantes HCN, CO₂, N₂O et N₂ ; d'autre part, la présence de H₂O, H₂, HCOOH, NH₃ et NO₂ n'est pas détectée.

Le tableau 14 donne les compositions obtenues par les références citées et les résultats ONERA.

Tableau 14

	Suryanarayana et Graybush [16]	Beyer [17]	ONERA
Méthode d'analyse	Spectrométrie de masse Octogène	Spectrométrie de masse Octogène/P.U.	Spectrométrie de masse Octogène
Température (°C)	T < T _{fusion}		298 > T _{fusion} = 276
Pression	?	10 ⁻³ à 10 ⁻¹ mbars	10 ⁻² à 1,5 mbars
Vitesse de pyrolyse	?	Très grande	0,4 mm.s ⁻¹
Composés	Fraction molaire (%)	Spectre ?	Fraction molaire (%)
HCN	4,5 (100 % ¹⁴ N)	42	20,4
H ₂ O	0		6,7
H ₂	0		1,2
CO ₂	8,5		1,1
N ₂ O	40 (99 % ¹⁴ N- ¹⁵ N) (1 % ¹⁵ N- ¹⁴ N)	100	14,2
HCOOH	0		0,2
NH ₃	0		0,7
NO ₂	0	54	15,8
HCHO	22,9	39	15,4
NO	9,9 (100 % ¹⁴ N)	27	19,1
N ₂	9,6 (100 % ¹⁴ N- ¹⁵ N)		3,5
CO	4,1		1,9
TOTAL	99,5		

4 - CONCLUSION

Quoique les propergols homogènes soient un sujet d'étude assez ancien, leurs mécanismes de combustion et les mécanismes d'action des additifs permettant de créer des effets de plateau et de mesa présentaient encore d'importantes incertitudes ayant pour conséquence des interprétations très différentes des phénomènes.

Les résultats des analyses de gaz sont rassemblés sur la figure 6 ; elles ont apporté les éclaircissements suivants :

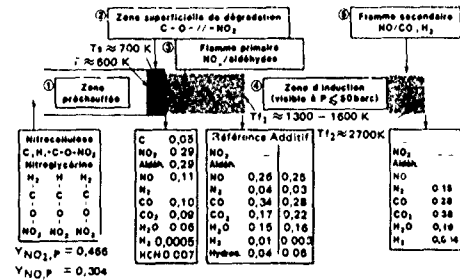


Fig. 6 - Résultats (Y_i) de la combustion d'un propergol homogène chaud (P.C. = 1100 cal.g⁻¹)

- sur les gaz produits par la dégradation en phase condensée :

L'analyse des gaz naissants est réalisée dans des conditions très proches de celles d'une combustion sous pression (réalisation de temps de séjour très courts). Cela permet la mise en évidence de NO₂ (Y_a ≈ 29%) dont la présence n'était antérieurement pas observée directement, d'aldéhydes HCHO (Y_a ≈ 17%) et de (CHO)₂ (Y_a ≈ 11,7%) et de résidus carbonés. La dégradation est donc bien initialisée par la rupture des liaisons CO - NO₂. Cette analyse montre aussi que des réactions NO₂-aldéhydes donnant NO, CO, CO₂, H₂O se produisent dès la phase condensée, rendant improbable le prélèvement de gaz totalement "naissants". La comparaison entre propergol de référence et avec additif montre que les additifs n'agissent pas au niveau de la phase condensée. Une étude thermogravimétrique de la stabilité des additifs montre que ceux-ci subissent la dégradation du propergol sans transformation notable.

- Au niveau des gaz résultant de la zone de flamme primaire :

L'analyse des gaz dans la zone d'induction montre que la flamme primaire est bien due essentiellement aux réactions chimiques entre NO₂ et les aldéhydes. Cependant, un début de réduction de NO s'y produit. Elle montre aussi que l'action des additifs a bien lieu à ce niveau de la combustion. Ils modifient les réactions de production et de consommation du carbone, conduisant à des gaz plus brûlés. Ces résultats sont confirmés par des expériences de simulation menées en parallèle (réaction NO₂/aldéhyde, d'où E_a = 5 kcal.mole⁻¹, réaction aldéhyde/additif → C, CO₂). La présence d'additif renforce donc la flamme primaire dont le flux de conduction vers la surface est plus intense et permet la naissance d'un effet de survitesse.

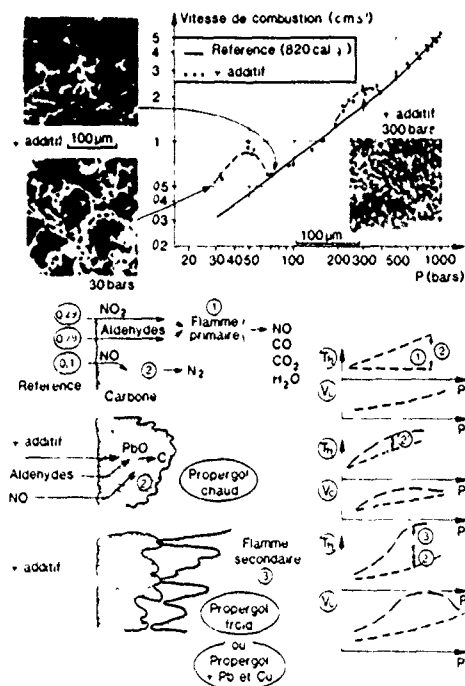


Fig 7 - Effets de survitesse

Le mécanisme proposé pour la première survitesse est présenté par la figure 7. L'effet de survitesse est lié à la présence d'une trame carbonée à la surface du propergol. Cette trame provient de réactions entre aldéhydes (issus de la phase condensée, en quantités d'autant plus importantes que le propergol est riche en nitrocellulose) et les résidus des sels de plomb. Cette trame a pour effet d'augmenter les réactions entre NO et carbone et, dans le cas où le résidu carboné est très important, de servir d'accroche flamme pour la flamme secondaire.

En outre, la surface d'échantillons, éteints brutalement par une dépressurisation rapide et examinés au microscope électronique à balayage, montre clairement la présence de la trame carbonée pendant la survitesse et sa disparition après le retour au niveau de la référence. Pour le propergol chaud, cette trame est beaucoup plus faible que pour le propergol froid, et de même pour l'effet de survitesse.

Pour expliquer la disparition de la trame carbonée, deux mécanismes peuvent être envisagés :

- 1) L'augmentation de la réactivité dans la flamme primaire induit des réactions entre les espèces chimiques et le carbone qui finit par se consommer plus vite qu'il ne se forme ; dans ces conditions, la survitesse disparaît progressivement (effet plateau) ;
- 2) Lorsque la trame est très importante, elle peut s'arracher brusquement de la surface, d'où un retour brutal de la vitesse au niveau de la référence (effet mesa).

L'efficacité de la technique de pyrolyse linéaire sous vide pour réaliser la dégradation rapide d'un matériau dans des conditions assurant le figeage des réactions entre les espèces chimiques produites a été démontrée par les résultats obtenus sur les propergols homogènes. Il a donc été possible d'envisager l'extension de ces expériences à des produits plus récemment introduits dans la fabrication des propergols solides : les nitramines, en particulier l'octogène.

Comme les propergols homogènes, l'octogène brûle avec une flamme étagée formée à partir des gaz de dégradation de la phase condensée. L'analyse de ces gaz a donc été réalisée. La composition obtenue est essentiellement caractérisée par la présence en abondance équivalente des oxydants NO_2 $\gamma = 22,2\%$ et N_2O $\gamma = 19,1\%$ et des combustibles HCHO $\gamma = 14,1\%$ et HCN $\gamma = 16,8\%$. La présence de NO $\gamma = 17,5\%$ et N_2 $\gamma = 3,0\%$ montre que des réactions se produisent aussi dès la phase condensée. Des investigations aux étapes intermédiaires de la combustion ne peuvent être menées de la même manière que pour les propergols homogènes : même aux basses pressions, la détermination du profil thermique montre que les différentes zones de flammes sont très serrées. Il est très difficile d'y glisser une sonde de prélèvement.

Des améliorations peuvent être apportées :

- à la technique de pyrolyse linéaire par rayonnement, en particulier par une augmentation des vitesses de pyrolyse, de manière à réduire encore les temps de séjour et à approcher au plus près des conditions réelles de combustion. Seule cette technique permettrait d'étudier les propergols froids plus intéressants : survitesse plus importante, résidus carbonés en plus grande quantité et dont le rôle paraît plus marqué. La pyrolyse par laser est peut-être une solution. Pour l'instant, elle présente des difficultés de mise au point. L'utilisation d'une source type corps noir très puissante est également possible, mais certainement plus lourde à mettre en oeuvre ;

- aux prélèvements dans la zone d'induction par une réduction des dimensions de la sonde pour pouvoir effectuer les prélèvements à pression plus élevée et donc étudier des survitesses plus importantes. Ceci est très difficile, en raison du rétrécissement de la zone d'induction en présence d'additif et de la présence de résidus carbonés. Il faudrait, en fait, utiliser une méthode d'analyse sans prélèvement.

REFERENCES BIBLIOGRAPHIQUES

- [1] G. Lengellé, J. Duterque, C. Verdier, A. Bizot and J.F. Trubert
Combustion mechanisms of double base solid propellants
17th Symposium (International) on Combustion, Leeds, 20-25th August 1978
- [2] G. Lengellé, A. Bizot, J. Duterque and J.F. Trubert
Steady-state burning of homogeneous propellants in fundamentals of solid propellant combustion
K.K. Kuo and M. Summerfield
Vol. 90 of Progress in Astronautics and Aeronautics, 1984.
- [3] C.A. Heller and A.S. Gordon
Structure of the gas phase combustion region of a solid double base propellant.
The Journal of Physical Chemistry vol. 59 nr 8, 1955.
- [4] J. Cobbo Ferreira
Analyse et modélisation de la combustion d'un propergol homogène et de l'action des additifs
Thèse de Docteur Ingénieur, Université de Poitiers, novembre 1982.
- [5] D.J. Hewkin, J.A. Hicks, J. Powling and H. Watts (E.R.D.E)
The combustion of nitric ester based propellants : ballistic modification by lead compounds
Combustion, Science and Technology, vol. 2, p. 307-327, 1971.
- [6] A.J.B. Robertson
The thermal decomposition of explosives
Trans. Faraday Soc. 45 (85-93), 1949.
- [7] J.J. Batten, D.C. Murdie
The thermal decomposition of nitramines at temperature below the melting point
Australian J. Chem. 23, 737-747, 1970.

- [8] M.W. Beckstead, R.L. Derr, C.F. Price
The combustion of solid monopropellants and composite propellants
13th Symp. (Int.) on Combustion 1047-1056, 1971.
- [9] T.J. Boggs, C.F. Price, D.E. Zurn, R.L. Derr, E.J. Dibble
Temperature sensitivity of deflagration rates of cyclotetramethylene tetranitramine (HMX)
13th JANAF Combustion meeting, 1976.
- [10] J.D. Cosgrove, A.J. Owen
The thermal decomposition of 1, 3, 5 trinitrohexahydro 1, 3, 5 triazine (RDX)
Combustion and Flame 22 (13-18 et 19-22), 1974.
- [11] J.N. Bradley, A.K. Butler, W.D. Capey, J.R. Gilbert
Mass spectrometry study of the thermal decomposition of 1, 3, 5 triazine (RDX)
J. Chem. Soc., Faraday Trans. 1, 73 (11) 1789-95, 1977.
- [12] M. Ben-Reuven, L.H. Cavany, R.J. Vichenevetsky, M. Summerfield
Flame zone and surface reaction model for deflagration RDX
16th Symp. (Int.) on Combustion, 1223-1233, 1976.
- [13] F.G. Rauch, A.J. Fanelli
The thermal decomposition kinetics of RDX above the melting point
J. Phys. Chem. 78, p. 1164, 1964.
- [14] A.E. Fogel'zang, B.S. Svet'lov, Y.Y. Adzhemyan, S.M. Kolyasov, O.I. Sergienko, S.M. Petrov
Combustion of explosives compounds with nitrogen-nitrogen bonds
Combustion explosions and shock waves vol. 12, nr 6, 1976.
- [15] J.J. Rocchio, A.A. Juhasz
HMX thermal decomposition chemistry and its relation to HMX composite propellant combustion
11th JANAF Combustion meeting, vol. 1, p. 247, 1974.
- [16] B. Suryanarayana, R.J. Graybush, J.R. Autera
Thermal degradation of secondary nitramines
Chemistry and Industry, vol. 12, p. 2177-2178, 1967.
- [17] R.A. Beyer
Molecular beam sampling mass spectrometry of high heating rate pyrolysis : description of data
acquisition system and pyrolysis of HMX in a polyurethane binder
U.S. N.T.I.S AD. A054328, 1978 (ARBRL-MR-02816 - AD-E-430016).
- [18] N. Kubota
Combustion mechanisms of nitramine composite propellants
18th Symp. (Int.) on Combustion, 187-194, 1981.
- [19] Bulusu (Suryanarayana), T. Axenrod, G.W.A. Milne
Electron impact fragmentation of some secondary aliphatic nitramine
Organic Mass Spectrometry, vol. 3, p. 13-21, 1970.
- [20] J. Stals
Chemistry of aliphatic unconjugated nitramines - Part 7
Trans. Faraday Soc. 67, p. 1768, 1971.
- [21] F. Volk, H. Schubert
Massen spektrometrische untersuchungen von explosivstoffen
Explosivstoffe 1/1968, p. 2-10
- [22] S.F. Sarner
Propellant Chemistry, 1966

Ces travaux ont été effectués en partie sous contrats de la DRET (Direction des Recherches, Etudes et Techniques, Délégation Générale de l'Armement) et de la SNPE (Société Nationale des Poudres et Explosifs).

MEASUREMENTS OF DISTRIBUTED COMBUSTION*

by

M.W. Beckstead, P.C. Braithwaite†, and D.L. Gordon**
 Brigham Young University
 Chemical Engineering Dept
 350 Clyde Building
 Provo, Utah 84602, USA

ABSTRACT

Acoustic suppressants are commonly added to low smoke and smokeless propellants to avoid the problem of combustion instability. Although some suppressants are considered to be inert, most actually react with the combustion products. If a particle reacts while traversing a relatively large portion of the system, the interchange of energy between the burning particle and the acoustic environment can result in either a driving or damping contribution to the acoustics of the system, which is referred to as distributed combustion. Instead of using actual solid propellants, an experimental technique was developed to study this mechanism utilizing a gas-fired Rijke burner. Advantages of this approach allow testing an additive independent of the propellant burning surface, avoiding the use of solid propellants, and allowing for independent control of frequency, O/F ratio, temperature, and particle addition.

Al and ZrC are additives commonly used in solid propellants to suppress combustion instability. Experimental results obtained using Al and ZrC in the Rijke burner indicate that both additives cause an increase in the acoustic growth rate when compared to growth rates obtained without any particles in the system. The increase caused by Al is significantly greater than that caused by ZrC, which is expected because the reaction of Al releases more than twice the energy ZrC does. The increase in the acoustic growth rate due to distributed combustion was found to be directly related to the heat of reaction.

INTRODUCTION & BACKGROUND

Various ingredients are routinely added to solid propellants for the purpose of suppressing acoustic combustion instability. However, the basis for selecting the type, size and concentration of particle is not well founded. Furthermore, additives that seem to work in T-burners do not necessarily work in motors and an additive that works in one motor does not necessarily work in a different motor (1). Additives also appear to be frequency dependent, working in one frequency range but not another (1). The confusion and disarray of knowledge on the subject clearly indicates that an in-depth study is warranted.

During the 1970's when T-burners were being adapted to measure the characteristics of metallized propellants, there were several experimental results that were never totally resolved (see for example References 2, 3 and associated articles). For example, at identical test conditions the variable area T-burner usually gave significantly different particle damping values than did the end burning, pulsed T-burner. Also, the velocity coupled T-burner gave significantly different results than an end vented burner with the same propellant and at identical test conditions (4). One reason for the observed differences could be that aluminum agglomeration occurs differently in the different configurations. A second reason could be the effects of distributed combustion. In an end burning configuration, the particle residence time is relatively long and the aluminum is most likely to burn relatively close to the propellant surface. On the other hand, for side burning configurations with larger areas, residence times will definitely be shorter, and it is more likely that the aluminum will burn throughout a significant length of the burner, possibly leaving the burner incompletely oxidized. Calculations (5) have shown that this is highly probable, and are shown in Figure 1. The figure shows that for the specified conditions, and for a propellant area ratio of 6 or greater, aluminum agglomerates of 80 μm or greater will not burn completely before leaving the burner. This means that the aluminum agglomerate will be burning throughout the cavity, interacting with the acoustic wave, which is in effect, distributed combustion.

The process of distributed combustion has generally been ignored in acoustic analyses of rocket motors in the past. It is usually assumed that the particle additive (usually Al), burns close enough to the propellant surface to be treated as a boundary condition.

Acoustic suppressants have also been added to low smoke and smokeless propellants for the past decade. For many years aluminum was a panacea for combustion instability. However, as the motivation to eliminate smoke in rocket exhausts increased, aluminum began to be eliminated from propellant formulations. In an attempt to avoid combustion instability, other ingredients were sought that would act as acoustic suppressants.

*This work was performed under contract AFOSR 83-0157 with Dr. Leonard Caveny as program manager.

†Current address: Morton-Thiokol, Wasatch Division, Brigham City, Utah.

**Current address: IRECO Incorporated, Salt Lake City, Utah.

In an attempt to understand the mechanistic action of acoustic suppressants, various possible mechanisms will now be considered and discussed. There appear to be three predominant mechanisms whereby additives can influence or suppress an acoustic wave:

- (1) Viscous energy dissipation due to particle drag (i.e. the classical particle damping).
- (2) Modification of the combustion response function due to interaction of the additive with the burning surface. (This could be suppressive or additive).
- (3) Distributed energy release of a reacting additive interacting with the acoustic wave (this also could either suppress or drive an acoustic wave).

Particle Damping

Particle damping due to viscous drag is a well-established phenomenon. Tempkin and Dobbins (6) and Carhart and Epstein (7) established the theoretical basis for particle damping, verifying the theory by measuring the damping of aerosols on acoustic waves (6,8) (see also reference 9). The equations derived by Epstein and Carhart were simplified by Tempkin and Dobbins, although the basic theory was not altered. The work of Tempkin and Dobbins was later modified slightly by Culick (10) who arrived at the following equation:

$$\alpha_D = -1/2 \frac{C_m}{(1 + C_m)} \sum_i \left(\frac{\omega^2 \tau_i}{1 + \omega^2 \tau_i} \right) X_i \quad (1)$$

where α is the acoustic damping coefficient in sec^{-1} , ω is the angular frequency, C_p is the mass fraction of particulate matter, X_i is the mass fraction of particulate matter with diameter D_i , and τ_i is the viscous relaxation time, $\rho D_i^2 / 18\mu$. This equation shows that the damping provided by a given particle is primarily dependent on the particle diameter and the frequency of oscillation. However, it is also a function of the particle concentration, particle density and the viscosity of the gas.

More recently, workers at NWC (11,12,13) have performed a series of experiments using various burners with propellants containing well characterized particles. Their measurements before, during and after combustion compare extremely well with their corresponding calculations, verifying quantitatively particulate damping theory in a combustion environment. They used an end burning T-burner which results in relatively large residence times for the particles, minimizing any effects of distributed combustion. In such a system, low flow rates and large residence times, cause the aluminum to burn completely to aluminum oxide close to the burning surface.

In the work reported by Derr (12) two different types of propellant were used, one containing 5% aluminum oxide and the other containing 10% aluminum oxide (all other ingredients were identical). In each case the initial particle size distribution of aluminum oxide was identical, and each of the propellants were tested at three different frequencies, 280, 700, and 1800 Hz. After burning the propellant, the particles were collected and analyzed. The measured particle size distribution was then used to calculate the theoretical damping. Kraeutle et al. (11) extended the work by varying the particle size distribution while holding the amount of aluminum oxide in each propellant constant. Agreement between the experimental results and the theoretical predictions is shown in Figure 2.

Apparent discrepancies exist between the NWC particle damping results and motor data where conflicting results have been observed based on particle damping theory. Particles do cause a certain amount of damping, but obviously they do not always provide sufficient damping to completely stabilize some motors. The lack of a totally stable motor can be erroneously interpreted as a total absence of particle damping. It is readily apparent from equation (1) that particle damping is a very strong function of both frequency and particle diameter. Thus, it is not surprising that a particle that damps well at one frequency may not damp well at a different frequency. For example, at 300 Hz and 1% concentration, a 12 μm particle provides 4 sec^{-1} of damping, whereas a 2 μm particle provides negligible damping. At 30,000 Hz and 1% concentration, the 2 μm particle provides 320 sec^{-1} damping compared to the 12 μm particle's 10 sec^{-1} of damping.

Although particle damping can be considered a well-established phenomenon, predictions of motor results based on particle damping theory alone are very often disappointing. Cases have occurred in both motor and T-burners where suppressant particle size or type has been changed based on particle damping theory only to result in worse oscillations (1). If a theory cannot correctly predict experimental results, how can the theory be considered to be quantitatively correct? It can, if there are several mechanisms competing with each other! It appears that experimental observations often referred to as "particle damping" are actually the result of several combined mechanisms including particle damping, distributed combustion, and possibly surface response modification.

Surface Response Modification

Solid particles added to a propellant for particulate damping can have a catalytic influence on the propellant combustion, modifying the transient combustion response.

The best documented example of this is probably Al_2O_3 (14). Al_2O_3 is the particulate product of aluminum combustion and has been added to propellants as an "inert" to study and verify particle damping (11,13). However, Al_2O_3 is also a weak burn rate catalyst used to increase the burn rate of composite propellants (14). Similar metallic oxides are also known to have catalytic effects on propellant combustion. If an additive influences the steady burning of a propellant, it would also be expected to influence the transient response of the propellant also. Therefore, additives such as Al_2O_3 can be expected to cause or change the measured response of a propellant. Crump (14) found this to be the case with Al_2O_3 in composite propellants.

Particle size is also an important factor. Finer particles normally exhibit greater catalytic effect on the steady state burn rate than coarser particles due to the relatively large available specific surface area for a given volume or weight of additive. The same trend should be expected with the transient combustion. Furthermore, such an effect might also be expected to be frequency dependent due to the very short characteristic times of fine particles compared to coarse particles. Therefore, the effect of an additive such as Al_2O_3 should be expected to be dependent on the particle size as well as on the test frequency. This is an area where little is known and future research is needed to clarify the effect of additives on the propellant response function.

Variable Energy Release (Distributed Combustion)

When ZrC was first added to propellants it was considered to be an "inert" additive. However, ZrO_2 was found in nozzle entrance areas, and thermochemical calculations show that oxidation of the ZrC is to be expected. Aluminum is also known to react relatively far from the burning propellant surface for certain test conditions. In reference 5 a model was developed to calculate the effect of distributed combustion on viscous particle damping of an acoustic wave. The model accounted for the changing particle size of burning aluminum for both original aluminum particles and agglomerated aluminum. The unagglomerated aluminum was assumed to burn directly to oxide smoke while the agglomerates were assumed to form both oxide smoke and a surface oxide, ultimately forming oxide caps of a specified size. The calculations were compared to variable area T-burner data for a typical aluminized composite propellant. The calculated results show that significant amounts of the metal can leave the burner unburned, causing a change in damping for changing residence time. The results, shown in Figure 3, invalidate the usual assumption that particle damping is independent of propellant area ratio. The calculated particle damping changed by a factor of two over the typical range of conditions used in variable area T-burners. Thus, it can be anticipated that variable area T-burners and end burning, pulsed T-burners should measure different particle damping values as observed. For actual motors, the anticipated damping could also be significantly different from what would be calculated based on T-burner data.

The Rijke Burner

The complex environment inside a burning fullscale rocket motor is a very difficult (and expensive) place to obtain experimental data. As a result different devices have been used to simulate the acoustic environment created inside a rocket. Most of these devices have been some form of T-burner, but some other devices have also been used. The Rijke burner used in the present study, see Figure 4, is a gas burner with a cylindrical body and a flameholder, usually a wire screen, placed in the lower half of the tube. As the gases burn, longitudinal model acoustic oscillations are generated. Rayleigh (14) offered the first correct explanation of the origin of the oscillations present in a Rijke tube (the Rijke tube differs from the Rijke burner in that the Rijke tube utilizes natural convection without combustion while the Rijke burner utilizes forced convection and combustion). He stated that for the oscillations to be sustained, heat must be added to the gas at the moment of greatest compression or taken away at the point of greatest expansion.

Although the T-burner has been widely used to study unstable propellant combustion there are several advantages to using a Rijke burner for studying additives. First, because the Rijke burner does not use solid propellant, an additive can be tested independently of the propellant burning, allowing the study of the effects of distributed combustion without interference due to possible modification of the burning surface response. Second, the system can easily be tested with or without particles, thus evaluating system effects which is very difficult to do in a T-burner. Third, a high pressure environment is required to burn solid rocket propellant efficiently while the Rijke burner can operate at atmospheric pressure. This makes it easier to observe the behavior of an additive in the Rijke burner as well as reducing operating costs significantly. Finally, various types of particles (reactive or inert) can be tested under identical conditions to better identify actual mechanistic action.

Diederichsen (16) has also used the Rijke burner to study acoustic suppressants. The majority of his work was concerned with the characterization of the burner without particles; however, he did test a small number of additives. Diederichsen ranked the additives he tested in order of increasing effectiveness as follows: aluminum flake, atomized aluminum, titanium dioxide, magnesium oxide and asbestos powder, magnesium, aluminum oxide, and silica ('Microsil'). Unfortunately due to limitations within his experimental system he was only able to obtain qualitative results (ie. limiting pressure amplitude rather than growth rates). Also, he did not document the sizes of

the additives used which would have been very useful in evaluating the suppressants from a theoretical basis.

The Rijke burner used in the current work is shown in Figure 4. It burns a mixture of propane, oxygen and nitrogen and is water cooled. Optical quality quartz tubes of varying length are placed on top of the burner and the flame is stabilized on a 20 mesh stainless steel screen. The burner frequency is varied by varying the length of quartz tubing and adjusting the length of the lower section. Gas flowrates to the burner are controlled with precision rotometers. A fluidized bed particle feeder which is suspended from an electronic balance is currently used to determine the continuous flowrate of particles into the burner.

As the gases burn, acoustic oscillations of variable amplitude develop in the Rijke burner. To control (start and stop) the oscillations and obtain the growth rate of these oscillations, a paddle was developed which slides across the top of the quartz tube changing the acoustic velocity boundary condition shutting off the oscillations. It then is withdrawn back to its initial location allowing the oscillations to grow to their steady state value. The oscillations are monitored with high frequency pressure transducers, the transducer output is amplified and then recorded on a high speed oscillograph. To ensure the efficient collection of data both the paddle and oscillograph are controlled by a micro-computer.

Extensive testing was performed to characterize the burner and determine optimum test conditions for the study. Temperature profiles were measured for each of the particle types as well as for the gas only condition. Data were taken with 1/32 inch (0.79 mm) sheath diameter type K thermocouples (Chromel-Alumel). The measured profiles are shown in Figure 5. Although the equilibrium flame temperature is approximately 2500 K, the measured temperatures are generally much lower throughout the burner. This is due in part to the fact that the thermocouple nearest the flame was located in the water cooled section of the burner and as a result produced low temperature readings. Despite the qualitative nature of the measured temperature profiles, it is important to note that the temperatures in the Rijke burner are higher when aluminum and zirconium carbide are present than when no particles have been added to the system. This is apparently a result of the energy added to the system when the aluminum or zirconium carbide particles burn. A second very important observation is that the gas temperatures are very low indicating significant heat losses through the Rijke burner. This indicates that the usual assumption of the gas temperature being constant throughout the length of the burner is not accurate.

Results and Discussion

To study the effects of distributed combustion in an acoustic environment Al and ZrC were added to the Rijke burner in varying amounts. Acoustic growth rate and limiting pressure amplitude measurements were made for each test case and were used to evaluate the effect of distributed combustion and particle damping. A sample acoustic growth curve for a test involving Al is shown in Figure 5. A major difficulty in determining growth rates when Al or ZrC are added is that oscillations grow so quickly in the Rijke burner that the number of data points in the linear portion of the growth curve is limited. Data were obtained with each additive varying the weight percent of the additive. Figure 7 shows that both particle additives caused the acoustic growth rates to increase significantly over the baseline case without particles. In both cases the acoustic growth rates increased as the mass loading increased, and as expected the growth rates for tests using Al were higher than those using ZrC.

The reactions of Al and ZrC are:



On a weight basis the heats of reaction for Al and ZrC are -7.4 Kcal/gm Al and -3.1 Kcal/gm ZrC respectively.

The rate of reaction cannot be calculated a priori but it can be anticipated qualitatively. Aluminum burns by first melting and vaporizing. Then the oxidizing medium and Al vapor diffuse together to react at a location above the particle surface. ZrC has a much higher melting and boiling point, such that it is more likely to react in the solid phase without melting. The oxidizer must diffuse to the surface of the solid ZrC and react heterogeneously which is usually a slower process than a vapor phase reaction. Also, the heterogeneous reaction will most likely be diffusion limited and therefore would be independent of pressure. Therefore, it is probable that Al reacts more rapidly than ZrC. Because Al probably reacts more rapidly and its reaction releases more than twice the energy of the ZrC reaction, Al is expected to have a greater influence on the acoustics of the system than ZrC.

Assuming that the increase in the acoustic growth rate is directly related to the heat of reaction, it should be possible to divide the acoustic growth rate by the appropriate heat of reaction and arrive at a normalized acoustic growth rate which should be a direct measure of distributed combustion. To determine the acoustic growth rate due to distributed combustion the average acoustic growth rate (33) sec^{-1} of the baseline case was subtracted from the growth rates obtained with Al and ZrC present. (Note that this procedure neglects any catalytic effects which may occur due to the

particles). The results of these calculations are shown in Figure 8 for the 7 μm ZrC and 13 μm Al. While some of the normalized growth rates for the ZrC appear slightly higher than those for Al, within the data scatter the two sets of data are equivalent, indicating that the amount of energy release is the primary mechanism leading to the distributed combustion.

In addition to the acoustic growth rates, the limiting pressure amplitude was measured for each test. The limiting pressure amplitude is determined by the non-linear damping within the system and should indicate which non-linear mechanism is dominant. The calculated linear particle damping due to 13 μm Al or 7 μm ZrC used in the experiments is $\sim 40 \text{ sec}^{-1}$ at 8% loading, the differences in particle sizes and densities compensating for each other. The damping value is very small when compared to the acoustic growth rates measured in the Rijke burner, but is virtually identical for the two different particles. If the limiting amplitude is determined by the non-linearities of the particle damping, then the limiting pressure amplitude for the two cases would be expected to be similar because of the similarity in particle characteristics and calculated linear particle damping. If the limiting amplitude is determined by the non-linearities of the combustion, then the measured amplitudes for the two additives would be expected to be different, perhaps proportional to the heat of reaction. Figure 9 shows that for both types of particles the limiting amplitude decreased as the mass loading increased, and as expected the actual amplitude for the two cases for a given mass loadings was virtually the same. Because of the similarities in the limiting amplitudes, one might expect the non-linear particle damping to be the dominant non-linear mechanism present rather than non-linearities associated with the combustion.

CONCLUSIONS

An initial study of two acoustic suppressants commonly used in solid rocket propellants has been performed. A Rijke burner was used to create an acoustic environment which is similar to that found in a solid propellant rocket motor. Because the Rijke burner does not use solid propellant, it was possible to study the effect of the additives without the catalytic influence the additive might have on the propellant response function. An increase in the acoustic growth rate was observed when Al and ZrC were each added to the system. This increase was apparently the result of energy being added to the system by the distributed combustion of the additive particles. It also appears that the increase in the acoustic growth rate due to distributed combustion is directly related to the heat of reaction of a given particle, as shown in Figure 8. This being the case, the larger the heat of reaction a given acoustic suppressant has, the more significant effect it is likely to have on the acoustics of the system. It is believed that this work represents the first quantitative study of the mechanism of distributed combustion in an acoustic environment.

REFERENCES

1. Condon, J. A., personal communication, Hercules, ABL, Cumberland, MD, 1980.
2. Derr, R.L., Price, C.F., and Culick, F.E.C., "Analysis of T-Burner Data Obtained by AFRPL Workshop Participants for a Metallized Propellant (ANB-3066)," 9th JANNAF Combustion Meeting, Vol 1, (Dec. 1972), p 299.
3. Beckstead, M.W., "An Overview of the Status of the T-Burner as a Combustion Stability Evaluation Tool for Metallized Propellants, 9th JANNAF Combustion Meeting, Vol 1, (Dec 1972), p 267.
4. Michell, P.L., "Status of Velocity Coupling," 13th JANNAF Combustion Meeting, Vol II, Dec. 1976, CPIA No. 281, pp 71-94.
5. Beckstead, M.W., Richards, R.S., and Brewster, B.S. "Distributed Combustion Effects on Particle Damping," AIAA J., Vol 22, No. 3, March 1984 pp 383.
6. Temkin, S. and Dobbins, R.A. "Attenuation and Dispersion of Sound by Particulate-Relaxation Processes" J. Acoust. Soc. Amer., Vol. 40, No. 2 (1966) pp 317-324.
7. Epstein, P.S. and Carhart, R.R. "The Absorption of Sound in Suspensions and Emulsions, 1. Water Fog in Air" J. Acoust. Soc. Amer., Vol. 25, No. 3, (May 1953), pp 553-556.
8. Dobbins, R.A., and Temkin, S., "Measurements of Particulate Acoustic Attenuation," AIAA Journal, Vol. 2, No. 6, (June 1964).
9. Zink, J.W., and Delasso, L.P., "Attenuation and Dispersion of Sound by Solid Particles Suspended in a Gas," J. Acoust. Soc. Amer., Vol. 30, No. 8, (Aug. 1958).
10. Culick, F.E.C., "T-Burner Testing of Metallized Solid Propellants," AFRPL-TR-74-28, AFRPL, Edwards, CA, (Oct. 1974).
11. Kraeutle, K.J., Derr, R.L., Mathes, H.B., and Dehority, G.L., "Combustion Instability Studies Using Metallized Solid Propellants: Additional Experimental Evidence for the Validity of Particle Damping Theory," 13th JANNAF Combustion Meeting, Vol. II, CPIA Pub. No. 281, Dec. 1976, pp 155-166.

12. Derr, R.L., Kraeutle, K.J., Mathes, H. B., and Dehority, G.L., "Combustion Instability Studies Using Metallized Solid Propellants: Part I, Experimental Verification of Particle Damping Theory" 12th JANNAF Combustion Meeting, CPIA Pub. No 273, Vol. II, Dec. 1975, pp 155-165.
13. Krautle, K.J., Mathes, H.B., and Derr, R.L., "The Role of Particulate Damping in the Control of Combustion Instability by Aluminum Combustion," AGARD Conference Proceedings No. 259, Solid Rocket Motor Technology, p 15-1.
14. Crump, J.E., "Combustion Instability in Minimum Smoke Propellants, Part 1. Experimental Techniques and Results," NWC TP 5936, Nov. 1977.
15. Rayleigh, J.W.S., "The Explanation of Certain Acoustical Phenomena," Nature, Vol. 18, (1878).
16. Diederichsen, J., "A Singing Flame as a Tool for Evaluation of Damping Agents for Solid Propellant Rocket Motors," Combustion and Flame, Vol. 7, (Mar. 1963).

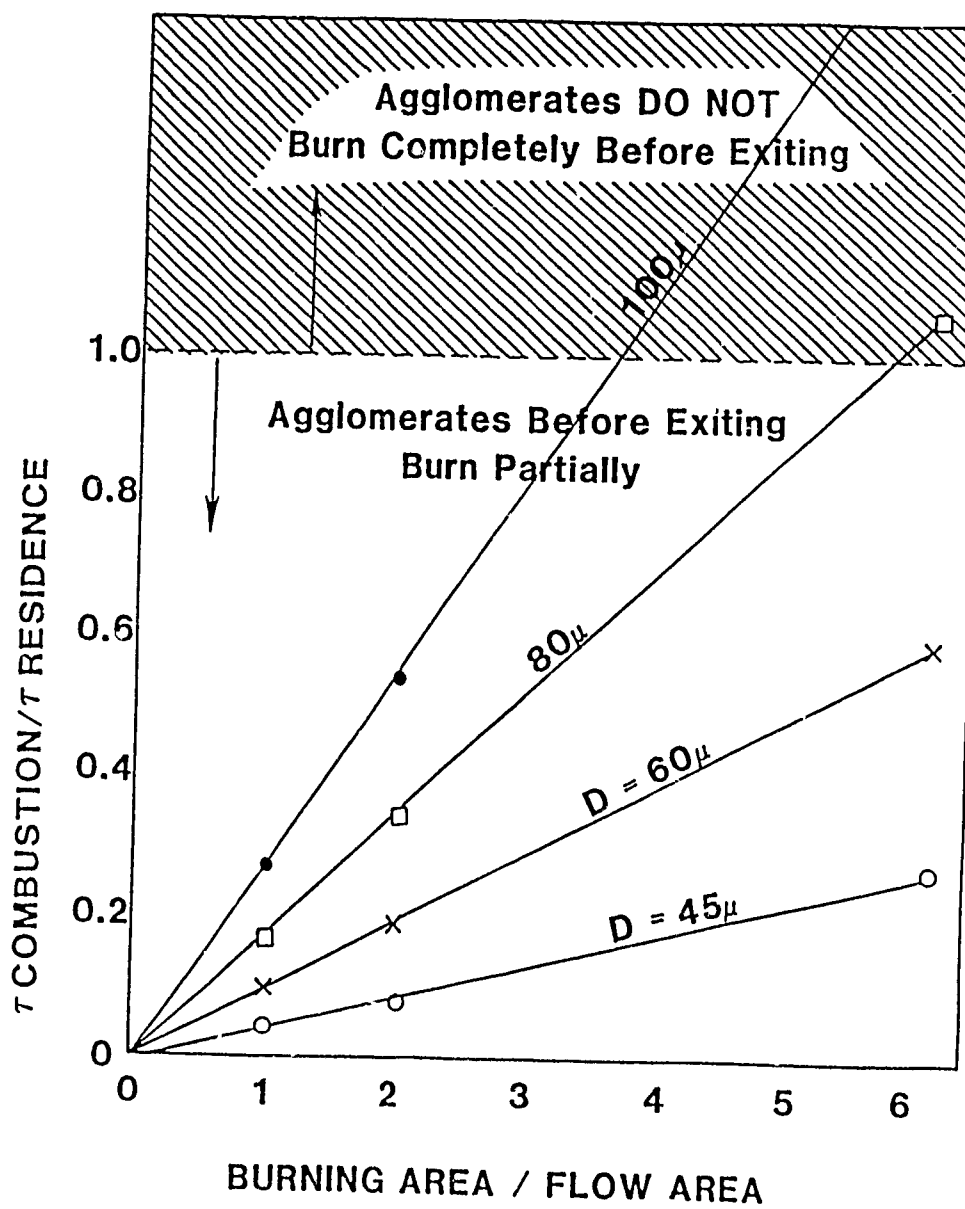


FIGURE 1. COMPARISON OF ALUMINUM AGGLOMERATE COMBUSTION AND RESIDENCE TIMES FOR AN 800 Hz BURNER / τ 3.4 MPa (500 PSI) AND 0.81 CM/SEC (0.32 IN/SEC) VARYING THE RELATIVE AMOUNT OF PROPELLANT.

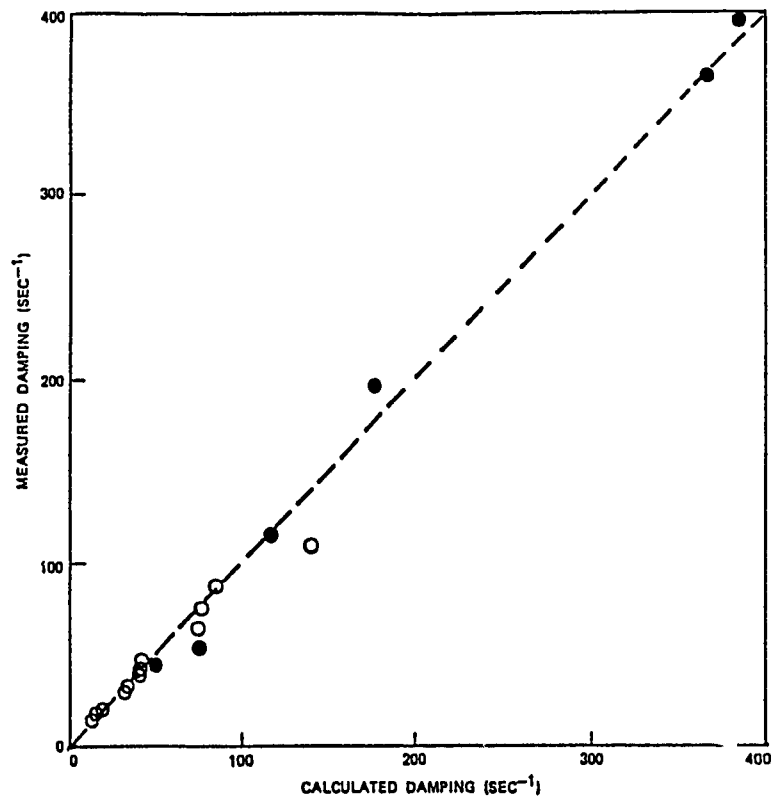


FIGURE 2: Measured Versus Calculated Damping for Aluminized Propellants A and B (●) and for Propellants C, D, E, and F Which Were Loaded With Aluminum Oxide Particles (○).

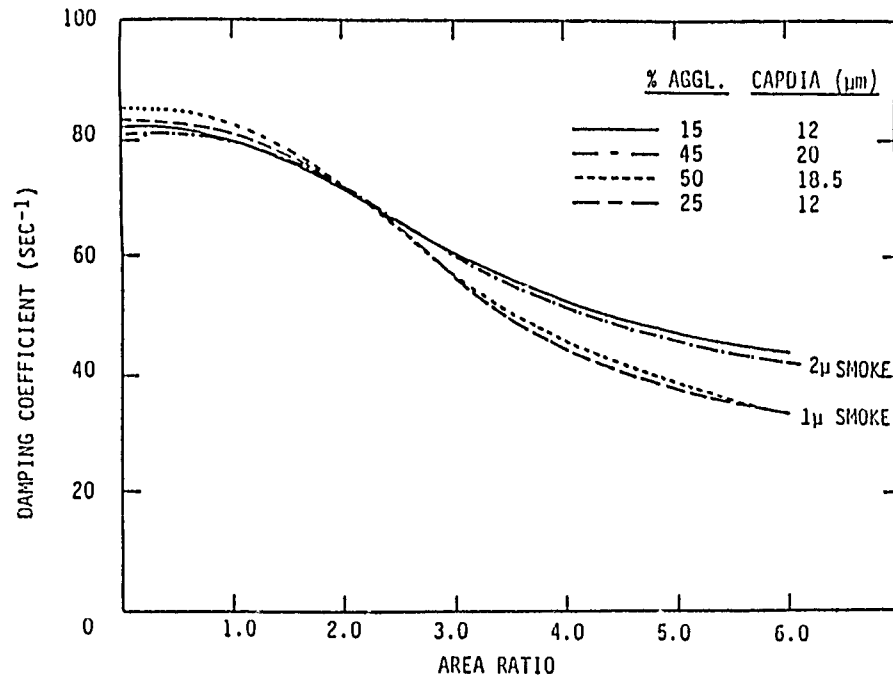


FIGURE 3: CALCULATED DAMPING VERSUS AREA RATIO FOR 800 Hz TEST CONDITIONS.

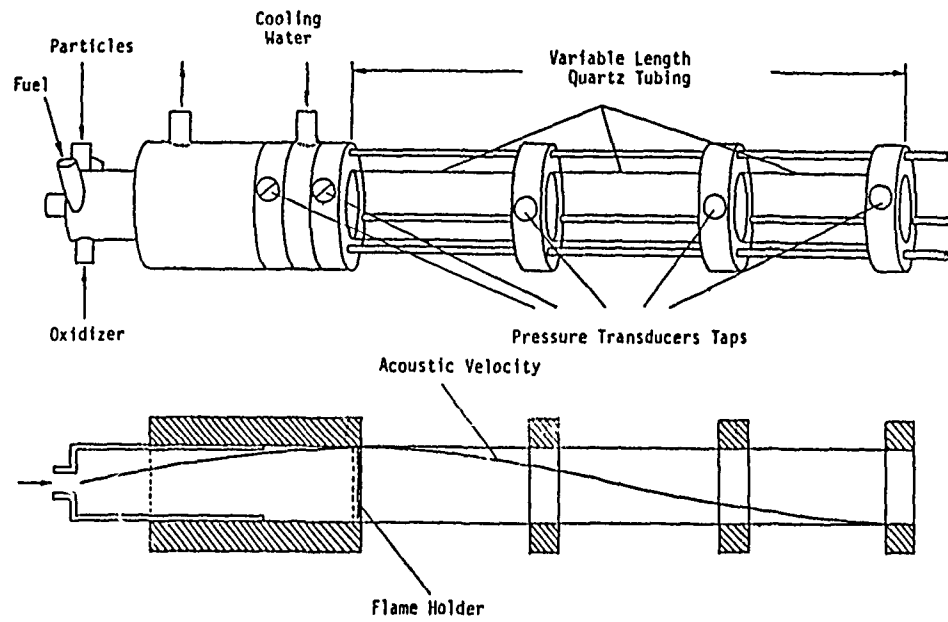


Figure 4. Sketch of Rijke tube burner used.

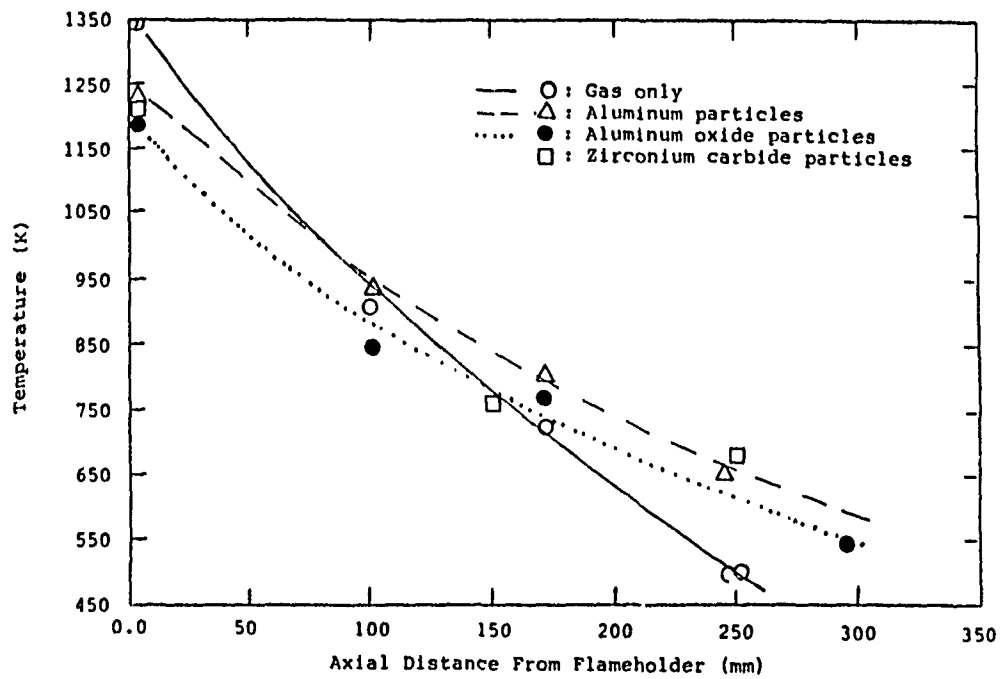


Figure 5. Temperature distribution in the Rijke burner with and without particle additives present.

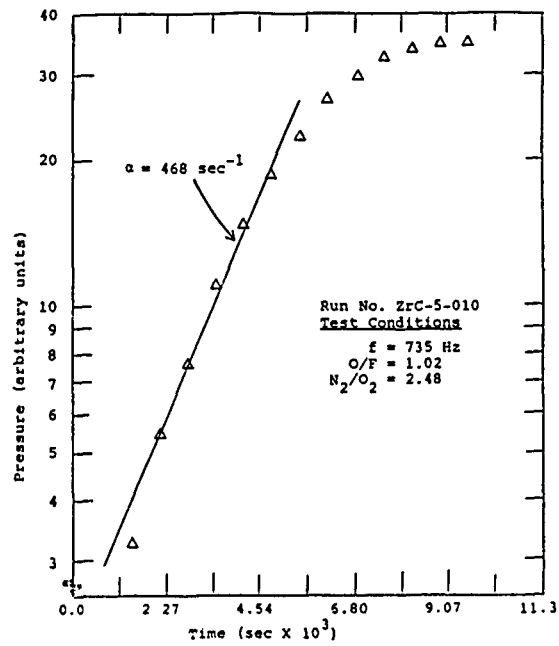


Figure 6. Growth of pressure oscillations in the Rijke burner with zirconium carbide particles present.

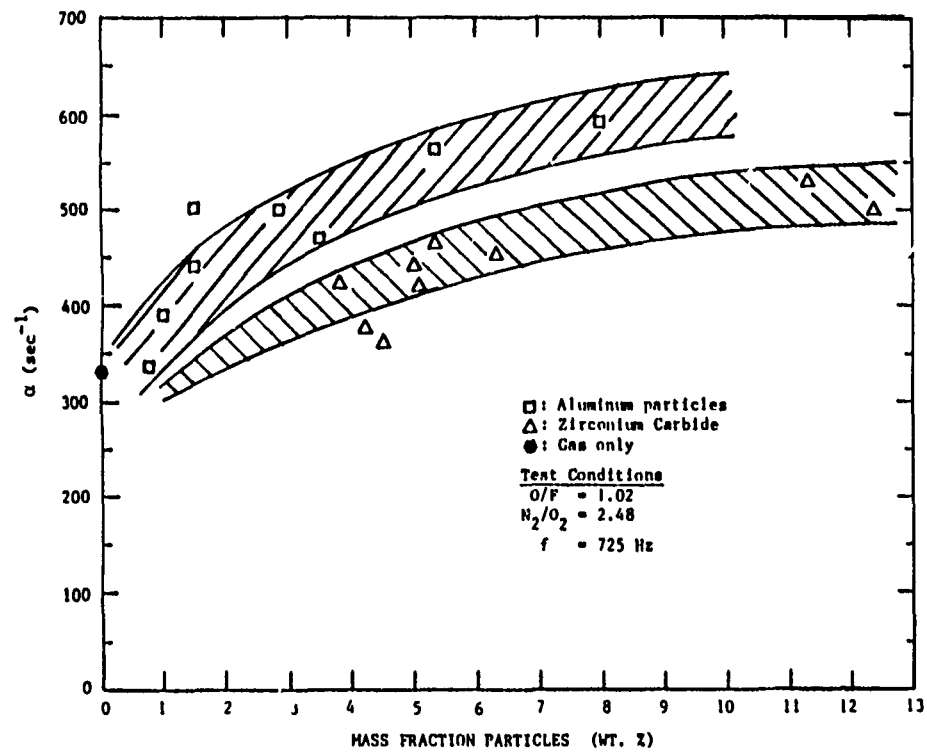


Figure 7. Acoustic growth rate (α) in the Rijke burner vs. mass fraction aluminum and zirconium carbide.

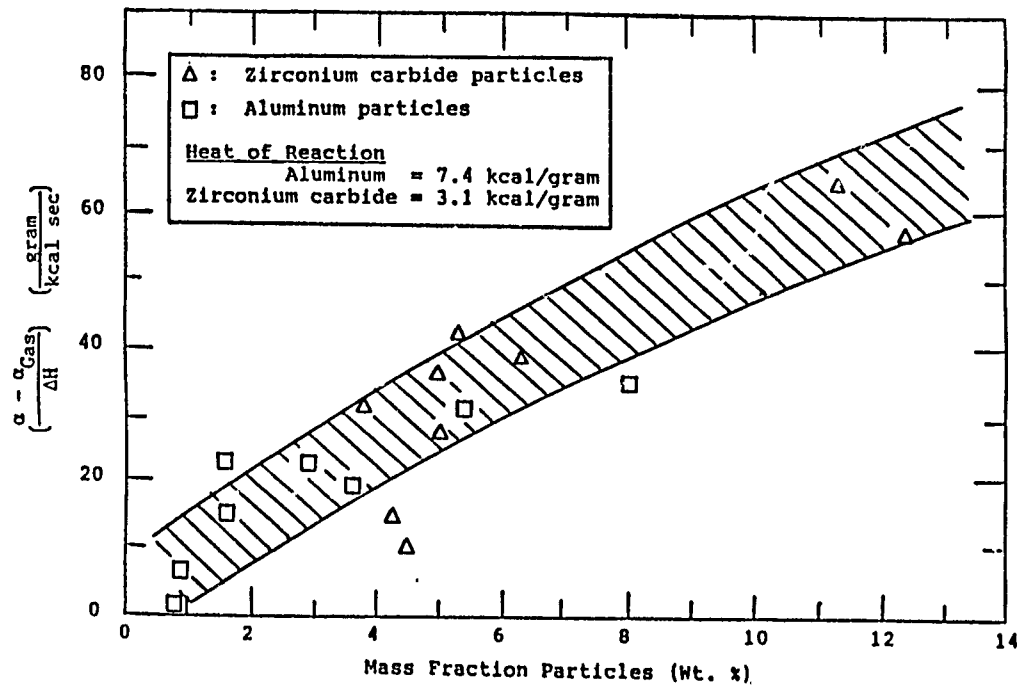


Figure 8. "Pseudo" acoustic growth rate vs. mass fraction of 13 micron aluminum and 7 micron zirconium carbide (mass mean diameter).

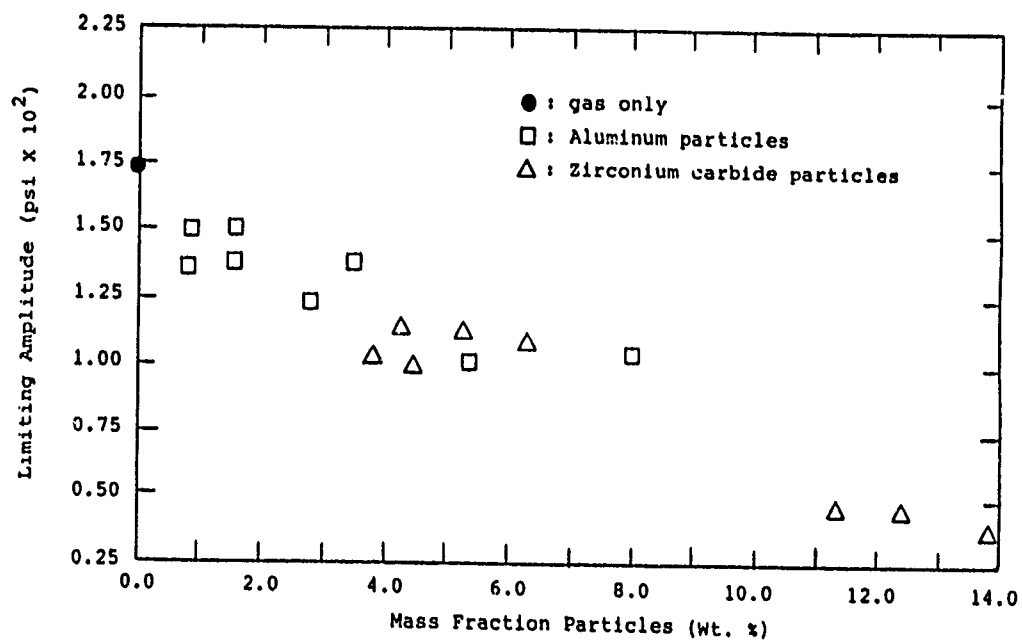


Figure 9. Limiting pressure amplitude vs. mass fraction aluminum and zirconium carbide in the Rijke burner.

DISCUSSION

P.Ramette, FR

How do you explain that on Fig. 5 of your paper the addition of AL, AL_2O_3 or ZrC leads to a reduction of temperature immediately behind the flame holder? The difference in the case of AL_2O_3 amounting to 160°K.

Author's Reply

The reduction in flame temperature is probably due to two reasons. Primarily, the particles before they ignite reduce the temperature near the flame holder. As the particles ignite and burn downstream of the flame holder then the temperature should rise, relative to the 'gas only' condition. This is in fact the observed behaviour.

The second and less important reason is data scatter. However this scatter should be random but with all three particles the temperature was reduced. Therefore this second reason is less plausible than the first.

REPORT DOCUMENTATION PAGE			
1. Recipient's Reference	2. Originator's Reference	3. Further Reference	4. Security Classification of Document
	AGARD-CP-391	ISBN 92-835-0387-2	UNCLASSIFIED
5. Originator	Advisory Group for Aerospace Research and Development North Atlantic Treaty Organization 7 rue Anceite, 92200 Neuilly sur Seine, France		
6. Title	SMOKELESS PROPELLANTS		
7. Presented at	the Propulsion and Energetics Panel 66th (A) Specialists' Meeting, held in Florence, Italy, 12 - 13 September 1985.		
8. Author(s)/Editor(s)	Various		9. Date
			January 1986
10. Author's/Editor's Address	Various		11. Pages
			174
12. Distribution Statement	This document is distributed in accordance with AGARD policies and regulations, which are outlined on the Outside Back Covers of all AGARD publications.		
13. Keywords/Descriptors	<ul style="list-style-type: none"> ↳ Inhibitors ↳ Minimum smoke ↳ Particle collection ↳ Plume analysis ↳ Reduced smoke ↳ Rocket propulsion ↳ Signature of propellants ↳ Smokelessness ↳ Smoke measurements 		
14. Abstract	<p>The Conference Proceedings contain 11 unclassified papers presented at the Propulsion and Energetics 66th (A) Specialists' Meeting on Smokeless Propellants, which was held on 12-13 September 1985 in Florence, Italy.</p> <p>The Technical Evaluation Report is included at the beginning of the Proceedings. Questions and answers of the discussions follow each paper. The Specialists' Meeting was arranged in the following sessions: A Review of Smokeless Propellant Technology (1); Prediction and Measurement of Signature (3); Chemistry of Smokeless Propellants (12); and Smoke Measurements (4).</p> <p>The purpose of the Specialists' Meeting was to bring together specialized experts in the field of smokeless propellants in order to discuss the definitions of the various degrees of smokelessness, and provide the results of the investigations performed in the last years. The achievements were discussed in the Technical Evaluation Report, which suggests also several subjects for future investigations.</p>		

<p>AGARD Conference Proceedings No. 391 Advisory Group for Aerospace Research and Development, NATO SMOKELESS PROPELLANTS Published January 1986 174 pages</p> <p>The Conference Proceedings contain 11 unclassified papers presented at the Propulsion and Energetics 66th(A) Specialists' Meeting on Smokeless Propellants, which was held on 12-13 September 1985 in Florence, Italy.</p> <p>The Technical Evaluation Report is included at the beginning of the Proceedings. Questions and answers of the discussions follow each paper. The Specialists' Meeting was arranged in the following sessions: A Review of Smokeless</p> <p>P.T.O.</p>	<p>AGARD-CP-391</p> <p>Inhibitors Minimum smoke Particle collection Plume analysis Reduced smoke Rocket propulsion Signature of propellants Smokelessness Smoke measurements</p>	<p>AGARD Conference Proceedings No. 391 Advisory Group for Aerospace Research and Development, NATO SMOKELESS PROPELLANTS Published January 1986 174 pages</p> <p>The Conference Proceedings contain 11 unclassified papers presented at the Propulsion and Energetics 66th(A) Specialists' Meeting on Smokeless Propellants, which was held on 12-13 September 1985 in Florence, Italy.</p> <p>The Technical Evaluation Report is included at the beginning of the Proceedings. Questions and answers of the discussions follow each paper. The Specialists' Meeting was arranged in the following sessions: A Review of Smokeless</p> <p>P.T.O.</p>	<p>AGARD-CP-391</p> <p>Inhibitors Minimum smoke Particle collection Plume analysis Reduced smoke Rocket propulsion Signature of propellants Smokelessness Smoke measurements</p>
<p>AGARD Conference Proceedings No. 391 Advisory Group for Aerospace Research and Development, NATO SMOKELESS PROPELLANTS Published January 1986 174 pages</p> <p>The Conference Proceedings contain 11 unclassified papers presented at the Propulsion and Energetics 66th(A) Specialists' Meeting on Smokeless Propellants, which was held on 12-13 September 1985 in Florence, Italy.</p> <p>The Technical Evaluation Report is included at the beginning of the Proceedings. Questions and answers of the discussions follow each paper. The Specialists' Meeting was arranged in the following sessions: A Review of Smokeless</p> <p>P.T.O.</p>	<p>AGARD-CP-391</p> <p>Inhibitors Minimum smoke Particle collection Plume analysis Reduced smoke Rocket propulsion Signature of propellants Smokelessness Smoke measurements</p>	<p>AGARD Conference Proceedings No. 391 Advisory Group for Aerospace Research and Development, NATO SMOKELESS PROPELLANTS Published January 1986 174 pages</p> <p>The Conference Proceedings contain 11 unclassified papers presented at the Propulsion and Energetics 66th(A) Specialists' Meeting on Smokeless Propellants, which was held on 12-13 September 1985 in Florence, Italy.</p> <p>The Technical Evaluation Report is included at the beginning of the Proceedings. Questions and answers of the discussions follow each paper. The Specialists' Meeting was arranged in the following sessions: A Review of Smokeless</p> <p>P.T.O.</p>	<p>AGARD-CP-391</p> <p>Inhibitors Minimum smoke Particle collection Plume analysis Reduced smoke Rocket propulsion Signature of propellants Smokelessness Smoke measurements</p>

<p>Propellant Technology (1), Prediction and Measurement of Signature (3), Chemistry of Smokeless Propellants (12), and Smoke Measurements (4)</p> <p>The purpose of the Specialists' Meeting was to bring together specialized experts in the field of smokeless propellants in order to discuss the definitions of the various degrees of smokelessness, and provide the results of the investigations performed in the last years. The achievements were discussed in the Technical Evaluation Report, which suggests also several subjects for future investigations.</p> <p>ISBN 92-835-0387-2</p>	<p>Propellant Technology (1), Prediction and Measurement of Signature (3); Chemistry of Smokeless Propellants (12), and Smoke Measurements (4)</p> <p>The purpose of the Specialists' Meeting was to bring together specialized experts in the field of smokeless propellants in order to discuss the definitions of the various degrees of smokelessness, and provide the results of the investigations performed in the last years. The achievements were discussed in the Technical Evaluation Report, which suggests also several subjects for future investigations.</p> <p>ISBN 92-835-0387-2</p>
<p>Propellant Technology (1); Prediction and Measurement of Signature (3), Chemistry of Smokeless Propellants (12); and Smoke Measurements (4)</p> <p>The purpose of the Specialists' Meeting was to bring together specialized experts in the field of smokeless propellants in order to discuss the definitions of the various degrees of smokelessness, and provide the results of the investigations performed in the last years. The achievements were discussed in the Technical Evaluation Report, which suggests also several subjects for future investigations.</p> <p>ISBN 92-835-0387-2</p>	<p>Propellant Technology (1), Prediction and Measurement of Signature (3); Chemistry of Smokeless Propellants (12); and Smoke Measurements (4)</p> <p>The purpose of the Specialists' Meeting was to bring together specialized experts in the field of smokeless propellants in order to discuss the definitions of the various degrees of smokelessness, and provide the results of the investigations performed in the last years. The achievements were discussed in the Technical Evaluation Report, which suggests also several subjects for future investigations.</p> <p>ISBN 92-835-0387-2</p>